

CATION CHELATING [2]CATENANES AND CYCLOPHANES BASED ON 2,2'-BIPYRIDINE



UNIVERSITY
of
GLASGOW

© Philip Ross Mackie

A thesis submitted for the degree of Doctor of Philosophy
Department of Chemistry, University of Glasgow, October 1998

ProQuest Number: 13815614

All rights reserved

INFORMATION TO ALL USERS

The quality of this reproduction is dependent upon the quality of the copy submitted.

In the unlikely event that the author did not send a complete manuscript and there are missing pages, these will be noted. Also, if material had to be removed, a note will indicate the deletion.



ProQuest 13815614

Published by ProQuest LLC (2018). Copyright of the Dissertation is held by the Author.

All rights reserved.

This work is protected against unauthorized copying under Title 17, United States Code
Microform Edition © ProQuest LLC.

ProQuest LLC.
789 East Eisenhower Parkway
P.O. Box 1346
Ann Arbor, MI 48106 – 1346

GLASGOW
UNIVERSITY
LIBRARY

11388 (copy 1)

*This thesis is dedicated to the
memory of Anne Ross MacLennan.*



Acknowledgements

Firstly, I would like to thank Mum, Dad and Neil without whose support and generosity none of this would have been possible. I would also like to thank my supervisors, Drs. Andy Benniston and Bob Peacock for their patience and sound advice over the duration of the project. Thanks are also due to Drs. Ken Muir, Dimitri Yufit, Simon Teat and especially Dr Louis Farrugia for a great deal of help with X-ray crystallography. The picosecond photophysical studies carried out by Professor A. Harriman at the Université Louis Pasteur de Strasbourg and the corresponding nanosecond time-resolved spectroscopy carried out with the assistance of Dr Andy M^cLean at the University of Paisley are gratefully acknowledged.

I would also like to thank my colleagues in the research office without whom my time in Rm. A4-30 would have been much less enjoyable. In addition I would like to thank Paul L., Graham, Campbell, Rose, Dave K., Dave E., Iain and Paul N. for all their help at various times in the last three years.

Finally, I would like to thank the EPSRC for funding.

Abbreviations

AIBN	Azobisisobutyrylnitrile
b	broad
bipy	bipyridine
CT	Charge Transfer
d	doublet
DCM	Dichloromethane
DHB	Dihydroxybenzene (hydroquinone)
DMB	Dimethoxybenzene
DMF	Dimethylformamide
DMSO	Dimethylsulphoxide
EDA	Electron Donor-Acceptor
EI	Electron Impact
Et	Ethyl
EtOAc	Ethyl Acetate
EtOH	Ethanol
FAB	Fast Atom Bombardment
IR	Infrared
m	multiplet
Me	Methyl
MeCN	Acetonitrile
MeOH	Methanol
MHz	Megahertz
MLCT	Metal to Ligand Charge Transfer
mmol	millimoles
MS	Mass Spectrometry
NBA	3-nitrobenzyl alcohol
NBS	N-Bromo Succinimide
NMR	Nuclear Magnetic Resonance
Petrol	Petroleum Ether 40 - 60°C
Ph	Phenyl
ppm	parts per million
q	quartet
s	singlet
t	triplet
TLC	Thin Layer Chromatography
THF	Tetra Hydro Furan
TMPD	Tetra Methyl Phenylene Diamine
UV	Ultraviolet
VIS	Visible

Summary

The research presented in this thesis lies within the general area of supramolecular chemistry. More specifically, this project involved the synthesis of cyclophanes and [2]catenanes which contained both cation chelating 2,2'-bipyridine units and π -electron accepting and donating moieties.

The cyclophane systems are composed of either one or two cation chelating units and two bipyridinium electron accepting units. They were assembled either by employing template syntheses whereby the electron deficient cyclophanes formed electron donor-acceptor (EDA) complexes with electron donating threads or by employing a 'pre-coordination' strategy. The former route produces pseudo-rotaxane species which may be easily de-threaded to yield cyclophane products. The latter synthetic route involves coordinating cyclophane precursors with metal centres, so as to overcome the unfavourable conformation of the 2,2'-bipyridine-based precursors, and performing ring closure reactions under refluxing conditions.

The [2]catenane structures are composed of two interlocked rings, one of which is an electron donating aromatic crown ether, the other being a π -electron deficient cation chelating cyclophane. The catenated systems were synthesised in a similar manner to their analogous cyclophanes, with the difference that upon ring closure, an interlocked structure is produced rather than a pseudo-rotaxane species - the EDA interaction is thus locked within the structure.

The primary aim of the project was to construct models for the photosynthetic reaction centre such as those in the purple photosynthetic bacteria *Rhodospseudomonas viridis* and *Rhodobacter sphaeroides*. Cation chelating [2]catenanes were identified as possessing the necessary structural features to adequately model the vectorial electron transfer that is present in the natural systems. The secondary aims of the project were to characterise and investigate the properties of the [2]catenanes and their related cyclophanes as ligands, guests for aromatic electron donors and as potential components of molecular devices.

Four cyclophane structures were constructed, each of which consisted of either one or two cation chelating 2,2'-bipyridyl units. All four systems were

characterised by NMR spectroscopy and mass spectrometry and their electrochemical properties investigated.

Cyclophanes **L1** and **L2** were characterised structurally by X-ray diffraction techniques, as was the precursor to these systems, **P1** and its ruthenium bipyridyl complex $\text{Ru}(\text{bipy})_2(\text{P1})^{4+}$. The structures confirmed that the pre-coordination strategy produces a cyclophane precursor which possesses a conformation more favourable towards cyclisation than its non-complexed equivalent. The cyclophane structures indicated that addition of 2,2'-bipyridine units to the cyclophane structures increased the cavity size and thus weakened binding of aromatic electron donors. This was confirmed by the measurement of binding constants for a range of such donors with **L1** and **L2**. The X-ray structure of the inclusion complex between **L1** and the donor thread **T1** revealed the geometry of the interactions between such electron deficient cyclophanes and their complementary electron rich guests.

The coordination chemistry of cyclophanes **L1** and **L2** was investigated, particularly as regards the formation of multiple - cyclophane aggregates. In addition, photoactive metal centres such as ruthenium and osmium tris-bipyridyl were appended to cyclophane **L1**. Photoinduced electron transfer (PET) was observed to occur upon investigation of $\text{Ru}(\text{bipy})_2(\text{L1})^{6+}$ by time-resolved fluorescence and absorption spectroscopy. The precursor complex $\text{Ru}(\text{bipy})_2(\text{P1})^{4+}$ was also subjected to photophysical investigation and no PET was observed.

Three analogous [2]catenanes were constructed and characterised by NMR spectroscopy and MS techniques. The properties of the interlocked species were investigated by UV-VIS spectroscopy and by cyclic voltammetry. The structure of one catenated structure, **L5**, was determined by X-ray diffraction and the interlocked nature of the compound confirmed. The coordination chemistry of this compound was investigated particularly as regards the construction of photoactive assemblies. Photoinduced electron transfer (PET) was observed to occur upon investigation of $\text{Ru}(\text{bipy})_2(\text{L5})^{6+}$ by time-resolved fluorescence and absorption spectroscopy in much the same way as had occurred in $\text{Ru}(\text{bipy})_2(\text{L1})^{6+}$. However, the complex which featured the catenated ligand possessed an inherent redox asymmetry between its two chemically identical electron acceptors, thus vectorial electron transfer was achieved.

Contents

	<i>Page</i>
Dedication	ii
Acknowledgements	iii
Abbreviations	iv
Summary	v
Contents	vii
Chapter 1 Introduction	1
1.1 Introductory Remarks	2
1.2 Supramolecular Chemistry	2
1.3 Molecular Recognition	5
1.4 Cyclophanes as Molecular Receptors	8
1.5 Molecular and Supramolecular Devices	10
1.6 [2]Catenanes and Their Role as Supramolecular Devices	21
1.7 Properties of Supermolecules and Supramolecular Assemblies	45
1.8 Aims and Objectives	57
1.9 References	58
Chapter 2 Experimental	65
2.1 Instrumentation	66
2.2 Chemicals and Solvents	69
2.3 Synthesis	74
2.4 Aromatic Electron Donor - Acceptor Binding Experiments	124
2.5 References	127
Chapter 3 Cyclophanes	130
3.1 Introduction	131
3.2 Precursors	135
3.3 Cyclophane L1	143
3.4 Cyclophane L2	164
3.5 Cyclophanes L3 and L4	172
3.6 References	177

Chapter 4	[2]Catenanes	179
4.1	Introduction	180
4.2	[2]Catenane L5	184
4.3	[2]Catenane L6	193
4.4	[2]Catenane L7	201
4.5	References	205
Chapter 5	Photophysical Studies	207
5.1	Introduction	208
5.2	Properties of Ru(bipy) ₂ (P1)(PF ₆) ₄	214
5.3	Properties of Ru(bipy) ₂ (L1)(PF ₆) ₆	226
5.4	Properties of Ru(bipy) ₂ (L5)(PF ₆) ₆	229
5.5	References	232
Chapter 6	Future Directions	234
6.1	Introduction	235
6.2	Electron Donor - Acceptor Complexes	236
6.3	Schiff Base Chemistry	246
6.4	References	252
Chapter 7	General Conclusions	253
Appendices		ix

Chapter 1

Introduction

1.1 Introductory Remarks

The research presented in this thesis falls within the general area of supramolecular chemistry. This topic encompasses an extremely diverse and prolific area of research, therefore it is impossible to provide a comprehensive description of all aspects of the field in this introduction.

Rather, it is hoped that these the following pages will provide a general overview of the roots, terminology and current status of supramolecular chemistry, identifying some general aims and concepts as well as providing some specific examples of recently published work. Brief reviews of some specific topics which are regarded as being particularly noteworthy and relevant to the work presented in this thesis will be undertaken in addition to brief discussions on some intriguing properties of supramolecular and molecular systems including photoinduced electron transfer, redox properties and host guest chemistry.

1.2 Supramolecular Chemistry

The concept and term “supramolecular chemistry” were introduced in 1978 by Jean - Marie Lehn “as a development and generalisation of earlier work”¹. The work to which Lehn was referring was the selective binding of alkali metal cations by macrocyclic and macropolycyclic ligands, crown ethers and cryptands². The key to the development of alkali metal complexation chemistry into supramolecular chemistry was the concept of *molecular recognition*, which by generalisation to include all intermolecular interactions and processes grew into the field as it is known today.

Although the term “supramolecular chemistry” is relatively recent, the subject has roots that extend back a great number of years³. Early concepts of molecular recognition were put forward by Ehrlich who identified the importance of *binding* of molecules and introduced the concept of the *receptor*. In 1894, Fischer presented the now ubiquitous ‘lock and key’ concept of steric fit, thus introducing the concept of complementarity (in particular geometric complementarity) as a basis of molecular recognition. Building on these two contributions, Werner introduced the idea of coordination (of ligands to metals), a concept which may be generalised

to relate to the affinity of partner molecules for each other when entering into a molecular interaction³. It is possible to trace some of the terminology of supramolecular chemistry to the mid - 1930's when the term "Übermolecule" was used to describe highly organised systems such as the acetic acid dimer which result from simple intermolecular interactions.

In addition to temporal depth, supramolecular chemistry also has roots in a wide variety of scientific disciplines, covering the chemical, physical and biological features of chemical species which are composed of organised molecular assemblies held together by means of intermolecular interactions. These roots extend into synthetic organic chemistry, coordination chemistry and include both experimental and theoretical studies of molecular interactions. There are also strong analogies to biochemical and biological processes that involve substrate binding (host - guest chemistry) and with materials science, in particular, in the development of molecular devices.

To understand the field of supramolecular chemistry, it is sagacious to review the broad aims of molecular chemistry. Synthetic molecular chemistry provides chemists with the means to produce new molecules and materials which may have novel properties. This is made possible by use of an wide array of highly sophisticated and powerful methods which may be used for the construction of complex molecular structures. Such structures are fashioned by the making and breaking of covalent bonds between atoms in a predictable fashion. Molecular chemistry is, thus, concerned with the chemistry of the covalent bond; with discovering and applying the rules that govern the structures, properties and reactivity of molecular species.

In the same way that the field of molecular chemistry is based on the covalent bond, supramolecular chemistry is based on the chemistry of molecular assemblies and of the intermolecular bond⁴. It is concerned with the next step in complexity beyond the molecule; the supermolecule and the organised polymolecular system, both of which are held together by non - covalent interactions (figure 1.1). Supramolecular chemistry may then be defined as "chemistry beyond the molecule", where supermolecules and intermolecular forces are the equivalents of molecules and covalent bonds in molecular chemistry.

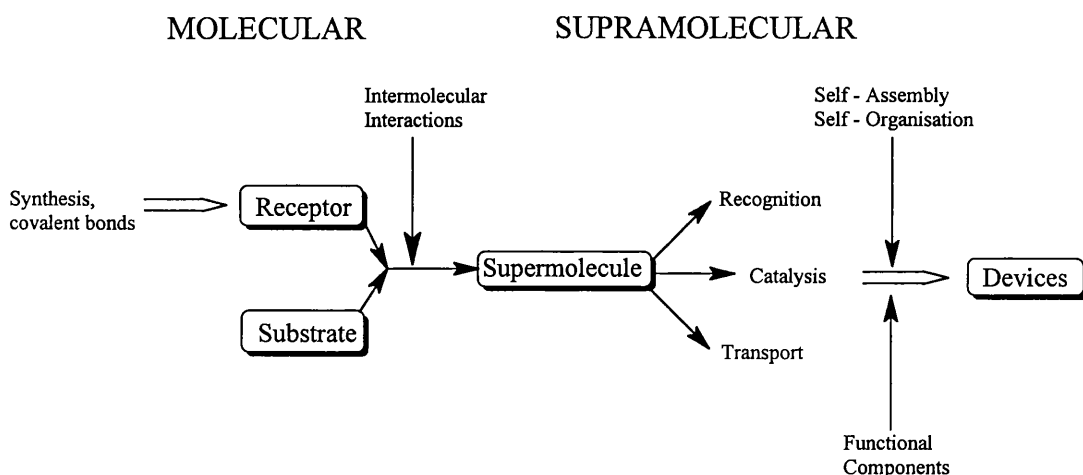


Figure 1.1: Relationship between molecular and supramolecular chemistry.

Non - covalent interactions control the behaviour of molecules and how they interact with one another - they control both the stability and selectivity of molecular associations and so the tendency of molecular components to bind. Molecular interactions form the basis of highly specific recognition, catalytic, transport and regulation processes which occur in biology^{3,4}. There are many examples of such processes including: substrate binding to a receptor protein, enzymatic reactions, assembling of multiprotein complexes, immunological antigen-antibody association, intermolecular reading, translocation and transcription of genetic code, regulation of gene expression by DNA binding proteins, entry of a virus into a cell, signal transduction by neurotransmitters and cellular recognition.

There are many types of molecular interaction, which all have different degrees of strength, directionality and distance dependence. Some particularly important examples are: hydrogen bonding, van der Waal's interactions (both attractive and repulsive), electrostatic forces, metal - ligand coordination and donor - acceptor interactions (such as those between π - electron rich and complementary π - electron poor aromatic systems). The strength of these interactions varies from strong for metal - ligand coordination to moderate for hydrogen bonding to weak for donor - acceptor interactions. In general, however, intermolecular forces are weaker than covalent bonds, with the result that supramolecular systems are thermodynamically, kinetically and dynamically less stable than molecules.

Supramolecular systems are defined both by the nature of the forces that hold them together and by the spatial arrangement (or “architecture”) of the components that constitute them.

The components of a supermolecule have been named “receptor” and “substrate”, the substrate usually being the smaller component whose binding is desired.^{3,4} Molecular receptors are defined as being chemical species held together by covalent bonds which are able to selectively complex ions or molecules. Binding of a substrate makes use of various intermolecular interactions (as listed previously), leading to production of a supermolecule. The design of the receptor determines, to a large extent, which substrate is bound in a multi - substrate system. Selective binding of a specific substrate to its receptor to yield a supermolecule involves a molecular recognition process. For a substrate to effectively bind to a receptor, the receptor must possess multiple binding sites which cooperatively contact and attract the binding sites of the substrate without generating strong non - bonded repulsions: in other words the receptor and substrate must be complementary.

The design of artificial systems capable of displaying selective binding requires knowledge and manipulation of the energetic and stereoelectronic features of the intermolecular forces within the architecture of the supermolecule.

Supermolecules and their properties will be the focus of this introduction, however, it should be noted that there are in fact two broad areas³ in supramolecular chemistry:

(1) Supermolecules; well defined discrete oligomolecular species consisting of a receptor and complementary substrate(s).

(2) Supramolecular assemblies; polymolecular entities that are composed of an undefined number of components which are produced by spontaneous assembly. Examples of such assemblies are phases such as films, layers, membranes, vesicles, micelles and mesomorphic phases, which have well defined microscopic order and predictable macroscopic characteristics.

1.3 Molecular Recognition

Molecular recognition³⁻⁷ is a logical extension of the previously referred to ‘lock and key’ concept. It is currently enjoying great popularity in the field of

supramolecular chemistry and beyond now that it is possible to construct and exploit synthetic receptor molecules that can, in simple terms, simulate the specificity exhibited by enzymes. Some examples of supramolecular systems which can recognise either ions (crown ethers, azamacrocycles, cryptands and spherands)^{1-4,6} or organic substrates (calixarenes, cyclophanes) are given in figure 1.2. In theory, for any given substrate (molecule or ion), an appropriate receptor molecule can be designed.

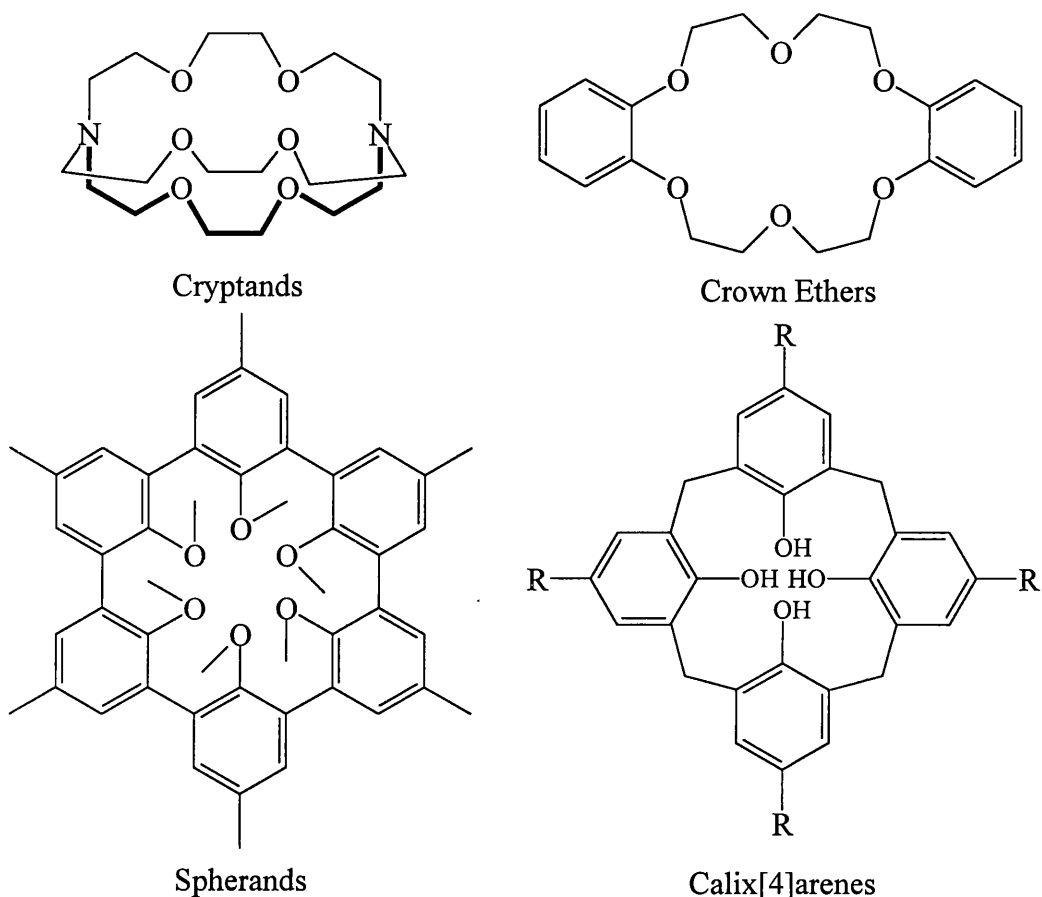


Figure 1.2: Some synthetic receptor molecules.

Before this can be attempted, however, the concepts behind molecular recognition must be explored. The term 'molecular recognition' can be defined as a process which involves both binding and selectivity of a substrate by a receptor^{1,3,4}. To achieve this, consideration of the energetics of the intermolecular association and the information involved in the binding process must be considered. Simple binding (e.g. of the previously discussed acetic acid dimer) does not constitute molecular recognition because in such cases there is no pattern recognition process occurring during the course of the interaction. The stability of a supramolecular assembly is

derived both from the energy of the interaction and by the amount of information used to produce the assembly. The implication of this statement is that information storage and readout on the molecular scale is a requirement of the recognition process.

The concept of molecular information may be succinctly stated as: “in order to achieve selective complexation of a substrate by a receptor, chemical information must be stored in the receptor and read out by the substrate” ^{2(a)}. This may be accomplished by careful design of receptors whereby the stored information is stored in the architecture of the receptor and read out during the complexation process. The rate of information readout is determined by the rates of association and dissociation of the receptor and acceptor.

A number of forms of information may be encoded within a receptor for example: topological information, binding site control and response to environmental factors. Receptor topology may contain information in its shape and size, the connectivity within the receptor, the conformation of the receptor and the manner in which this changes upon complexation with the substrate and, in specific cases, the chirality of the receptor or its binding sites. The control of binding sites may be effected *via* their number, size and shape, arrangement within the architecture of the receptor and by their electronic properties (charge, polarity, polarisability and van der Waals attractions and repulsions). Environmental effects largely involve the solvation of the complexed and uncomplexed species by the medium and the balance between solvation of the substrate by the medium and complexation by the receptor.

Recognition implies both geometrical and interactional complementarity between the receptor and its substrate (i.e. matching binding sites in the correct positions). This rational leads to the *double complementarity* principle whereby both geometrical and energetic features of receptor - substrate interactions must be considered when molecular interactions are under investigation. This concept is unifying in that it includes both the early geometrical ‘lock and key’ theories and also more rigorous kinetic and thermodynamic examinations of molecular interactions. This analysis is useful because it provides a quantitative basis for the consideration of recognition processes so that interaction parameters and functions

may be employed, allowing the use of molecular modelling in the investigation of such interactions.³

The ultimate goal of molecular recognition must be to adequately mimic the exquisitely organised chemical systems found in biological systems such as enzymes and nucleic acids which perform marvels of specificity in a most complicated yet elegant fashion.⁶

1.4 Cyclophanes as Molecular Receptors

Many classes of synthetic receptor molecules (see figure 1.2) have been studied by a variety of research groups since the inception of supramolecular chemistry. Cyclophanes are particularly valuable as synthetic receptor molecules because they allow the possibility of locating groups precisely within the molecular architecture⁸. It is possible, using the many synthetic strategies available for constructing cyclophanes, to build “nests”, “multi - floor structures”, helices, macropolycyclics, macro - hollow tubes and most importantly in the context of this thesis, hollow cavities and novel ligand systems.

Cyclophane chemistry has become a major component of supramolecular chemistry, specifically in the area of molecular recognition, because in addition to their role as receptors⁸ they have found application as models for intercalation, and as building blocks of organic catalysts.

The roots of cyclophane chemistry go back to 1899, when Pellegrin succeeded in synthesising perhaps the simplest possible cyclophane (figure 1.3), [2,2] - metacyclophane (a feat repeated by Baker in 1950).

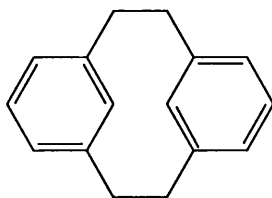


Figure 1.3: [2,2] - metacyclophane.

Since this discovery, a number of advances in cyclophane chemistry have been made: the most notable of these have been discussed at length by Vögtle and others^{8,9} and hence will only be briefly outlined here. The development of *ansa*

compounds (figure 1.4) by Lüttringhaus in 1937 was an important progression because they were produced using modern synthetic techniques.

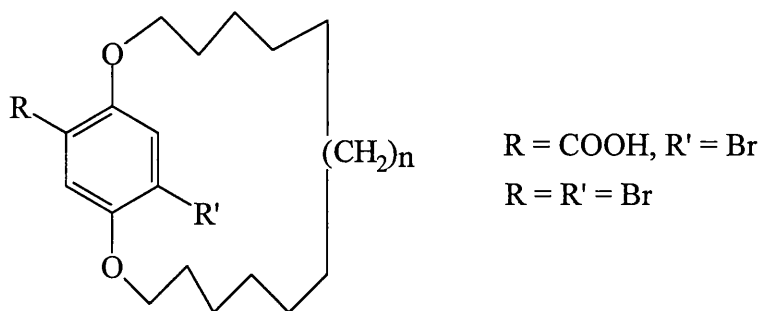


Figure 1.4: The *ansa* cyclophanes.

The *ansa* cyclophanes are aliphatic bridged benzene derivatives which fit into the modular system which is currently used to name cyclophanes. Further advances in this field were made by Huisgen (cyclisation by high dilution Friedel - Crafts acylation in 1952) and by Stetter (who synthesised the bridged benzidine molecules very similar in connectivity to systems of contemporary interest - see figure 1.5).

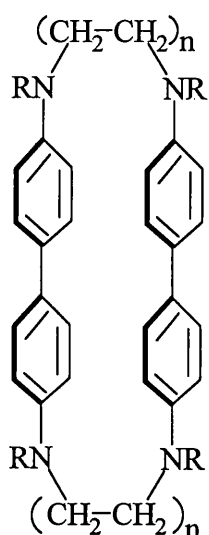


Figure 1.5: Bridged benzidine cyclophanes.

The 'age of cyclophanes' truly began in 1949 when Brown and Farthing synthesised [2,2] - paracyclophane by pyrolysis of *p*-xylene, using a process first described by Swarc. Cram and Steinberg built on this work to synthesise [2,2]-paracyclophane by a **directed** synthesis⁹ - this was an important advance in that it introduced a more sophisticated approach to cyclophane synthesis. Subsequently, these synthetic routes to paracyclophane were surpassed by the high yielding route

of Marsh (which involved heating of $p\text{-CH}_3\text{C}_6\text{H}_4\text{CH}_2\text{N}(\text{CH}_3)_3\text{OH}$). When, in 1967, Pederson discovered the crown ethers^{2(b)} modern cyclophane chemistry had begun.

1.5 Molecular and Supramolecular Devices

Molecular devices are structurally organised, functional chemical systems which form part of larger supramolecular arrays^{3,4,10}. The development of such devices is dependant upon the design of functional molecular components which will perform their function in the correct sequence in order to achieve the desired purpose of the supramolecular system. The components require an external trigger to operate in the correct sequence and they may be classified according to the stimulus to which they respond as photo-, electro- (redox-), iono-, magneto-, thermo-, mechano- or chemoactive.

The term 'machine' has recently been applied¹¹ to such chemical systems, whereby the components of the machine are the chemical subunits which are made to perform unique operations at the molecular level. Molecular switches provide an example of such devices (or machines) in which the relative position of molecular subunits is altered by an external reagent such as light or through redox or chemical changes.

Molecular receptors (such as the cyclophanes described previously) are potential components of supramolecular devices when they are capable of some additional function, whether that function is communicating to the external operator that a substrate has bound (molecular sensors)¹², acting as reagents or catalysts to a substrate, or performing a transportation process. To achieve multiple functionality, (i.e. molecular recognition plus an addition function(s)) a component must contain several subunits that are capable of interacting with one another. The mode of operation of the device, be it (1) photoactive, (2) redoxactive or (3) an ionophore depends on the nature of the substrate with which it was designed to interact.

(1) Photoactive supramolecular assemblies^{4,11} consist of individual photoactive (and commonly redoxactive) components which are in close proximity and thus interact with one another. This causes a perturbation to the ground- and excited-state properties of the individual components; thus the supramolecular assembly has electrochemical and photophysical properties that are different from its

constituent parts. This effect enables a number of processes to occur in the supramolecular entity that cannot occur in the isolated molecular components, for example: photoinduced energy transfer, charge separation by electron transfer¹³ (or proton transfer), perturbation of the probability and energy of electronic transitions, modification of redox potentials (and thus thermodynamic driving forces) and regulation of binding and reaction by photoexcitation (photocatalysis).

It is possible to envision a multi-step process occurring in the operation of a photoactive supramolecular assembly. If a simple two component (receptor and substrate) system is considered, on binding of the two components to produce the supermolecule and photoexcitation of the complex, one of a number of routes may be followed^{4(a)} (figure 1.6). It is possible to carry out a photochemical reaction, to initiate a reaction or to perform an energy or electron transfer process. The products of these processes may be either the dissociated receptor - substrate pair, the supramolecular complex or some products that result from the reaction of the substrate with the receptor.

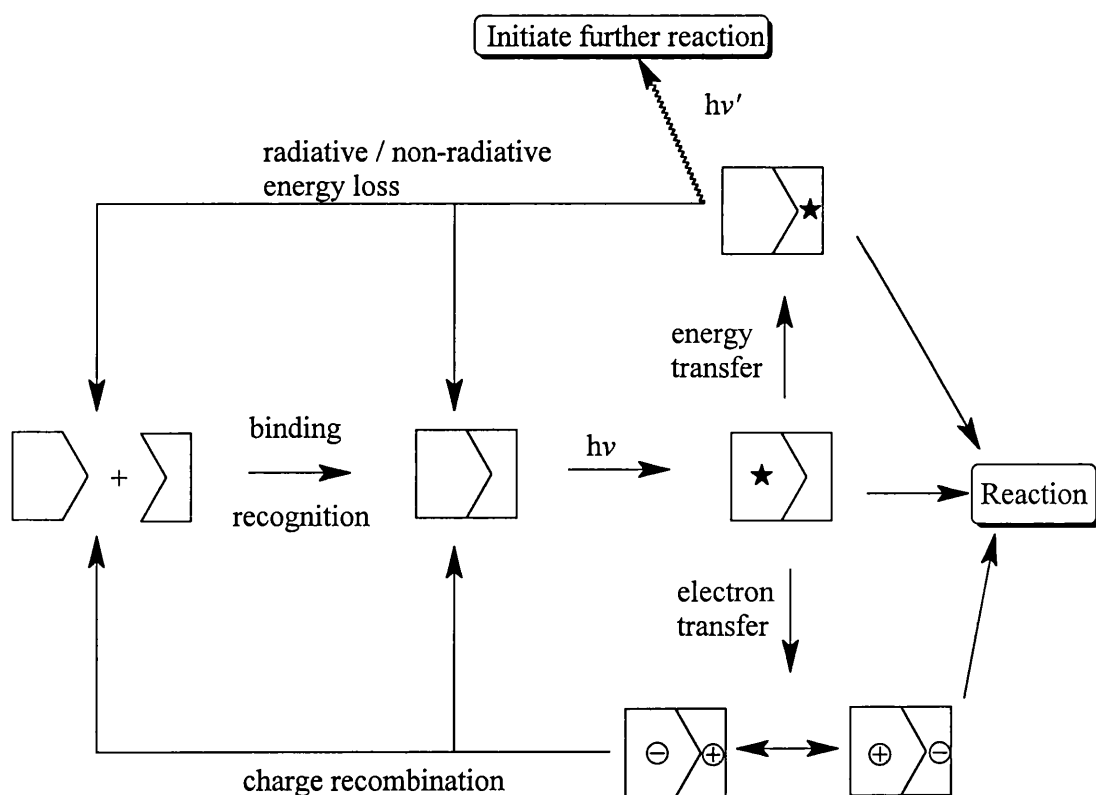


Figure 1.6: Photochemistry of supramolecular assemblies.

The three processes that can occur upon excitation of the supramolecular assembly may be illustrated by the salient examples described below.

The receptor - substrate complex may react upon photoexcitation in a number of ways. A particularly interesting example is the case where a coordination compound such as $[\text{Co}(\text{CN})_6]^{3-}$ is bound by a polyammonium macrocycle¹⁴ (figure 1.7). Excitation of the complex with light results in the temporary breaking of the Co-CN bonds. For the free cyano - cobalt complex in aqueous solution, this would lead to aquation of the cobalt atom at all six coordination sites. However, when the cyano - cobalt compound is complexed with a polyammonium macrocycle, dissociation of some of the CN^- groups is hindered, so preventing aquation in these positions. Thus, the extent and geometry of aquation of the cyano - cobalt complex (and so geometry of further substitution) may be controlled by use of a molecular receptor.

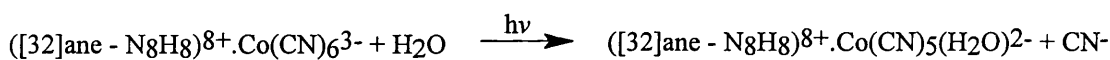
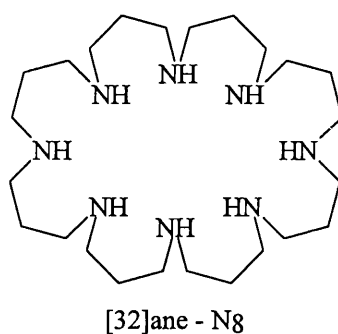


Figure 1.7: Polyammonium macrocycles as functional molecular receptors.

Energy transfer is a topic of great interest in supramolecular chemistry. Most interest centres on the conversion of light from, for example, short wavelength (UV) radiation to long wavelength (visible) radiation *via* an absorption - energy transfer - emission pathway. Lanthanide ions, in particular europium and terbium, and their complexes with cryptands (especially the cryptand bipy.bipy.bipy) have been extensively investigated in this respect and are found to produce quantum yields of between 0.02 and 0.03. More recently, europium and terbium complexes with calix[4]arenes¹⁵ (figure 1.8) have been found to perform a similar function as the cryptands but to provide improved quantum yields of around 0.2 (in the case of terbium) by offering improved encapsulation of the metal ion thus limiting contact with water molecules (water being an extremely efficient quencher of lanthanide fluorescence). These systems work by similar mechanisms, whereby ultraviolet light

is absorbed by the ligand (either the calixarene or the bipy cryptand); the energy is transferred to the bound lanthanide by an energy transfer process, whereupon the energy is released as visible light.

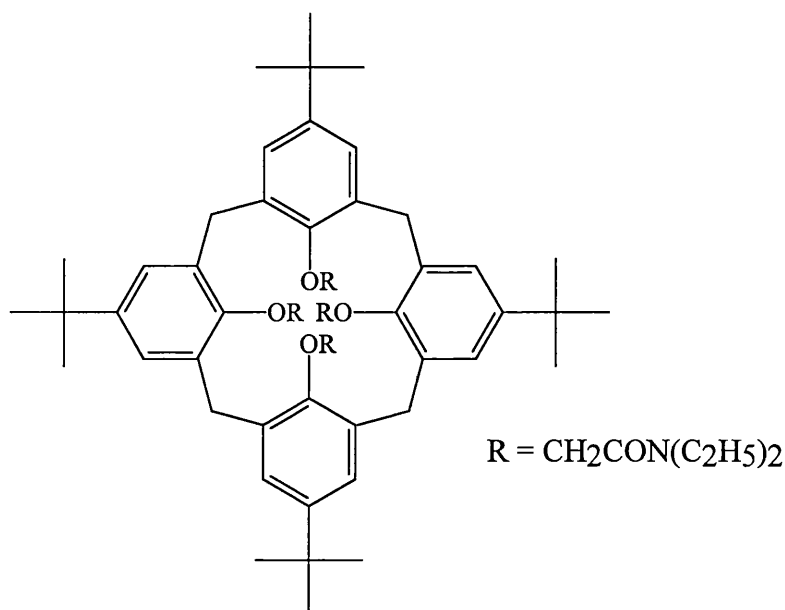


Figure 1.8: A calix[4]arene used in an energy transfer system.

Systems which are capable of electron transfer abound in the recent literature. Photoinduced electron transfer¹³ (photogeneration of charge separated states) is of interest both for photocatalytic systems (e.g. artificial photosynthesis) and in signal transduction (e.g. in sensor applications). The former application is of specific relevance to the research presented in this thesis and will be discussed in detail in section 1.7. However, in basic terms, an artificial photosynthesis system consists of three components^{4(a), 16(a)} (figure 1.9); a light harvesting unit (photosensitiser), an electron carrier (relay) and catalysts to facilitate hydrogen and oxygen production from water. A number of sensitisers have been employed in the literature, for example, metal - polypyridine complexes, metal porphyrins and semiconducting materials. Relays that have proved useful include methyl viologen and its derivatives and more complex compounds such as cobalt - sepulchrate.^{16(b)} The generation of oxygen and hydrogen from water requires the scaling of a formidable activation barrier. This may be overcome by the use of catalysts such as Pt, Ru, Os, RuO₂ and IrO₂.

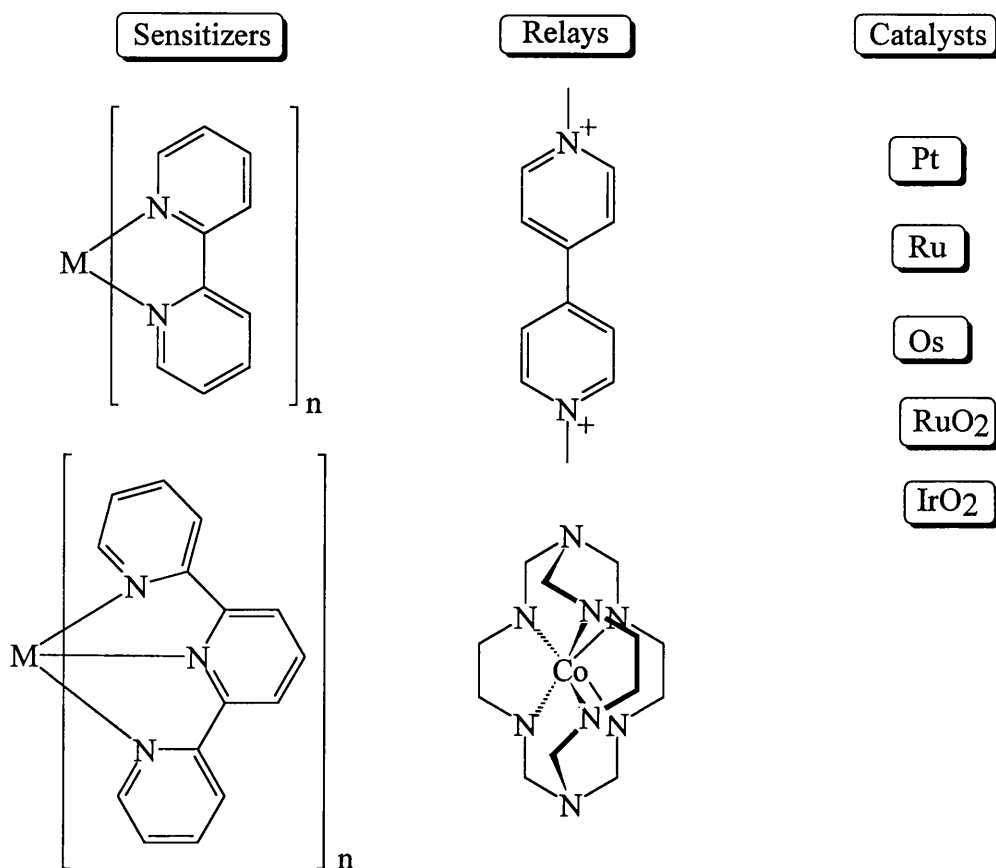
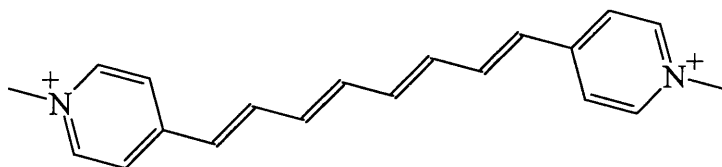


Figure 1.9: The three components of an artificial photosynthetic system.

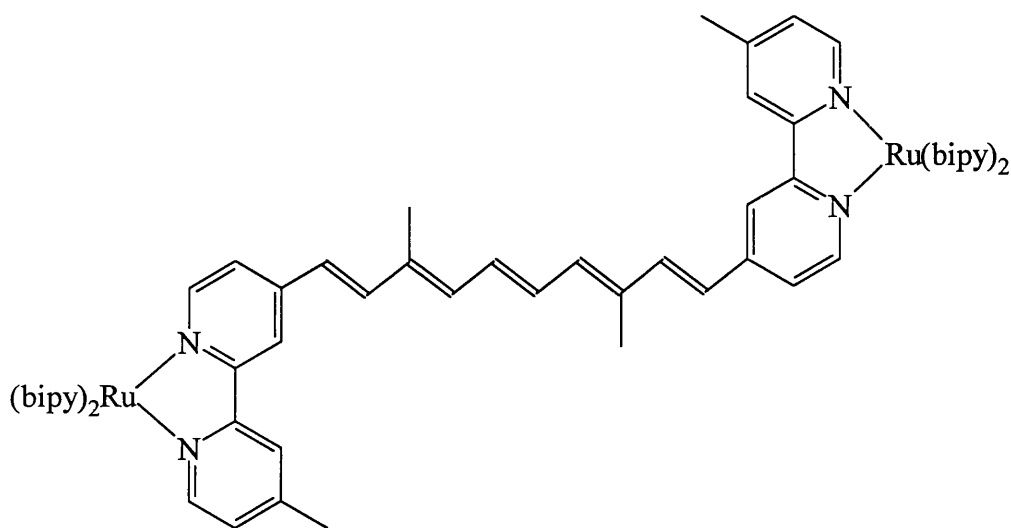
(2) Redoxactive supramolecular systems^{4(a)} have been envisioned as being potentially useful in the development molecular wires, diodes, transistors and rectifiers. Currently, the area attracting the most attention is the development of molecular wires and shuttles, which may be regarded as being the most important and fundamental components of an electronic network (or circuit) as they permit electron flow and act a junctions between various parts of the system.

Molecular wires are generally based on polyvinyl³ systems which permit electron transfer through the length of the chain by virtue of their conjugated π - orbitals. Such wires may be constructed from carotene¹⁷ or caroviologen derivatives (figure 1.10). The caroviologens have been shown to possess a length suitable for spanning a bilayer membrane in a sodium dihexadecylphosphate vesicle, with the hydrosoluble pyridinium groups being placed close to the negatively charged inner and outer surfaces of the vesicle^{4(a)}. These molecules clearly have the potential to act as reversible electron channels through membranes or, in conjunction with polymeric supports, as molecular nanocircuits in molecular electronic devices.

Building on this approach, if photo- or redoxactive groups are appended onto the ends of the polyene chain it is possible to create systems where the active groups communicate with one another (i.e. are coupled) over large distances. Alternatively, with unsymmetrical substitution push-pull polyenes have been shown to display interesting nonlinear optical properties¹⁷.



A Caroviologen



A Symmetrically Substituted Carotene Derivative

Figure 1.10: Molecular wires.

Electronic devices based on molecular shuttles are a comparatively recent innovation, pioneered primarily in the laboratories of Sauvage, Stoddart and Kaifer¹⁸.

A salient example¹⁹ is given by the [2]rotaxane system shown in cartoon form in figure 1.11.

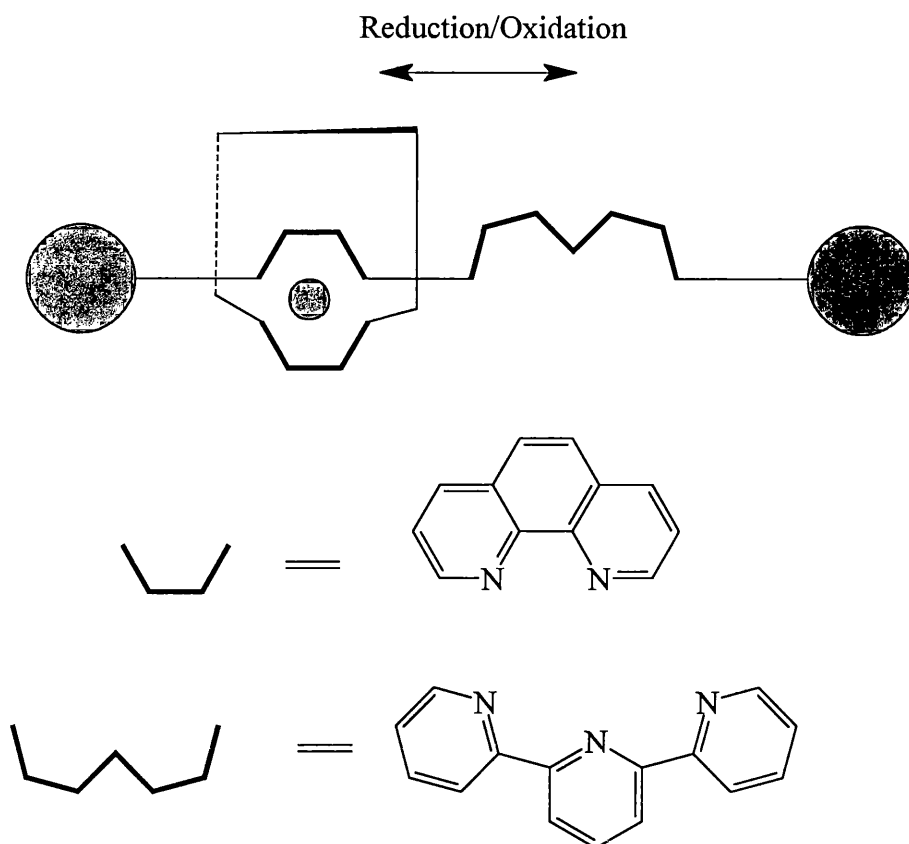
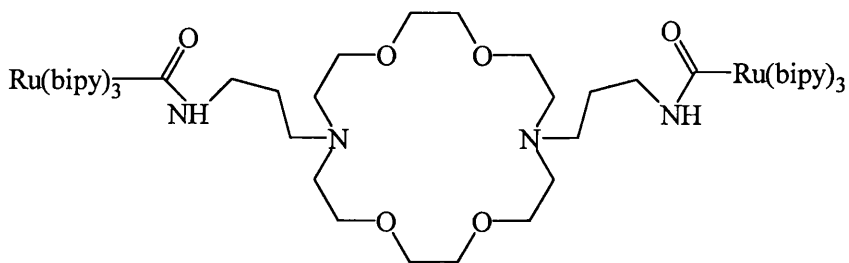


Figure 1.11: A redox - driven molecular shuttle.

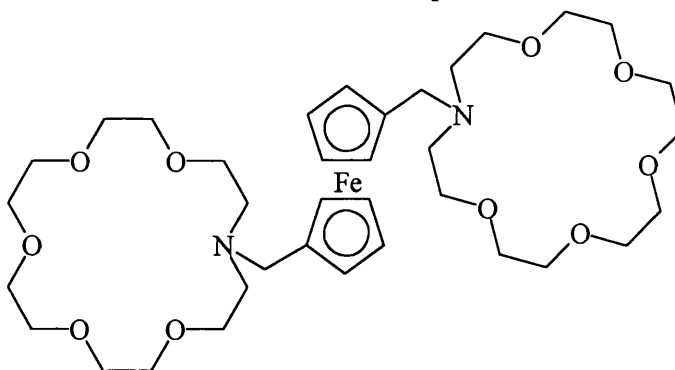
The rotaxane consists of a 'thread' which contains two cation chelating sites - one ditopic and one tritopic. The 'bead', which is a cyclophane, contains a ditopic chelating unit. Initially, a copper (I) ion is bound by both the bead and the thread at ditopic binding sites, allowing the complex to be tetrahedral, as is preferred by the metal ion in the +1 oxidation state. On oxidation to copper (II) however, the preferred geometry is five - coordinate - a geometry that may be accommodated by movement of the metal ion and the bead to the second, tritopic binding site on the thread. This process is reversible, thus this system represents a redox - driven molecular shuttle assembly.

(3) Ionic molecular devices are defined as being supramolecular systems which react to ionic stimuli^{4(a)}. This field of research is based upon the study of molecular recognition events that are involved in biological signalling - processes that are controlled by the binding of ions (for example, processes mediated by potassium, sodium, calcium and acetylcholine ions).

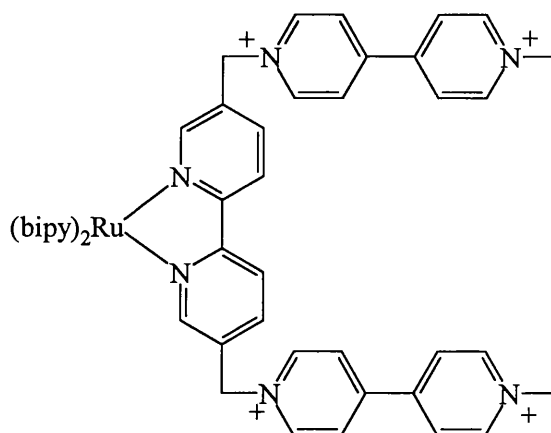
There are clearly a vast number of potential components for ionic devices - a wide variety of synthetic molecular receptors are available, including crown ethers, cryptands and macrocyclic structures to name but a few. The substrate (positive or negative ions) also has an abundance of variations - ions contain a significant^{3,4(a),14} amount of information in their charge (polarity, magnitude), their size and shape (geometrical complementarity) and also in their desired binding modes (preference for tetrahedral, square pyramidal, octahedral or other coordination geometries). Ionic molecular devices may generally be divided into two classes; sensors and transport devices. In an ion transportation device, there are three important functions that are required before successful operation can occur; binding of the substrate, triggering of the transportation event by an external stimulus (light or redox changes for example), followed by transportation of the ion. Selectivity^{4(c),7(b)} is an important aspect of ion recognition and synthetic receptors which are capable of performing an ion recognition function are of particular interest. In this regard, the work of Beer²⁰ and co-workers has been particularly noteworthy as systems have now been developed which can recognize either cations, anions or both cations and anions together in one sensory assembly. Examples²¹ of molecules with an anion recognition function are abundant, e.g. acyclic ruthenium bipyridyl-polypyridinium receptors (figure 1.12) which have been shown to coordinate chloride and bromide in 1:1 stoichiometries with magnitudes of around $10^2 \text{ dm}^3\text{mol}^{-1}$. The binding of anions may be followed by observing the significant cathodic perturbations of the pyridinium reduction couple of the receptor. Recognition of cation binding has been achieved by employing azo-crown ethers which are covalently bound to a ferrocene electrochemical signalling unit. Upon binding of cations in the azo-crown, the ferrocene/ferrocenium redox couple is perturbed, moving to a significantly more positive potential. Both cations and anions may be bound within the same ionophore by utilising a cooperative binding strategy whereby an azo-crown ether compound containing two ruthenium bipyridine-amide subunits firstly binds a potassium ion thus enhancing the binding of a chloride anion by means of electrostatic interactions which work in concert with halide-amide hydrogen bonding interaction (figure 1.12). Binding of both ions may be easily followed by changes in the fluorescence spectrum of the receptor.



Cation/Anion Receptor



Cation Receptor



Anion Receptor

Figure 1.12: Functional synthetic ion receptors.

Biological ion transport occurs by movement of ions along channels which show a selectivity for specific ions^{4(a)}. Due to the complex nature of such channels, wholly synthetic analogues have not been investigated extensively. There are, however, a number of approaches to artificial ion channels using, for example, aggregates of polyether macrocycles (such as those described by Gokel)²², macrocyclic peptides, macrocyclic polyamines in tubular mesophases (discotic liquid

crystals) and in Lehn's "bouquet" - type chundle (channels based on bundles of polyether chains) molecules^{3,4(a),4(c)}.

These systems operate as ion channels by orienting their macrocyclic cores along an axis using either liquid crystal columnar stacking in the case of tubular mesophases, by use of molecular scaffolding to hold the macrocycles in the desired orientation,²² or by grafting several transmembrane chains (i.e. polyether chains of sufficient length to span bi-lipid membranes) onto a functional macrocycle, thus delineating a channel structure. An example of such a chundle molecule is given in figure 1.13.

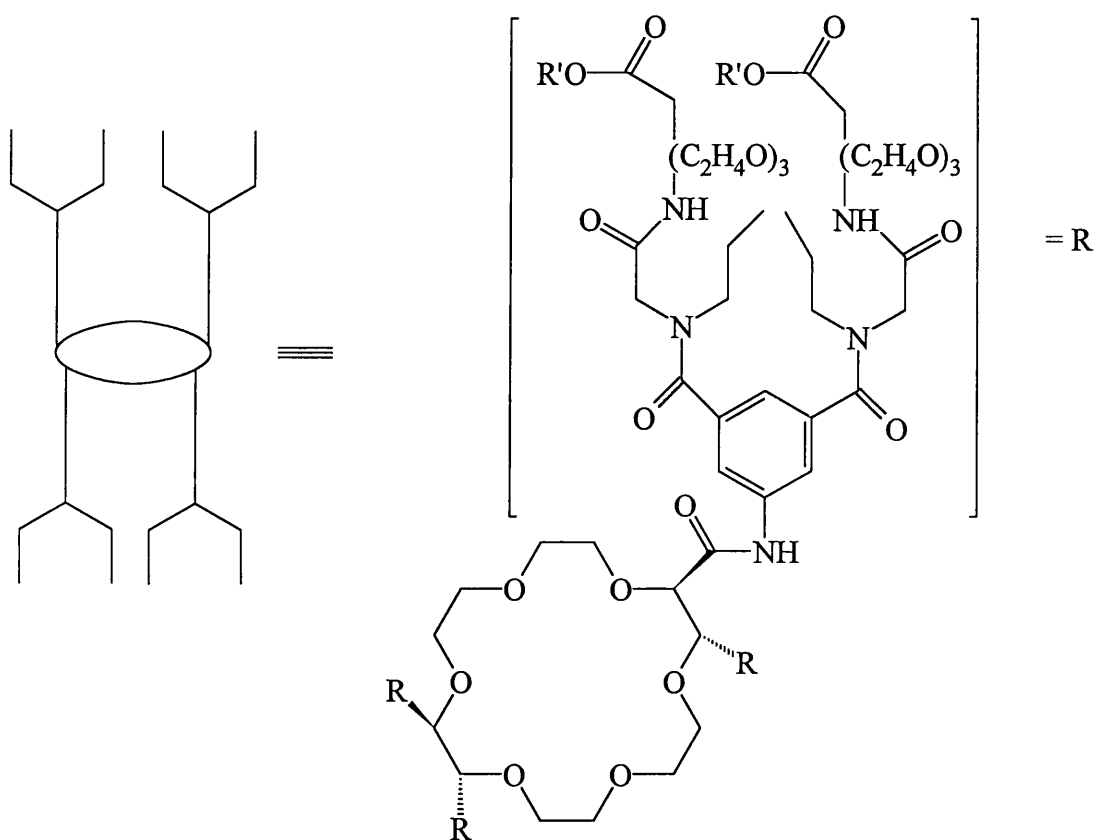


Figure 1.13: A synthetic ion channel (chundle molecule).

Molecular systems which are capable of selectively sensing ions are of interest in supramolecular chemistry as they are in commerce¹² in, for example, ion selective electrodes. The basic design features of such systems must include both a selective binding and a signal transduction component. Signal transduction may be in the form of an optical or electrical output or as a change in the physical properties of the system such as mass, conductivity or capacitance. A particularly interesting

family of systems of this type are the fluoroionophores, which undergo drastic changes in their fluorescence and absorption properties under cation complexation. An example of a fluoroionophore is presented in figure 1.14. This system consists of a fluorophore (a merocyanine derivative known as “DCM”) which is covalently linked to an ionophore (an azo - crown ether). DCM is known to undergo intramolecular charge transfer from the electron rich amino group (the azo - crown) to the electron poor dicyanomethylene subunit. The crown acts as a tuner to the photoinduced charge transfer as complexation of a cation diminishes the amount of electron flow by reducing the electron donating ability of the nitrogen atom in the crown. This effect is much more pronounced for cations of higher charge density such as Mg^{2+} and Ca^{2+} .

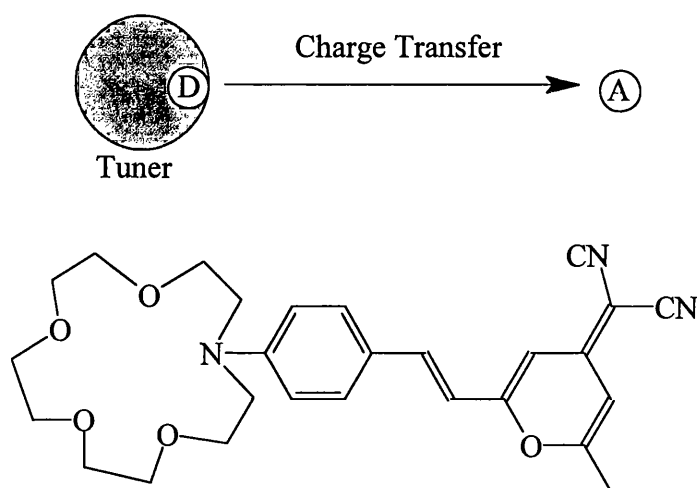


Figure 1.14: An example of a fluoroionophore.

There are further complications with this system, which are apparent from the slight changes in position and shape of the fluorescence maximum upon cation binding. It was found that fluorescence lifetime is unaffected by cation binding and that fluorescence quantum yield is decreased as expected - however there are large differences in the absorption spectra between the free and complexed sensor. An explanation for these observations may be that photo-ejection of the cation is occurring: upon charge transfer from the nitrogen atom to the acceptor, this atom is rendered positively polarised and thus it repels the cation which is bound within the azo - crown. This feature may prove to be a useful molecular device, as the system can function as a light driven cation pump.

1.6 [2]Catenanes and Their Role as Supramolecular Devices

Because of the unique structural features of catenanes (and rotaxanes) research into these molecules as supramolecular devices is growing¹¹. There are a wide variety of approaches to the synthesis of catenanes, ranging from purely statistical reactions to more complicated directed and templated reactions. The method of construction of a catenane and the functions it performs are, of course, directly related to the components that make up the supermolecule and how they assemble. In the recent literature it is possible to find an incredibly diverse sweep of functional components that have been incorporated into catenane systems - for example: fullerenes; cyclodextrins; charged or neutral aromatic electron acceptors such as the paraquat dication, the dication of diazapyrene and the diimine of pyromellitic anhydride; aromatic electron donors often based on naphthoxy and phenoxy derivatives or tetrathiafulvalene residues; chelating units such as 1,10 - phenanthroline and 2,2' - bipyridine; peptides; electron donating and accepting porphyrins; intrinsically chiral units such as bi-naphthol and hydrobenzoin residues; a variety of heterocycles such as thiophene, pyridine and furan; metallomacrocycles and organometallic units; photoswitchable azobenzene - based moieties and isophthaloyl fragments cyclised using ether, amide or sulphonamide linkages. When surveying such a diverse field it is convenient to classify catenanes according to their method of construction and to review the properties of related systems concurrently.

Before beginning such a review, however, it is helpful to consider the origins and historical background of catenane chemistry²³. A catenane is composed of interlocked rings, the most simple case being the [2]catenanes (the number in parentheses referring to the number of rings locked together in the system). Catenanes are topological isomers of the rings from which they are constructed but they possess different chemical and topological properties from their constituent parts. [2]Catenanes are not normally chiral, however it is possible to introduce chirality into catenane systems by introducing directionality into the rings of the catenane (e.g. Vögtle and co-workers introduced topological chirality into an isophthaloyl based system by using asymmetric linker units²⁴ - three amide and one sulphonamide, as shown in figure 1.15).

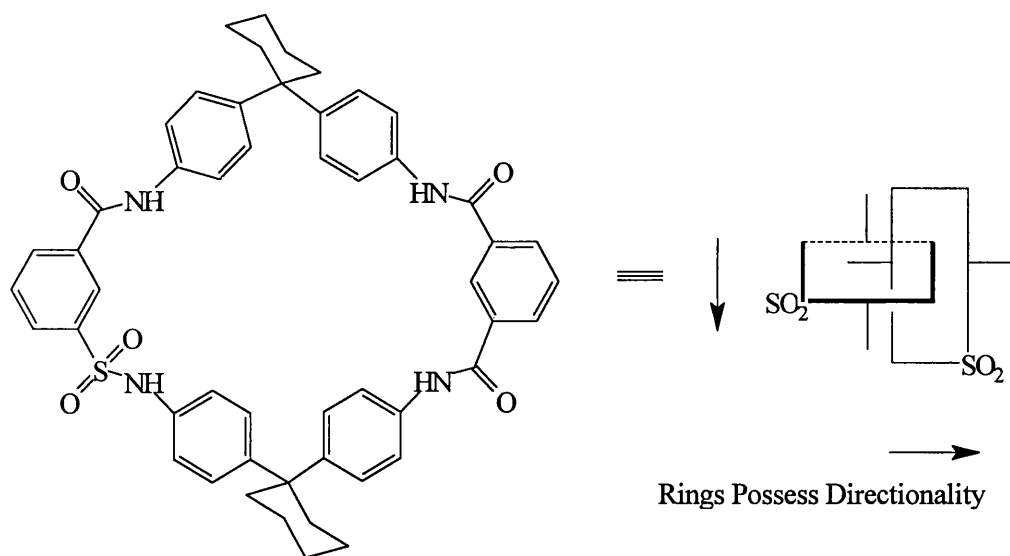


Figure 1.15: A chiral [2]catenane - rings with a sense of direction.

It is also possible to introduce chirality into catenated systems by introducing chiral axes (e.g. Stoddart and co-workers added bi-naphthol derivatives²⁵ to one cyclophane component of a [2]catenane, see figure 1.16) or by creating a chiral plane in the catenane (e.g. naphthyl - paraquat based cyclophane constructed by Stoddart and co-workers,²⁶ figure 1.17).

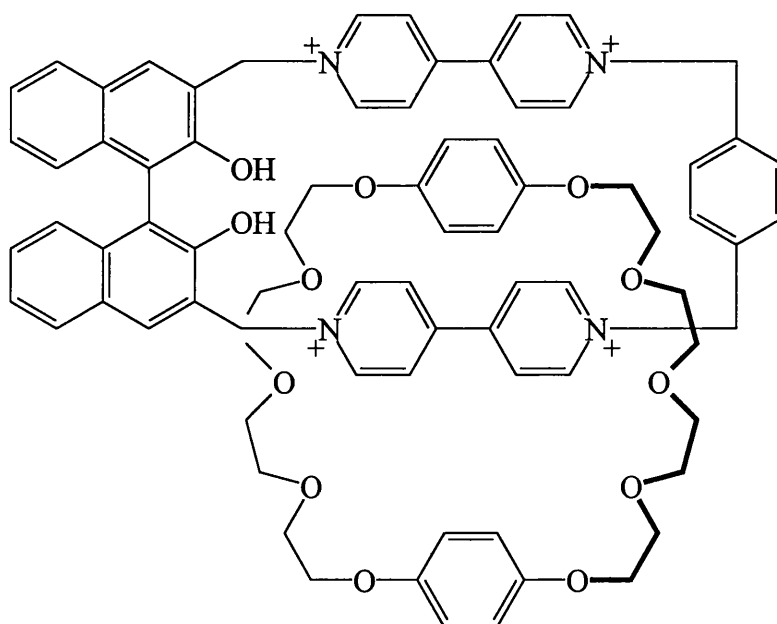


Figure 1.16: A [2]catenane with a chiral axis.

Separation of the topological enantiomers produced in the above systems is unusual - however they may sometimes be resolved by chiral shift reagents in NMR experiments.

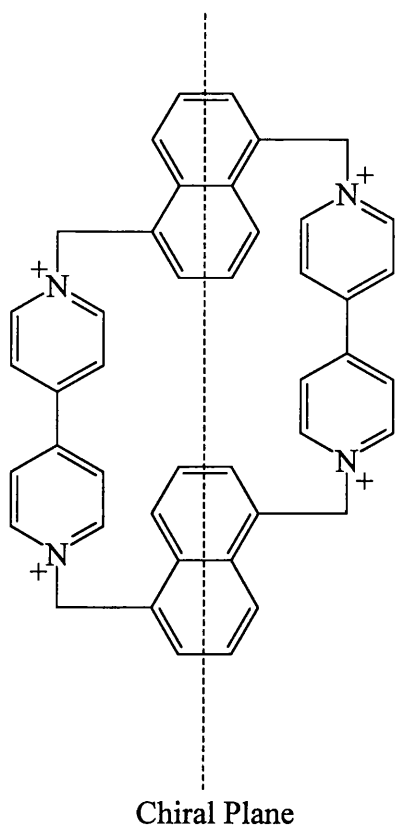


Figure 1.17: Acceptor cyclophane residue with a chiral plane.

In addition to chiral [2]catenane systems, bis - [2]catenane systems with chiral planes have been synthesised by Stoddart and co-workers²⁷, as shown in figure 1.18. The bis - catenane exhibits averaged D_2 symmetry (averaged due to rapid rotations and migrations of the crown ether molecules in the catenane).

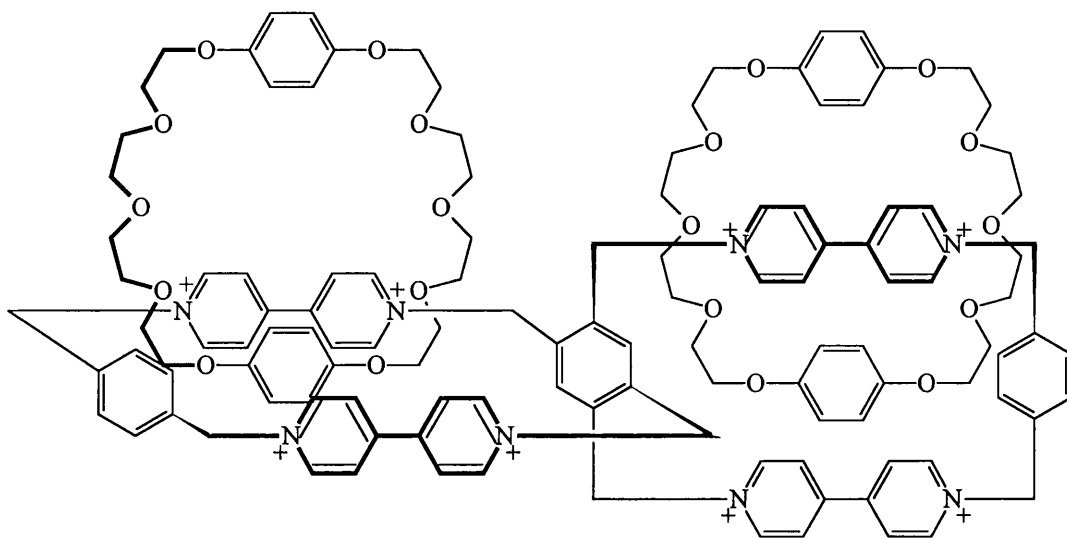


Figure 1.18: A bis - [2]catenane with a chiral plane.

In biological systems a large variety of topological isomers have been identified. DNA, both single and double stranded, forms a number superstructures

which have been implicated in the replication of genomes. These superstructures occur where the central axis of the DNA double helix has been bent, twisted or knotted into various forms of tertiary structure. A particularly relevant example is given by duplex circular DNA, which is made up of two complete, closed rings which forms superstructures when linked together such as supercoils, catenanes and knots.²³ These features may be replicated using synthetic DNA in conjunction with solid supports to construct novel superstructures as has been reported by Seeman and co-workers.²⁸ DNA superstructures are defined by a ‘linking number’ - the algebraic sum of the number of supercoils and the number of helical turns in the duplex. The linking number is independent of any distortions that may occur in the molecule but it may be altered by enzymes known as topoisomerases which operate by breaking DNA chains.

DNA is clearly a special case in that it contains a double stranded cycle - the term ‘linking number’ is not appropriate to more simple systems. As an alternative, the term ‘crossing number’ has been employed, which is defined as being the minimum number of crossing points in a two dimensional representation of the supramolecular system in question (figure 1.19).

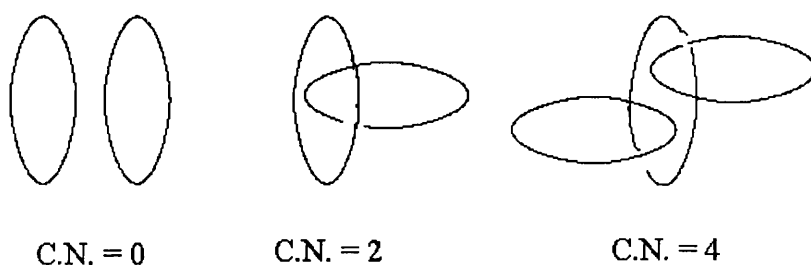


Figure 1.19: Definition of crossing number.

Systems with interlocked rings have been known to exist for sometime - they were discussed as early as 1912 by Willstätter, however it was only until the 1960’s that Frisch and Wasserman described the routes by which catenanes may conceivably be synthesised.²⁹ “the formation of interlocking rings may be accomplished by the statistical threading of one ring by a linear molecule which is to be formed into the second ring”. This approach assumes that the first ring is large enough to adopt a conformation that provides a cavity large enough for the linear molecule to thread through. A further approach identified by Frisch and Wasserman was noted: “alternatively, the two rings may be constructed about a central core, a

procedure that should give rise to much higher yields of interlocked rings". More recent approaches to catenane synthesis involve the Möbius strip approach, which may be considered as a compromise between statistical threading and a directed synthesis, and the template approach - by far the most common method for synthesising catenanes in the recent literature.

1.6.1 Catenanes from Statistical Threading

The concept behind this method of catenane construction is very simple: a molecular thread which is functionalised at both ends is passed through a cyclic molecule and subsequently cyclised to yield a catenane. Since the probability that the cyclisation reaction will occur whilst the linear molecule is threaded through the macrocycle is low, this synthetic strategy does not produce high yields of catenane products.

The first synthetic catenane was, however, produced by this type of strategy by Wasserman in 1960, although the pure compound could not be isolated. Despite the obvious drawbacks, the fact that this strategy produced a catenane gave credence to the statements of Frisch and Wasserman regarding the syntheses of catenanes. It should be noted that this approach does not consider any recognition process between the cyclic and linear molecules - often these compounds contain little or no functionality, although the presence of van der Waals interactions between two hydrocarbon rings have been noted by Schill and co-workers.³⁰

The limiting factor of statistical syntheses is, therefore, the random nature of the reaction - however this may be overcome by introducing associative interactions between the component molecules (a template process). This approach was first considered by Lüttringhaus and co-workers in 1958, and involved the production of a rotaxane - like inclusion compound between hydrophobic α - or β -cyclodextrin and aromatic long chain dithiols.³¹ This attempt did not lead to the production of a [2]catenane structure (this was achieved in 1993 by Stoddart and co-workers³² using β -cyclodextrin, with a diphenyl derivative as substrate - cyclisation was effected by way of amide linkages - see figure 1.20), however it illustrated a means by which high yields of catenane structures may be obtained.

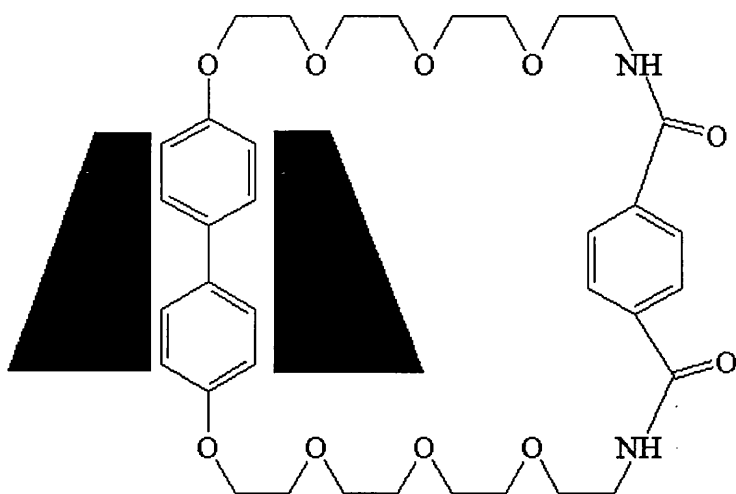


Figure 1.20: A cyclodextrin containing catenane.

1.6.2 Directed Catenane Synthesis

The synthetic route most commonly identified with this strategy was devised by Schill and Lüttringhaus.³³ It involves a multi - step synthesis which begins from a rigid aromatic core - the key to this procedure in that it imposes intramolecular cyclisation leading to a catenated product. The strategy involves a cyclisation which produces a cyclophane precursor which has functional groups maintained in fixed positions. A second directed cyclisation then occurs to produce two interlocked rings which are tethered to an aromatic core. Cleavage of the covalent links between the core and one of the rings leads to the production of a true [2]catenane.

Because of the large number of steps involved, however, this type of synthesis is not commonly employed in the large scale preparation of [2]catenanes. An example of this strategy, however is the synthesis of a [2]-[cyclohexatetraoctane] [cyclooctacosane] catenane by Schill²³ and co-workers is given in figure 1.21.

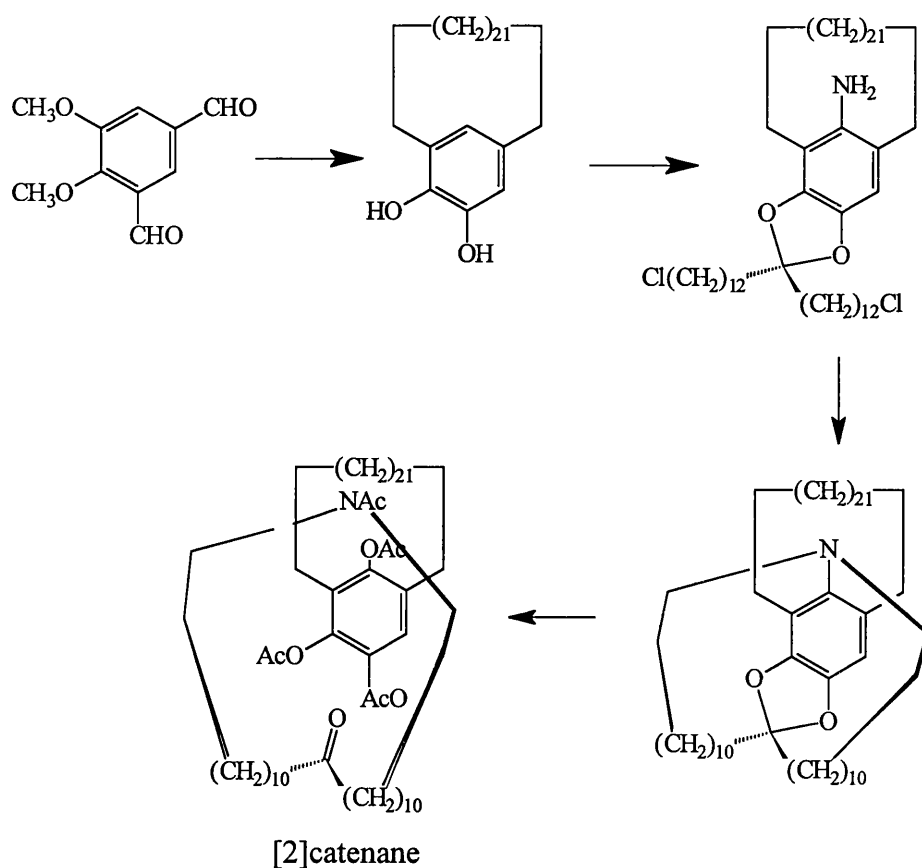


Figure 1.21: A catenane produced by a directed synthesis.

1.6.3 Catenanes from Möbius Strips

This approach, initially considered by Wasserman and Schill^{29,34} and more recently by Walba³⁵ is based on ladder shaped molecules (figure 1.22), or on the overlapping, labile metallomacrocycles of Fujita and Ogura³⁶, (see figure 1.23).

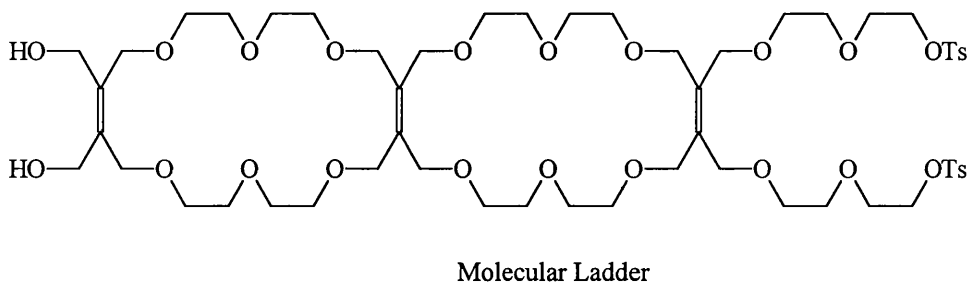


Figure 1.22: A möbius strip precursor constructed by Walba *et al.*

For this mechanism of catenane synthesis to work, the ends of the ladder shaped molecule must have the ability to twist so that a möbius strip is produced. The number of twists determines the product that is isolated after the vertical 'rungs' are removed. Zero twists leads to the production of two separate cyclic molecules,

one twist leads to a large macrocycle (the sum of the two smaller cycles joined end to end) whereas two twists results in the creation of a [2]catenane.

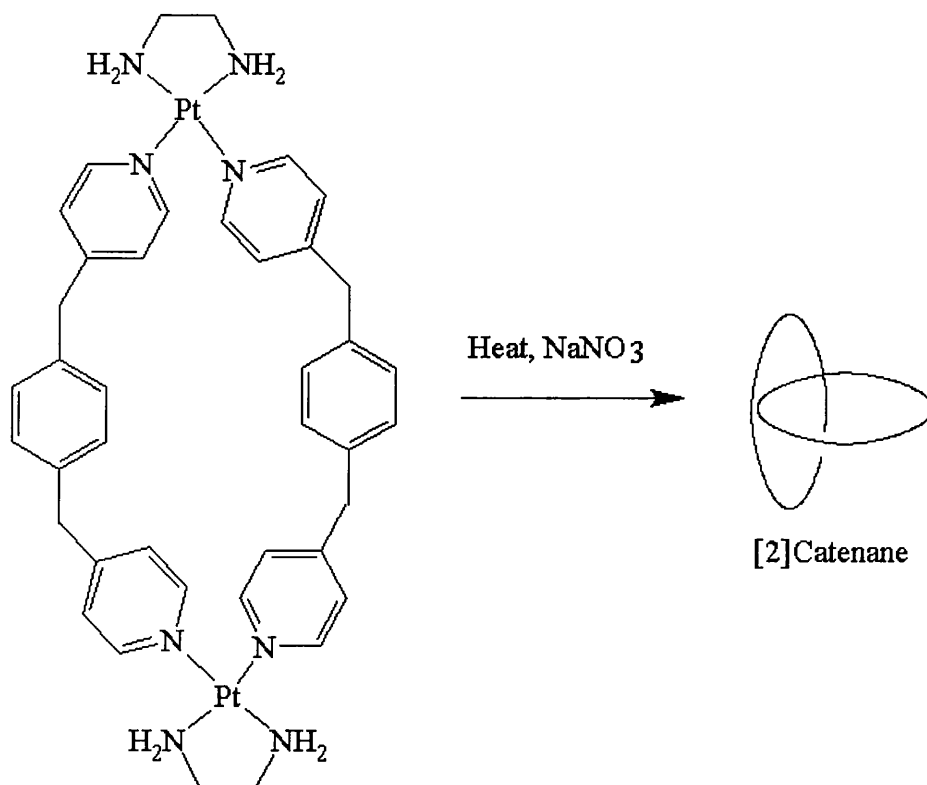


Figure 1.23: Fujita and Ogura's catenating metallomacrocycle.

The system reported by Fujita and Ogura³⁶ assembles by a similar route in that the number of twists is determined by the dissociation and subsequent reformation of platinum - pyridine bonds after intertwining of the ligands has occurred (the driving force being hydrophobic interactions and edge to face aromatic contacts).

Related reactions based upon metathesis of macrocyclic polyolefins³⁷ are also random - the key step is an intramolecular metathesis reaction which takes place in a large flexible polyolefinic rings after a degree of twisting has occurred. The yield of catenane produced by this method is very small.

These approaches are similar to a statistical threading reaction in that they have a random nature - the number of twists achieved prior to cyclisation determines the outcome. Given this limitation, the Möbius strip mechanism is not widely used to synthesise [2]catenane structures.

1.6.4 Catenanes from Transition Metal Templates

Due to their ability to arrange ligands around themselves in predictable geometries, transition metals have been used as templates for a number of years in a variety of systems. The use of transition metals as templates is well documented - the central concept may be stated as follows:³⁸ when organic residues form a complex with a transition metal, nucleophilic attack is often facilitated and electrophilic attack is retarded by the charge on the cationic metal centre. When this is combined with the stereochemical requirements on the ligand imposed by the metal, reactions which may not have been entropically favourable become so in the coordination sphere of the metal. Thus, the metal acts as a template for the synthesis³⁹ of, for example, macrocyclic compounds which would otherwise be synthesised in low yield. Early examples of this type of synthesis are: Reppe's cyclooctatetraene synthesis, where four acetylenic compounds assemble around a nickel ion; the templated synthesis of metallophthalocyanins, and the synthesis of the 'classic' templated Schiff base tetradentate macrocycles (figure 1.24) as first obtained and characterised by Curtis in 1961.⁴⁰

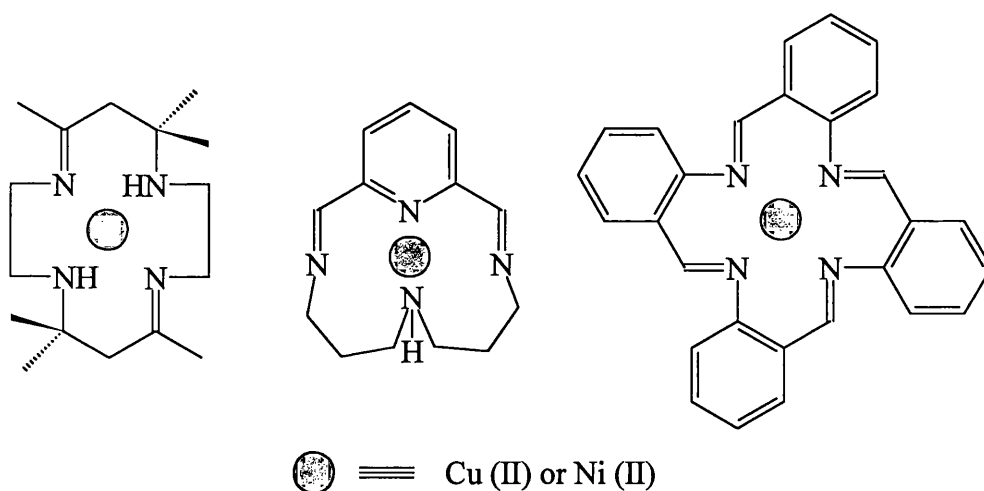


Figure 1.24: Early templated Schiff base macrocycles.

It may be noted that the syntheses described above are largely two dimensional - they involve the synthesis of single macrocycles. Examples of three dimensional templates based on transition metals are, however less common. Examples of such a strategy are the synthesis of cobalt sepulchrate by Sargeson,⁴¹ as well as by a number of encapsulating clathrate - type molecules.

The use of transition metals to build three dimensional molecular structures is thus possible, and indeed this approach has been exploited by Sauvage and co-

workers to construct interlocked rings.²³ It was recognised by Sauvage that to synthesise catenated structures using transition metals as templates, it is necessary to set ligands around the metal such that reactive groups are available for cyclisation at a later stage in the reaction. Two possible strategies to achieve catenane formation from a metal template were identified: (1) bring two acyclic ligands together and cyclise both together, or (2) form a complex between one acyclic and one cyclic molecule and subsequently cyclise the former to produce a catenane (figure 1.25).

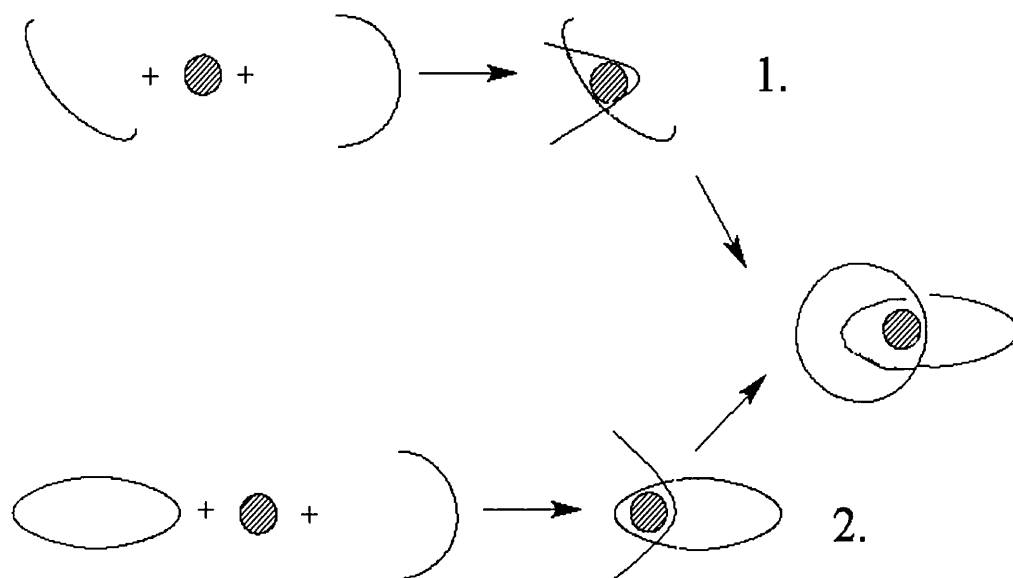


Figure 1.25: Two possible strategies to metal templated catenanes.

The first strategy is rather straightforward but as a total of four connections are required, it was found to be, as expected, lower yielding than the second strategy. The second strategy is more sophisticated, in that it requires the synthesis of a macrocycle prior to complexation with the acyclic unit and therefore the final cyclisation step requires only two connections to be made. On a statistical basis this reaction must produce a higher yield than the first route. The advantage of this method is also its main drawback however, as the synthesis of the cyclic molecule may not be trivial. The second strategy was also employed by Sauvage, and did indeed give improved yields of catenane product in the final step, however the complexity of this route ruled against it being used except in the case where catenanes containing mixed (different in terms of functionality, size etc.) rings were being synthesised.

The initial chelating unit chosen by Sauvage was based on 2,9 - disubstituted - 1,10 - phenanthroline (in particular the di-anisyl derivative) which was known to form stable pseudotetrahedral complexes in which the two ligands encapsulate the metallic centre.²³ Copper (I) complexes display this geometry, thus they were chosen as ideal building blocks for the templated synthesis of catenanes: the first compound produced by this procedure⁴² (named catenates to reflect their ligating nature) is shown in figure 1.26. Note that ring closure was effected by use of polyether linkages.

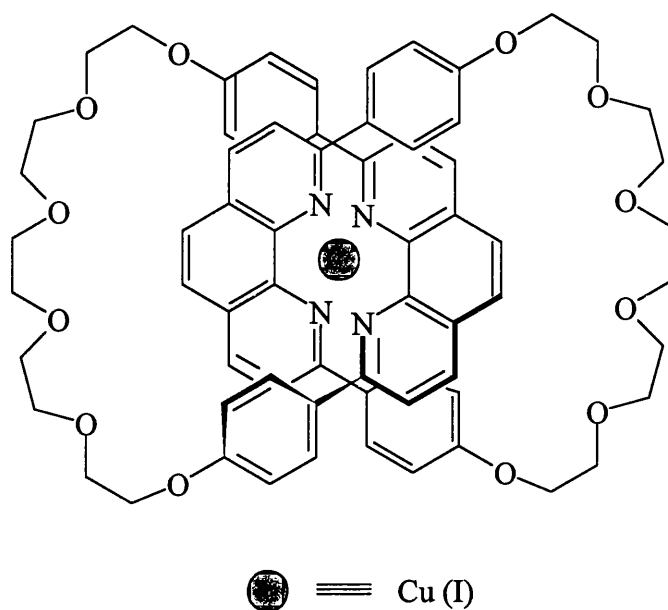


Figure 1.26: The first [2]catenate.

The metal template may be removed by use of a cyanide extraction, yielding the free ligand (named a catenand) which has a quite different geometry to the corresponding complexed compound. The chelating phenanthroline units rotate so as to be as far apart as possible upon de-complexation (unless they are prevented from doing so by the addition of 'locking' groups which hinder passing of one ring through the other)⁴³ - however this effect is reversible upon addition a metal cation. Catenands have a diverse coordination chemistry; a variety of metals in variable oxidation states (low oxidation states are stabilised by the encapsulating ligands) may be complexed by the ligands, in addition catenate complexes have been noted to display an unusual kinetic inertness towards de-complexation.²³

Since the first catenates and catenands were identified, a large number of developments have occurred, such as the development of a doubly - interlocked

catenated structures⁴⁴ (see figure 1.27). These structures represent the next level up in the complexity of [2]catenanes. Doubly - interlocked [2]catenanes are interesting because unlike simple [2]catenanes they are always chiral and in addition, due to the tightness of the structure, the constituent cyclophanes glide through each other at a much slower rate than their more simple isomers.

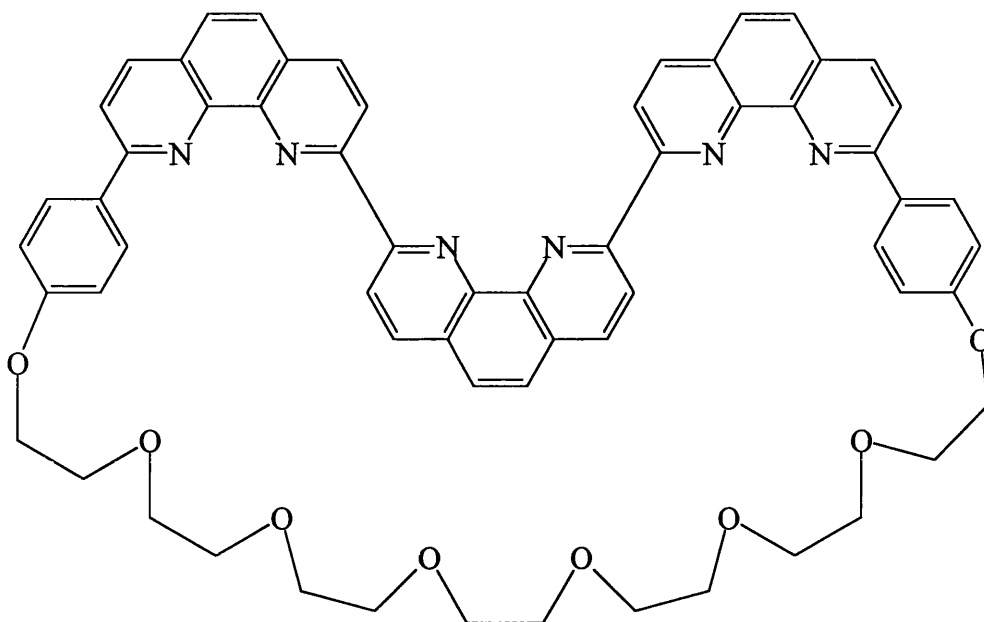


Figure 1.27: Component cyclophane of a doubly - interlocked [2]catenate.

By changing the residues with which the final cyclisation is carried out so that they contain additional functional groups, a diverse range of chemical and physical properties may be incorporated into the basic [2]catenate structure. For example by use of a multidentate ligand containing two terminal terpyridyl units along with the standard phenanthroline chelator (figure 1.27), an interlocked structure may be constructed⁴⁵ which consists of a central (templating) copper (I) phenanthroline complex and two ruthenium (II) terpyridyl complexes which act as linker units - effecting ring closure thus producing the interlocked system. It has also proved possible to assemble one metallomacrocyclic with a ruthenium terpyridyl complex, add it to a copper atom and a second multidentate ligand and ring close with a third metal ion thus producing a hetero-trimetallic system incorporating interlocked rings.

A particularly interesting example with regard to the operation of interlocked systems as molecular devices is the case of a [2]catenate which demonstrates redox

control of the ring gliding motion within its copper (I) complex. This was achieved by combining both ditopic phenanthroline and tritopic terpyridyl chelating units on the same cyclophane (c.f. the molecular shuttle presented in figure 1.11) and synthesising a [2]catenate structure with copper (I) in the usual way.⁴⁶ Upon oxidation of the metal centre to copper (II), the preferred geometry is changed from tetrahedral to octahedral - a change that can be accommodated (reversibly) by rotation of the rings (one at a time) so that the metal becomes chelated by the tritopic terpyridyl chelators, thus allowing octahedral geometry.

The central part of the above catenates may also be used to construct donor - acceptor porphyrin arrays⁴⁷ where the usual ring closure step to produce the interlocked system is performed using heterometallic porphyrin derivatives thus creating the system depicted in cartoon form in figure 1.29. Initial indications were that this system may indeed perform as a model for the photosynthetic reaction centre 'special pair' of porphyrins.

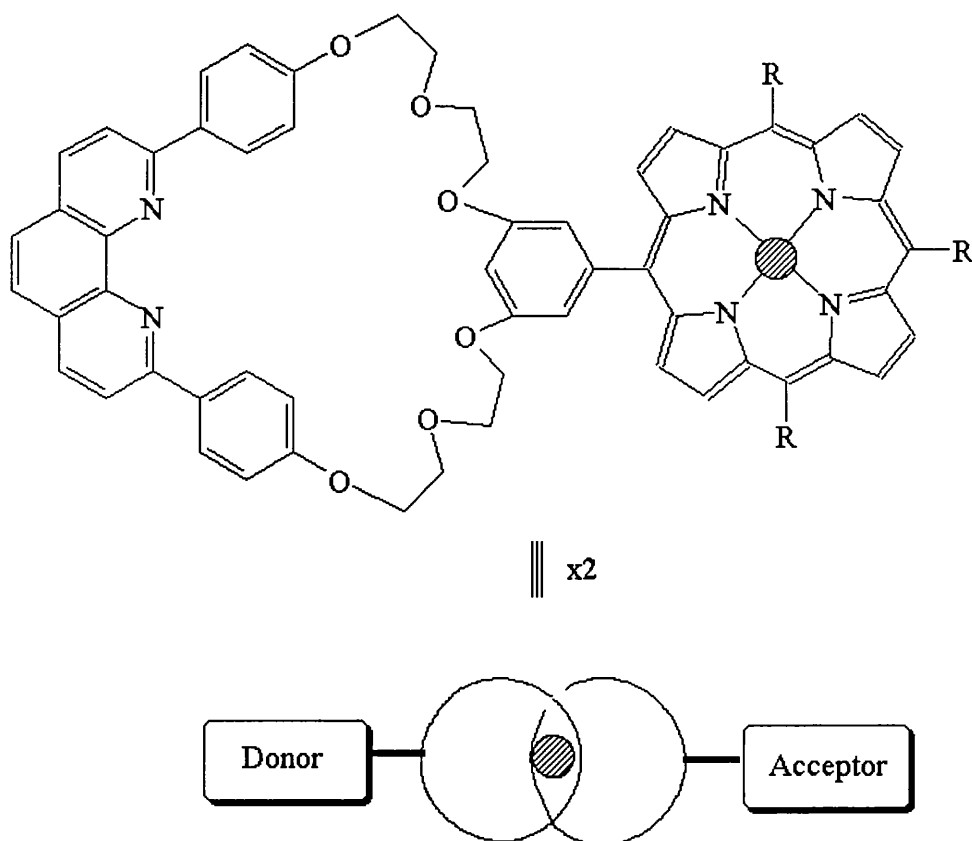


Figure 1.28: Catenates as linker units in porphyrin arrays.

As a further example of the versatility of the catenate system described here, a number of groups have recently included derivatives of the basic catenate system in polymeric arrays. Such systems are of interest because of their potential rheological and mechanical properties. [2]Catenates have been derivatised with amines⁴⁸ (for inclusion in polyamides), cyclised as part of poly(ethylenamine) polymers⁴⁹ and copolymerised with rigid blocks as part of polyester macromolecules.⁵⁰

A link is provided between catenanes assembled by use of metal templates and those assembled *via* $\pi - \pi$ interactions by the system depicted in figure 1.30.

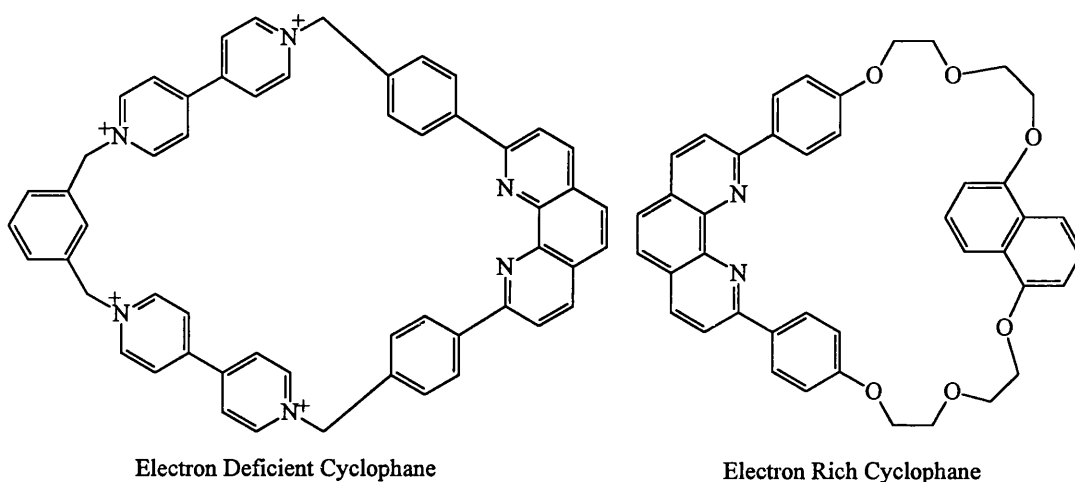


Figure 1.29: Components of a ‘switchable’ bi-modal [2]catenate structure.

This system has been described as a hybrid [2]catenane,⁵¹ as it contains both cation chelating units (which were used to assemble the system) and π - electron rich and π - electron poor aromatic units suitable for the formation of donor - acceptor complexes. It is possible to convert (or ‘switch’) between these two modes by adding or removing the metal cation. The switching process may be easily followed by absorption spectroscopy *via* the appearance (on deprotonation) or disappearance (on protonation) of a charge transfer band that results from interaction of the aromatic donor - acceptor pair.

1.6.5 Catenanes Templated by $\pi - \pi$ Interactions

Non - covalent interactions between aromatic molecules have become very important in the synthesis and in determining the properties of supramolecular assemblies.⁵² They control a number of molecular recognition and self - assembly

events such as: the packing of aromatic compounds in the solid state; template directed syntheses; molecular recognition of hosts by synthetic (and natural) guests as well as a multitude of examples in biology such as base pair stacking in DNA and control of the three dimensional structure of proteins. The term $\pi - \pi$ interaction is defined as being a non - covalent interaction between delocalised π - systems including interactions between aromatic molecules. Such interactions involve the interplay of several different effects which can be categorised as follows:

- (1) van der Waals interactions which are the sum of the dispersive and repulsive interactions between the interacting molecules.
- (2) Electrostatic interactions between static molecular charge distributions.
- (3) Induction energy, which is the interaction between the static molecular charge distribution of one molecule and the proximity induced change in the charge distribution of the other.
- (4) Charge transfer, which is the stabilization of a complex due to mixing of the ground state with the charge separated excited state.
- (5) Desolvation, whereby the interacting molecules must be desolvated prior to complexation. The complex may be stabilised or destabilised by the solvent depending on polarity and solvophobic effects.

In the current literature there are two approaches towards describing the interactions between aromatic systems: the first, favoured by Hunter,⁵³ ascribes the attractive interactions between aromatic molecules primarily to electrostatic interactions (although solvent effects are also recognised as being important) between the negatively charged π - orbitals of the first molecule and the positively charged σ - framework of the second molecule (figure 1.30).

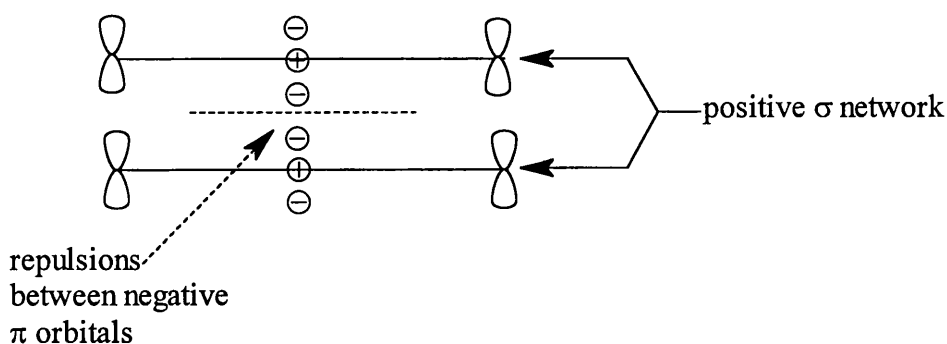


Figure 1.30: Electrostatic model of face to face $\pi - \pi$ interactions.

This model for arene - arene interactions predicts, therefore, that if no other factors are in operation, the strongest complex will be formed where the $\pi - \pi$ interactions are minimised - i.e. between two electron poor aromatics.

In contrast, the second model, favoured by Stoddart,⁵⁴ ascribes the attractive interactions between π - electron rich and complementary π - electron poor aromatic molecules to the formation of an electron donor acceptor (EDA) complex, as evidenced by the production of a charge transfer (CT) band in the absorption spectrum. The CT band arises from an electronic transition within molecular orbitals formed by direct overlap of appropriate HOMO - LUMO π - orbitals of the two interacting aromatics.⁵⁵ In addition to this effect, the strong binding noted in a number of such systems (see below) is attributed to C-H... π edge to face interactions⁵⁶ allied to electrostatic and hydrogen bonding interactions between polyether chains and charged π - electron poor aromatics.⁵⁷

It is likely that the first model is generally correct for most aromatic - aromatic interactions but other factors such as those described in the second model may become more important in specific instances. With this in mind, the supramolecular systems described below will be described largely in terms of the EDA model.

The discovery by Stoddart that an aromatic crown ether based on a hydroquinone derivative could form a 1:1 inclusion complex with the paraquat dication in both solution and the solid state led to a prolific field of supramolecular research based on the associative interactions between aromatic electron donors and their complementary aromatic electron acceptors (EDA complexes).⁵⁸ Initially, inclusion compounds and a [2]catenane (figure 1.31) were constructed - the solid state structure of the catenane demonstrated the existence of non-covalent electrostatic and dispersive interactions that are associated with sandwiching parallel layers of hydroquinol derivatives with paraquat dicationic derivatives (in the form of a tetracationic cyclophane), leading to a continuous π - stack along one crystallographic axis. The efficient synthesis of the [2]catenane was attributed to a template effect between the partially formed acceptor cyclophane and the donor crown ether - a fact that distinguished this system from previously synthesised organic catenanes.

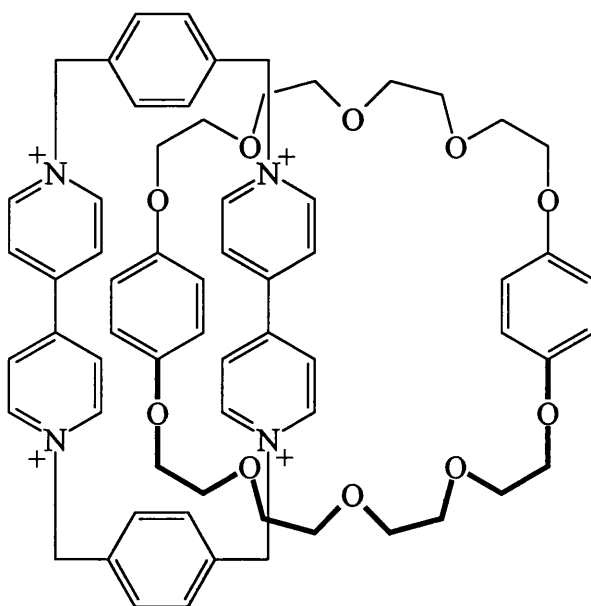


Figure 1.31: The first EDA [2]catenane.

In addition to the yield enhancing template effect, the methodology pioneered by Stoddart was easily accessible as ring closures to produce catenated structures involved simple nucleophilic substitutions. This accessibility has led to a wide proliferation in systems which are based on this synthetic route - figure 1.32 provides a glimpse of a selection of 'building blocks' that have been incorporated into the macrocyclic donor or acceptor components of these catenated systems.^{54(c)}

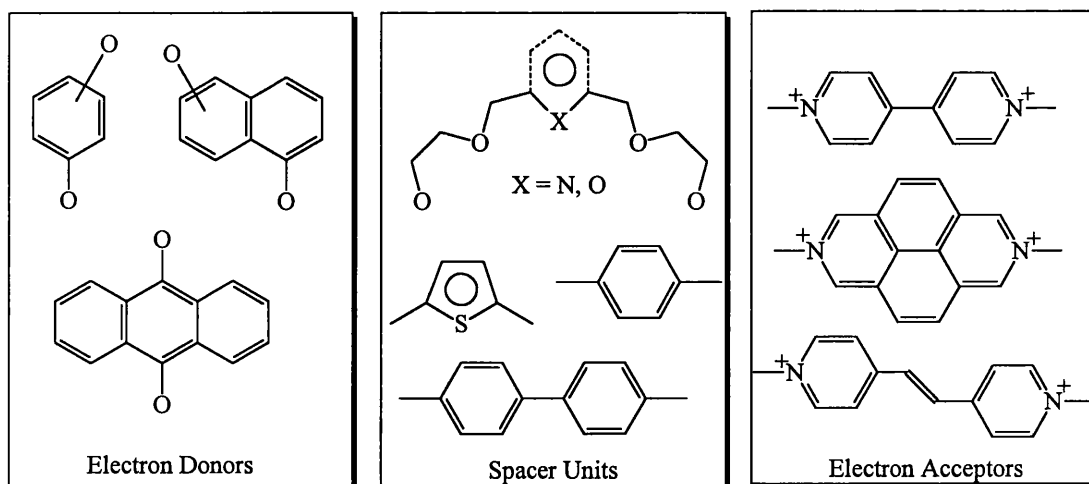


Figure 1.32: Stoddart's 'molecular meccano' toolbox.

Clearly, it is not practicable to describe every development in this field since its inception nearly ten years ago (in any case a number of reviews are available for this purpose). Rather, a selection of examples which have a bearing on the research presented in this thesis will be detailed.

Since the development of the first EDA [2]catenane, a great deal of effort has been devoted to producing [n]catenanes⁵⁹ (polycatenanes) due to the promise they hold as materials with interesting properties. A number of [3]catenanes have been synthesised, however, higher catenanes have proved somewhat more difficult to synthesise. A recent paper by Stoddart and co-workers has demonstrated that the same procedure used to produce the first [2]catenane may be extended to produce [5]- (olympiadane), [6]- and [7]catenanes by use of appropriate components (figure 1.33).

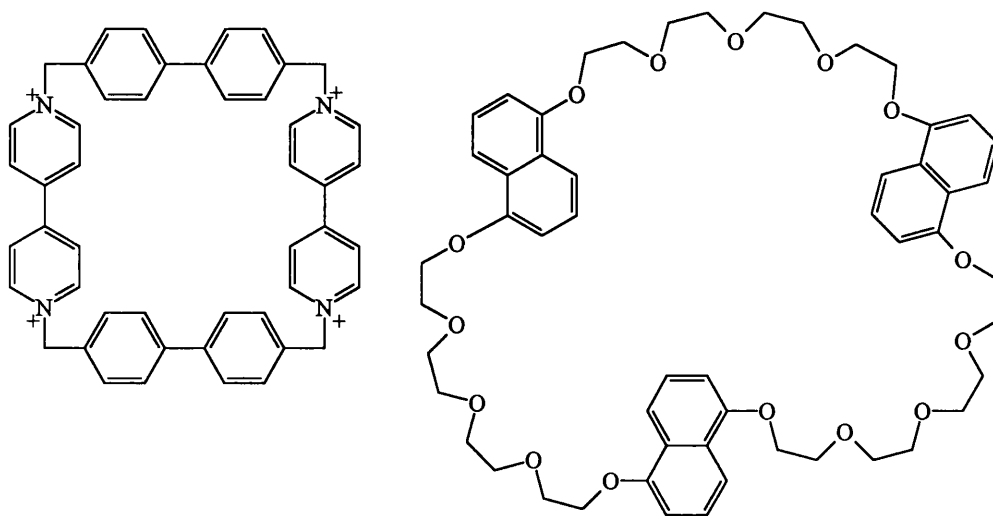


Figure 1.33: Components of [n]catenanes.

An alternative approach to producing catenane containing polymeric materials is to co-polymerise functionalised [2]catenanes with complementary monomers (to date no pure polycatenane has been produced). This is achieved by placing functional groups such as carboxylic or hydroxyl groups on each of the macrocyclic rings of the [2]catenane and carrying out a step - growth polymerisation reaction. Using this method, a bis - hydroxyl [2]catenane derivative has successfully been polymerised with bis(4 - isocyanatophenyl)methane to produce a polyurethane⁶⁰ of number average molecular weight $M_n = 26.5 \text{ kg mol}^{-1}$.

Moving on from the mechanical properties of catenanes to their photophysical and electrochemical properties, some examples of catenane structures which may be of use as molecular devices are given in the next few paragraphs. Gokel, Kaifer and co-workers have synthesised a catenated system based on the original EDA catenane (c.f. figure 1.31) which is attached *via* thio bridges to a gold electrode surface.⁶¹ The aim of this work was to use self - assembly to create

catenane structures on a gold surface, thus controlling the molecular organisation at the electrode - solution interface.

The inclusion of porphyrins in catenate structures has been discussed previously (c.f. figure 1.28), however using porphyrins as components in one of the macrocyclic rings to produce novel catenated species has not been discussed. Gunter and co-workers have constructed both inclusion complexes and [2]catenanes using porphyrins straddled with hydroquinol - polyether chains.⁶² Tetracationic acceptor cyclophane may be clipped onto the hydroquinol chain thus producing catenane structures which have an acceptor paraquat group held in close proximity to an electron donating porphyrin unit. Porphyrins are well known for their photophysical and redox properties and it has been shown that there is electron transfer from the zinc - porphyrin to the proximal paraquat moiety.

A number of models for supramolecular devices based on systems containing $\pi - \pi$ EDA interactions have been constructed, some of the most interesting being those that are 'photoswitchable' - examples being the azobenzene based systems produced by Vögtle and co-workers⁶³ and Stoddart's vinyl - viologen systems⁶⁴ (figure 1.34).

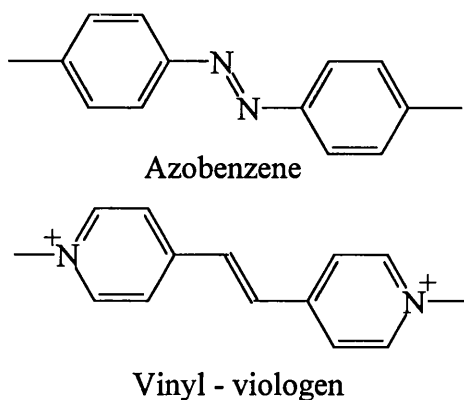


Figure 1.34: Photoswitchable catenane components.

The azobenzene containing [2]catenanes are isomerised upon irradiation with UV light, leading to a 40:60 *Z* to *E* ratio. Production of the *Z* isomer brings the paraquat units closer together and so restricts rotation of the crown ether around the acceptor unit. In contrast, however, the vinyl - viologen derivatised [2]catenanes are not photoswitchable - instead of isomerising the vinyl unit, irradiation simply produces light induced electron transfer in the charge transfer complex. The

counterpart non - catenated cyclophane analogue does, however, demonstrate the expected isomerisation.

The systems described above have all been based on charged (e.g. dicationic) electron accepting units and dioxyarene - based polyether donor units. Becher and co-workers have, however, pioneered the incorporation of tetrathiafulvalene (TTF) in macrocyclic arrays⁶⁵ (figure 1.35) which may then function as donors in EDA complexes, [2]- and [3]catenanes and pseudocatenanes. In addition Sanders and co-workers have constructed intriguing neutral electron accepting units (including metallomacrocyclic components) based on pyromellitic anhydride diimide⁶⁶ (and its naphthyl derivative). Such units (figure 1.35) are of particular interest because they remove the need for electrostatic stabilization of a dicationic acceptor unit - thus enabling clearer investigation of the nature of the EDA interaction.

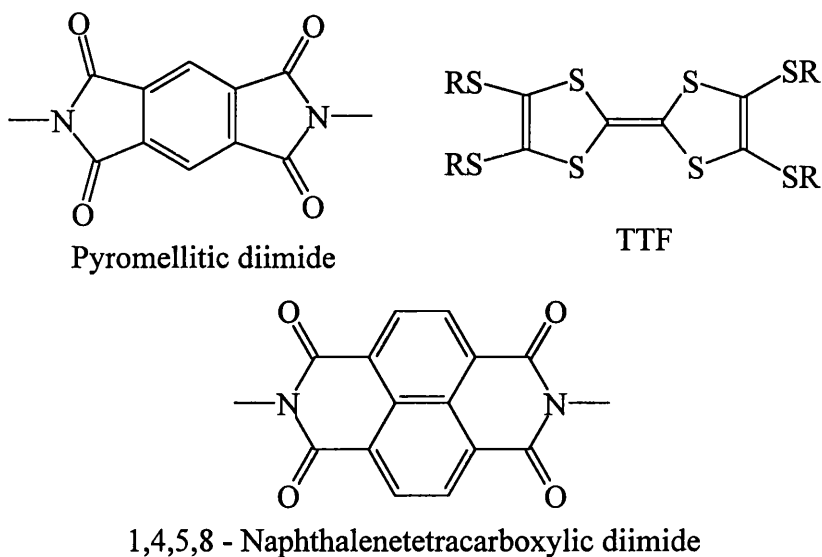


Figure 1.35: Novel components in EDA based [2]catenanes.

Very recently, Stoddart and co-workers have published the synthesis, some solid state structures and a limited investigation of some properties of a number of systems which were based on the cation chelating 4,4' - dimethyl - 2,2' - bipyridyl unit.⁶⁷ Such systems are also the focus of the research presented in this thesis. Curiously, in the above paper, compounds were generally synthesised in a manner which appears to be contrary to the aim of templated synthesis, as high dilution, high temperatures or high pressures were employed rather than ambient temperature and pressure methodologies. Perhaps even more curious is the fact that in a previous publication by the same group concerning the incorporation of directly analogous

3,3' - dimethyl - biphenyl units into EDA complexes and [2]catenanes²⁵ (figure 1.36) an entirely different (template) strategy was employed.

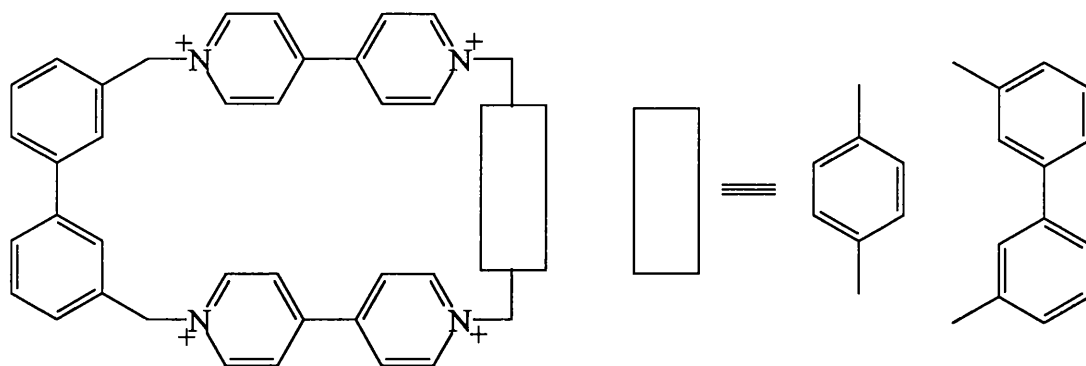


Figure 1.36: 3,3' - Dimethyl - biphenyl based components of EDA complexes and [2]catenanes.

Despite this apparent discrepancy, the synthesis of [2]catenanes and other supramolecular species may be very efficiently carried out by use of a combination of π - π interactions, electrostatic interactions and hydrogen bonding. Correspondingly, the next section deals with systems efficiently assembled using hydrogen bonding as the main driving force, with the support of a variety of arene - arene interactions.

1.6.6 Catenanes Templated by Hydrogen Bonding

Catenane structures which are templated by and incorporate hydrogen bonds as the main structure determining feature are somewhat less common than the those based on EDA interactions or transition metal templates. Indeed, examples of this type of structure in the literature have largely focussed on interlocked macrocyclic components based on amides or their analogues such as sulphonamides. The first amide based [2]catenanes were reported independently by Hunter⁶⁸ and Vögtle⁶⁹ in 1992 and were based on hindered anilide structures. The [2]catenane synthesised by Hunter was produced (in 34% yield) as a by-product in the synthesis of an artificial receptor for *p* - benzoquinone (figure 1.37).

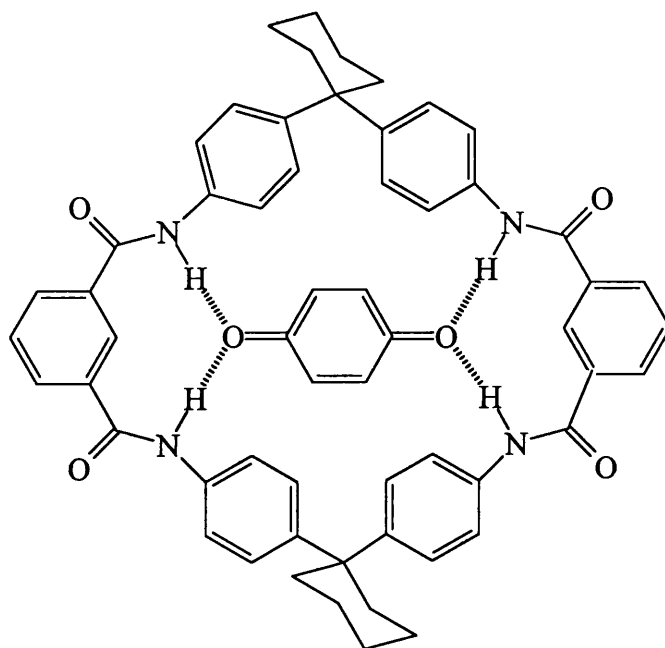


Figure 1.37: Artificial *p* - benzoquinone receptor.

Initially the catenane structure was elucidated by FAB mass spectrometry and by very elegant NMR experiments from which a number of hydrogen bonded interactions (and π - π interactions) were identified, the most important of these being the intermolecular H - bonding interactions between amide N-H and C=O groups. This was subsequently confirmed by X-ray crystallographic studies. In addition it was found that gliding of one ring through the other is prohibited, with the activation barrier being some 73 kJmol^{-1} - thus the catenane exists in two enantiomeric forms at room temperature.

The contemporary [2]catenane structure produced by Vögtle and co-workers was identical to that of Hunter except that it possessed a methoxy group on the

isophthaloyl unit - the aim was to synthesise 'basket' molecules by derivatising the expected macrocycle at these positions. Since this discovery, asymmetrically substituted catenanes have been synthesised by altering the substitution patterns and synthetic strategies employed.⁷⁰ Substituted [2]catenanes have also been used to produce oligomeric catenane arrays (degrees of polymerisation of up to 5) *via* copolymerisation with rigid co-monomers under Suzuki conditions.⁷⁰ However, attempts to exchange furan or pyridine units for isophthaloyl units have generally proved to be difficult or impossible.⁷¹ Exchange of amide groups for sulphonamide groups allows for the production of rings with a 'sense of direction', as previously discussed (c.f. figure 1.15), and in addition, such linkages may be used to produce 'pretzel' shaped molecules.⁷⁰ This is made possible by employing the enhanced acidity of sulphonamide protons with respect to analogous amide protons - selective deprotonation followed by alkylation with bi-functional iodoalkanes of a suitable chain length results in production of the desired compound (figure 1.38).

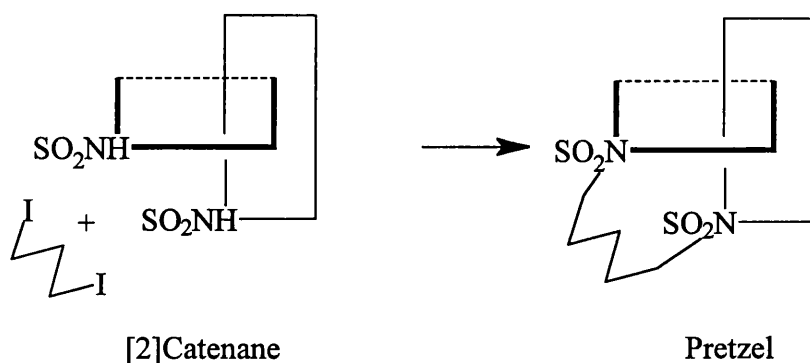


Figure 1.38: Synthesis of pretzel - type molecules from [2]catenanes.

The systems described above suffer from the problem that the catenane assembly process is not tolerant to simple modifications to the precursors. In addition it is not always particularly desirable that rotation of one ring about the other be prevented. The [2]catenanes reported by Leigh and co-workers, conversely, are readily accessible, easily functionalised and possess the conformational and dynamic properties expected of interlocked systems.

The first such system⁷² was identified in 1995, and was formed by a serendipitous side - reaction in the synthesis of a molecular receptor for carbon dioxide (figure 1.39). The synthetic route to this catenane has proved to be quite general, with a number of derivatives having been reported to date.⁷³ The yields of catenated species are independent of functional variation in the reactants, however

variations in dynamic and structural properties have been noted. More specifically, substitution of the isophthaloyl unit prevents complete circumrotation of one cyclophane through the other - thereby locking the two sides of each macrocycle in different chemical environments (so lowering the symmetry of the system).

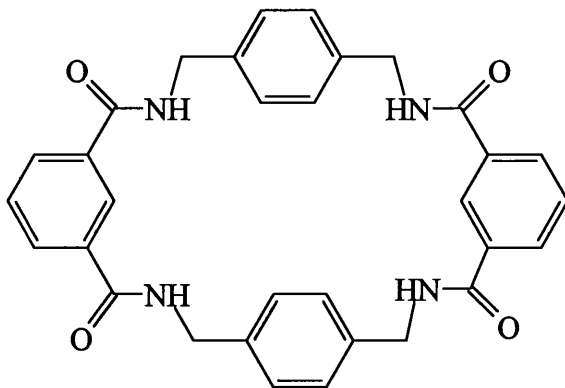


Figure 1.39: One macrocyclic component of Leigh's [2]catenane.

Recent developments in this field have centred on the templated assembly of benzylic amide cyclophanes around peptides to produce template rotaxanes. Such systems have been shown to demonstrate strong solvent effects which may be exploited to produce molecular shuttle devices.⁷⁴

1.7 Properties of Supramolecules and Supramolecular Assemblies

The range of properties displayed by supramolecular systems are numerous and diverse as has been described previously. The properties that are of particular interest in this body of work are those that relate to photoinduced electron transfer, electrochemistry and molecular recognition, host - guest interactions. The latter property has been discussed at length above but the former properties merit further discussion particularly in relation to ruthenium(II) tris-bipyridyl and methyl viologen subunits as these are the parts of the molecular architecture which are deemed photo- and/or redoxactive.

Light - harvesting by plants may be regarded as the single most important natural process occurring on the Earth.¹¹ The design and synthesis of artificial light harvesting systems has, thus, received considerable interest in recent years. Systems have been constructed from a multitude of chemical species including europium and terbium cryptates,³ calix[4]arenes¹⁵, pendant arm macrocycles and photoactive rotaxanes and catenanes. In addition, ruthenium, osmium and rhenium - polypyridine complexes⁷⁵ have found application as part of donor - relay - acceptor arrays^{16(a)}. The design of such systems has been aided greatly by the solving of the X-ray structure of the photosynthetic reaction centre (RC) for the bacteria *Rhodospseudomonas viridis* by Deisenhofer and Michel in 1989,⁷⁶ as this provided a means of visualising the concepts that are necessary to their successful operation. In the photosynthetic RC the processes that occur may be summarised as follows: excitation by photons of the correct energy of a donor molecule (porphyrin 'special pair') causes an electron to migrate along a series of electron acceptors, to finally rest in a quinone based electron acceptor, thus producing a pair of redox ions. The separation and relative orientations of the donor and acceptor residues play a major role in the control of individual electron transfer steps. In addition, it has been determined that electron transfer proceeds only along the L branch of two almost identical sets of electron transfer reagents.⁷⁷ The means by which this is achieved centres on the different effective dielectric constant of the media immediately surrounding the M and L branches: a slightly higher polarity around the L branch favours electron transfer along this direction.

The requirements for the construction of synthetic models of this system are that the active subunits must be arranged spatially in such a way so that the system is capable of not only photoinduced electron transfer but also directional (or vectorial) electron flow.

1.7.1 Photoinduced Electron Transfer

Photoinduced electron transfer is the branch of photochemistry dealing with the property of photoactive molecules to act as strong oxidising or reducing species when in their excited states.¹³ Such molecules are often better electron donors (or acceptors) when in their excited states than when they are in their ground states - thus they may be described as photosensitisers as when excited they can induce chemical changes in surrounding chemical species by electron transfer.

To understand the concept of photoinduced electron transfer it is convenient to look at the two main topics involved: photochemistry and electron transfer.

(a) Photochemical reactions begin with the absorption of light by chemical species in their ground state leading to the formation of an excited state (figure 1.40): - these have different properties and reactivity from ground states.

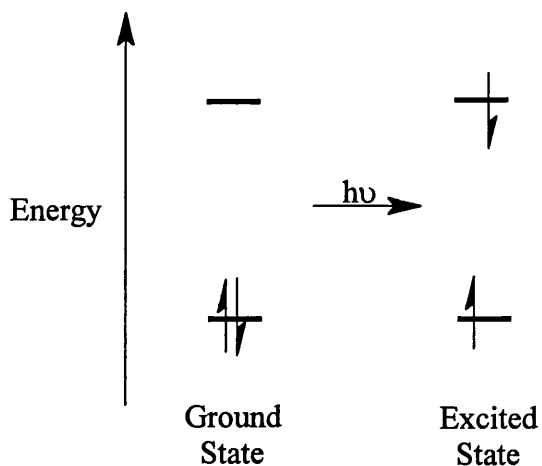


Figure 1.40: Formation of an excited state.

Electronic transitions may occur between molecular orbitals in a number of systems, such as simple organic molecules (e.g. $\pi - \pi^*$ transitions in alkenes and $n - \pi$ transitions in carbonyl compounds) and in transition metal complexes (e.g. metal centred $d - d$ transitions, ligand based $\pi - \pi$ transitions and metal to ligand [or vice versa] charge transfers [MLCT or LMCT]). Transitions occur from the ground state of a molecule, named the singlet ground state (S_0) because the spins of the electrons

in this orbital are paired; in systems containing one unpaired electron (e.g. free radicals) doublet species exist and a system in which there are two unpaired electrons (of parallel spin) a triplet state is produced. Excited states may be found in either of two spin states: singlet (S_n) or triplet (T_n). Each state is a 'packet' of vibrational energy levels, representing the various possible nuclear geometries. Transitions normally occur from lowest vibrational state of the S_0 level into any higher vibrational level of the excited singlet state - this is known as a 'vertical' or 'Franck - Condon' transition. Subsequent to this, relaxation occurs *via* changes in bond lengths and angles and in the solvation sphere of the molecule so that the first vibrational energy level of the first excited state is thermally populated. This state is highly energetic and may therefore lose its energy by either of two routes; by radiative (for example fluorescence) or non - radiative (internal conversion, intersystem crossing) pathways. A particularly interesting example of intersystem crossing is the conversion of singlet excited states to form triplet states, a process which involves a spin flip of an orbital electron. Triplet states occur where electrons are in parallel spin states and so in different orbitals (Pauli exclusion principle). In accordance with Hund's rule, triplets are of lower energy than the singlet states from which they originate as shown in figure 1.41. As intersystem crossing involves a spin flip, it is a 'forbidden' transition in quantum mechanical terms and so has a lower probability than singlet to singlet transitions.

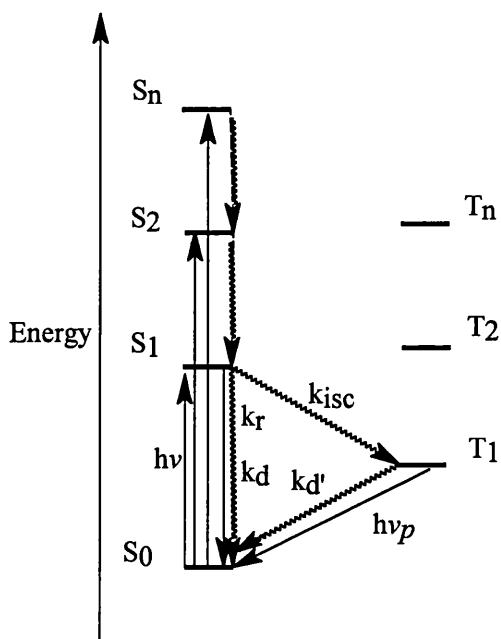


Figure 1.41: A state energy diagram.

As transitions from triplet states are forbidden, they are generally much longer lived and so available for electron (and energy) transfer reactions otherwise known as quenching pathways.

(b) Quenching⁷⁸ may be defined as deactivation of an excited state by an external reagent (intra- or intermolecular) which is a molecule in the ground state. Quenching processes may occur over relatively long distances through space or *via* a flexible or rigid spacer unit. In solution, the polarity and viscosity of the medium determines both the motions and the proximity of the sensitizer - quencher pair. In photoinduced electron transfer, the process of quenching generates a radical ion pair (where both charged species have an odd number of electrons) consisting of the oxidised donor and the reduced acceptor where the rate of electron transfer is written as k_{et} (or alternatively as k_{cs}). The yield of ion pairs produced in this manner may be measured by comparing the rate of electron transfer with that of an analogous system, or by measuring the quantum efficiency:

$$\phi_{IP} = k_{et}/k_{et} + k_{en} + k_d + k_{other}$$

where k_{en} = rate of energy transfer, k_d = rate of radiationless deactivation and k_{other} = rate for photochemical pathways. The lifetime of the ion pair formed by electron transfer is defined by:

$$\tau_{IP} = 1/k_{ret}$$

where k_{ret} = rate of electron return - i.e. the rate at which the original ground state reactants are generated from the charge separated state.

The process of photoinduced electron transfer therefore depends on two discrete processes - formation of the equilibrated excited state and subsequent electron transfer. The latter step depends on the ability of excited states to act as strong electron donors (or acceptors) which is in turn dependent upon thermodynamic factors. These factors are manifest in the ionisation potential (or electron affinity) of the excited state - such states are often more able to donate or accept electrons than their analogous ground states. The explanation for this behaviour is that the excited electron occupies a high energy antibonding orbital, which is positioned at a greater separation distance from the nucleus - the Coulombic energy holding the electron to the positive nucleus is reduced, thus the ionisation potential is reduced. Ionisation potentials are a useful guide to the thermodynamic feasibility of an electron transfer reaction but redox potentials are

more useful for the solution phase as they include factors such as solvation and Coulombic effects. Figure 1.42 shows the state diagram for the ionisation of an electron donor in the ground and excited states.

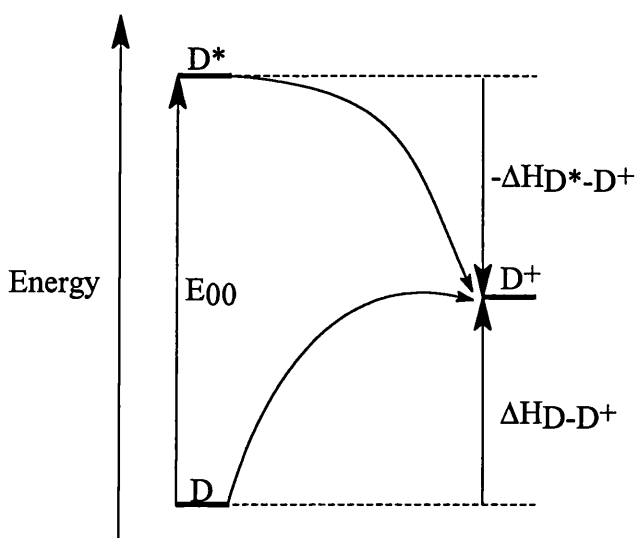


Figure 1.42: Ionisation of an electron donor in ground and excited states.

From the diagram, it is obvious that $-\Delta H_{D^*-D^+} + \Delta H_{D-D^+} = E_{00}$ so that $-\Delta G_{D^*-D^+} - T\Delta S_{D^*-D^+} + \Delta G_{D-D^+} + T\Delta S_{D-D^+} = E_{00}$ where the entropy terms are related to structural and solvation changes between the initial and final electron transfer states. If these terms are disregarded (for the purposes of this discussion) then, $-\Delta G_{D^*-D^+} - \Delta G_{D-D^+} = E_{00}$ i.e. the free energy of electron transfer from D^* is more negative than that from D by an amount equal to the energy of the excited state. Thus, by careful matching of an electron acceptor with a suitable photosensitiser (i.e. thermodynamically favourable reaction, correct lifetime of excited state) an efficient electron transfer reaction can occur. The free energy change for an electron transfer between an excited donor and a ground state acceptor may be written in terms of their electrode potentials:

$$\Delta G_{el}(eV) = nF[E^0(D^+/D^*) - E^0(A/A^{\cdot})]$$

$$\text{or } \Delta G_{el}(eV) = nF[E^0(D^+/D) - E^0(A/A^{\cdot}) - \Delta G_{00}]$$

where ΔG_{00} is the free energy in electron volts corresponding to the equilibrium energy E_{00} . Thus, the free energy of electron transfer may be quantified by measurement of experimental parameters.

Having established that a photoinduced electron transfer reaction is thermodynamically favourable, it is important to recognise the fact that the solvent

plays a vital role in the solution phase.⁷⁹ The solvent determines how close the two interacting species may approach, and also how quickly they may dissociate subsequent to electron transfer. In addition, a polar solvent can reorganise and so stabilise the charge on the ions formed by this process, thus prolonging the charge separated state (by screening the ions from one another) and possibly separating the constituent ions to such large distances that they are no longer an ion pair.

Collisions with solvent molecules are a central part of the Marcus theory of photoinduced electron transfer, as described below.

1.7.2 The Marcus Theory of Photoinduced Electron Theory^{13,79,80}

When an electron donor and acceptor approach from a large distance, they reach an encounter distance where their frontier orbitals begin to interact. At this point they form a supermolecule which is the precursor to electron transfer. The precursor state undergoes a change in nuclear organisation to produce a transition state subsequent to which electron transfer occurs. The states that exist immediately before and after electron transfer may be represented by parabolic functions which represent idealised energy curves - each point on the curve represents a discrete nuclear geometry and energy associated with a particular nuclear configuration. Where the two curves intersect represents the energy and nuclear configuration of the transition state - the energy term is the activation energy for the electron transfer process at a nuclear geometry unique to the transition state (figure 1.43).

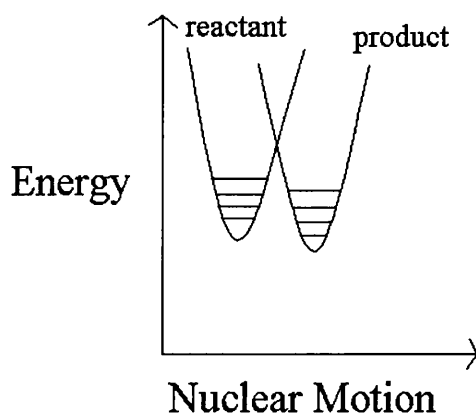


Figure 1.43: Representation of transition state for electron transfer.

The transition state energy, ΔG_{et}^\ddagger is reached through collisions between reacting molecules and neighbouring solvent molecules in the surrounding medium - energy is supplied by these vibrational collisions prior to electron transfer. Once the transition state is reached, the electron is transferred, thereby allowing conservation of energy. In the transition state, electron transfer is virtually instantaneous as compared to nuclear motion (the Franck - Condon principle) so that no nuclear motions occur during transfer. Subsequent to electron transfer the 'successor' state rapidly undergoes thermal equilibration with the surrounding medium.

Adiabatic interactions occur where there is strong interaction between the precursor and product states and so their zero - order states become strongly perturbed. Electron transfer is much more probable in the adiabatic case than in non - adiabatic systems, as in the former electron transfer occurs entirely on one potential surface (i.e. one continuous curve). When the interaction energy becomes large, ΔG_{et}^\ddagger is reduced - at this point resonance stabilisation of the transition state becomes the dominant force. Such situations arise when exciplexes are formed and charge transfer occurs at diffusion controlled rates.

In the case of more weakly adiabatic systems, the major problem is to determine how reacting systems can overcome free energy barriers and finally proceed to the product state. The factors that determine the nature of the transition state in electron transfer generally include the bond changes that take place during formation of the transition state and the changes in the solvent molecules during electron transfer. The free energy of activation for electron transfer is thus related to the driving force for the reaction and to the reorganisation energy:

$$\Delta G_{et}^\ddagger = \lambda/4(1 + \Delta G_{et}/\lambda)^2$$

Total reorganisation energy may be split into two terms; inner and outer sphere reorganisation energy. The inner sphere term refers to energy changes accompanying changes in bond lengths and angles during electron transfer, whereas the outer sphere term relates to the energy change as the solvent shells surrounding the reactants rearrange, which is in turn related to the polarisation of the solvent molecules surrounding the reactant pair.

The activation energy for an electron transfer process consists of solvent and bond contributions, with the overall feasibility of the process being determined by the thermodynamic driving force. The rate constant for electron transfer from an excited state to a quencher is dependant upon the activation energy of electron transfer and, thus, the driving force and reorganisation energy according to the above equation. As the driving force, ΔG_{el} , increases so does the rate of electron transfer until the rate reaches a maximum (where ΔG_{el}^\ddagger equals zero). However, subsequent increases in ΔG_{el} result in a diminishing rate of electron transfer as ΔG_{el}^\ddagger begins to increase again. The quadratic dependency of the rate of electron transfer on the thermodynamic driving force gives rise to two kinetic domains: the normal region where $-\Delta G_{el} < \lambda$ and the inverted region where $-\Delta G_{el} > \lambda$ (figure 1.44).

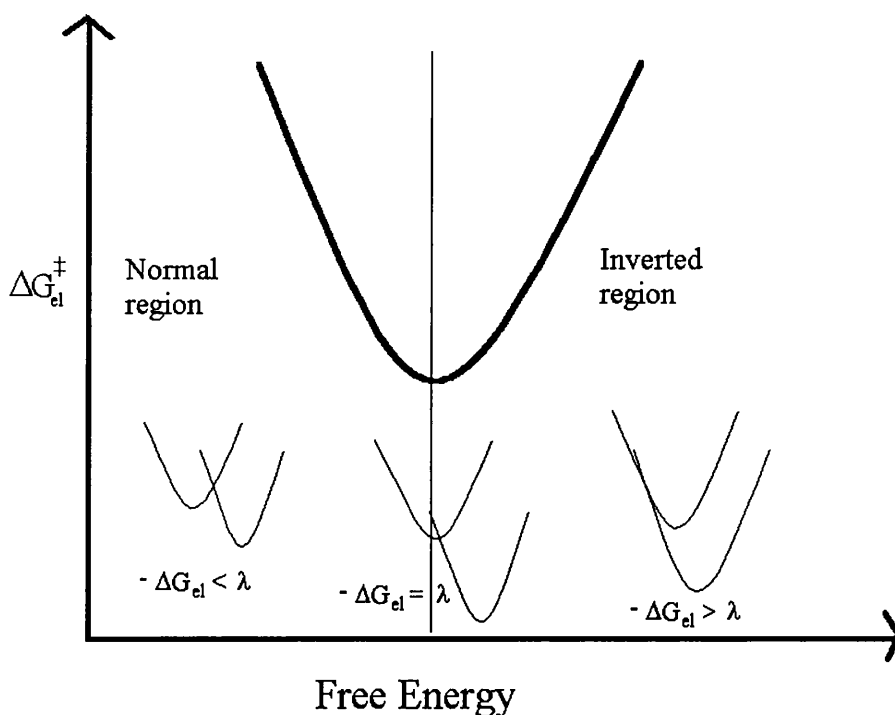


Figure 1.44: The normal and inverted regions in Marcus theory.

1.7.3 Photophysical and Electrochemical Properties of $\text{Ru}(\text{bipy})_3^{2+}$

Ruthenium (II) tris - bipyridyl was one of the first transition metal complexes to be investigated for its excited state properties as an oxidant and reductant.¹³ The complex and its substituted derivatives absorb light from the UV region down to about 520nm - the characteristic red colour of the complex being due

to an intense metal to ligand d, π^* charge transfer transition.⁸¹ The complex is luminescent, with the emitting states identified as being the spin forbidden counterparts of the charge transfer transition. There is a large apparent Stokes shift (absorbing and emitting states are different so this is not a true Stokes shift) with the absorption and luminescence maxima being well separated - thus self absorption is not an important factor.

A great deal of discussion has taken place regarding the nature of the excited state - whether the excited electron is localised on one bipy π^* orbital or delocalised throughout the entire ligand system.⁸² The ordering and spin characteristics of the emitting states have also been the subject of intense debate. The generally accepted view is that the emitting state consists of a manifold of closely spaced localised excited states which are predominantly triplet in nature. They are populated from delocalised singlet states formed by the absorption process *via* an intersystem crossing operation.

Substitution of the ligand causes both wavelength shifts and intensity changes in the electronic transitions of the complex, however there is evidence that the ordering of levels in the excited state singlet and triplet manifolds is invariant to such derivatisation.⁸³

In addition to the singlet and triplet excited states, high energy d-d states have been detected and implicated in the photo-decomposition of $\text{Ru}(\text{bipy})_3^{2+}$ at high temperatures.⁸² These states are important as they can explain the temperature dependence of the observed rate constant for decay of the excited state. The study of emission lifetimes and quantum yields has confirmed that the radiative (k_r) and non-radiative (k_{nr}) rate constants are largely temperature independent whereas deactivation of the excited state *via* the d-d states (k'^0) was found to be temperature dependent, such that the overall rate constant may be defined as follows.

$$k_{\text{obs}} = k_r + k_{nr} + k'^0 \exp(-E_a/k_bT)$$

The model for the excited states of ruthenium tris - bipyridyl and its derivatives may thus be described by a three level model as shown in figure 1.45.

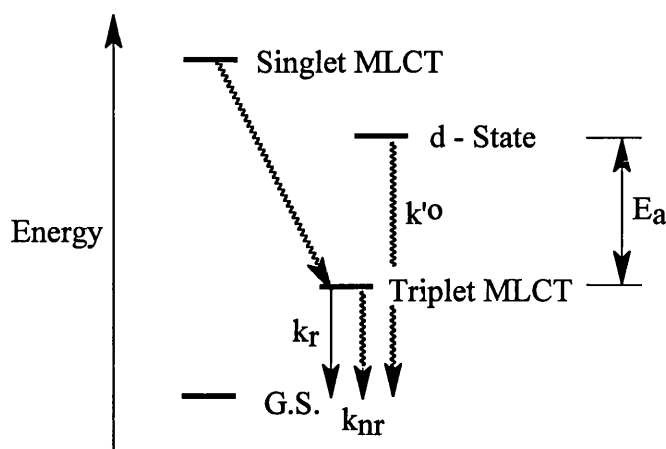


Figure 1.45: Excited states of Ru(bipy)₃²⁺.

In addition to the non - radiative decay pathways described above, the choice of solvent has a significant effect on the luminescence characteristics (and in particular k_{nr}) of Ru(bipy)₃ and its derivatives. It has been argued that the importance of solvents on the luminescence may be attributable to energy gap effects whereby excited state energy is trapped by solvent acceptor vibrations and that solvent properties are important as regards the stability of the initial and final states of the prospective charge transfer complex (as discussed previously).⁷⁹

As there are a number of excellent reviews on the luminescence of Ru(bipy)₃²⁺ and the effects of the medium on it, these themes will not be discussed further at this point.^{75,79,82}

The incorporation of Ru(bipy)₃²⁺ into so - called “light harvesting devices” has been of particular interest in recent years. A number of systems involving both intra- and intermolecular quenching of Ru(bipy)₃²⁺ emission, often using viologen derivatives as the ground state quencher have been reported. The excited state of ruthenium tris - bipyridyl is a strong reducing agent, losing an electron to oxidising substrates and generating the ruthenium (III) complex.⁸⁴ In solution, it is well known that methyl viologen will quench the luminescence of the ruthenium moiety, the rate constant being bimolecular, i.e. intermolecular, as expected.⁸⁵ By constructing ruthenium complexes with bipyridine ligands derivatised with polyether chains containing electron rich aromatic units and forming EDA complexes with electron deficient tetracationic cyclophanes, Dürr and Willner *et al* have been able to measure the rates of a number of photoinduced electron transfer reactions.⁸⁶ Recently, they have constructed a [2]catenane based on the same principle⁸⁷ (figure

1.46) which has a rate of electron transfer measured at $2.6 \times 10^7 \text{ s}^{-1}$ - the rate constant is first order because the excited state donor and the quencher are mechanically linked together (so they cannot diffuse apart).

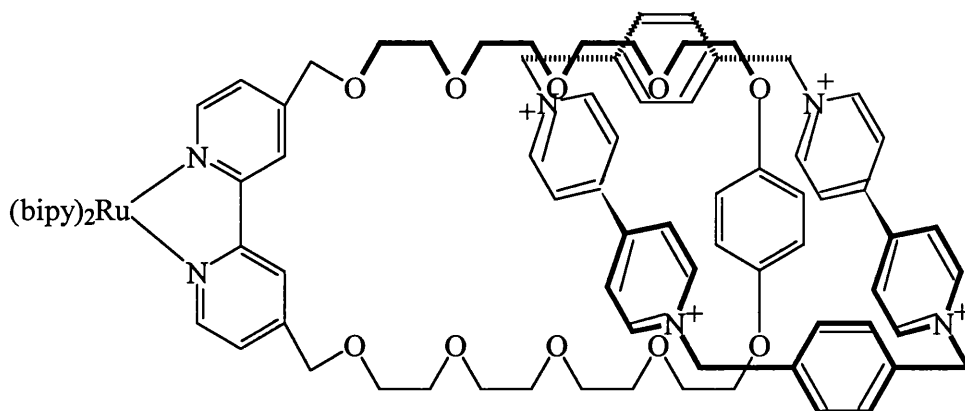


Figure 1.46: A [2]catenane capable of displaying intramolecular photoinduced electron transfer.

By covalently attaching viologen derivatives to bipyridine ligands with variable spacer lengths, a number of groups⁸⁸ have produced systems which are capable of photoinduced electron transfer with either unimolecular (through bonds interaction, short spacer length) or bimolecular (through space, long spacer length) rate constants. By employing functionalised viologen derivatives as electron relay devices, the group of Dürr and Willner⁸⁹ have extended this strategy to construct sensitiser - relay - acceptor triads whereby large spatial charge separations have been achieved (figure 1.47).

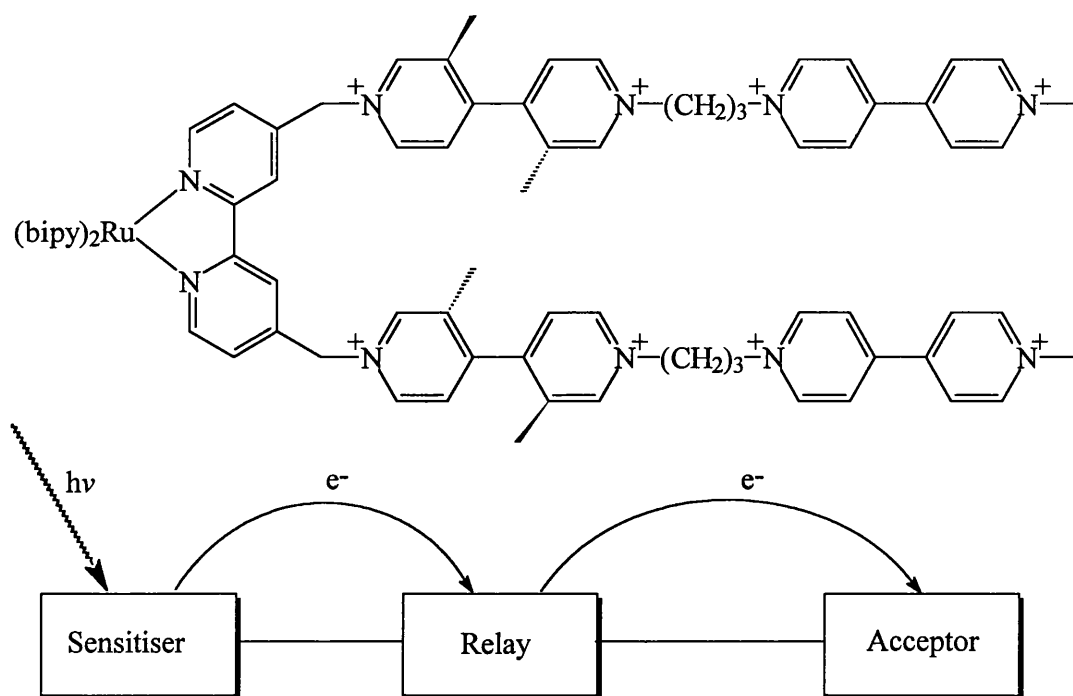


Figure 1.47: A sensitizer - relay - acceptor triad.

The systems described above all suffer to a greater or lesser degree from extremely efficient back electron transfer (charge recombination) due to the relatively strong oxidising ability⁸⁴ of $Ru(bipy)_3^{3+}$ - whilst this potentially allows the construction of a photo - driven cycle, it presents a limit to the usefulness of ruthenium tris - bipyridyl as a component in photoactive molecular devices.

1.8 Aims and Objectives

The primary aim of the research presented in this thesis was to construct and characterise supramolecular systems which possessed the ability to model the photosynthetic reaction centre. To achieve this aim, it was convenient to employ established methods for the construction of catenanes and cyclophanes, such as utilising associative interactions between complementary aromatic electron donors and acceptors, and combining such syntheses with transition metal based chemistry so as to make use of the intriguing photochemical properties of ruthenium (and osmium) tris bipyridyl moieties.

[2]Catenanes and their analogous cyclophanes were chosen as target molecules due to the fact that they presented a means of producing chemically identical model systems which were capable (or not) of displaying redox asymmetry between two identical electron accepting units.

The secondary objectives of this research were to investigate the host - guest chemistry of some of the model systems synthesised and to study the nature of the π - π interactions involved, where possible, using solid state structures; assemble polymolecular arrays by use of transition metals as linker units and also to investigate the electrochemical and photophysical (where appropriate) properties of the molecular and supramolecular systems produced.

1.9 References

- [1] Lehn, J.M. *Pure Appl. Chem.*, 1978, **50**, 871.
- [2] (a) Lehn, J.M. *Structure and Bonding*, 1973, **16**, 1. (b) Pederson, C.J. *Angew. Chem. Int. Ed. Engl.*, 1988, **27**, 1021.
- [3] Lehn, J.M. *Supramolecular Chemistry*, VCH, Weinheim, 1995.
- [4] (a) Lehn, J.M. *Angew. Chem. Int. Ed. Engl.*, 1989, **27**, 89. (b) Various papers in *Supramolecular Chemistry*, NATO ASI Series, (Eds. Balzani, V.; De Cola, L.), Kluwer Academic Publisher, Dordrecht, 1992. (c) Vögtle, F. *Supramolecular Chemistry*, Wiley, Chichester, 1991.
- [5] Lehn, J.M. in *Frontiers in Supramolecular Organic Chemistry and Photochemistry*, (Eds. Schneider, H.J.; Dürr, H), VCH, Weinheim, 1991.
- [6] Cram, D.J. *Angew. Chem. Int. Ed. Engl.*, 1988, **27**, 1009.
- [7] (a) Schneider, H.J.; Blatter, T.; Cuber, U.; Juneja, R.; Schiestel, T.; Scheider, U.; Theis, I.; Zimmermann, P. in *Frontiers in Supramolecular Organic Chemistry and Photochemistry*, (Eds. Schneider, H.J.; Dürr, H), VCH, Weinheim, 1991. (b) Various papers in *Principles of Molecular Recognition*, (Eds. Buckingham, A.D.; Legon, A.C.; Roberts, S.M.), Blackie Academic and Professional, London, 1993.
- [8] Vögtle, F. *Cyclophane Chemistry*, Wiley, Chichester, 1993.
- [9] Cram D.J. in *Cyclophanes, A Series of Monographs*, (Eds. Keehn, P.M.; Rosenfeld, S.M.), Academic Press, 1983.
- [10] Willner, I.; Willner, B. in *Frontiers in Supramolecular Organic Chemistry and Photochemistry*, (Eds. Schneider, H.J.; Dürr, H), VCH, Weinheim, 1991.
- [11] Benniston A.C. *Chem. Soc. Rev.*, 1996, 427.
- [12] Various papers in *Fluorescent Chemosensors for Ion and Molecule Recognition*, (Ed. Czarnik A.W.), American Chemical Society, Washington D.C., 1992.
- [13] Kavernos, G.J. *Fundamentals of Photoinduced Electron Transfer*, VCH, New York, 1993.
- [14] Balzani, V.; Ballardini, R.; Gandolfi, M.T.; Prodi, L.; in *Frontiers in Supramolecular Organic Chemistry and Photochemistry*, (Eds. Schneider, H.J.; Dürr, H), VCH, Weinheim, 1991.
- [15] Ungaro, R.; Pochini, A. in *Frontiers in Supramolecular Organic Chemistry and Photochemistry*, (Eds. Schneider, H.J.; Dürr, H), VCH, Weinheim, 1991.

- [16] (a) Dürr, H.; Bossman, S.; Kilbury, H.; Trierweiler, H.P.; Schwartz, R. in *Frontiers in Supramolecular Organic Chemistry and Photochemistry*, (Eds. Schneider, H.J.; Dürr, H), VCH, Weinheim, 1991. (b) Houlding, V.; Geiger, T.; Kölle, U.; Grätzel, M. *J. Chem. Soc. Chem. Commun.*, 1982, 681.
- [17] Benniston A.C.; Gouille, V.; Harriman, A.; Lehn, J.M.; Marczinke, B. *J. Phys. Chem.*, 1994, **98**, 7798.
- [18] A number of 'molecular shuttle' devices have been published in the recent literature, see for example: (a) Amabilino, D.B.; Ashton, P.R.; Boyd, S.E.; Gómez - López, M.; Hayes, W.; Stoddart, J.F. *J. Org. Chem.*, 1997, **62**, 3062. (b) Anelli, P.L.; Asakawa, M.; Ashton, P.R.; Bissell, R.A.; Clavier, G.; Górski, R.; Kaifer, A.E.; Langford, S.J.; Mattersteig, G.; Menzer, S.; Philp, D.; Slawin, A.M.Z.; Spencer, N.; Stoddart, J.F.; Tolley, M.S.; Williams, D.J. *Chem. Eur. J.*, 1997, **3**, 1113. (c) Martinez - Diaz, M.V.; Spencer, N.; Stoddart, J.F. *Angew. Chem. Int. Ed. Engl.*, 1997, **36**, 1904. (d) Gong, C.; Gibson, H.W. *Angew. Chem. Int. Ed. Engl.*, 1997, **36**, 2331.
- [19] Gavina, P.; Sauvage, J.P. *Tetrahedron Lett.*, 1997, **38**, 3521.
- [20] For reviews of the work of Beer see: (a) Beer, P.D.; Wheeler, J.W.; Moore, C. in *Supramolecular Chemistry*, NATO ASI Series, (Eds. Balzani, V.; De Cola, L.), Kluwer Academic Publishers, Dordrecht, 1992. (b) Beer, P.D. in *Transition Metals in Supramolecular Chemistry*, NATO ASI Series, (Eds. Fabbrizzi, L.; Poggi, A.), Kluwer Academic Publishers, Dordrecht, 1994. (c) Beer, P.D. *J. Chem. Soc. Chem. Commun.*, 1996, 689. (d) Beer, P.D. *Acc. Chem. Res.*, 1998, **31**, 71.
- [21] For examples of an: (a) anion receptor see Beer, P.D.; Fletcher, N.C.; Wear, T.J. *Inorg. Chim. Acta*, 1996, **251**, 335. (b) cation receptor see Chen, Z.; Pilgrim, A.J.; Beer, P.D. *J. Chem. Soc. Faraday Trans.*, 1995, **91**, 4331. (c) anion and cation receptor see Beer, P.D.; Dent, S.W.; Fletcher, N.C.; Wear, T.J. *Polyhedron*, 1996, **15**, 2983.
- [22] For examples see: (a) Munoz, S.; Mallen, J.; Nakano, A.; Chen, Z.; Gay, I.; Echegoyen, L.; Gokel, G.W. *J. Am. Chem. Soc.*, 1993, **115**, 1705. (b) Munoz, S.; Mallen, J.; Nakano, A.; Chen, Z.; Gay, I.; Echegoyen, L.; Gokel, G.W. *J. Chem. Soc. Chem. Commun.*, 1992, 520. (c) Chen Z.; Gokel, G.W.; Echegoyen, L. *J.*

- Org. Chem.*, 1991, **56**, 3369. (d) De Wall, S.L.; Wang, K.; Berger, D.R.; Watanabe, S.; Hernandez, J.C.; Gokel, G.W. *J. Org. Chem.*, 1997, **62**, 6784.
- [23] Dietrich - Buchecker, C.O.; Sauvage, J.P. *Chem. Rev.*, 1987, **87**, 795.
- [24] Ottenshildebrandt, S.; Schmidt, T.; Harren, J.; Vögtle, F. *Liebigs Ann. Chem.*, 1995, 1855.
- [25] Asakawa, A.; Ashton, P.R.; Boyd, S.E.; Brown, C.L.; Menzer, S.; Pasini, D.; Stoddart, J.F.; Tolley, M.S.; White, A.J.P.; Williams, D.J.; Wyatt, P.G. *Chem. Eur. J.*, 1997, **3**, 463.
- [26] Ashton, P.R.; Boyd, S.E.; Menzer, S.; Pasini, D.; Raymo, F.M.; Spencer, N.; Stoddart, J.F.; White A.J.P.; Williams, D.J.; Wyatt, P.G. *Chem. Eur. J.*, 1998, **4**, 299.
- [27] Ashton, P.R.; Reder, A.S.; Spencer, N.; Stoddart, J.F. *J. Am. Chem. Soc.*, 1993, **115**, 5286.
- [28] Seeman, N.C.; Chen, J.H.; Du, S.M.; Mueller, J.E.; Zhang, Y.W.; Fu, T.J.; Wang, Y.L.; Wang, H.; Zhang, S.W. *New J. Chem.*, 1993, **17**, 739.
- [29] Frisch, H.L.; Wasserman, E.J. *J. Am. Chem. Soc.*, 1961, **83**, 3789.
- [30] Schill, G.; Schweickert, N.; Fritz, H.; Vetter, W. *Angew. Chem. Int. Ed. Engl.*, 1983, **22**, 889.
- [31] Lüttringhaus, A.; Cramer, F.; Prinzbach, H.; Henglein, F.M. *Liebigs Ann. Chem.*, 1958, **613**, 185.
- [32] Armspach, D.; Ashton, P.R.; Moore, C.P.; Spencer, N.; Stoddart, J.F.; Wear, T.J.; Williams, D.J. *Angew. Chem. Int. Ed. Engl.*, 1993, **32**, 854.
- [33] Original reference: Schill, G.; Lüttringhaus, A. *Angew. Chem.*, 1964, **76**, 567, see also reference 23.
- [34] Schill, G. *Catenanes, Rotaxanes and Knots*, Academic, New York, 1971.
- [35] Walba, D.M.; Homan, T.C.; Richards, R.M.; Haltiwanger, R.C. *New J. Chem.*, 1993, **17**, 661.
- [36] See for example: (a) Fujita, M.; Ogura, K. *Bull. Chem. Soc. Japan*, 1996, **69**, 1471. (b) Fujita, M.; Ogura, K. *Coord. Chem. Rev.*, 1996, **148**, 249. (c) Fujita, M.; Ibukuro, F.; Seki, H.; Kamo, O.; Imanari, M.; Ogura, K. *J. Am. Chem. Soc.*, 1996, **118**, 899. (d) Fujita, M.; Ibukuro, F.; Yamaguchi, K.; Ogura, K. *J. Am.*

- Chem. Soc.*, 1995, **117**, 4175. (e) Fujita, M.; Ibukuro, F.; Hagihara, H.; Ogura, K. *Nature*, 1994, **367**, 720.
- [37] Wasserman, E.; Ben-Efraim, D.A.; Wolovsky, R. *J. Am. Chem. Soc.*, 1970, **92**, 2132.
- [38] Cotton, F.A.; Wilkinson, G. *Advanced Inorganic Chemistry, Fifth Edition*, Wiley, New York, 1988, pp. 346.
- [39] Original reference: Reppe, W.; Schlichting, O.; Klager, K.; Toepel, T. *Liebigs Ann. Chem.*, 1948, **560**, 1, see also reference 23.
- [40] Curtis, N.F. *J. Chem. Soc.*, 1960, 4409.
- [41] Creaser, I.I.; Harrowfield, J.M.; Herlt, A.J.; Sargeson, A.M.; Springborg, J. *J. Am. Chem. Soc.*, 1977, **99**, 3181.
- [42] Dietrich-Buchecker, C.O.; Sauvage, J.P.; Kintzinger, J.P. *Tetrahedron Lett.*, 1983, **24**, 5095.
- [43] Dietrich-Buchecker, C.O.; Sauvage, J.P.; Weiss, J. *Tetrahedron Lett.* 1986, **27**, 2257.
- [44] (a) Dietrich-Buchecker, C.O.; Leize, E.; Nierengarten, J.F.; Sauvage, J.P.; van Dorsselaer, A. *J. Chem. Soc. Chem. Commun.*, 1994, 2257. (b) Nierengarten, J.F.; Dietrich-Buchecker, C.O.; Sauvage, J.P. *J. Am. Chem. Soc.*, 1994, **116**, 375.
- [45] Cardenas, D.J.; Sauvage, J.P. *Inorg. Chem.*, 1997, **36**, 2777.
- [46] Cardenas, D.J.; Livoreil, A.; Sauvage, J.P.; *J. Am. Chem. Soc.*, 1996, **118**, 11980.
- [47] Amabilino, D.B.; Sauvage, J.P. *J. Chem. Soc. Chem. Commun.*, 1996, 2441.
- [48] Shimada, S.; Ishikawa, K.; Tamaoki, N. *Acta Chem. Scand.*, 1998, **52**, 374.
- [49] Suh, J.H.; Lee, S.H. *J. Org. Chem.*, 1998, **63**, 1519.
- [50] Weidmann, J.L.; Kern, J.M.; Sauvage, J.P.; Geerts, Y.; Muscat, D.; Müllen, K. *J. Chem. Soc. Chem. Commun.*, 1996, 1243.
- [51] Amabilino, D.B.; Dietrich-Buchecker, C.O.; Livoreil, A.; Perezgarcia, L.; Sauvage, J.P.; Stoddart, J.F. *J. Am. Chem. Soc.*, 1996, **118**, 3905.
- [52] Hunter, C.A. *Chem. Soc. Rev.*, 1994, **23**, 101.
- [53] Hunter, C.A. *Angew. Chem. Int. Ed. Engl.*, 1993, **32**, 1584.
- [54] See for example: (a) Stoddart, J.F. in *Frontiers in Supramolecular Organic Chemistry and Photochemistry*, (Eds. Schneider, H.J.; Dürr, H), VCH, Weinheim,

1991. (b) Fyfe, M.C.T.; Stoddart, J.F. *Acc. Chem. Res.*, 1997, **30**, 393. (c) Gillard, R.E.; Raymo, F.M.; Stoddart, J.F. *Chem. Eur. J.*, 1997, **3**, 1933.
- [55] Benniston, A.C.; Harriman, A. *J. Am. Chem. Soc.*, 1994, **116**, 11531.
- [56] Nishio, M.; Unezawa, Y.; Hirota, M.; Takeuchi, Y. *Tetrahedron*, 1995, **51**, 8665.
- [57] Amabilino, D.B.; Ashton, P.R.; Brown, C.L.; Córdova, E.; Godínez, L.A.; Goodnow, T.T.; Kaifer, A.E.; Newton, S.P.; Pietraszkiewicz, M.; Philp, D.; Raymo, F.M.; Reder, A.S.; Rutland, M.T.; Slawin, A.M.Z.; Spencer, N.; Stoddart, J.F.; Williams, D.J. *J. Am. Chem. Soc.*, 1995, **117**, 1271.
- [58] Ashton, P.R.; Goodnow, T.T.; Kaifer, A.E.; Reddington, M.V.; Slawin, A.M.Z.; Spencer, N.; Stoddart, J.F.; Vicent, C.; Williams, D.J. *Angew. Chem. Int. Ed. Engl.*, 1989, **28**, 1396.
- [59] Examples of polycatenanes: (a) Amabilino, D.B.; Ashton, P.R.; Balzani, V.; Boyd, S.E.; Credi, A.; Lee, J.Y.; Menzer, S.; Stoddart, J.F.; Venturi, M.; Williams, D.J. *J. Am. Chem. Soc.*, 1998, **120**, 4295. (b) Ashton, P.R.; Boyd, S.E.; Claessens, C.G.; Gillard, R.E.; Menzer, S.; Stoddart, J.F.; Tolley, M.S.; White, A.J.P.; Williams, D.J. *Chem. Eur. J.*, 1997, **3**, 788. (c) Ashton, P.R.; Brown, C.L.; Chrystal, E.J.T.; Parry, K.P.; Pietraszkiewicz, M.; Spencer, N.; Stoddart, J.F. *Angew. Chem. Int. Ed. Engl.*, 1991, **30**, 1042.
- [60] Menzer, S.; White, A.J.P.; Williams, D.J.; Belohradsky, M.; Hamers, C.; Raymo, F.M.; Shipway, A.N.; Stoddart, J.F. *Macromolecules*, 1998, **31**, 295.
- [61] Lu, T.B.; Zhang, L.; Gokel, G.W.; Kaifer, A.E. *J. Am. Chem. Soc.*, 1993, **115**, 2542.
- [62] (a) Gunter, M.J.; Hockless, D.C.R.; Johnston, M.R.; Skelton, B.W.; White, A.H. *J. Am. Chem. Soc.*, 1994, **116**, 4810. (b) Gunter, M.J.; Johnston, M.R. *J. Chem. Soc. Chem. Commun.*, 1992, 1163.
- [63] (a) Bauer, M.; Muller, W.M.; Muller, U.; Rissanen, K.; Vögtle, F. *Liebigs Ann. Chem.*, 1995, 649. (b) Vögtle, F.; Muller, W.M.; Muller, U.; Bauer, M.; Rissanen, K. *Angew. Chem. Int. Ed. Engl.*, 1993, **32**, 1295.
- [64] Ashton, P.R.; Ballardini, R.; Balzani, V.; Credi, A.; Gandolfi, M.T.; Menzer, S.; Perez-Garcia, L.; Prodi, L.; Stoddart, J.F.; Venturi, M.; White, A.J.P.; Williams, D.J. *J. Am. Chem. Soc.*, 1995, **117**, 11171.

[65] For examples see: (a) Nielsen, M.B.; Thorup, N.; Becher, J. *J. Chem. Soc. Perkin Trans. I*, 1998, 1305. (b) Li, Z.T.; Stein, P.C.; Becher, J.; Jensen, D.; Mork, P.; Svenstrup, N. *Chem. Eur. J.* 1996, **2**, 624. (c) Li, Z.T.; Stein, P.C.; Svenstrup, N.; Lund, K.H.; Becher, J. *Angew. Chem. Int. Ed. Engl.*, 1995, **34**, 2524. See also: Asakawa, M.; Ashton, P.R.; Balzani, V.; Credi, A.; Hamers, C.; Mattersteig, G.; Montalti, M.; Shipway, A.N.; Spencer, N.; Stoddart, J.F.; Tolley, M.S.; Venturi, M.; White, A.J.P.; Williams, D.J. *Angew. Chem. Int. Ed. Engl.*, 1998, **37**, 333.

[66] (a) Hamilton, D.G.; Davies, J.E.; Prodi, L.; Sanders, J.K.M. *Chem. Eur. J.*, 1998, **4**, 608. (b) Hamilton, D.G.; Sanders, J.K.M.; Davies, J.E.; Clegg, W.; Teat, S.J.

[67] Ashton, P.R.; Balzani, V.; Credi, A.; Kocian, O.; Pasini, D.; Prodi, L.; Spencer, N.; Stoddart, J.F.; Tolley, M.S.; Venturi, M.; White, A.J.P.; Williams, D.J. *Chem. Eur. J.*, 1998, **4**, 590. See also: Benniston, A.C.; Mackie, P.R.; Harriman, A. *Tetrahedron Lett.*, 1997, **38**, 3577 and Benniston A.C.; Mackie, P.R.; Farrugia, L.J.; Parsons, S.; Clegg, W.; Teat, S.J. *Platinum Metals Rev.*, 1998, **42**, 100.

[68] (a) Adams, H.; Carver, F.J.; Hunter, C.A. *J. Chem. Soc. Chem. Commun.*, 1995, 809. (b) Hunter, C.A. *J. Am. Chem. Soc.*, 1992, **114**, 5303.

[69] Vögtle, F.; Meier, S.; Hoss, R. *Angew. Chem. Int. Ed. Engl.*, 1992, **31**, 1619.

[70] Jager, R.; Vögtle, F. *Angew. Chem. Int. Ed. Engl.*, 1997, **36**, 930.

[71] Ottenshildebrandt, S.; Nieger, M.; Rissanen, K.; Rouvinen, J.; Meier, S.; Harder, G.; Vögtle, F. *J. Chem. Soc. Chem. Comm.*, 1995, 777.

[72] Johnston, A.G.; Leigh, D.A.; Nezhat, L.; Smart, J.P.; Deegan, M.D. *Angew. Chem. Int. Ed. Engl.*, 1995, **34**, 1212.

[73] Johnston, A.G.; Leigh, D.A.; Pritchard, R.J.; Deegan, M.D. *Angew. Chem. Int. Ed. Engl.*, 1995, **34**, 1209.

[74] Lane, A.S.; Leigh, D.A.; Murphy, A. *J. Am. Chem. Soc.*, 1997, **119**, 11092.

[75] Various articles in *Transition Metals in Supramolecular Chemistry*, NATO ASI Series, (Eds. Fabbrizzi, L.; Poggi, A.), Kluwer Academic Publishers, Dordrecht, 1994.

[76] Deisenhofer, J.; Michel, H.; *Angew. Chem. Int. Ed. Engl.*, 1989, **28**, 829.

- [77] Benniston, A.C.; Mackie, P.R.; Harriman, A. *Angew. Chem. Int. Ed. Engl.*, 1998, **37**, 354.
- [78] Bowen, E.J. in *Luminescence in Chemistry*, (Ed. Bowen, E.J.), D. van Nostrand, London, 1968.
- [79] Chen, P.; Meyer, T.J. *Chem. Rev.*, 1998, **98**, 1439.
- [80] Marcus, R.A. *Ann. Rev. Phys. Chem.*, 1964, **15**, 155.
- [81] Cook, M.J.; Lewis, A.P.; MaAuliffe, G.S.G.; Skarda, V.; Thomson, A.J.; Glasper, J.C.; Robbins, D.J. *J. Chem. Soc. Perkin Trans. II*, 1984, 1293.
- [82] Krause, R.A. *Structure and Bonding*, 1987 **67**,1.
- [83] Cook, M.J.; Lewis, A.P.; MaAuliffe, G.S.G.; Skarda, V.; Thomson, A.J.; Glasper, J.C.; Robbins, D.J. *J. Chem. Soc. Perkin Trans. II*, 1984, 1303.
- [84] Cook, M.J.; Lewis, A.P.; MaAuliffe, G.S.G.; Skarda, V.; Thomson, A.J.; Glasper, J.C.; Robbins, D.J. *J. Chem. Soc. Perkin Trans. II*, 1984, 1309.
- [85] Bock, C.R.; Meyer, T.J.; Whitten, D.G. *J. Am. Chem. Soc.*, 1974, **96**, 4710.
- [86] (a) Kropf, M.; Joselevich, E.; Dürr, H.; Willner, I. *J. Am. Chem. Soc.*, 1996, **118**, 655. (b) David, E.; Born, R.; Kaganer, E.; Joselevich, E.; Dürr, H.; Willner, I. *J. Am. Chem. Soc.*, 1997, **119**, 7778. (c) Seiler, M.; Dürr, H.; Willner, I.; Joselevich, E.; Doron, A.; Stoddart, J.F. *J. Am. Chem. Soc.*, 1994, **116**, 3399.
- [87] Hu, Y.Z.; van Logen, D.; Schwarz, O.; Bossman, S.; Dürr, H.; Huch, V.; Veith, M. *J. Am. Chem. Soc.*, 1998, **120**, 5822.
- [88] (a) Kelly, L.A.; Rodgers, M.A.J. *J. Phys. Chem.*, 1995, **99**, 13132. (b) Clark, C.D.; Debad, J.D.; Yonemoto, E.H.; Mallouk, T.E.; Bard, A.J. *J. Am. Chem. Soc.*, 1997, **119**, 10525.
- [89] (a) Seiler, M.; Dürr, H. *Synthesis*, 1994, 83. (b) Zahauy, E.; Seiler, M.; Marx-Tibbon, S.; Joselevich, E.; Willner, I.; Dürr, H.; O'Connor, D.; Harriman, A. *Angew. Chem. Int. Ed. Engl.*, 1995, **34**, 1005.

Chapter Two

Experimental

2.1 Instrumentation

2.1.1 General

UV-VIS spectra were obtained on a Shimadzu UV - 3101PC spectrophotometer. Reference and sample spectra were collected using optically matched 1cm quartz cuvettes. Corrected spectra were produced by sample - reference subtraction using the Shimadzu UVPC suite of programs.

Ambient temperature two dimensional $^1\text{H} - ^1\text{H}$ COSY NMR spectra were obtained on a Bruker Avance DPX 400 FT - NMR spectrometer using the Bruker XWIN - NMR suite of programs. Low temperature two dimensional NMR spectra and all one dimensional NMR spectra were obtained on a Bruker AM360 360 MHz FT - NMR spectrometer using the Bruker Aspect 3000 suite of programs. Carbon spectra were obtained at 90 MHz using either broad band or DEPT sequences. All samples were referenced internally to solvent resonances. Deuterated solvents were purified by freeze - thaw degassing and stored under a nitrogen atmosphere.

Infrared spectra were obtained on a Nicolet Impact 410 spectrophotometer using the OMNIC suite of programs and on a Perkin Elmer Paragon 1000 FT - IR photospectrometer. Samples were prepared as 8mm diameter KBr discs using 300mg of KBr and a press force of 8 tons or as thin films between NaCl plates.

Steady state fluorescence spectra were obtained on a SPEX Fluoromax spectrofluorimeter using the DM3000 suite of programs. Spectra were obtained in a 1cm quartz cuvette.

2.1.2 Mass Spectrometry

Electron Impact (EI) and Fast Atom Bombardment (FAB) mass spectra were obtained by Mr T. Ritchie using a JEOL JMS 700 ("The MStation") mass spectrometer. FAB mass spectra were obtained from a sample matrix consisting of the sample and 3 - nitro benzyl alcohol (NBA).

Electrospray mass spectra were obtained from the EPSRC Mass Spectrometry Service Centre at Swansea. Electrospray mass spectra were obtained, typically, using a mobile phase of acetonitrile - 1% formic acid with cone voltages varying from 20V to 90V.

2.1.3 Electrochemistry

Cyclic Voltamograms (CVs) were obtained using an EG&G PARC Model 175 universal programmer and a Model 173 potentiostat with a Model 178 electrometer. CVs were recorded using a Linseis LY1400 plotter. All CV were obtained in dry, nitrogen degassed acetonitrile solutions containing 0.2M tetra butyl ammonium tetrafluoroborate background electrolyte. Unless otherwise stated, the reference electrode was Ag/AgNO₃ saturated acetonitrile solution, the working electrode was glassy carbon and the counter electrode was platinum. Potentials were converted so that they were referenced to the standard calomel electrode (SCE) by scaling to a new “zero” at - 0.29V with respect to the Ag/AgNO₃ zero¹.

2.1.4 X - ray Crystallographic Data Collection

Crystallographic data were obtained from a number of sources, using both conventional laboratory X-ray sources and the synchrotron radiation source at CLRC Daresbury.

At the University of Glasgow, data was collected by Drs. Louis Farrugia, Dimitri Yufit and Ken Muir on an Enraf - Nonius CAD4 diffractometer using graphite monochromated (Mo-K_α) X - ray radiation ($\lambda = 0.71069\text{\AA}$). Data collection was facilitated by use of CAD4 Express software and data reduction was effected by the XCAD4 program.

At the University of Edinburgh, data was obtained by Dr Simon Parsons on a Stoe Stadi-4 diffractometer using graphite monochromated (Cu-K_α) X - ray radiation ($\lambda = 1.54178\text{\AA}$). Data collection was facilitated by use of the Stoe DIF4 program and data reduction was effected by use of the Stoe REDU4 program.

At the University of Durham, data was obtained by Dr Dimitri Yufit on a Siemens SMART CCD area detector using graphite monochromated (Mo-K_α) X-ray radiation ($\lambda = 0.71073\text{\AA}$). Data collection was effected by use of the SMART suite of programs, frame integration was achieved by use of the SAINT program and absorption corrections performed by the SADABS program.

Crystallographic data obtained using the synchrotron radiation source at Daresbury was collected with the assistance of Dr Simon Teat and Professor William Clegg at Station 9.8. The station specialises in single crystal diffraction from

small or weakly diffracting samples which are inaccessible to conventional laboratory X - ray sources. This was made possible by the high photon flux produced by the SRS 5 Tesla Wiggler magnet. The wavelength of the radiation was variable but was generally close to that produced by a conventional molybdenum source. A Siemens SMART CCD area detector was used for data collection in combination with the SMART suite of programs. Frame integration was achieved by use of the SAINT program and absorption corrections performed by the SADABS program.

All crystallographic data was collected in the ω - 2θ scan mode at low temperatures, typically in the range 160 to 220K, using crystals mounted on glass fibres. Structure solution and refinement was carried out using the Glasgow WinGX - 96² suite of programs, in particular SIR 92³ and SHELXL 93⁴.

2.1.5 Time Resolved Fluorescence/Transient Absorbance Studies

(a) Picosecond Time Resolved Data

Laser spectroscopic studies which required time-resolution on the picosecond scale were performed by Professor Anthony Harriman at the Université Louis Pasteur. The measurements⁵ were made using a mode-locked, frequency doubled Antares 76S Nd:YAG laser as the excitation pump for a Coherent Model 700 pyromethene dual-jet dye laser. The spectrometer was run at 10 Hz and the output pulse was split to produce excitation and monitoring pulses. Output from the pyromethene dye laser was at 565nm with a pulse width of 0.3ps. The monitoring pulse was delayed with a computerised optical delay stage and spectra were acquired with a Princeton dual diode array spectrograph. About 600 individual laser shots were averaged for each time delay and kinetic profiles were constructed by overlaying spectra collected at about 50 different delay times. Kinetic profiles were analysed by non - linear least squares iteration using global analysis methodology.

(b) Nanosecond time Resolved Data

Laser spectroscopic studies which required time - resolution on the nanosecond scale were performed with the assistance of Dr Andrew McLean at the University of Paisley. The measurements were made using a Spectron Laser Services SL803 Q-switched Nd YAG solid state laser at 532nm. The laser pulse

duration was 15ns at an output energy of 800 μ J. Laser energy was monitored using a Laser Precision Corp. RM-6600 universal radiometer. Transient fluorescence spectra were recorded using an Applied Photophysics photomultiplier, an Applied Photophysics f/3.4 monochromator and a Tektronix TDS520 two channel digitising oscilloscope. All data was analysed using an On Line Instrument Systems kinetic fit (1989) program.

2.1.6 Molecular Modelling

Molecular modelling was undertaken using the Hyperchem (release 4.5 for windows, © Hypercube Inc. 1994) molecular modelling and simulation software. Geometry optimisations of molecular models were carried out using the MM⁺ force field, utilising a Polak - Ribiere algorithm, terminating at an RMS gradient of 1×10^{-4} kcal/ \AA mol. The use of such models proved to be a powerful tool in determining whether a successful outcome to a synthetic strategy was likely and also whether the target molecule would have the desired shape, and thus function, prior to embarking on protracted synthetic procedures.

2.2 Chemicals and Solvents

Chemicals, their suppliers and purity used in preparative work are listed in table 2.2.1. Solvents and purification techniques are listed in table 2.2.2.

Table 2.2.1 Chemicals, Suppliers and Purity

Acetic Acid (Glacial)	(Prolabo)	100%
Adipic Acid	(Koch - Light)	99%
(L)-Alanine	(Sigma)	99%
Aluminium Oxide, Neutral (Brockmann Grade 1)	(BDH)	99+ %
Ammonium Chloride	(Fisons)	99.5%
Ammonium Hexafluorophosphate	(Fluka)	98%
2,2'-Azobis-(2-methylpropionitrile) (AIBN)	(Janssen)	98+ %
Barium Carbonate	(BDH)	99.5%
Benzyl Bromide	(Aldrich)	98%
4-(Benzyloxy)phenol	(Lancaster)	98+ %

2,2'-Bipyridine	(Aldrich)	99+ %
4,4'-Bipyridine	(Lancaster)	98%
N-Bromosuccinimide (NBS)	(Aldrich)	99%
Bromo-Trimethylsilane	(Aldrich)	97%
Cyclohexene	(Aldrich)	99%
2-(2-Chloroethoxy)ethanol	(Lancaster)	99%
2-[2-(2-Chloroethoxy)ethoxy]ethanol	(Aldrich)	98%
Copper (I) Oxide	(BDH)	97.5%
<i>p</i> -Cyanobenzylbromide	(Aldrich)	99%
α,α' -Dibromoxylene	(Aldrich)	97%
1,1-Dichloroethene	(Aldrich)	99%
Dihydroxybenzene (DHB)	(Fluka)	99%
1,5-Dihydroxynaphthalene	(Aldrich)	97%
Dimethoxybenzene (DMB)	(Aldrich)	99%
4,4'-Dimethyl-2,2'-Bipyridine	(Aldrich)	99%
4,4'-Dimethyl-diphenyl	(R.N. Emanuel)	99%
Dimethylglyoxime	(Avocado)	99%
4,7-Dimethyl-1,10-Phenanthroline	(Aldrich)	98%
Disodium(+)- <i>O,O'</i> -dibenoxyl-D-tartrate	(Aldrich)	99%
Ferrocene	(BDH)	99%
1,1'-Ferrocenedicarboxylic Acid	(Aldrich)	96%
(L)-Glutamic Acid	(Sigma)	99%
Hydrochloric Acid	(Fisher)	S.G. 1.18
Iron Sulphate Heptahydrate	(BDH)	98%
Lithium Chloride	(BDH)	99%
Lithium Aluminium Hydride	(EGA)	96%
Magnesium Sulphate	(BDH)	99%
Nickel Aluminium Alloy	(Riedel De Haen)	97%
Osmium Trichloride Hydrate	(Strem)	#54.25%
Oxalyl Chloride	(Aldrich)	99%
Palladium	(Lancaster)	10% on carbon
Palladium Hydroxide	(Aldrich)	20% on carbon (moist)

3-Picoline	(Aldrich)	99%
Phosphorous Pentoxide	(Riedel De Haen)	98.5%
Phthalic Anhydride	(Aldrich)	99%
Potassium <i>t</i> -Butoxide	(Aldrich)	95%
Potassium Carbonate	(May & Baker)	99%
Potassium Nitrate	(Koch -Light)	99.9%
Pyridine	(Aldrich)	99+ %
Ruthenium Trichloride Hydrate	(Johnson Matthey)	#42.75 %
Selenium Dioxide	(Aldrich)	99.8%
Sephadex LH-20	(Fluka)	-----
Sephadex G-15	(Sigma)	-----
Sephadex G-25	(Aldrich)	-----
Silica Gel 40-60 μ m	(PhaseSep)	99.5%
Silver Hexafluorophosphate	(Fluka)	98%
Sodium Acetate	(Hopkin & Williams)	99%
Sodium Carbonate	(BDH)	99.9%
Sodium Chloride	(Fisons)	99.9%
Sodium Hydride	(Aldrich)	60% Dispersion in Mineral Oil
Sodium Hydroxide	(Fisons)	97%
Sodium Iodide	(BDH)	99%
Sodium Sulphite Heptahydrate	(Riedel De Haen)	96%
Sodium Tetrafluoroborate	(Aldrich)	98%
Sodium Tetrphenylborate	(Aldrich)	99.5%
Succinic Acid	(BDH)	99%
Sulphuric Acid	(Prolabo)	95%
(L)-Tartaric Acid	(BDH)	99.5%
Tetraethylene Glycol	(Aldrich)	99%
Tetrafluoroboric Acid Etherate	(Aldrich)	85%
Tetramethylphenylenediamine (TMPD) Dihydrochloride	(Aldrich)	96%
<i>p</i> -Toluene Sulphonyl Chloride	(Aldrich)	98%
Trifluoroacetic Acid	(Aldrich)	99%
Zinc Triflate	(Aldrich)	98%

Purity stated as % metal in salt.

Table 2.2.2 Solvents and Purification Methods

Acetone	Distilled from potassium carbonate under N ₂ .
Acetonitrile	Distilled from calcium hydride under N ₂ .
Benzene	Distilled from sodium benzophenone under N ₂ .
<i>t</i> - Butyl Alcohol	Stored over 4Å sieves.
Carbon Tetrachloride	Distilled from phosphorous pentoxide under N ₂ .
Chloroform	Distilled from phosphorous pentoxide under N ₂ .
Cyclohexane	Distilled from sodium under N ₂ .
Dichloromethane	Distilled from calcium hydride under N ₂ .
Diethylether	Distilled from sodium benzophenone under N ₂ .
Dimethylformamide	Dried over magnesium sulphate and stored over 4Å sieves.
Dimethylsulphoxide	Stored over 4Å sieves.
Dioxane	Distilled from sodium benzophenone under N ₂ .
Ethanol	Twice distilled from magnesium turnings and iodine under N ₂ . Stored over 4Å sieves.
Ethyl Acetate	Distilled from calcium hydride under N ₂ .

Ethylene Glycol	Stored over magnesium sulphate.
Methanol	Stored over 4Å sieves.
Nitromethane	Stored over 4Å sieves.
40 - 60°C Petroleum Ether	Distilled from sodium under N ₂ .
Tetrahydrofuran	Distilled from sodium benzophenone under N ₂ .
Toluene	Distilled from sodium under N ₂ .

2.3 Synthesis

2.3.1 Precursors

(a) 4,4'-Bis(bromomethyl)-2,2'-bipyridine

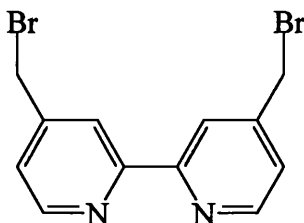
The literature procedure⁶ for brominating 4,4'-dimethyl-2,2'-bipyridine produces a yield of only 30%. The literature procedure involves a thermal reaction between N-bromosuccinimide and the dimethyl compound in carbon tetrachloride, using AIBN as a radical initiator, followed by extensive column chromatography to yield pure product. In an effort to improve the yield of this reaction, a variety of synthetic routes⁷, summarised in table 2.3.1, were attempted: all involve irradiation of the reaction mixture. Many of the variations involved subtle changes in reaction conditions, solvent mixture or reactant concentrations thus only the most productive method is detailed below.

Reagent Used	Solvent Mixture	AIBN/DCE Added?		Yield (%)
CuBr ₂	Acetic Acid	N	N	NIL
NBS	DCM	N	N	20
NBS	1:1 DCM/CCl ₄	N	N	20
NBS	CCl ₄	Y	N	30
NBS	95:5 DCM/CCl ₄	Y	N	45
NBS	95:5 DCM/CCl ₄	Y	Y (500mg)	NIL
NBS	95:5 DCM/CCl ₄	Y	Y (30mg)	NIL
NBS	Benzene	Y	N	5

Table 2.3.1 Summary of Bromination Conditions

The use of 1,1 - dichloroethene (DCE) was conceived⁸ with the hope of controlling the bromine radical chain (DCE is known to be an excellent radical scavenger) thus preventing over - bromination of the dimethyl compound. Clearly the DCE had too powerful an effect on the radical chain - an effect that will be discussed later in this thesis.

Most Productive Route to 4,4'-Bis(bromomethyl)-2,2'-bipyridine.



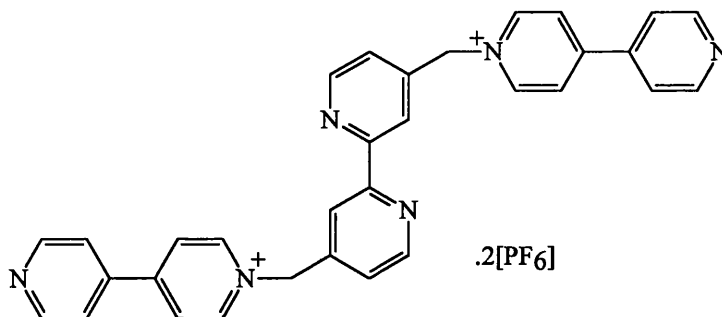
To a mixture of 4,4'-dimethyl-2,2'-bipyridine (9.84g, 53.5mmol) and N-bromosuccinimide (19.72g, 111mmol) in dry carbon tetrachloride/dichloromethane (95:5, 370ml) was added AIBN (100mg). The resulting solution was stirred and heated gently (40°C) whilst being irradiated with a 500W halogen lamp under a nitrogen atmosphere for three hours.

After the reaction had cooled, the reaction vessel was immersed in ice water in order to precipitate all the succinimide by-product. The reaction mixture was filtered and the remaining solution was evaporated to dryness *in vacuo*. The residue was partitioned between dichloromethane (200ml) and distilled water (200ml) and the organic layer concentrated *in vacuo* before being purified by column chromatography [SiO₂, DCM/Acetone/Methanol (97:2:1)]. The product may be precipitated from the concentrated eluent as a colourless solid by the addition of cyclohexane.

Yield = 8.16g , 45.0%

¹H NMR (CDCl₃): 4.46 (s, 4H); 7.34 (dd, J = 1.7Hz, J' = 5.0Hz, 2H); 8.42 (s, 2H); 8.65 (d, J = 5.0Hz, 2H).

(b) **4,4'-Bis(methylene-4,4'-bipyridinium)-2,2'-bipyridine
Bis(Hexafluorophosphate)⁹ (P1)**



A solution of 4,4'-Bis(bromomethyl)-2,2'-bipyridine (0.914g, 2.67mmol) in dry acetonitrile (110ml) was added over 6 hours to a solution of 4,4'-bipyridine (1.018g, 6.52mmol) in dry, refluxing acetonitrile (100ml). Heating was continued for 18 hours. After the solution had cooled to room temperature, the yellow precipitate was filtered off and washed with acetonitrile (50ml) and diethyl ether (50ml) before being dissolved in water (500ml). The aqueous solution was washed with diethyl ether (4 x 200ml) and then concentrated *in vacuo*. A saturated aqueous solution of ammonium hexafluorophosphate was added to the concentrated aqueous solution until no further precipitation was observed. The precipitate was filtered off and washed with water (30ml), methanol (30ml) and diethyl ether (30ml). Finally, the product was recrystallised from acetone - water to afford the product as a cream coloured solid.

Yield = 1.42g, 64.7%

¹H NMR (d₆ - acetone): 6.33 (s, 4H); 7.64 (dd, J = 2.0Hz, J' = 5.0Hz, 2H); 8.00 (dd, J = 6.2Hz, J' = 1.7Hz, 4H); 8.66 (s, 2H); 8.77 (bd, J = 7.0Hz, 4H); 8.80 (d, J = 5.2Hz, 2H); 8.87 (d, J = 6.2Hz, 4H); 9.51 (d, J = 7.2Hz, 4H).

FAB - MS (NBA matrix) m/z = 639 (M - PF₆)⁺; 493 (M - 2PF₆)⁺.

Calculated for C₃₂H₂₆N₆P₂F₁₂ C: 48.98%, H: 3.32%, N: 10.71% found C: 47.28%, H: 3.69%, N: 9.87%.

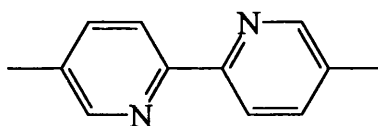
Electrochemical data: E_{1/2} = - 0.88V (2e) vs SCE.

(c) **Raney Nickel W7-J¹⁰**

Nickel - aluminium alloy (1:1, 25g) was added in portions to a solution of sodium hydroxide (32g) in water (150ml) over 15 minutes. The reaction was carried out in a 1L conical flask immersed in an ice-bath and equipped with a very efficient (mechanical) stirrer to control frothing. The temperature quickly reached 80-85°C.

As soon as the addition of the alloy was complete, the cooling bath was removed and stirring was continued for 1.5 hours to control frothing. When the reaction began to subside and the temperature began to fall, the flask was immersed in a boiling water bath and gentle stirring was continued for 30minutes. The stirrer was then removed and distilled water (200ml) added. The supernatant liquid was decanted and the catalyst then washed by decantation with distilled water (8 x 200ml). The pyrophoric catalyst was stored under distilled water.

(d) **5,5'-Dimethyl-2,2'-bipyridine¹⁰**



Wet Raney Nickel W7-J catalyst (20g) was placed in a 1L three - necked flask fitted with a condenser (closed at the top with a stopper), a dropping funnel containing 3-picoline (50ml) and a connection to a water pump. The flask was slowly evacuated and warmed in a water bath - care was taken to avoid loss of catalyst by frothing. After two hours at 100°C over 20mm Hg the flask was removed from the water bath. The 3-picoline was then added to the catalyst *via* the dropping funnel, care being taken to avoid access of air until the catalyst had been thoroughly wetted. The stopper was then removed and the mixture refluxed for two days.

After this time, the catalyst was filtered off (CARE - pyrophoric!) and quickly washed with hot 3-picoline. The unreacted 3-picoline was removed by distillation (B.Pt. 144.1°C / 767mm Hg) and the residue extracted with boiling 60 - 80° petroleum ether. This solution was purified by passage through a column of alumina (DCM was used to aid elution), the solvent evaporated and the resulting product recrystallised from ethanol to give colourless needles.

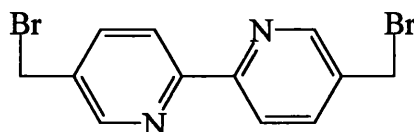
Yield = 390mg, 3.8%.

The low yield of this product may be attributable to a number of problems with the reaction work-up; it is difficult to wash the pyrophoric catalyst with sufficient hot picoline without exposing it to air, the 3-picoline “bumps” excessively under distillation (even with very a gentle heating increment) and also the alumina column seems to irreversibly adsorb some product.

$^1\text{H NMR}$ (CDCl_3): 2.34 (s, 6H); 7.56 (dd, $J = 1.7\text{Hz}$, $J' = 8.0\text{Hz}$, 2H); 8.21 (d, $J = 8.0\text{Hz}$, 2H); 8.45 (s, 2H).

EI - MS $m/z = 184$ (M^+).

(e) **5,5'-Bis(bromomethyl)-2,2'-bipyridine^{11(a)}**



5,5'-Dimethyl-2,2'-bipyridine (390mg, 2.12mmol) and N-bromosuccinimide (870mg, 4.88mmol) were refluxed in carbon tetrachloride (300ml) for 4 hours in the presence of AIBN (35mg, 0.212mmol).

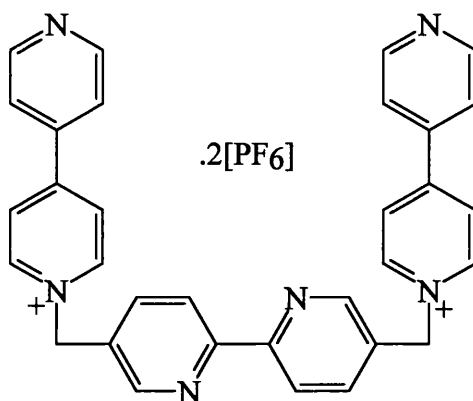
After this time, the solution was concentrated *in vacuo*, cooled in an ice bath and the precipitated succinimide filtered off. The solvent was then removed and the residue was purified by column chromatography [SiO_2 , CHCl_3] to yield the pure product.

Yield = 254mg, 35%.

$^1\text{H NMR}$ (CDCl_3): 4.51 (s, 4H); 7.83 (dd, $J = 2.3\text{Hz}$, $J' = 8.2\text{Hz}$, 2H); 8.37 (d, $J = 8.0\text{Hz}$, 2H); 8.66 (s, 2H).

EI - MS $m/z = 342$ (M^+); 217 ($\text{M} - \text{Br}$)⁺; 182 ($\text{M} - 2\text{Br}$)⁺.

**(f) 5,5'-Bis(methylene-4,4'-bipyridinium)-2,2'-Bipyridine
Bis(hexafluorophosphate) (P2)^{11(b)}**



A similar procedure to that used in 2.3.1 (b) was employed to produce this precursor molecule with the exception that 5,5'-Bis(bromomethyl)-2,2'-bipyridine (50mg, 0.15mmol) in dry acetonitrile (20ml) was used rather than the 4,4'-derivative. 4,4'-bipyridine (58.2mg, 0.37mmol) in dry acetonitrile (20ml) was refluxed with the bromomethyl compound as in 2.3.1 (b).

Yield = 23.0mg, 12.1%.

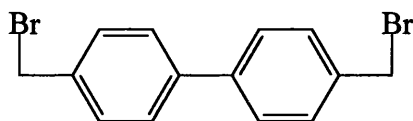
The poor yield may again be attributed to the reaction work-up: compound P2 seems to have a greater solubility in methanol than does P1 - some product may have been lost during the methanol wash.

¹H NMR (d₃ - acetonitrile): 5.89 (s, 4H); 7.83 (dd, J = 1.6Hz, J' = 4.5Hz, 4H); 8.03 (dd, J = 2.2Hz, J' = 8.2Hz, 2H); 8.38 (d, J = 6.9Hz, 4H); 8.56 (d, J = 8.2Hz, 2H); 8.84 (s, 2H); 8.87 (m, 4H); 8.93 (d, J = 6.9Hz, 4H).

FAB - MS (NBA matrix) m/z = 693 (M - PF₆)⁺.

(g)

4,4'-Bis(bromomethyl)-diphenyl¹²



4,4'-Dimethyl-diphenyl (2.5g, 13.74mmol) and N-bromosuccinimide (4.88g, 27.48mmol) were refluxed in carbon tetrachloride (500ml) for 4 hours in the presence of AIBN (23mg, 0.14mmol).

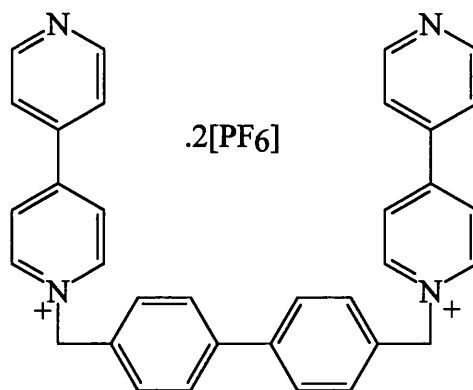
After this time the solution was cooled to room temperature and the succinimide by-product filtered off. Removal of the solvent *in vacuo* yielded the product.

Yield = 3.51g, 75.2%.

¹H NMR (CDCl₃): 4.54 (s, 4H); 7.48 (bm, 8H).

EI - MS m/z = 340 (M⁺); 260 (M - Br)⁺; 181 (M - 2Br)⁺.

(h) **4,4'-Bis(methylene-4,4'-bipyridinium)-diphenyl
Bis(hexafluorophosphate) (P3)¹²**



A similar procedure to that used in 2.3.1 (b) was employed to produce this precursor molecule with the exception that 4,4'-Bis(bromomethyl)-diphenyl (3.18g, 9.35mmol) in dry acetonitrile (100ml) was used instead of a bipyridine derivative. 4,4' - bipyridine (3.50g, 22.41mmol) in dry acetonitrile (120ml) was refluxed with the bromomethyl - diphenyl compound as in 2.3.1 (b).

Yield = 6.80g, 93.0%.

¹H NMR (d₆ - acetone): 6.19 (s, 4H); 7.84 (m, 8H); 8.12 (m, 4H); 8.72 (d, J = 6.95Hz, 4H); 8.95 (dd, J = 1.5Hz, J' = 4.6Hz, 4H); 9.42 (d, J = 7.0Hz, 4H).

FAB - MS (NBA matrix) m/z = 637 (M - PF₆)⁺.

(i) **cis-[Ru(2,2'-bipyridine)₂Cl₂].xH₂O¹³**

RuCl₃.3H₂O (7.8g, 29.8mmol), 2,2'-bipyridine (9.36g, 60.0mmol) and LiCl (8.4g, 2mmol) were heated at reflux in reagent grade DMF (50ml) for 8 hours. The reaction was stirred magnetically throughout this period.

After the reaction mixture had cooled to room temperature, reagent grade acetone (250ml) was added and the resultant solution cooled to 0°C overnight. Filtering yielded a red - violet solution and a dark green - black microcrystalline product. The solid was washed three times with water (25ml) followed by diethyl ether (25ml) and then dried by suction.

Yield = 7.68g, 62.0%.

(j) **cis-[Ru(bipy)₂(pyridine)₂]Cl₂¹⁴**

cis-[Ru(2,2' - bipyridine)₂Cl₂].xH₂O (7.0g, 14.5mmol) was refluxed for three hours in a solution of distilled water (140ml) and pyridine (70ml). During this time the reaction mixture changed in colour from black to light orange. After the reaction

mixture had cooled to ambient temperature, the filtered solution was evaporated to dryness, the brown residue taken up in methanol (140ml) and the complex precipitated as orange needles by the addition of diethyl ether. After standing for one hour the crystals were collected and washed with ether.

Yield = 8.79g, 94.7%

(k) Resolution of Λ -cis-[Ru(bipy)₂(pyridine)₂]²⁺

An aqueous solution of 0.5M disodium (+)-*O,O'*-dibenzoxy-L-tartrate (45ml) was added to a solution of cis-[Ru(bipy)₂(pyridine)₂]Cl₂ (4.5g, 7.0mmol) in distilled water (90ml). The mixture was stirred for 10 minutes, and then the solvent was allowed to evaporate naturally in a darkened cupboard for 10 days. After this time, the dark red crystals of Λ -cis-[Ru(bipy)₂(pyridine)₂][(+)-*O,O'*-dibenzoxy-L-tartrate]¹⁵ were collected by filtration. The product was washed with cold water and air dried.

Yield = 1.14g, 33.5%.

The optical purity of this compound was confirmed by obtaining the Circular Dichroism (CD) spectrum of the product. The CD spectrum was recorded on a Jobin Yvon HRS 2 spectrometer and recorded using a Venture RE 541 recorder. The CD spectrum observed for the product was exactly as expected, being the exact obverse of the Δ -diastereoisomer as reported in the literature. At low energies the CD is strongly positive (for example, at 360nm, $\Delta\epsilon = 25.92$) and at higher energies the CD is negative.

(l) cis-[Os(2,2' - bipyridine)₂Cl₂].xH₂O¹⁶

Lithium chloride (0.95g, 22.4mmol) was dissolved in dry, degassed DMF (25ml) with gentle warming. Osmium trichloride hydrate (0.50g, 1.68mmol) was added to the reaction mixture under nitrogen, followed by 2,2'-bipyridine (0.53g, 3.40mmol). The reaction mixture was refluxed for three hours, whereupon the solution became brown - red in colour. Upon cooling to room temperature methanol (10ml) was added to the reaction mixture. To ensure complete reduction of Os (III) to Os(II), a dilute aqueous solution of sodium sulphite was then added to the reaction mixture dropwise, with stirring, until the reaction mixture became deep purple - red in colour. The reaction mixture was then added to reagent grade acetone (300ml) and cooled to 0°C overnight to yield a dark red crystalline precipitate which was isolated by filtration and washed with distilled water (to

remove excess lithium chloride) prior to drying *in vacuo* for six hours at room temperature.

Yield = 250mg, 25.8%.

¹H NMR (d₆ - DMSO): 7.13 (m, 4H); 7.73 (m, 4H); 8.56 (d, J = 6.5Hz), 4H); 8.81 (m, 4H).

FAB - MS (NBA matrix): m/z = 574 (M⁺).

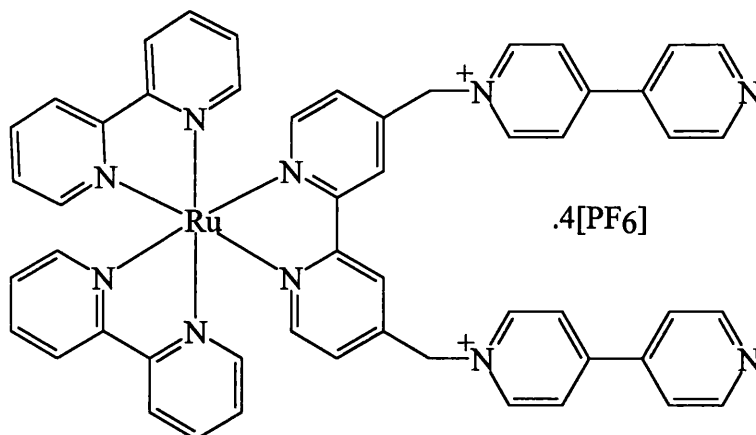
Calculated for C₂₀H₂₀N₄Cl₂O₂O_s C: 39.41%, H: 3.31%, N: 9.19% found C: 39.71% H: 3.43% N: 9.86%

(m) Copper (I) Tetrakis(acetonitrile) Hexafluorophosphate¹⁷

Copper (I) oxide (5.7g, 0.04mol), dried over phosphorous pentoxide, was suspended in acetonitrile (25ml) and tetrafluoroboric acid etherate (11.4g, 0.08mol) was added. the mixture was heated for one hour with stirring to reflux temperatures and then filtered whilst hot. The solid residue was washed with hot acetonitrile (20ml) and the combined filtrates allowed to cool to room temperature whereupon the colourless crystalline product precipitated. The product was filtered off and washed with diethyl ether. The compound was stored over phosphorous pentoxide in a nitrogen atmosphere.

Yield = 15.60g, 82.5%. M.Pt. = 158 - 161°C (lit. = 167°C).

(n) [Ru(2,2'-bipyridine)₂(4,4'-Bis(methylene-4,4'-bipyridinium-2,2'-Bipyridine)] Tetrakis(hexafluorophosphate)⁹



Compound **P1** (375mg, 0.48mmol) and Λ -cis-[Ru(bipy)₂(pyridine)₂][(+)-*O,O'*-dibenzoyl-L-tartrate] (450mg, 0.46mmol) were added to ethylene glycol (12ml, 10% distilled water) in a 25ml round bottomed flask. The reaction mixture was stirred and heated to 120°C for four hours before being cooled to room temperature and diluted with distilled water (18ml).

The resultant solution was then filtered and a saturated aqueous solution of ammonium hexafluorophosphate was added dropwise to the filtrate until no further precipitation was observed. The solid was collected by filtration and washed with distilled water. The material was then purified by column chromatography [SiO₂, MeOH / 2N NH₄Cl / MeNO₂ (7:2:1)].

Yield = 425mg, 62.3%.

¹H NMR (d₆ - acetone): 6.28 (s, 4H); 7.55 (m, 4H); 7.65 (d, J = 5.7Hz, 2H); 7.96 - 7.98 (m, 4H); 8.01 (m, 4H); 8.11 (d, J = 5.8Hz, 2H); 8.19 (m, 4H); 8.62 (d, J = 6.4Hz, 4H); 8.75 - 8.81 (m, 6H); 8.90 (m, 4H); 9.28 (d, J = 6.3Hz, 4H).

FAB - MS (NBA matrix) and Electrospray MS: m/z = 1343 (M - PF₆)⁺; 1197 (M - 2PF₆)⁺; 1052 (M - 3PF₆)⁺.

Calculated for C₅₆H₅₂N₁₀P₄F₂₄Ru C: 43.02%, H: 3.35%, N: 8.96%, found C: 42.86%, H: 3.14%, N 9.05%.

Electrochemical data: E_{1/2} = 1.27V (1e); E_{1/2} = - 0.90V (2e) vs SCE.

(o) [Os(2,2'-bipyridine)₂][(4,4'-Bis(methylene-4,4'-bipyridinium)-2,2'-Bipyridine)] Tetrakis(hexafluorophosphate)⁹

A similar synthetic strategy to that employed in 2.3.1 (n) above was used to produce this compound, expect that the reaction mixture contained cis-[Os(2,2'-bipyridine)₂Cl₂].xH₂O (103mg, 0.16mmol) and compound P1 (168.7mg, 0.21mmol) in ethylene glycol (5.5ml, 10% water). The reaction mixture was heated to 160°C rather than 120°C to facilitate reaction of the osmium complex.

Yield = 70mg, 27.0%.

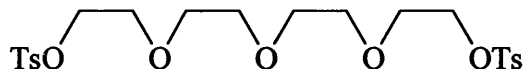
¹H NMR (d₆ - acetone): 6.31 (s, 4H); 7.47 (m, 6H); 7.84 - 7.99 (m, 10H); 8.25 (d, J = 6.4Hz, 4H); 8.65 (d, J = 6.9Hz, 4H); 8.73 - 8.74 (m, 6H); 9.04 (m, 4H); 9.30 (d, J = 8.9Hz, 4H).

Electrospray MS: m/z = 1433 (M - PF₆)⁺; 1287 (M - 2PF₆)⁺; 1141 (M - 3PF₆)⁺.

Electrochemical data: E_{1/2} = 0.81V; E_{1/2} = - 0.85V vs SCE.

2.3.2 Crown Ethers and Related Guest Molecules

(a) **Tetraethyleneglycol Bitosylate¹⁸**

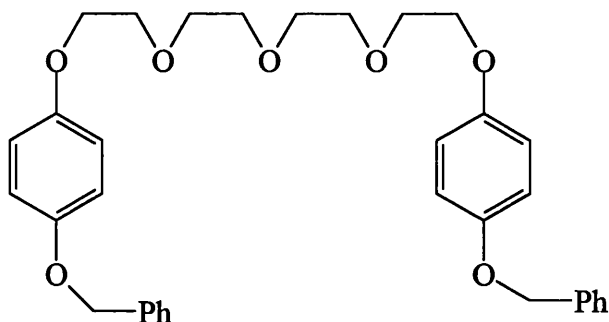


A 3L three necked round bottomed flask equipped with a mechanical stirrer, dropping funnel and thermometer was charged with *p* - toluene sulphonyl chloride (216g, 1.13mol) dissolved in acetone (500ml). Tetraethylene glycol (110g, 0.57mmol) was added to the solution and the mixture was cooled to below 15°C. Meanwhile, sodium hydroxide (45g, 1.13mol) was dissolved in distilled water (250ml) and the solution cooled to room temperature. The cooled sodium hydroxide solution was added dropwise to the mixture, keeping the temperature below 20°C. When the last sodium hydroxide solution had been added, the mixture was stirred for a further one hour, then added to three litres of iced water whilst being stirred vigorously. The product was extracted from the water using dichloromethane (3 x 300ml). The solvent was removed *in vacuo* to yield a pale yellow oil.

Yield = 215.8g, 80.6%.

¹H NMR (CDCl₃): 2.37 (s, 6H); 3.57 (m, 8H); 3.59 (m, 4H); 3.63 (m, 4H); 7.33 -7.86 (dd, J = 8.0Hz, J' = 74.6Hz, AA'BB' system, 8H).

(b) 1,11-Bis[4-(benzyloxy)phenoxy]-3,6,9-trioxaundecane¹⁹



A solution of 4-(benzyloxy)phenol (35.08g, 175mmol) in dry DMF (280ml) was added over 20 minutes to a suspension of sodium hydride (8.65g 60% dispersion in mineral oil, washed previously with cyclohexane) in dry DMF (120ml), with stirring under a nitrogen atmosphere.

After an additional 15 minutes, tetraethyleneglycol bitosylate (46.4g, 90.8mmol) dissolved in dry DMF (400ml) was added over a two and a half hours and the temperature was raised to 80°C. Stirring and heating were continued for 24 hours.

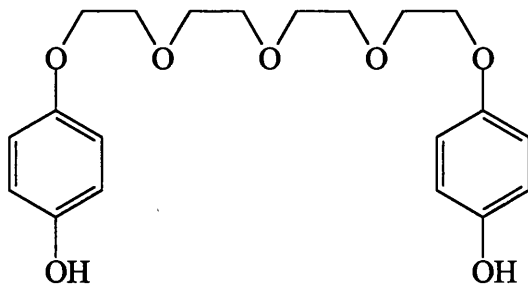
After the reaction had cooled to room temperature, the slight excess of NaH was quenched by the addition of a few drops of distilled water. The solvent was then removed *in vacuo* and the residue partitioned between dichloromethane (500ml) and water (280ml). The organic phase was washed with water and dried (MgSO₄).

Evaporation of the solvent *in vacuo* afforded a solid residue which on recrystallisation from ethanol / cyclohexane (2:1) afforded the product as a cream solid.

Yield = 39.4g, 77.8%.

¹H NMR (CDCl₃): 3.64 (m, 8H); 3.76 (m, 4H); 4.02 (m, 4H); 4.93 (s, 4H); 6.79 (m, 8H); 7.18 - 7.34 (m, 10H).

(c) 1,11-Bis(4-hydroxyphenoxy)-3,6,9-trioxaundecane²⁰



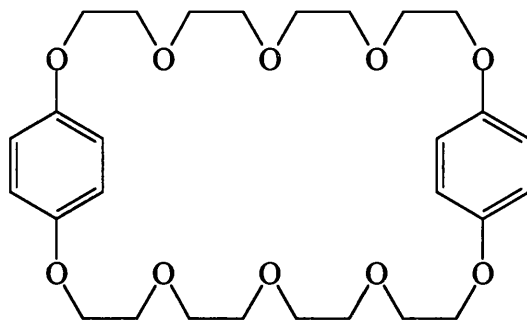
A solution of 1,11-Bis[4-(benzyloxy)phenoxy]-3,6,9-trioxaundecane (39.0g, 75mmol) in ethanol (300ml) to which cyclohexene (330ml) had been added was placed in a round bottomed flask. Palladium hydroxide (20% on carbon, moist, 9.54g) was added and the suspension was stirred under reflux for three hours. After filtration of the catalyst (which was then recycled for further use), the solvent was removed *in vacuo* to yield the product as a viscous pale yellow oil.

Yield = 24.95g, 83.7%.

¹H NMR (CDCl₃): 3.59 - 3.74 (m, 8H); 3.67 (m, 4H); 3.97 (m, 4H); 6.63 (bs, 8H).

(d) 1,4,7,10,17,23,26,28,32-Decaoxa[13,13]paracyclophane¹⁹

(34C10)



A solution of 1,11 - Bis(4-hydroxyphenoxy) - 3,6,9 - trioxaundecane (24.95g, 70mmol) in dry THF (500ml) and a solution of tetraethyleneglycol bitosylate (33.86g, 72mmol) in dry THF (600ml) were added simultaneously over two hours to a stirred suspension of NaH (9.50g, 60% dispersion in mineral oil, washed previously with cyclohexane) in dry THF (600ml) under nitrogen. The mixture was refluxed for five days before being cooled to room temperature. Excess NaH was quenched by the addition of a few drops of distilled water and the solvent was removed *in vacuo*. The residue was then partitioned between DCM (500ml) and water (300ml). Sodium chloride was added to break up the emulsion that formed during the partitioning process. The organic phase was washed with 2N HCl (160ml) and distilled water (160ml), dried (MgSO₄) and finally concentrated *in vacuo*.

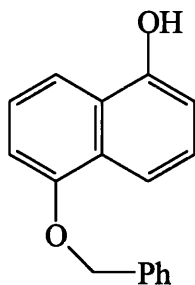
Column chromatography [SiO₂, diethyl ether/chloroform/methanol (68:30:2)] afforded the product as a white solid upon removal of solvent from the eluent. Finally, the product was recrystallised from acetone- cyclohexane.

Yield = 1.99g, 5.8%.

¹H NMR (CDCl₃): 3.60 - 3.68 (m, 16H); 3.78 (m, 8H); 4.02 (m, 8H); 6.79 (s, 8H).

EI - MS: m/z = 536 (M⁺).

(e) **1-Benzoxyl-5-hydroxyl naphthalene**²¹



A solution of 1,5-dihydroxy naphthalene (1g, 6.25mmol) in DMF (50ml) was added to a stirred suspension of potassium carbonate (0.97g, 7mmol) in DMF (50ml). After 30 minutes benzyl bromide (1.07g, 6.25mmol) in DMF (30ml) was added dropwise whilst maintaining the reaction mixture at ambient temperature. Stirring was continued for 18 hours.

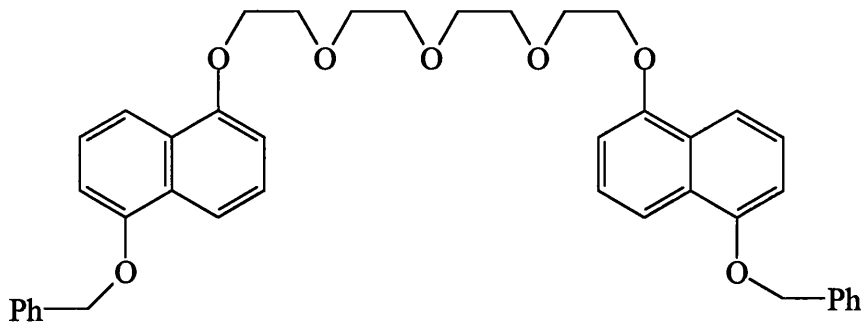
After this time the solvent was removed *in vacuo* and the residue was partitioned between DCM (80ml) and distilled water (30ml). The organic phase was washed with distilled water, dried (MgSO₄) and the solvent was removed *in vacuo*. The residue was purified by column chromatography [SiO₂, chloroform].

Yield = 230mg (15.6%).

¹H NMR (CDCl₃): 5.24 (s, 2H); 5.48 (bs, 1H); 6.84 (d, J = 7.4Hz, 1H); 6.91 (d, J = 7.6Hz, 1H); 7.27 - 7.54 (m, 7H); 7.77 (d, J = 8.5Hz, 1H); 7.94 (d, J = 8.5Hz, 1H).

EI -MS: m/z = 250 (M⁺).

(f) 1,11-Bis[5'-(benzyloxy)naphthoxy]-3,6,9-trioxaundecane²¹



A similar procedure to that used to prepare the phenoxy - analogue (2.3.2 (b)) was used to prepare this compound with a few minor modifications as noted below.

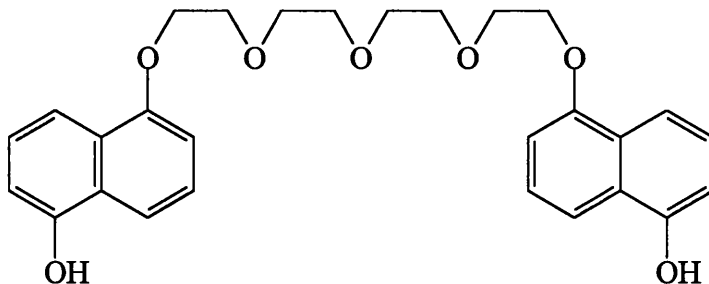
The reaction mixture contained 1-benzoyl-5-hydroxyl naphthalene (3.80g, 15.39mmol) in dry DMF (100ml), sodium hydride (1.90g, 60% dispersion in mineral oil, washed previously with cyclohexane) in dry DMF (40ml) and tetraethylene glycol bitosylate (3.90g, 7.72mmol) in dry DMF (100ml). The reaction mixture was stirred and heated for 18 hours at 70°C. The residue obtained after work up of the reaction was purified by column chromatography [SiO₂, chloroform / diethyl ether / methanol (35:45:20)].

Yield = 4.00g, 39.5%.

¹H NMR (CDCl₃): 3.77 (m, 4H); 3.80 (m, 4H); 3.97 (m, 4H); 4.02 (m, 4H); 5.21 (s, 4H); 6.83 (d, J = 7.6Hz, 2H); 6.91 (d, J = 7.7Hz, 2H); 7.43 - 7.59 (m, 14H); 8.01 - 8.09 (m, 4H).

EI and FAB (NBA matrix) MS: m/z = 658 (M⁺).

(g) 1,11-Bis[5'-(hydroxy)naphthoxy]-3,6,9-trioxaundecane²²



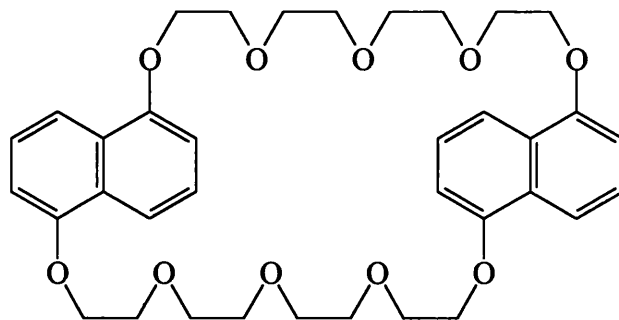
1,11-Bis[5'-(benzyloxy)naphthoxy]-3,6,9-trioxaundecane (4.00g, 6.08mmol) was refluxed with Palladium (1.2g, 10% on carbon) in ethanol (90ml) under a hydrogen atmosphere. After 19 hours the catalyst was filtered off and solvent was removed *in vacuo* to yield the product as a viscous brown oil.

Yield = 1.97g, 69.8%.

¹H NMR (d₃ - acetonitrile): 3.57 - 3.65 (m, 8H); 3.93 (m, 4H); 4.05 (m, 4H); 6.96 (m, 4H); 7.34 (m, 4H); 7.75 (m, 4H).

EI - MS: m/z = 478 (M⁺).

(h) 1,4,7,10,13,24,27,30,33,36-Decaoxa[13,13]-(1,5)
naphthophane (1/5DN38C10)²¹



A similar procedure to that used to prepare the phenoxy - analogue (2.3.2 (d)) was used to prepare this compound with a few minor modifications as noted below.

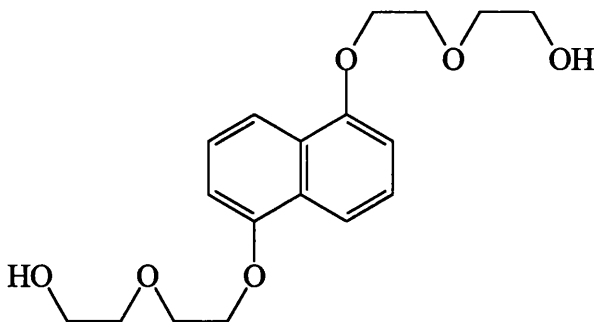
The reaction mixture contained 1,11-Bis[5'-(hydroxy)naphthoxy]-3,6,9-trioxaundecane (1.97g, 4.12mmol) in dry THF (75ml), tetraethylene glycol bitosylate (2.19g, 4.36mmol) in dry THF and NaH (0.92g, 60% dispersion in mineral oil, washed previously with cyclohexane) in THF (85ml). The reaction mixture was refluxed for 6 days. Subsequent to work up of the reaction and purification of the residue using the previously detailed chromatographic technique, a second column chromatography [SiO₂, ethyl acetate] step was employed to remove any small traces of impurity that remained.

Yield = 530mg, 20.9% (after first column); 66.2mg, 2.6% (after second column).

¹H NMR (d₃ - acetonitrile): 3.62 (m, 16H); 3.96 (m, 8H); 4.28 (m, 8H); 6.85 (d, J = 10Hz, 4H); 7.34 (t, J = 10Hz, 4H); 7.85 (d, J = 10Hz, 4H).

EI - MS: m/z = 636 (M⁺).

(i) 1,5-Bis[(hydroxyethoxy)-ethoxy]naphthalene (T1)²³



A solution of 1,5-dihydroxynaphthalene (8.0g, 50mmol) in dry *t*-butyl alcohol (50ml) was added to a solution of potassium *t*-butoxide (12.3g, 110mmol) in dry *t*-butyl alcohol (50ml) under nitrogen. The mixture was refluxed for 2 hours and then 2-(2-chloroethoxy) ethanol (13.70g, 110mmol) was added over 15 minutes. Refluxing was continued for 6 hours.

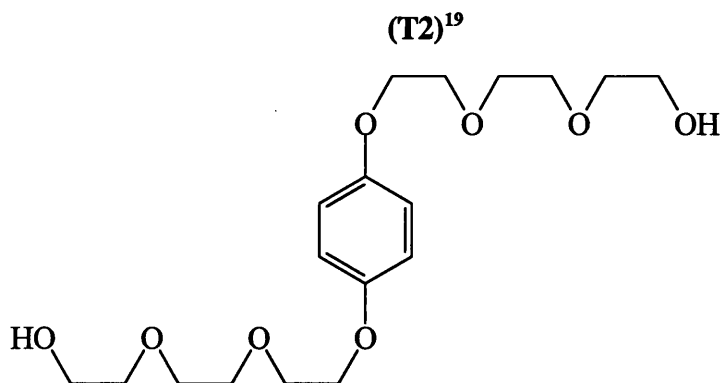
After this time, the reaction mixture was cooled to room temperature and filtered. The solid residue was washed with DCM (50ml) and the combined organic solutions evaporated *in vacuo* and the residue dissolved in DCM (100ml). The organic solution was washed with 2N HCl (30ml) and distilled water (2 x 30ml) and then dried (MgSO₄). The solution was concentrated *in vacuo* and the residue purified by column chromatography [SiO₂, ethyl acetate / 5% methanol].

Yield = 12.8g, 74.9%.

¹H NMR (CDCl₃): 3.74 (m, 8H); 3.95 (m, 4H); 4.26 (m, 4H); 6.81 (d, J = 7.92Hz, 2H); 7.32 (t, J = 7.9Hz, 2H); 7.85 (d, J = 7.9Hz, 2H).

EI - MS: m/z = 336 (M⁺).

(j) 1,4-Bis[2-{2-(2-hydroxyethoxy)ethoxy}ethoxy]benzene



A similar procedure to that used to prepare the naphthoxy - analogue (2.3.2 (i)) was used to prepare this compound with a few minor modifications as noted below.

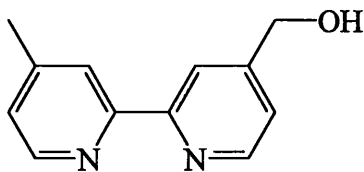
The reaction mixture contained 1,4-dihydroxybenzene (5.5g, 50mmol) in dry *t*-butyl alcohol (50ml), potassium *t*-butoxide (12.3g, 110mmol) in dry *t*-butyl alcohol and 2-[2-(2-chloroethoxy)ethoxy]ethanol (18.5g, 110mmol). The reaction mixture was refluxed for 65 hours.

Yield = 10.29g, 55.0%.

¹H NMR (CDCl₃): 3.57 (m, 12H); 3.65 (m, 4H); 3.80 (m, 4H); 4.04 (m, 4H); 6.82 (s, 4H).

EI - MS: *m/z* = 374 (M⁺).

(k) **4-Hydroxymethyl-4'-methyl-2,2'-bipyridine**



4-Bromomethyl-4'-methyl-2,2'-bipyridine (1.34g, 5.09mmol, obtained as a by-product from reaction 2.3.1 (a)) was dissolved in acetone (25ml) and vigorously refluxed with distilled water (100ml) and BaCO₃ (1.97g, 10mmol, iron free) for 48 hours.

After this time, the reaction mixture was filtered and the product extracted with chloroform (100ml). The solvent was evaporated *in vacuo* and the residue purified by column chromatography [SiO₂, DCM/acetone/methanol (94:2:4)] to yield the product.

Yield = 180.1mg, 17.7%.

¹H NMR (CDCl₃): 2.38 (s, 3H); 4.71 (s, 2H); 7.08 (d, J = 4.9Hz, 1H); 7.25 (d, J = 5.0Hz, 1H); 8.13 (s, 1H); 8.25 (s, 1H); 8.43 (d, J = 5.0Hz, 1H); 8.53 (d, J = 5.0Hz, 1H).

EI - MS: m/z = 199 (M⁺).

(l) **1,1'-Ferrocene diacidchloride²⁴**

1,1'-Ferrocene dicarboxylic acid (750mg, 2.74mmol) in dry DCM (15ml) was stirred with oxalyl chloride (1.5ml, 15mmol) and pyridine (1 drop) in the dark at ambient temperature for 12 hours.

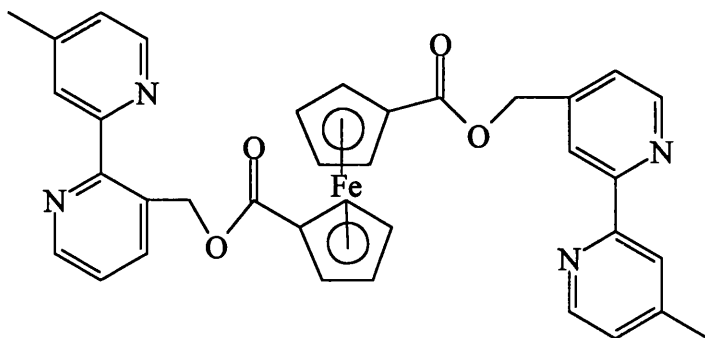
After this time, the mixture was refluxed for 6 hours, cooled to room temperature and the solvent removed *in vacuo*. The residue was continuously extracted with petrol (100 - 140°C) at 80°C to yield, on removal of the solvent, a dark red solid.

Yield = 400mg, 47.0%.

¹H NMR (CDCl₃): 4.75 (m, 4H); 5.04 (m, 4H).

I.R. (KBr disc): 1762cm⁻¹ ν(C=O).

(m) 1,1'-Ferrocene di(carboxy-4-methylene-4'-methyl-2,2'-bipyridine)



A solution of 1,1'-ferrocene diacidchloride (62.2mg, 0.20mmol) in dry DCM (20ml) was added dropwise to a solution of 4-hydroxymethyl-4'-methyl-2,2'-bipyridine (79.9mg, 0.40mmol) in dry DCM (30ml) with stirring and cooling (ice bath).

The reaction mixture was stirred for 1 hour after addition of the acid chloride was complete. The organic solution was washed several times with a NaHCO₃ solution, until the washings were no longer pink in colour, before being dried (MgSO₄). The solvent was removed *in vacuo* to yield a residue which was purified by column chromatography [SiO₂, DCM/10% methanol]. The fractions containing the orange product were evaporated to dryness immediately upon elution as it was found that the product spontaneously decomposed to a purple iron tris-bipyridyl derivative (confirmed by UV - VIS spectroscopy) when in solution.

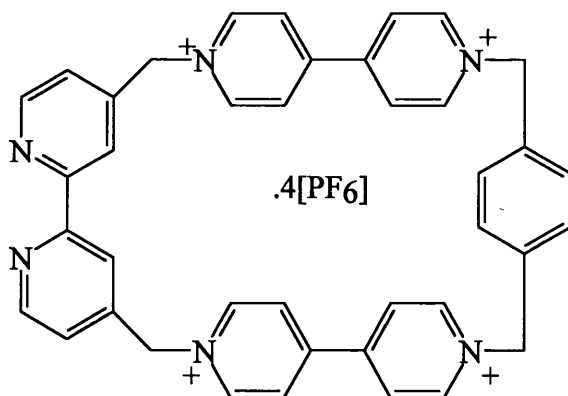
Yield = 10mg, 7.8%.

¹H NMR (CDCl₃): 2.51 (s, 6H); 4.49 (t, J = 1.9Hz, 4H); 4.54 (t, J = 1.9Hz, 4H); 5.37 (s, 4H); 7.25 (m, 2H); 7.32 (bd, J = 5.4Hz, 2H); 8.31 (s, 2H); 8.68 (d, J = 5.0Hz, 2H); 8.73 (s, 2H); 8.79 (d, J = 5.3Hz, 2H).

EI - MS: m/z = 638 (M⁺); 292 [(M - Fe)/2]⁺.

2.3.3 Free Cyclophanes and [2] Catenanes

(a) Cyclo[bisparaquat-*p*-phenylene-2,2'-bipyridine] Tetrakis (hexafluorophosphate) (L1)



α,α' -Dibromo-*p*-xylene (45mg, 0.17mmol), compound **P1** (130mg, 0.166mmol) and template compound **T1** (173mg, 0.512mmol) were dissolved in dry DMF (5ml). Sodium iodide (5mg) was added to the clear solution and the reaction mixture was stirred at room temperature for 7 days.

After this time, the solvent was removed *in vacuo* to leave a red residue which was dissolved in the minimum distilled water (a small quantity of 2N NH₄Cl was used to aid dissolution of the residue). The aqueous solution was then extracted continuously at reflux with chloroform (100ml) for 5 days, during which time the solution changed from red to pale yellow in colour.

The aqueous solution was separated from the organic layer and evaporated to dryness *in vacuo*. The residue was then purified by column chromatography [Al₂O₃, acetonitrile/distilled water/saturated KNO₃ (aq) (10:3:0.1)]. The product containing fractions (second band to elute) were evaporated to dryness and dissolved in the minimum distilled water. A saturated aqueous solution of ammonium hexafluorophosphate was then added to the aqueous solution until on further precipitation occurred. The precipitate was taken up into a nitromethane solution and the solution washed several times with distilled water to remove excess NH₄PF₆ from the organic layer. Finally, removal of the solvent *in vacuo* yielded the product as a colourless solid.

Yield = 45.1mg, 23.1%.

¹H NMR (d₆ - acetone): 6.15 (s, 4H); 6.27 (s, 4H); 7.75 (s, 4H); 7.92 - 7.94 (dd, J = 5.0Hz, J' = 1.0Hz, 2H); 8.22 (s, 2H); 8.59 - 8.61 (d, J = 6.9Hz, 4H);

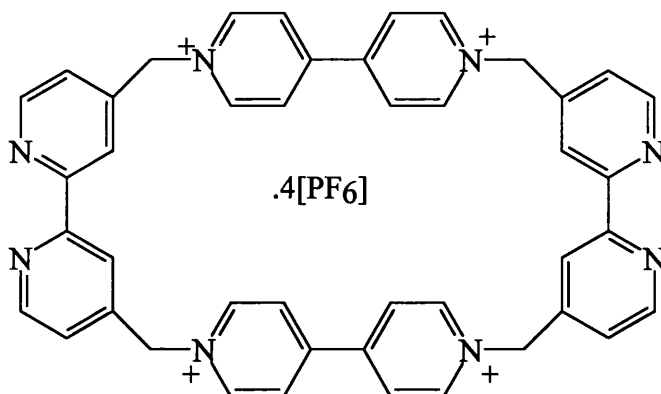
8.66 - 8.68 (d, J = 6.9Hz, 4H); 8.77 - 8.78 (d, J = 4.9Hz, 2H); 9.37 - 9.39 (d, J = 7.1Hz, 4H); 9.59 - 9.60 (d, J = 7.1Hz, 4H).

FAB - MS (NBA matrix): m/z = 1032 (M - PF₆)⁺, 888 (M - 2PF₆)⁺, 743 (M - 3PF₆)⁺.

Calculated for C₄₀H₃₄N₆P₄F₂₄ C: 40.75%, H: 2.89%, N: 7.13%, found C: 40.86%, H: 3.34%, N: 6.24%.

Electrochemical data: E_{1/2} = - 0.40V (2e); E_{1/2} = - 0.83V (2e) vs SCE.

(b) Cyclo[bisparaquat-bis-2,2'-bipyridine] Tetrakis
(hexafluorophosphate) (L2)



A similar procedure to that used to prepare the mono - bipy analogue (2.3.3 (a)) was used to prepare this compound with a few minor modifications as noted below.

The reaction mixture contained 4,4'-Bis(bromomethyl)-2,2'-bipyridine (42.0mg, 0.123mmol), compound P1 (96.3mg, 0.123mmol) and template compound T1 (127.6mg, 0.377mmol), with sodium iodide (1mg) in dry DMF (2ml). The purification steps were identical to those detailed above.

Yield = 8.3mg, 5.4%.

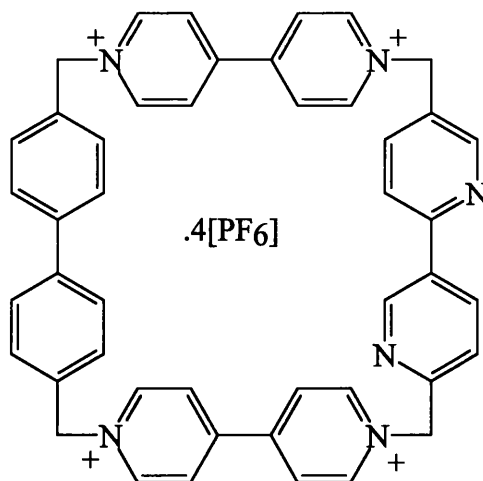
¹H NMR (d₆ - acetone): 6.29 (s, 8H); 7.96 - 7.97 (dd, J = 5.0Hz, J' = 1.0Hz, 4H); 8.40 (s, 4H); 8.66 - 8.68 (d, J = 7.0Hz, 8H); 8.81 - 8.83 (d, J = 5.0Hz, 4H); 9.57 - 9.58 (d, J = 7.0Hz, 8H).

FAB - MS (NBA matrix): m/z = 1111 (M - PF₆)⁺, 966 (M - 2PF₆)⁺, 821 (M - 3PF₆)⁺.

Calculated for C₅₃H₅₄N₈P₄F₂₄O₃: C: 44.49%, H 3.80%, N 7.83%, found C: 44.94%, H: 3.98%, N: 7.94%.

Electrochemical data: E_{1/2} = -0.34V (2e), E_{1/2} = -0.74V (2e) vs SCE.

(c) Cyclo[bisparaquat-diphenyl-2,2'-bipyridine] Tetrakis
(hexafluorophosphate) (L3)



A similar procedure to that used to prepare the 4,4'-derivatised bipy analogue (2.3.3 (a)) was used to prepare this compound with a few minor modifications as noted below.

The reaction mixture contained 5,5'-bis(bromomethyl)-2,2'-bipyridine (100.2mg, 0.29mmol), compound P3 (201.7mg, 0.258mmol) and template compound T1 (270.4mg, 0.800mmol), with sodium iodide (5.6mg) in dry DMF (6ml). After chloroform extraction of the reaction residue, it was necessary to filter the aqueous layer in order to remove an insoluble precipitate. The residue from the reaction work up was subjected to column chromatography [Al₂O₃, acetonitrile / distilled water / saturated KNO₃ (aq) (10:3:0.1)] three times rather than just one due to the difficulty encountered in purifying this ligand.

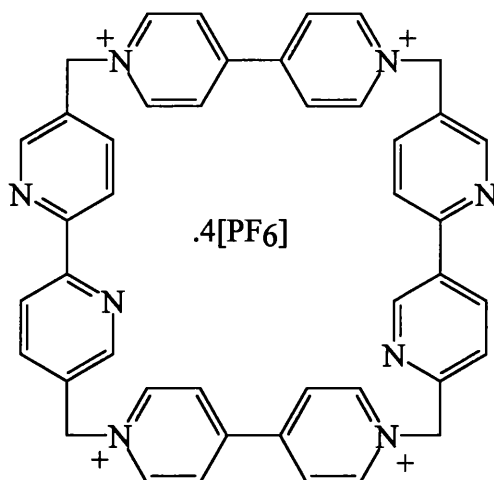
Yield = 3.4mg, 1.1%.

¹H NMR (d₆ - acetone); 6.20 (s, 4H); 6.33 (s, 4H); 7.69 - 7.76 (m, 8H); 8.26 - 8.29 (dd, J = 8.1Hz, J' = 2.0Hz, 2H); 8.40 - 8.43 (d, J = 8.1Hz, 2H); 8.74 - 8.76 (d, J = 7.1Hz, 4H); 8.77 - 8.79 (d, J = 6.9Hz, 4H); 9.01 (s, 2H); 9.52 - 9.54 (d, J = 7.1Hz, 4H); 9.58 - 9.60 (d, J = 7.0Hz, 4H).

FAB - MS (NBA matrix): m/z = 1110 (M - PF₆)⁺, 965 (M - 2PF₆)⁺, 820 (M - 3PF₆)⁺.

Electrochemical data: E_{1/2} = - 0.39V (2e), E_{1/2} = - 0.84V (2e) vs SCE.

(d) Cyclo[bisparaquat-bis-2,2'-bipyridine] Tetrakis
(hexafluorophosphate) (L4)



A similar procedure to that used to prepare the mono - bipy analogue (2.3.3 (c)) was used to prepare this compound with a few minor modifications as noted below.

The reaction mixture contained 5,5'-bis(bromomethyl)-2,2'-bipyridine (9.6mg, 0.028mmol), compound **P2** (22.0mg, 0.028mmol) and template compound **T1** (30.3mg, 0.089mmol), with sodium iodide (1mg) in dry DMF (2ml). After chloroform extraction of the reaction residue, it was necessary to filter the aqueous layer in order to remove an insoluble precipitate. The residue from the reaction work up was subjected to column chromatography [Al_2O_3 , acetonitrile/distilled water/saturated KNO_3 (aq) (10:3:0.1)] twice rather than just once, due to the difficulty encountered in purifying this ligand.

Yield = 2.9mg, 8.2%.

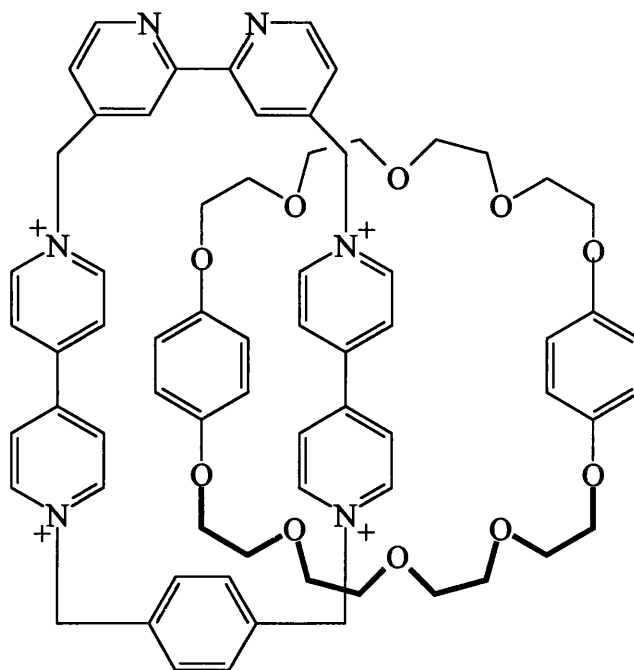
^1H NMR (d_6 - acetone): 6.33 (s, 8H); 8.27 - 8.30 (dd, $J = 8.4\text{Hz}$, $J' = 1.1\text{Hz}$, 4H); 8.41 - 8.44 (d, $J = 8.2\text{Hz}$, 4H); 8.74 - 8.76 (d, $J = 6.7\text{Hz}$, 8H); 9.02 - 9.03 (d, $J = 1.1\text{Hz}$, 4H); 9.58 - 9.59 (d, $J = 6.8\text{Hz}$, 8H).

FAB - MS (NBA matrix): 1111 ($\text{M} - \text{PF}_6$) $^+$, 966 ($\text{M} - 2\text{PF}_6$) $^+$, 821 ($\text{M} - 3\text{PF}_6$) $^+$.

Calculated for $\text{C}_{44}\text{H}_{36}\text{N}_8\text{P}_4\text{F}_{24}$ C: 42.04%, H: 2.87%, N: 8.92%, found C: 49.04%, H: 5.57%, N: 6.65% - sample may have been solvated e.g with acetone molecules.

Electrochemical data: $E_{1/2} = -0.38\text{V}$ (2e); $E_{1/2} = -0.80\text{V}$ (2e) vs SCE.

(e) { [2]-[34C10]-[Cyclo[bisparaquat-*p*-phenylene-2,2'-bipyridine]catenane} Tetrakis (hexafluorophosphate) (L5)⁹



A solution of compound **P1** (0.157g, 0.2mmol) in dry acetonitrile (5ml) was added to a stirred solution of **34C10** (0.291g, 0.52mmol) in dry acetonitrile (5ml) under nitrogen. A solution of α,α' - dibromo - *p* - xylene (0.053g, 0.2mmol) in dry acetonitrile (5ml) was then added. After 4 hours the reaction mixture became a deep red colour which preceded precipitation of a red solid.

After the reaction had been stirred at room temperature for 5 days, the precipitate was filtered off, washed with chloroform (10ml), dissolved in distilled water (30ml) and filtered to remove a small amount of insoluble polymeric material. The red acetonitrile solution which remains after the filtration was evaporated to dryness *in vacuo* and the combined residues were subjected to column chromatography [SiO_2 , methanol/2N NH_4Cl (aq)/nitromethane (7:2:1)].

The red fractions were concentrated *in vacuo* and a saturated aqueous solution of NH_4PF_6 was added until no further precipitation occurred. The solid was washed with warm water (20ml) before being recrystallised three times from acetone - distilled water.

Yield = 15.0mg, 4.3%.

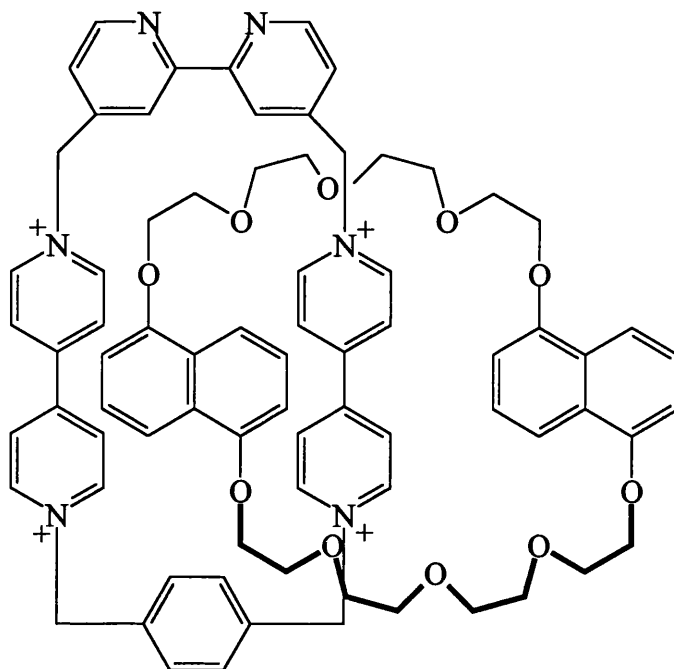
^1H NMR (d_6 - acetone): 3.46 (m, 8H); 3.61 (m, 8H); 3.89 - 3.93 (m, 16H); 6.08 (s, 4H); 6.15 (s, 4H); 7.94 (m, 2H); 8.00 (s, 4H); 8.10 - 8.14 (2 x d, J =

8Hz, 8H); 8.18 (m, 2H); 8.90 - 8.92 (d, J = 5Hz, 2H); 9.27 - 9.29 (d, J = 5.2Hz, 4H); 9.32 - 9.34 (d, J = 7.0Hz, 4H). Owing to relatively fast interchange of the bound - unbound dihydroxybenzene groups of the interlocked crown ether moiety, eight protons are missing. The appropriate signals are severely broadened into the baseline but upon cooling of the sample can be observed.

FAB - MS (NBA matrix): $m/z = 1569 (M - PF_6)^+$, $1425 (M - 2PF_6)^+$, $1279 (M - 3PF_6)^+$.

Electrochemical Data: $E_{1/2} = - 0.41V (1e)$; $E_{1/2} = - 0.54V (1e)$; $E_{1/2} = - 0.91V (2e)$ vs SCE.

(f) {[2]-[1/5DN38C10]-[Cyclo[bisparaquat-*p*-phenylene-2,2'-bipyridine]catenane} Tetrakis (hexafluorophosphate) (L6)



A solution of compound **P1** (19.7mg, 0.025mmol) in dry acetonitrile (3ml) was added to a stirred solution of **1/5DN38C10** (60.0mg, 0.094mmol) in dry acetonitrile (3ml) under nitrogen.

After 15 minutes, α,α' -dibromo-*p*-xylene (6.6mg, 0.025mmol) was added and the reaction mixture stirred at room temperature for 10 days.

After this time, the solvent was removed *in vacuo* to yield a purple - red residue which was purified twice by column chromatography [SiO₂, methanol/2N NH₄Cl/nitromethane (7:2:1)]. The purple - red fractions were collected, concentrated *in vacuo* and precipitated by the addition of a saturated aqueous solution of NH₄PF₆. The solid was washed with warm water (20ml) before being recrystallised three times from acetone - diisopropyl ether.

Yield = 10.0mg, 33.1%.

¹H NMR (d₆-acetone, 313K): 3.00 (bm, 4H); 3.14 (m, 4H); 3.45 (m, 4H); 3.68 (m, 6H); 3.87 (m, 6H); 3.96 (bm, 6H); 4.30 (bm, 2H); 5.79 - 5.83 (t, J = 7.96, 2H); 6.13 (m, 8H); 6.48 - 6.50 (d, J = 7.76Hz, 2H); 7.81 - 7.83 (d, J = 6.8Hz, 4H); 7.90 - 7.92 (d, J = 6.9Hz, 4H); 8.04 (m, 2H); 8.28 (s, 4H); 8.43 (s, 2H); 9.04 - 9.05 (d, J = 4.8Hz, 2H); 9.26 - 9.27 (d, J = 6.7Hz, 4H); 9.40 - 9.42 (d, J = 6.9Hz, 4H). Owing to relatively fast interchange of the bound - unbound

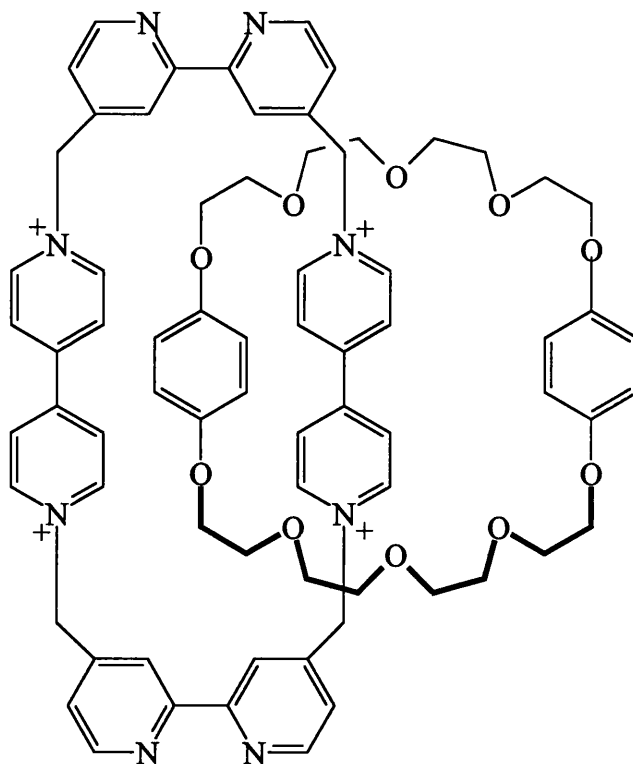
dihydroxynaphthalene groups of the interlocked crown ether moiety, eight protons are missing. The appropriate signals are severely broadened into the baseline but the use of variable temperature one dimensional and low temperature two dimensional $^1\text{H} - ^1\text{H}$ COSY NMR spectroscopy has allowed location of these signals. These experiments will be discussed later in this thesis.

FAB - MS (NBA matrix): $m/z = 1695 (\text{M} - \text{PF}_6)^+$, $1527 (\text{M} - 2\text{PF}_6)^+$, $1382 (\text{M} - 3\text{PF}_6)^+$, $1237 (\text{M} - 4\text{PF}_6)^+$.

Calculated for $\text{C}_{76}\text{H}_{78}\text{N}_6\text{O}_{10}\text{P}_4\text{F}_{24}$; C: 50.27%, H: 4.29%, N: 4.63%, found; C: 46.38%, H: 4.71%, N: 3.85% - sample may have been solvated e.g with acetone molecules.

Electrochemical Data: $E_{1/2} = -0.43\text{V} (1e)$; $E_{1/2} = -0.53\text{V} (1e)$; $E_{1/2} = -0.83\text{V} (1e)$; $E_{1/2} = -0.97\text{V} (1e)$ vs SCE.

(g) { [2]-[34C10]-[Cyclo[bisparaquat-bis-2,2'-bipyridine]catenane} Tetrakis (hexafluorophosphate) (L7)



A solution of compound T1 (65.3mg, 0.083mmol) in dry acetonitrile (1.5ml) was added with stirring to a solution of **34C10** (119.0mg, 0.222mmol) in dry acetonitrile (1.5ml) under nitrogen.

After 30 minutes, a solution of 4,4'-bis(bromomethyl)-2,2'-bipyridine (28.4mg, 0.083mmol) in dry acetonitrile (1ml) was added and the reaction mixture stirred for 10 days after the addition of sodium iodide (2mg).

After this time, the solvent was removed and the red residue was purified twice by column chromatography [SiO_2 , methanol/2N NH_4Cl /nitromethane (7:2:1)]. The red fractions were collected, concentrated *in vacuo* and precipitated by the addition of a saturated aqueous solution of NH_4PF_6 . The solid was washed with warm water (20ml) before being recrystallised from acetone - diisopropyl ether.

Yield = 1.5mg, 1.0%.

^1H NMR (d_6 - acetone): 3.37 (bm, 8H); 3.52 - 3.53 (m, 8H); 3.85 (m, 8H); 3.91 - 3.92 (m, 8H); 6.25 (s, 8H); 6.39 (s, 4H); 7.91 - 7.92 (d, $J = 4.7\text{Hz}$, 4H); 8.29 - 8.31 (d, $J = 6.7\text{Hz}$, 8H); 8.37 (s, 4H); 8.88 - 8.89 (d, $J = 4.7\text{Hz}$, 4H); 9.39 - 9.41 (d, $J = 6.7\text{Hz}$, 8H).

FAB - MS (NBA matrix): $m/z = 1647 (M - PF_6)^+$, $1502 (M - 2PF_6)^+$, $1357 (M - 3PF_6)^+$.

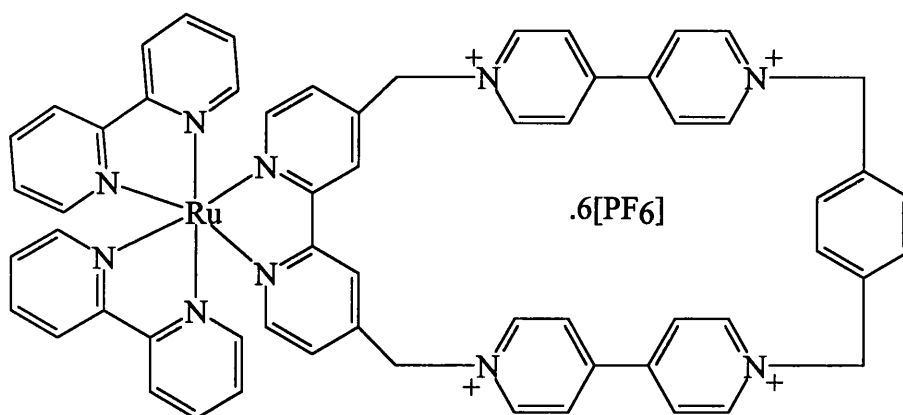
Electrochemical Data: $E_{1/2} = -0.43V (2e)$; $E_{1/2} = -0.73V (2e)$ vs SCE. It was not possible to resolve the separate reduction peaks for the first reduction of the “inside” and “outside” viologen units due to the extremely weak nature of the analyte solution.

(h) NMR Experiment: Formation of [2] Catenane L7.

The yield of reaction 2.3.3 (g) was obviously rather disappointing. As the reaction was repeated an number of times with no improvement to the yield, an NMR study was carried out with the aim of following the progress of the reaction over 5 days to try and determine where the reaction was failing. The reaction was carried out in a 5mm borosilicate NMR tube. The reaction mixture contained compound **P1** (24.4mg, 0.03mmol), 4,4' - bis(bromomethyl) - 2,2' - bipyridine (10.4mg, 0.03mmol) and **34C10** (41.9mg, 0.078mmol) in d_6 - DMSO (1ml, 2 drops D_2O added). NMR spectra were recorded every three hours for the first twelve hours and once a day thereafter. The results of this study are discussed later in this thesis.

2.3.4 Metal Complexes of Cyclophanes and [2] Catenanes

(a) $\text{Ru}(\text{bipy})_2(\text{L1})(\text{PF}_6)_6$



Method 1⁹

A solution of $[\text{Ru}(\text{bipy})_2(\text{P1})].4[\text{PF}_6]$ (73.2mg, 0.05mmol) in dry acetonitrile (25ml) was stirred and heated to reflux. α, α' -dibromo-*p*-xylene (13mg, 0.05mmol) in dry acetonitrile (20ml) was added dropwise. Sodium iodide (2mg) was added to the reaction mixture and refluxing was continued for 8 days.

After this time, the reaction mixture was cooled to room temperature and the solution was reduced in volume to c.a. 10ml. THF (30ml) was added to the concentrated solution and the precipitate produced was filtered off and air dried before being dissolved in the minimum distilled water. The crude product was precipitated by the careful addition of a saturated aqueous solution of ammonium hexafluorophosphate before being filtered off and washed with copious distilled water. Size exclusion column chromatography [sephadex LH - 20, acetonitrile] yielded the pure compound.

Yield = 65.5mg, 70.0%.

Method 2²⁵

A mixture of compound L1 (previously converted to the chloride salt, 3.14mg, 4.24×10^{-3} mmol) and $\text{Ru}(\text{bipy})_2\text{Cl}_2$ (2.09mg, 4.32×10^{-3} mmol) in dry ethanol (6ml) were refluxed for 48 hours.

After this time, the solvent was removed and the residue purified twice by size exclusion column chromatography [sephadex G-15, distilled water]. The product containing fractions (first band to elute) were concentrated *in vacuo* and the

product precipitated by the addition of a saturated aqueous solution of NH_4PF_6 . The red solid was removed by centrifugation and washed with copious distilled water, before being recrystallised from acetonitrile - diisopropyl ether.

Yield = 5.4mg, 68.0%.

^1H NMR (d_6 - acetone): 6.15 (s, 4H), 6.21 (s, 4H); 7.43 (m, 2H); 7.56 (m, 2H); 7.92 (s, 4H); 7.97 - 8.00 (t, $J = 6.4\text{Hz}$, 8H); 8.21 - 8.28 (m, 4H); 8.49 - 8.51 (d, $J = 6.2\text{Hz}$, 8H); 8.74 (s, 2H); 8.79 - 8.83 (m, 4H); 9.25 - 9.27 (d, $J = 6.2\text{Hz}$, 4H); 9.43 - 9.44 (d, $J = 6.3\text{Hz}$, 4H).

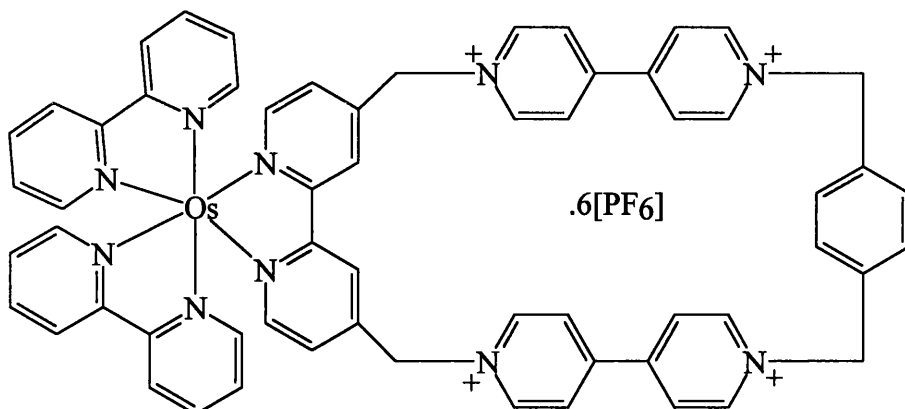
FAB - MS (NBA matrix): $m/z = 1737$ (M - PF_6)⁺, 1591 (M - 2PF_6)⁺, 1446 (M - 3PF_6)⁺.

Electrospray - MS: $m/z = 1736$ (M - PF_6)⁺, 795 (M - 2PF_6)²⁺, 482 (M - 3PF_6)³⁺.

Electrochemical Data: $E_{1/2} = 1.23\text{V}$ (1e); $E_{1/2} = -0.40\text{V}$ (2e); $E_{1/2} = -0.86\text{V}$ (2e) vs SCE.

A two dimensional ^1H - ^1H COSY NMR experiment that was carried out on this compound will be discussed later in this thesis.

(b)



A similar synthetic strategy to that employed for the ruthenium analogue in 2.3.4 (a) (method1) above, was used to synthesise Os(bipy)₂(L1)(PF₆)₆, with a few minor modifications as noted below.

The reaction mixture contained [Os(bipy)₂(P1)].4[PF₆] (24.6mg, 0.015mmol) and α,α' -dibromo-*p*-xylene (4.0mg, 0.015mmol) and sodium iodide (1mg) in dry acetonitrile (35ml).

The product was purified by column chromatography [Al₂O₃, methanol/2N NH₄Cl/nitromethane (7:2:1)] followed by size exclusion column chromatography [sephadex LH-20, acetonitrile].

Yield = 15.7mg, 60.0%.

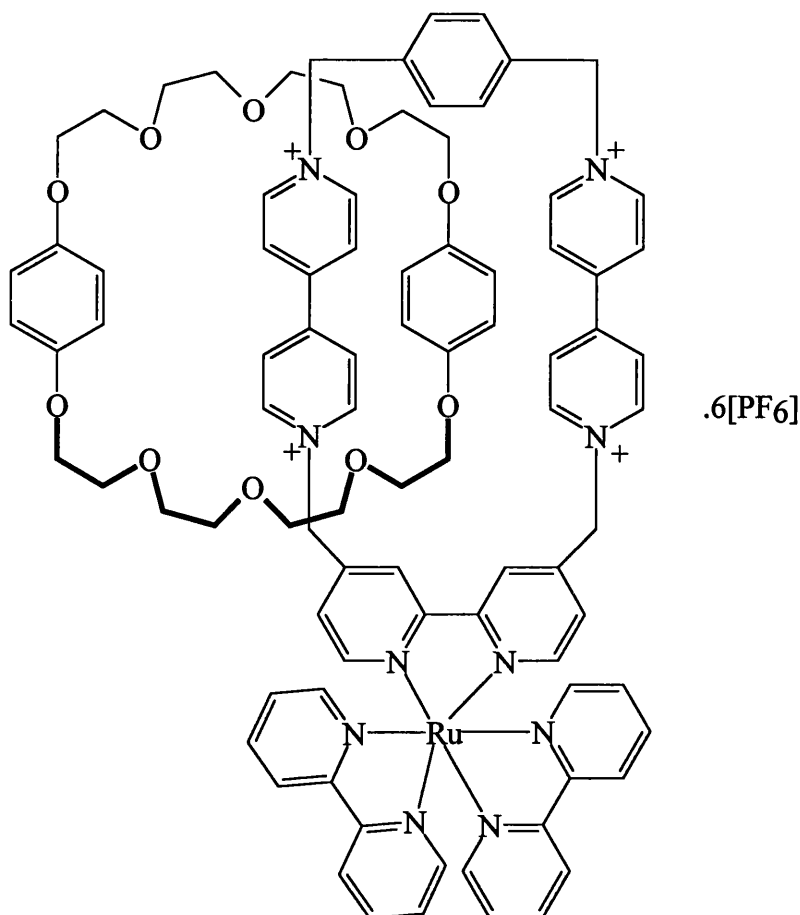
¹H NMR (d₆ - acetone): 6.18 (bs, 8H); 7.33 - 7.39 (m, 2H); 7.49 (t, J = 9.6Hz, 2H); 7.78 - 7.80 (d, J = 9.6Hz, 2H); 7.87 - 7.89 (m, 4H); 7.89 (s, 4H); 8.01 (m, 4H); 8.13 - 8.15 (d, J = 5.3Hz, 2H); 8.49 - 8.51 (d, J = 4.8Hz, 8H); 8.76 - 8.78 (d, J = 8.3Hz, 4H); 8.96 (s, 2H); 9.38 - 9.39 (d, J = 6.3Hz, 4H); 9.46 - 9.48 (d, J = 5.8Hz, 4H).

FAB - MS (NBA matrix): m/z = 1824 (M - PF₆)⁺, 1682 (M - 2PF₆)⁺, 1536 (M - 3PF₆)⁺.

Electrospray - MS: m/z = 1825 (M - PF₆)⁺, 840 (M - 2PF₆)²⁺, 511 (M - 3PF₆)³⁺.

Electrochemical Data: E_{1/2} = 0.82V (1e); E_{1/2} = - 0.41V (2e); E_{1/2} = - 0.75V (2e) vs SCE.

(c)



A similar synthetic strategy to that employed to synthesise Ru(bipy)₂(L1)(PF₆)₆ in 2.3.4 (a) (method 2) was used to synthesise this compound.

The reaction mixture contained [2]catenane L5 (previously converted to the chloride salt, 4.3mg, 2.52 x 10⁻³mmol) and Ru(bipy)₂Cl₂ (1.2mg, 2.54 x 10⁻³mmol) in dry ethanol (6ml).

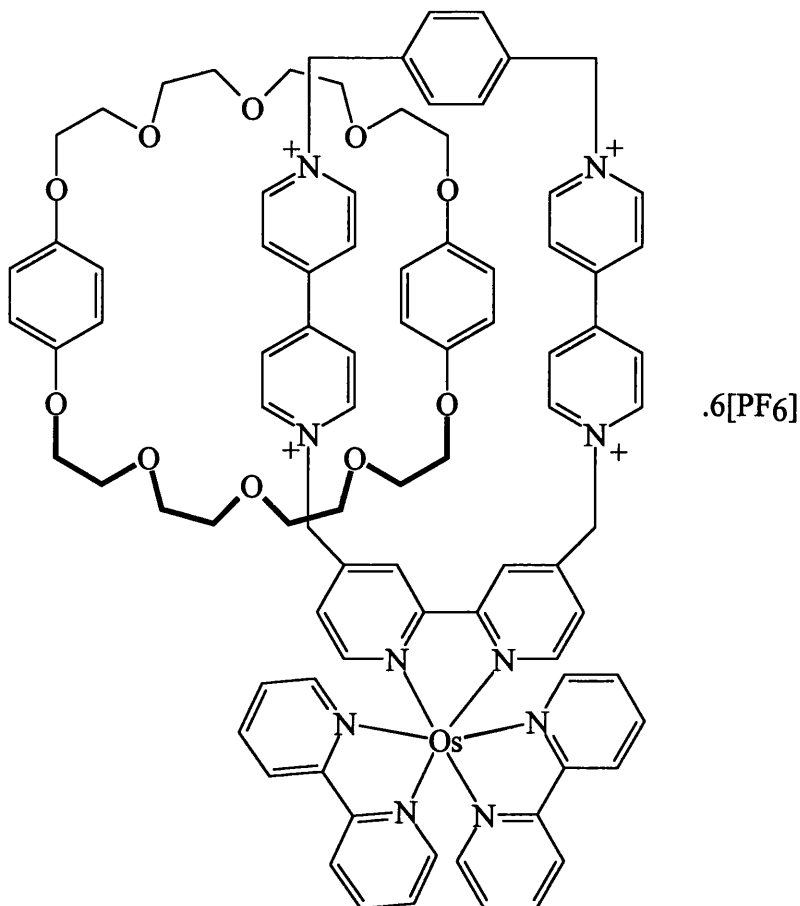
Yield = 7.7mg, 94.0%.

¹H NMR (d₆ - acetone): 3.45 - 3.48 (m, 4H); 3.61 - 3.63 (m, 8H); 3.69 - 3.72 (m, 8H); 3.79 - 3.85 (m, 12H); 3.93 - 4.10 (m, 4H); 6.10 (s, 4H); 6.23 (s, 4H), 6.26 (s, 4H); 7.57 - 7.73 (q, J = 7.5Hz, 4H); 7.92 - 7.94 (d, J = 5.6Hz, 2H); 7.98 (s, 4H); 8.00 - 8.02 (d, J = 5.3Hz, 2H); 8.02 - 8.22 (m, 10H); 8.23 - 8.31 (m, 4H); 8.34 - 8.36 (d, J = 5.7Hz, 2H); 8.82 - 8.87 (m, 6H); 9.34 - 9.36 (d, J = 5.0Hz, 8H).

Electrospray - MS: m/z = 661 (M - 3PF₆)³⁺, 460 (M - 4PF₆)⁴⁺, 339 (M - 5PF₆)⁵⁺.

(d)

Os(bipy)₂(L5)(PF₆)₆



To a solution of [Os(bipy)₂(P1)].4[PF₆] (31.3mg, 0.02mmol) in dry degassed acetonitrile (2ml) was added a solution of **34C10** (31.9mg, 0.06mmol) in dry degassed acetonitrile (3ml) with stirring, under nitrogen.

After 15 minutes, a solution of α,α' -dibromo-*p*-xylene (5.3mg, 0.02mmol) in dry degassed acetonitrile (2ml) was added. The reaction mixture was stirred at room temperature for 10 days after the addition of NaI (1mg).

After this time, the solvent was removed *in vacuo* and the brown residue purified by column chromatography [SiO₂, methanol/2N NH₄Cl(aq)/nitromethane (7:2:1)]. The product containing fractions (first brown band to elute) were collected, concentrated *in vacuo* and precipitated by the careful addition of a saturated aqueous solution of NH₄PF₆. The brown solid was taken up into a solution of nitromethane, which was washed several times with distilled water to remove any excess NH₄PF₆. Finally, the solvent was removed *in vacuo* to yield the product as a brown solid.

Yield = 1.1mg, 2.2%.

^1H NMR (d_6 - acetone): 3.31 - 3.33 (m, 8H); 3.44 - 3.49 (m, 8H); 3.60 - 3.65 (bm, 8H); 3.76 - 3.87 (m, 8H); 6.13 (s, 4H); 6.28 (s, 4H); 6.33 (s, 4H); 7.53 - 7.57 (t, $J = 8.3\text{Hz}$, 2H); 7.69 - 7.71 (t, $J = 5.4\text{Hz}$, 2H); 7.82 - 7.84 (d, $J = 5.5\text{Hz}$, 2H); 7.94 - 8.00 (m, 2H); 8.03 (s, 4H); 8.13 - 8.28 (m, 12H); 8.83 - 8.88 (m, 8H); 9.40 - 9.42 (d, $J = 6.9\text{Hz}$, 8H).

Electrospray - MS: $m/z = 1108$ (M - 2PF_6) $^{2+}$, 690 (M - 3PF_6) $^{3+}$, 481 (M - 4PF_6) $^{4+}$.

(e) $\text{Cu}^{\text{I}}(\text{L1})_2(\text{PF}_6)_8(\text{BF}_4)^{(2\theta)}$

A solution of compound **L1** (1.8mg, $1.5 \times 10^{-3}\text{mmol}$) in dry, degassed d_6 - acetone (0.9ml) was placed in a 5mm borosilicate NMR tube fitted with a subseal top so that the reaction may be performed under a nitrogen atmosphere. $[\text{Cu}^{\text{I}}(\text{CH}_3\text{CN})_4][\text{BF}_4]$ (5.1mg, 0.015mmol) in dry, degassed d_6 - acetone (0.5ml) was added *via* an accurate syringe in $2\mu\text{L}$ aliquots and a ^1H NMR spectrum recorded after each titration. When addition of $[\text{Cu}^{\text{I}}]$ had no further effect, a final ^1H NMR spectrum was recorded and the solvent removed *in vacuo* to yield the product in quantitative yield.

^1H NMR (d_6 - acetone): 6.21 (s, 8H); 6.25 (s, 8H); 7.89 (s, 8H); 8.17 (m, 4H); 8.56 (m, 16H); 8.71 (m, 4H); 8.78 (m, 4H); 9.40 (m, 8H); 9.43 - 9.45 (d, $J = 6.3\text{Hz}$, 8H).

Electrospray - MS: Only very weak peaks relating to the complex could be observed: the complex degrades in the spectrometer to give the expected peaks for the free cyclophane.

(f) $\text{Cu}^{\text{I}}(\text{L2})_2(\text{PF}_6)_8(\text{BF}_4)$

An identical technique to that employed in 2.3.4 (e) above was used to synthesise this compound. The initial solution contained compound **L2** (2.7mg, $2.1 \times 10^{-3}\text{mmol}$) in dry degassed d_6 - acetone (0.6ml). The $[\text{Cu}^{\text{I}}]$ solution was as previous (5.1mg, 0.015mmol in 0.5ml d_6 - acetone).

After the addition of $10\mu\text{L}$ $[\text{Cu}^{\text{I}}]$ solution it was found that there were no signals apparent in the ^1H NMR spectrum and that a precipitate had formed in the sample tube.

(g) $\text{Cu}^{\text{I}}(\text{L3})_2(\text{PF}_6)_8(\text{BF}_4)$

An identical technique to that employed in 2.3.4 (e) above was again used to synthesise this compound. The initial solution contained compound **L3** (1.4mg, 1.1×10^{-3} mmol) in dry degassed d_6 - acetone (0.4ml). The $[\text{Cu}^{\text{I}}]$ solution contained $[\text{Cu}^{\text{I}}(\text{CH}_3\text{CN})_4][\text{BF}_4]$ (5.2mg, 0.016mmol in 0.5ml d_6 - acetone).

^1H NMR (d_6 - acetone): 6.21 (m, 16H); 7.55 (bm, 4H); 7.72 (m, 16H); 7.86 (m, 4H); 7.98 - 7.99 (d, $J = 4.8\text{Hz}$, 4H); 8.78 (m, 16H); 9.53 - 9.59 (m, 16H).

(h) $\text{Cu}^{\text{I}}(\text{L5})_2(\text{PF}_6)_8(\text{BF}_4)$ - Mass Spectrometer Scale Experiment.

$[\text{Cu}^{\text{I}}(\text{CH}_3\text{CN})_4][\text{BF}_4]$ (1.0mg, 0.0006mmol) in dry, degassed acetonitrile (5ml) was added to a solution of compound **L5** (0.1mg, 0.0006mmol) in dry, degassed acetonitrile (2ml) under a nitrogen atmosphere. The solution was concentrated *in vacuo*, mixed with the NBA matrix and then introduced into the FAB mass spectrometer.

FAB - MS (NBA matrix): $m/z = 3347 (\text{M} - \text{PF}_6\text{BF}_4)^+$, $3288 (\text{M} - 2\text{PF}_6)^+$, $3143 (\text{M} - 3\text{PF}_6)^+$.

(i) $\text{Fe}^{\text{II}}(\text{L1})_3(\text{PF}_6)_{14}$

To a solution of compound **L1** (18.9mg, 0.016mmol) in dry degassed acetonitrile (3ml) was added $\text{FeSO}_4 \cdot 7\text{H}_2\text{O}$ (1.5mg, 0.0054mmol) and NH_4PF_6 (1.8mg, 0.011mmol). The reaction mixture was stirred for 24 hours at room temperature.

After this time, the solvent was removed *in vacuo*, and the residue partitioned between distilled water (10ml) and nitromethane (10ml). The organic layer was washed several times with distilled water to remove excess inorganic salts, before being evaporated to dryness to yield the product as a red - purple solid in quantitative yield.

^1H NMR (d_6 - acetone): 6.15 (s, 12H); 6.18 (s, 12H); 7.67 - 7.68 (d, $J = 5.4\text{Hz}$, 6H); 7.88 (m, 18H); 8.47 - 8.49 (m, 24H); 8.63 (s, 6H); 9.17 - 9.19 (d, $J = 6.2\text{Hz}$, 12H); 9.38 - 9.40 (d, $J = 6.2\text{Hz}$, 12H).

Electrospray - MS: $m/z = 1149 (\text{M} - 3\text{PF}_6)^{3+}$; $825 (\text{M} - 4\text{PF}_6)^{4+}$; $631 (\text{M} - 5\text{PF}_6)^{5+}$; $502 (\text{M} - 6\text{PF}_6)^{6+}$.

Electrochemical Data: $E_{1/2} = 1.26\text{V}$ (1e); $E_{1/2} = -0.37\text{V}$ (2e); $E_{1/2} = -0.81\text{V}$ (2e) vs SCE.

(j) $\text{Zn}^{\text{II}}(\text{L1})_2(\text{PF}_6)_8(\text{CF}_3\text{SO}_3)_2^{(27)}$

A solution of compound **L1** (4.4mg, 3.7×10^{-3} mmol) in dry, degassed d_6 - acetone (0.9ml) was placed in a 5mm borosilicate NMR tube. $\text{Zn}(\text{CF}_3\text{SO}_3)_2$ (0.7mg, 0.0195mmol) in dry, degassed d_6 - acetone (0.1ml) was added to this solution *via* an accurate syringe.

After an ^1H NMR spectrum had been obtained, the solvent was removed *in vacuo* to yield the compound as a colourless solid in quantitative yield.

^1H NMR (d_6 - acetone): 6.19 (s, 8H); 6.27 (s, 8H); 7.87 (s, 4H); 8.39 (m, 4H); 8.56 - 8.58 (m, 16H); 9.00 (m, 4H); 9.12 (m, 4H); 9.43 - 9.45 (d, $J = 7.0\text{Hz}$, 8H); 9.56 - 9.58 (d, $J = 4.5\text{Hz}$, 8H).

Electrospray - MS: $m/z = 2212$ ($\text{M} - 3\text{PF}_6$) $^+$.

(k) $[\text{Zn}^{\text{II}}(\text{L2})_2(\text{PF}_6)_8(\text{CF}_3\text{SO}_3)_2]_n$

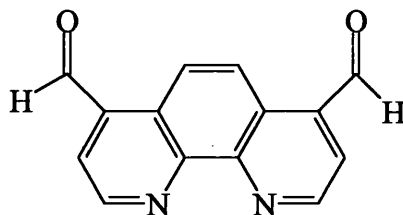
An identical technique to that employed in 2.3.4 (j) above was used to synthesise this compound. The initial solution contained compound **L2** (2.7mg, 2.1×10^{-3} mmol) in dry degassed d_6 - acetone (0.6ml). $\text{Zn}(\text{CF}_3\text{SO}_3)_2$ (10.2mg, in dry, degassed d_6 - acetone (1ml) or 0.04molL^{-1}) was added in $2\mu\text{L}$ aliquots.

After the addition of $2\mu\text{L}$ $[\text{Zn}^{\text{II}}]$ solution it was found that there were no signals apparent in the ^1H NMR spectrum and that a precipitate had formed in the sample tube. However upon the addition of $6\mu\text{L}$ $[\text{Zn}^{\text{II}}]$ solution some ^1H NMR signals re-appeared in the spectrum and the precipitate was observed to re - dissolve. After the addition of $8\mu\text{L}$ $[\text{Zn}^{\text{II}}]$ solution no further shifting of ^1H NMR resonances was observed.

^1H NMR (d_6 - acetone): 6.40 (s, 16H); 8.36 (d, $J = 6.5\text{Hz}$, 8H); 8.65 - 8.67 (d, $J = 7.1\text{Hz}$, 16H); 8.96 (s, 8H); 9.14 - 9.15 (d, $J = 5.2\text{Hz}$, 8H); 9.60 - 9.62 (d, $J = 6.6\text{Hz}$, 16H).

2.3.5 Schiff Base Chemistry

(a) 1,10-Phenanthroline-4,7-dicarbaldehyde²⁸

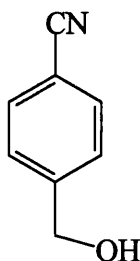


A mixture of 4,7-dimethyl-1,10-phenanthroline (1.0g, 4.8mmol) and selenium dioxide (2.5g, 22.6mmol) in dioxane (4% distilled water, 72ml) was heated under reflux for 2 hours and then filtered through powdered molecular sieves while still hot. The dialdehyde separated from the cold filtrate as colourless crystals (some decolourised by elemental selenium).

Yield = 146mg, 14.0%

¹H NMR (d₆ - DMSO): 8.28 (d, J = 3.6Hz, 2H); 9.12 (s, 2H); 9.44 (d, J = 3.6Hz, 2H); 10.68 (s, 2H).

(b) *p*-Cyanobenzyl alcohol²⁹



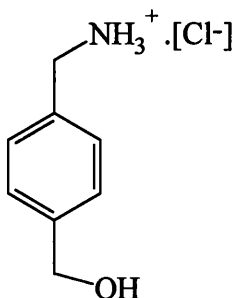
p-Cyanobenzyl bromide (4g, 0.02mol) was vigorously stirred and refluxed with distilled water (120ml) and BaCO₃ (7.7g) for 40 minutes. Chloroform extraction and vacuum distillation gave pure *p*-cyanobenzyl alcohol [B.Pt. = 145°C under 0.3mm Hg].

Yield = 2.30g, 85.0%

¹H NMR (CDCl₃): 2.82 (t, J = 0.54Hz, 1H); 4.71 (d, J = 0.54Hz, 2H); 7.52 (dd, J = 2.88Hz, J' = 0.72Hz, 4H).

¹³C NMR (CDCl₃): 63.96; 110.81; 118.80; 126.90; 126.93; 129.50; 132.19; 132.51; 146.37.

(c) ***p*-Hydroxybenzylamine hydrochloride²⁹**



p-Cyanobenzyl alcohol (2.30g, 17.3mmol) was reduced with LiAlH₄ (1.20g, 31.6mmol) in refluxing anhydrous diethyl ether (70ml) for 3 hours under nitrogen.

After this time distilled water (2ml) was dripped carefully into the reaction mixture, followed by 15% NaOH solution (2ml) and lastly more distilled water (6ml). Extraction with chloroform isolates the free base in solution and extraction of this organic solution with an aqueous solution of HCl (2N, 100ml) yields, on evaporation of the water, *p*-hydroxy benzylamine hydrochloride.

Yield = 3.55g, 118.3% (product obviously contained excess HCl).

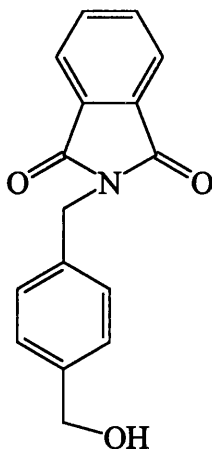
M.Pt. = 149°C (lit. 157 - 158°C).

¹H NMR (D₂O): 3.89 (s, 2H); 4.34 (s, 2H); 7.16 (m, 4H).

¹³C NMR (D₂O): 45.18; 65.75; 130.35; 131.23; 131.47; 131.70; 132.08; 143.46.

(d)

***p*-Phthalimidomethylbenzyl alcohol**



p-Hydroxybenzylamine hydrochloride (3.00g, 17.3mmol) and phthalic anhydride (2.59g, 34.1mmol) were dissolved in glacial acetic acid (35ml). Sodium acetate (2.87g, 35.0mmol) was then added and the reaction mixture was refluxed for 35 minutes. After this time the reaction mixture was cooled to 0°C and left overnight. The *N*-substituted phthalimide separated out and was recrystallised from ethanol.

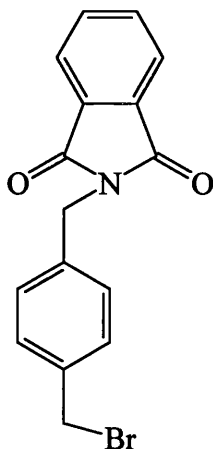
Yield = 160mg, 12.3%.

¹H NMR (CDCl₃): 4.53 (s, 2H); 4.85 (s, 2H); 7.41 (dd, *J* = 1.2Hz, *J*' = 4.3Hz, 4H); 7.81 (dd, *J* = 0.7Hz, *J*' = 6.5Hz, 4H).

¹³C NMR (CDCl₃): 41.21; 45.80; 123.39; 128.62; 128.93; 129.04; 132.06; 134.05; 136.58; 196.15; 214.16.

EI - MS: *m/z* = 285 (M.H₂O)⁺; 267 (M⁺); 250 (M - HO)⁺.

(e) ***p*-Phthalimidomethylbenzyl bromide³⁰**



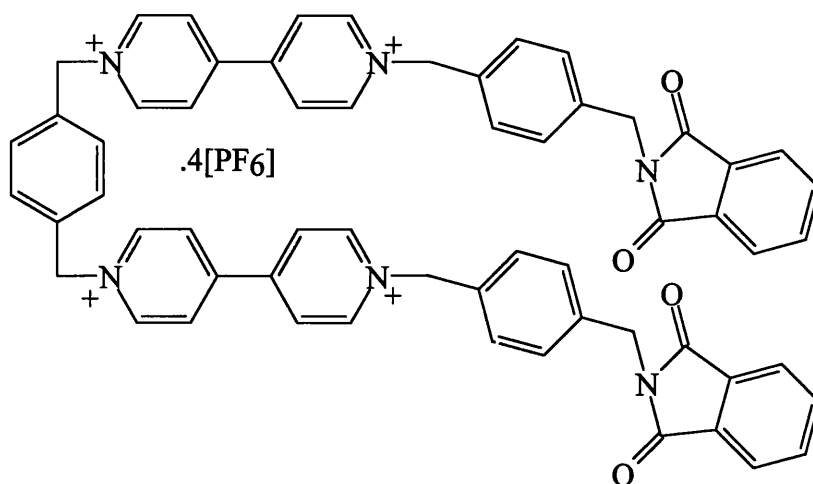
To a stirred room temperature solution of *p*-phthalimidomethylbenzyl alcohol (116mg, 0.43mmol) in dry chloroform (10ml) was added, dropwise, a solution of trimethylsilyl bromide (79mg, 0.645mmol) in dry chloroform (5ml). The reaction mixture was stirred for 3 days, the reaction being followed by TLC [SiO₂, CHCl₃] to check for complete reaction. The reagent, the solvent and the silyl ether by-product are volatile and were removed *in vacuo* to yield the product.

Yield = 127.4mg, 88.7%.

¹H NMR (d₆ - DMSO): 4.60 (s, 2H); 4.73 (s, 2H); 7.31 (dd, J = 12.0Hz, J' = 8.0Hz, 4H); 7.60 (m, 4H).

CI - MS (Positive ion, isobutane): m/z = 330 (M⁺); 250 (M - Br)⁺.

(f) **1,1' - [1,4 - Phenylenebis(methylene)][bis-*p*-phthalimido-methylbenzylbis-4,4'-bipyridinium] Tetrakis (hexafluorophosphate) (SB1)**



A solution of 1,1'-[1,4-phenylenebis(methylene)]bis-4,4'-bipyridinium bis(hexafluorophosphate) (136mg, 0.19mmol) in dry acetonitrile (30ml) was added over 6 hours to a solution of *p*-phthalimidomethylbenzyl bromide (127mg, 0.39mmol) in dry refluxing acetonitrile (30ml). Heating was continued for 18 hours.

After this time, the solution was cooled to room temperature concentrated *in vacuo*. The precipitate was filtered off and washed with acetonitrile (50ml) and diethyl ether (50ml) before being dissolved in the minimum distilled water. The aqueous solution was then washed with diethyl ether (4 x 50ml). The concentrated aqueous solution was then treated with a saturated aqueous solution of NH_4PF_6 until no further precipitation was observed. The precipitate was filtered off, washed with distilled water (50ml), methanol (50ml) and diethylether (50ml) before being recrystallised from acetone - water.

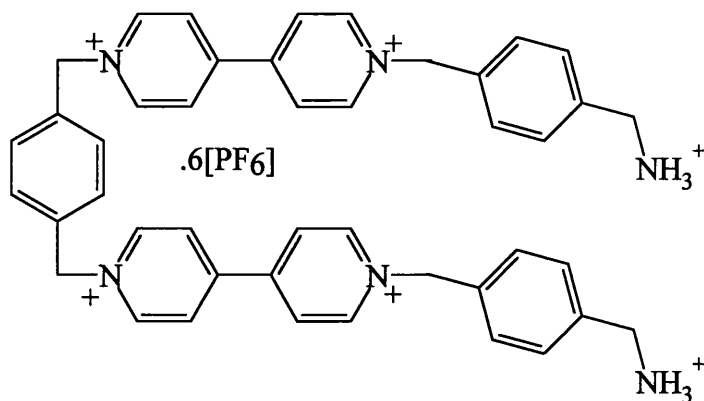
Yield = 180mg, 63.0%.

^1H NMR (d_6 - acetone): 4.75 (s, 4H); 5.87 (s, 4H); 5.93 (s, 4H); 7.35-7.55 (AA'BB', $J = 7.2\text{Hz}$, $J' = 1.2\text{Hz}$, 8H); 7.65 (s, 4H); 7.84 (m, 8H); 8.61 (m, 8H); 9.35 (m, 8H).

^{13}C NMR (d_6 - acetone): 40.20; 63.50; 63.95; 123.72; 127.31; 128.51; 129.78; 130.27; 131.70; 133.10; 135.18; 135.22; 138.90; 146.00; 150.12; 169.60.

FAB - MS (NBA matrix): $m/z = 1351$ (M - PF_6) $^+$; 1206 (M - 2PF_6) $^+$; 1061 (M - 3PF_6) $^+$.

(g) **1,1'-[1,4-Phenylenebis(methylene)][bis-*p*-aminomethylbenzylbis-4,4'-bipyridinium] Hexakis (hexafluorophosphate) (SB2)**



Compound **SB1** (previously converted to the chloride salt, 1.35g, 0.127mmol) was suspended in a mixture of glacial acetic acid (60ml) and concentrated HCl (60ml). The mixture was heated to reflux for 2 days.

After this time, the solution was cooled to room temperature and poured into cold water (5°C, 50ml). The phthalic acid by-product was removed by filtration and the filtrate was concentrated *in vacuo*. The product was precipitated by the dropwise addition of a saturated aqueous solution of ammonium hexafluorophosphate until no further precipitation was observed. The solid was filtered off and washed with water before being recrystallised from acetonitrile - distilled water.

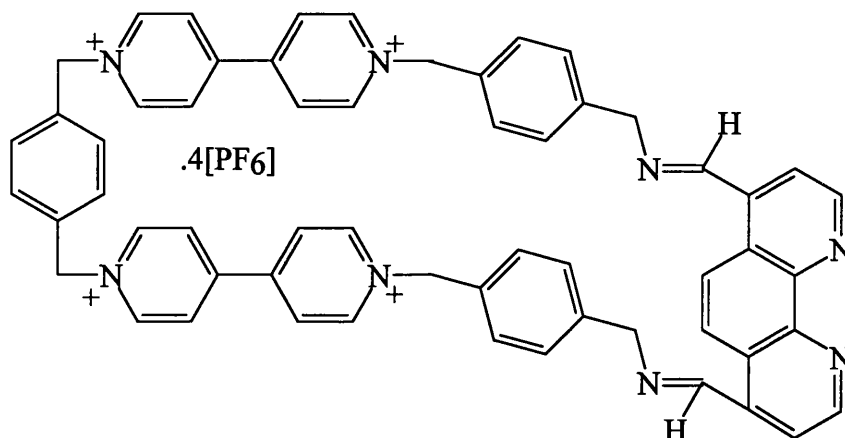
Yield = 0.88g, 45.1%.

¹H NMR (d₆ -acetone): 4.26 (s, partially obscured by a water peak, 4H); 6.04 (s, 4H); 6.06 (s, 4H); 7.53 - 7.67 (m, 8H); 7.70 (s, 4H); 8.67 - 8.68 (d, J = 6.8Hz, 8H); 9.30 - 9.32 (m, 8H).

¹³C NMR (d₆ - acetone): 51.52; 65.00; 65.13; 128.54; 129.60; 130.64; 130.88; 131.30; 131.72; 134.85; 135.25; 135.75; 146.73; 147.00; 151.44.

FAB - MS (NBA matrix): m/z = 1383 (M - PF₆)⁺; 1238 (M - 2PF₆)⁺; 1093 (M - 3PF₆)⁺; 948 (M - 4PF₆)⁺.

(h) Attempt to synthesise Cyclo[1,4-phenylenebis(methylene)][bis-4,4'-bipyridinium-*p*-methylenebenzyl]-1,10-phenanthroline-4,7-diimine Tetrakis(hexafluorophosphate) (L8)



A number of attempts were made to produce both the cyclophane and [2]catenane (with **34C10**) versions of this compound, but without success. The synthetic routes described below is an example of the typical conditions used in the attempted syntheses.

Method 1

1,10-Phenanthroline-4,7-dialdehyde (7.9mg, 0.033mmol) in dry DMSO (1ml) was added slowly to a room temperature mixture of compound **SB2** (52.0mg, 0.033mmol), compound **T1** (34.4mg, 0.099mmol) and pyridine (1 drop) in dry, degassed acetonitrile (6ml). Stirring was continued for 24 days, the reaction being monitored by sampling using FAB - MS.

Method 2

1,10-Phenanthroline-4,7-dialdehyde (7.8mg, 0.032mmol) in dry acetonitrile (25ml) was added slowly to a refluxing mixture of compound **SB2** (50.0mg, 0.032mmol) and pyridine (5.2mg, 0.065mmol) in dry, degassed acetonitrile (20ml). Stirring and heating were continued for 5 days, the reaction being monitored by sampling using FAB - MS.

2.4 Aromatic Electron Donor - Acceptor Binding Experiments

2.4.1 Benesi - Hildebrand Analysis.^{31,32}

This analysis assumes the formation of a 1:1 complex **SL** where **S** is the substrate and **L** is a ligand to which it binds. The essence of the technique is that a solution of the free substrate has a significantly different absorption spectrum from the complex **SL**. Therefore, the extent of binding may be followed simply by observing the changes in absorbance upon adding accurately measured quantities of **L** to a solution of **S** - the total concentration of **S** remains unchanged throughout.

In the specific context of the studies reported here, aliquots of an aromatic electron donor molecule (**DHB**, **DMB**, **TMPD**, **T1** or **T2**) are added to a solution of the receptor cyclophane (**L1** or **L2**). A charge transfer (**CT**) complex is produced and the growth of the **CT** band is followed by absorption spectroscopy. The initial receptor solution has zero molar absorbance at the wavelength where the **CT** band grows in.

To obtain binding constants from absorption data, the binding isotherm must first be derived. Assuming that Beer's law is followed by all species, then at zero ligand concentration;

$$A_0 = \epsilon_s b S_t$$

where S_t is substrate concentration, b is the pathlength and ϵ_s is the molar absorbance of **S**. On addition of ligand **L** (of concentration L_t), this becomes;

$$\begin{aligned} A_L &= \epsilon_s b [S] + \epsilon_L b [L] + \epsilon_{SL} b [SL] \\ &= \epsilon_s b S_t + \epsilon_L b L_t + \Delta \epsilon_{SL} b [SL] \end{aligned}$$

where $\Delta \epsilon_{SL} = \epsilon_{SL} - \epsilon_s - \epsilon_L$. The first and second terms of the above expression may be disregarded as they are equal to zero in the studies reported here. Combining this equation with the definition for a binding constant: $K_{SL} = [SL]/[S][L]$ leads to the expression;

$$\Delta A = K_{SL} \Delta \epsilon_{SL} b [S][L]$$

where $\Delta A = A - A_0$. As $S_t = [S] + [SL]$ then $[S] = S_t / (1 + K_{SL}[L])$, which gives;

$$\Delta A / b = S_t K_{SL} \Delta \epsilon_{SL} [L] / (1 + K_{SL}[L])$$

which is the binding isotherm for a 1:1 complex. The linearised form of this equation (below) is known as the Benesi - Hildebrand equation.

$$b/\Delta A = 1/S_t K_{SL} \Delta \epsilon [L] + 1/S_t \Delta \epsilon_{SL}$$

By plotting $S_t/\Delta A$ vs $1/[L]$, a straight line plot is obtained with a y - intercept of $1/\Delta \epsilon_{SL}$ and a gradient of $1/ K_{SL} \Delta \epsilon$ - thus the binding constant may be easily calculated.

2.4.2 ^1H NMR Techniques³¹

A similar premise is used in determining binding constants as was used in 2.4.1 above. In this case the binding constant under measurement pertains to a system containing a substrate **S**, a ligand **L** and a complex **SL** where **SL** is a 1:1 complex which is in fast exchange with **S** and **L**.

Initially **S** has a proton which comes into resonance at a frequency ν_s . As the ligand **L** is added and the complex is formed, this resonance becomes a weighted average of frequencies ν_s and ν_{SL} , whereby;

$$\nu_0 = f_{10}\nu_s + f_{11}\nu_{SL}$$

where f_{10} and f_{11} are weighted occupancy factors relating to the stability of **S** and **SL**. Thus the observed chemical shift may be expressed as;

$$\delta = f_{10}\delta_s + f_{11}\delta_{SL}$$

and as $f_{10} + f_{11} = 1$, then;

$$\delta = f_{11}(\delta_{SL} - \delta_s) + \delta_s$$

If chemical shift differences are defined as $\Delta = \delta - \delta_s$ and $\Delta_{11} = \delta_{SL} - \delta_s$ then assuming a 1:1 binding isotherm leads to the expression;

$$\Delta = \Delta_{11}K_{11}[L]/1 + K_{11}[L]$$

which in the linearised form gives the equation;

$$1/\Delta = 1/\Delta_{11}K_{11}[L] + 1/\Delta_{11}$$

where K_{11} is the binding constant of interest $[L]$ is the concentration of ligand added and Δ may be calculated from δ and δ_s which are measured experimentally. A plot of $1/\Delta$ vs $1/[L]$ gives a straight line plot with a y - intercept of $1/\Delta_{11}$ and a gradient of $1/\Delta_{11}K_{11}$ thus the binding constant may again be easily calculated.

Two important assumptions are made in this analysis:

(1) [L] is larger than [S] because L_t must equal [L], where;

$$\begin{aligned}L_t &= [L] + [SL] \\ &= [L](1 + K_{11}[S])\end{aligned}$$

so that L_t only equals [L] when $K_{11}[S] \ll 1$.

(2) It is assumed that when S and L bind, $SL = LS$. In addition it is assumed that S and L cannot bind to themselves.

2.4.3 Binding Constants from Fluorescence Quenching³³

Fluorescence is an enormously sensitive technique for studying molecular interactions and as such it has been described as the optimal signal transduction mechanism for sensing applications³⁴. Fluorescence is a sensitive technique because the observing wavelength is always longer than the exciting wavelength so that an output signal may be observed *versus* a zero (or near zero) background. What this means in practical terms is that any change in, for example, fluorescence must be due to interaction of the fluorophore with the fluorescence modulator.

Commonly fluorescence experiments involve binding of a fluorescent receptor to an analyte which modulates the fluorescence intensity of the receptor. In the context of the study reported here, the roles were reversed: the analyte (compound T1) is fluorescent ($\lambda_{max}=445\text{nm}$) in the unbound state, but upon addition of the receptor (compound L2) in accurately weighed aliquots, the fluorescence intensity is diminished. This quenching effect may be caused by the introduction of non - radiative energy loss pathways on formation of a charge transfer complex between the two compounds or by changes in the polarity of the environment around the fluorophore caused by complexation to the receptor.

The determination of the binding constant may be carried out using a standard analysis despite the unusual experimental conditions.

If F_0 is the intensity of fluorescence of the substrate at zero quencher concentration and F is the corresponding intensity at a given ligand concentration [L], then:

$$F_0/F = 1 + K[L]$$

where $K = [SL]/[S][L]$.

A linear plot of F_0/F *versus* [L] simply gives the binding constant K as the gradient of a straight line plot.

2.5 References

- [1] Kavarnos, G.J. *Fundamentals of Photoinduced Electron Transfer*, VCH, New York, 1993, 35.
- [2] Farrugia, L.J. *WinGX - 96 An Integrated System of Programs for the Solution, Refinement and Analysis of Single Crystal X-ray Diffraction Data*, 1996, University of Glasgow, UK.
- [3] Altomare, A.; Cascarano, G.; Giacovazzo, C.; Guagliardi, A. *J. Appl. Cryst.*, 1993, **26**, 343.
- [4] Sheldrick, G.M. *SHELXL93 Program for the Refinement of Crystal Structures*, 1993, University of Gottingen, Germany.
- [5] (a) Collin, J.P.; Harriman, A.; Heitz, V.; Odobel, F.; Sauvage, J-P. *J. Am. Chem. Soc.*, 1994, **116**, 5679. (b) Harriman, A.; Odobel, F.; Sauvage, J-P. *J. Am. Chem. Soc.*, 1995, **117**, 9461.
- [6] Gould, S.; Strouse, G.F.; Meyer, T.J.; Sullivan, B.P. *Inorg. Chem.*, 1991, **30**, 2942.
- [7] Various bromination strategies based on, for example, (a) Chaintreau, C.; Adrain, G.; Couturier, D. *Synth. Comms.*, 1981, **11**, 669. (b) Luning, U.; Skell, P.S. *Tetrahedron*, 1985, **41**, 4289. (c) Zhang, Y-H.; Dong, M-H.; Jiang, X-K.; Chow, Y.L. *Can. J. Chem.*, 1990, **68**, 1668. (d) Chow, Y.L.; Zhao, D-C. *J. Org. Chem.*, 1987, **52**, 1931. (e) Offerman, W.; Vogtle, F. *Synthesis*, 1977, 272. (f) Skell, P.S.; Day, J.C. *Acc. Chem. Res.*, 1978, **11**, 381. (g) Tanner, D.D.; Reed, D.W.; Tan, S.L.; Meintzer, C.P.; Walling, C.; Sopchik, A. *J. Am. Chem. Soc.*, 1985, **107**, 6576.
- [8] Luning, U.; Seshardi, S.; Skell, P.S. *J. Org. Chem.*, 1986, **51**, 2071.
- [9] Benniston A.C.; Mackie, P.R.; Harriman, A. *Tetrahedron Lett.*, 1997, **38**, 3577.
- [10] Sasse, W.H.F.; Whittle, C.P. *J. Chem. Soc.*, 1961, 1349.
- [11] (a) Eaves, J.G.; Munro, H.S.; Parker, D. *J. Chem. Soc. Chem. Commun.*, 1985, 684. (b) Beer, P.D.; Wheeler, J.W.; Grieve, A.; Moore C.P.; Wear, T. *J. Chem. Soc. Chem. Commun.*, 1992, 1225. Beer, P.D.; Fletcher, N.C.; Grieve,

- A.; Wheeler, J.W.; Moore, C.P.; Wear, T. *J. Chem. Soc. Perkin Trans. II*, 1996, 1545.
- [12] Ashton, P.R.; Menzer, S.; Raymo, F.M.; Shimizu, G.K.H.; Stoddart, J.F.; Williams, D.J. *J. Chem. Soc. Chem. Commun.*, 1996, 487.
- [13] Sullivan, B.P.; Salmon, D.J.; Meyer, T.J. *Inorg. Chem.*, 1978, **17**, 3334.
- [14] Dwyer, F.P.; Goodwin, H.A.; Gyarfas, E.C. *Aust. J. Chem.*, 1963, **16**, 544.
- [15] Hua, X.; von Zelewsky, A. *Inorg. Chem.*, 1995, **34**, 5791.
- [16] Kendrick - Geno, M.J.; Dawson, J.H. *Inorg. Chim. Acta.*, 1985, **97**, L41.
- [17] Meerween, H.; Hederich, V.; Wunderlich, K. *Ber. Dtsch. Pharm. Ges.*, 1958, **63**, 548.
- [18] Gardner, S. *B.Sc. Thesis*, 1995, University of Glasgow, UK.
- [19] Anelli, P.L.; Ashton, P.R.; Ballardini, R.; Balzani, V.; Delgado, M.; Gandolfi, M.T.; Goodnow, T.T.; Kaifer, A.E.; Philp, D.; Pietraszkiewicz, M.; Prodi, L.; Reddington, M.V.; Slawin, A.M.Z.; Spencer, N.; Stoddart, J.F.; Vicent, C.; Williams, D.J. *J. Am. Chem. Soc.*, 1992, **114**, 193.
- [20] Hanessian, S.; Liak, T.J.; Vanasse, B. *Synthesis*, 1981, 396.
- [21] Ashton, P.R.; Chrystal, E.J.T.; Mathais, J.P.; Parry, K.P.; Slawin, A.M.Z.; Spencer, N.; Stoddart, J.F.; Williams, D.J. *Tetrahedron Lett.*, 1987, **28**, 6367.
- [22] McCloskey, C.M. *Advan. Carbohydr. Chem.*, 1957, **12**, 137.
- [23] Asakawa, M.; Ashton, P.R.; Boyd, S.E.; Brown, C.L.; Gillard, R.E.; Kocian, O.; Raymo, F.M.; Stoddart, J.F.; Tolley, M.S.; White, A.J.P.; Williams, D.J. *J. Org. Chem.*, 1997, **62**, 26.
- [24] Lorkowski, H.J.; Pannier, R.; Werde, A. *J. Prakt. Chem.*, 1967, **35**, 149.
- [25] Preparation adapted from: Seiler, M.; Durr, H. *Synthesis*, 1994, 83.
- [26] Preparation adapted from: Amabilino, D.B.; Dietrich - Buchecker, C.O.; Livoreil, L.P.G.; Sauvage, J-P. *J. Am. Chem. Soc.*, 1996, **118**, 3905.
- [27] Preparation adapted from: Houghton, M.A.; Bilyk, A.; Harding, M.A.; Turner, P.; Hambley, T.W. *J. Chem. Soc. Dalton Trans.*, 1997, **15**, 2725.
- [28] Preparation adapted from: Bishop, M.M.; Lewis, J.; O'Donoghue, T.D.; Raithby, P.R. *J. Chem. Soc. Chem. Commun.*, 1978, 476.
- [29] Bardsley, W.G.; Ashford, J.S.; Hill, C.M. *Biochem. J.*, 1971, **122**, 557.
- [30] Jung, M.E.; Hatfield, G.L. *Tetrahedron Lett.*, 1978, **6**, 4483.

- [31] Connors, K.A. *Binding Constants: The Measurement of Molecular Complex Stability*, Wiley - Interscience, New York, 1987.
- [32] Benisi, H.A.; Hildebrand, J.H. *J. Am. Chem. Soc.*, 1949, **71**, 2703.
- [33] McCormick, D.B. in *Molecular Association in Biology* (Ed.: B. Pullman), Academic, New York, 1968, 377.
- [34] Czarnik, A.W. *Fluorescent Chemosensors for Ion and Molecule Recognition*, ACS Symposium Series 538, Washington D.C., 1992.

Chapter Three

Cyclophanes

3.1 Introduction

Cyclophanes ('bridged aromatic compounds') represent a central class of synthetic receptors in molecular recognition studies.¹ A wide variety of substrates from inorganic and organic ions to neutral molecules have been complexed by tailor-made cyclophanes. There are numerous examples of cyclophanes² which show host properties towards guest molecules and ions including crown ethers, spherands, calixarenes, porphyrins, cyclotrimeratrylenes and cryptophanes. To operate as effective host compounds it is desirable that cyclophanes must not be neither too rigid nor too flexible, as if they are too inelastic, their rates of complexation and de-complexation are too slow to be of practical use. If, conversely, the receptor is too flexible, there is either no cavity formed or the cavity is filled intramolecularly by portions of the ring itself. As cyclophanes may be constructed so as to have variable proportions of flexible aliphatic and rigid aromatic components, they are ideal sources of receptor molecules. Cyclophanes provide the opportunity to tune the cavity size and shape so as to be complementary to the substrate whose binding is being sought.

With the possibility of locating groups precisely in space, cyclophane chemistry has thus provided the building units for a number of interesting classes of compounds² and has become a major component of supramolecular chemistry. In addition, cyclophanes have been extensively employed in the study of molecular recognition processes because of the availability of a wide variety of three-dimensional molecular architectures.

In addition to the study of inclusion phenomena, it is possible to introduce into the rings of cyclophane systems substituents which can interact as ligands with metal cations.³ The formation of inclusion complexes is brought about by utilising *endoreceptors* i.e. binding sites which may be said to 'point inwards' towards the cyclophane cavity. In contrast, *exoreceptors* are orientated so as to 'point outwards' from the cyclophane ring so that binding of substrates outside of the cavity becomes possible (figure 3.1).⁴

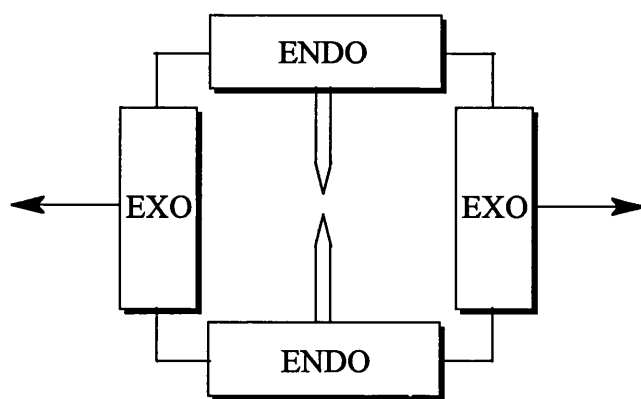


Figure 3.1: Definition of exoreceptors and endoreceptors.

Cyclophanes bearing endoreceptors are much more common than those bearing exoreceptors because cyclophane chemistry evolved as a means of studying inclusion phenomena. The design of such receptors has employed macrocyclic architectures containing rigid spacers that allow binding sites to be positioned on the walls of molecular cavities in such a way that they converge towards the bound substrate.³ This convergent approach, whereby endoreceptors effect an endo-recognition process for a complementary substrate, is one of the functions that the cyclophanes discussed in this chapter were designed to perform. The specific substrates for which the cyclophanes were designed are aromatic electron donor molecules. Such molecules are capable of forming EDA (electron donor acceptor) complexes with π - electron deficient units such as those based upon the paraquat dication (as discussed previously, see section 1.6.5). The work of Stoddart and co-workers is particularly relevant to this type of intermolecular interaction, indeed, the first cyclophane capable of forming an inclusion complex with electron rich aromatic molecules (employing EDA interactions) was synthesised by this group (figure 3.2).⁵

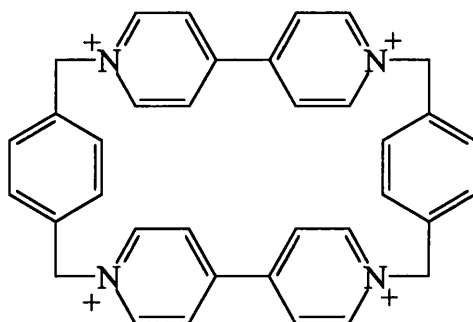


Figure 3.2: A cyclophane capable of convergent binding of aromatic electron donors.

From figure 3.2 it is evident that this receptor is not particularly functional in that it binds substrates but it does not have the ability to perform any additional functions. Further developments have taken place however, building on the basic system depicted above, including the development of cyclophanes containing both electron rich and electron poor subunits which allow the cyclophanes to recognise one another and so assemble into organised two and three dimensional solid-state structures,^{4,6,7} and the introduction of subunits containing elements of chirality (both planes and axes).^{8,9} It has been possible to bind a wide range of aromatic electron donors in such cyclophanes, with binding constants being in the general range 10 - 100 M⁻¹ for alkoxy-benzene¹⁰ donors and up to 6500M⁻¹ for systems based on naphthoxy¹¹ electron donors. In addition it has been possible to expand the size of the cavity of the cyclophane so that it becomes possible to employ these systems to study the phenomenon of second sphere coordination of metal complexes (figure 3.3).¹²

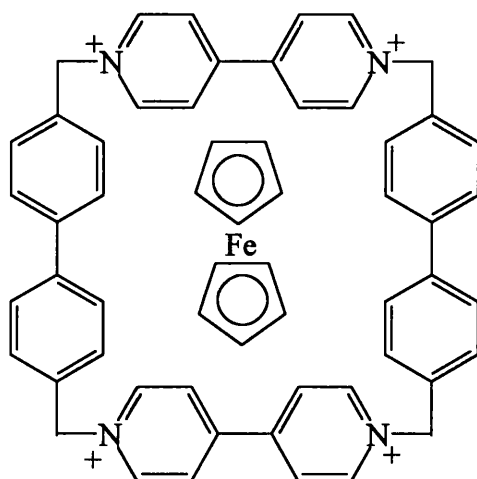


Figure 3.3: Second sphere coordination of ferrocene by a cyclophane receptor.

The syntheses and properties of cyclophanes capable of forming EDA complexes is, thus, well established. The next step towards the creation of functional assemblies (e.g. those which are photo- and/or redoxactive) was to combine cation chelating exoreceptors with endoreceptors in novel cyclophane systems. The use of *metallo-exoreceptors*³ allows the arrangement of ligands bearing recognition sites around a metal ion - thus large polymolecular arrays may be constructed which possess recognition sites in specific dispositions. An advantage of this approach is that the metal centre may change the properties of the cyclophane

by virtue of its charge, preferred coordination geometry or electronic properties (electron acceptor or donor properties in the ground or excited states). Chelating units such as 1,10-phenanthroline have been employed in this regard by Sauvage and co-workers (especially in catenate systems see: section 1.6.4) and 2,2'-bipyridine has been incorporated into receptor molecules by Beer (in acyclic systems see: section 1.5 part (3)) and Rebek¹³ (as part of crown ethers). The cyclophanes presented in this chapter employ 2,2'-bipyridine as a cation chelating exoreceptor.

2,2'-Bipyridine and its derivatives are renowned for their ability to form coordination complexes with metal ions of almost all groups in the periodic table.¹⁴ A description of the bonding in such complexes may be given by molecular orbital theory whereby coordinative bonds are formed between metal ions and ligands which are able to form both σ - and π - bonds. 2,2'-Bipyridine is both a σ -donor and π -acceptor ligand - the lone pair of electrons on the nitrogen atoms form a σ -bond with metal s-orbitals, and filled metal d-orbitals of the correct geometry can overlap with the unoccupied ligand π^* -orbitals - thus 'back-bonding' occurs. Because the ligand acts as soft σ -base and π -acid it is capable of stabilising transition metals in low oxidation states.

2,2'-Bipyridines are important in a wide variety of chemical fields: in coordination chemistry ($\text{Fe}(\text{bipy})_3^{2+}$ was identified by Blau in 1888); in analytical chemistry and in biological systems including enzymes. Many supramolecular systems have included bipyridine units, with the systems constructed by Lehn and co-workers being particularly interesting due to their intriguing topologies and their close analogies to biologically important systems. By joining several bipyridine units together it has been possible to construct, on addition of cations with tetrahedral coordination geometries (e.g. Cu (I)), a series of double-stranded double helices¹⁵ (or 'helicates'), an example of which is shown in figure 3.4.

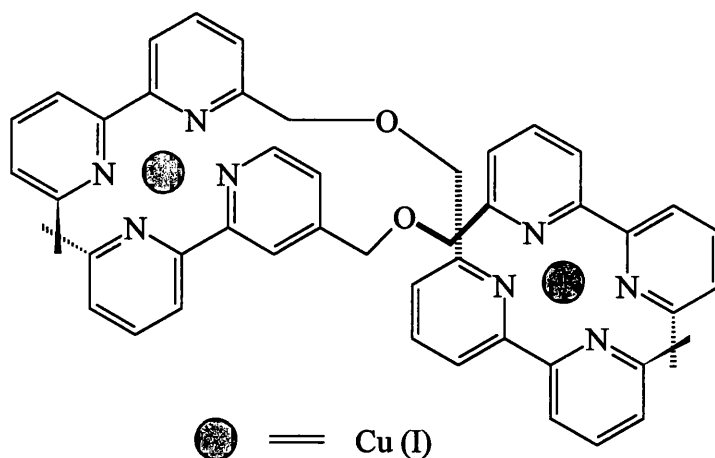


Figure 3.4: A 'Helicate' molecule.

3.2 Precursors

The precursor compound **P1**, 4,4'- bis(methylene-4,4'-bipyridinium)-2,2'-bipyridine bis(hexafluorophosphate), was prepared according to a route often used to synthesise cyclophane precursors containing viologen subunits.⁵ The high yielding synthetic route involves simple nucleophilic substitution reactions, performed using high dilution conditions so as to avoid the production of oligomers, followed by anion exchange. The ¹H NMR spectrum shows a relatively simple pattern as expected for a symmetrically substituted 2,2'-bipyridine (resonances are assigned in table 3.2.1), with only three signals for the chelating unit (figure 3.9), a singlet for the methylene linker unit and four sets of signals corresponding to the bipyridinium unit (two sets each for the protons α and β to the charged and neutral nitrogen atoms).

The low-energy conformation of 2,2'-bipyridine and its derivatives is well established¹⁴ as being the 'transoid' conformer where the nitrogen donor atoms on the chelating unit are as far apart as possible due to electrostatic repulsion of the lone pair of electrons on each of the nitrogen atoms. A molecular mechanics model of precursor **P1** (figure 3.5) indicates that this molecule should adopt the 'transoid' conformation as expected.

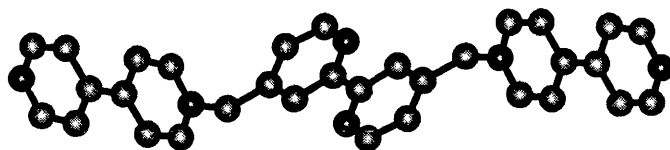


Figure 3.5: Molecular mechanics model of P1.

The geometry proposed by the molecular mechanics model was confirmed by the determination of the solid state structure of **P1.2**[PF₆] by X-ray diffraction analysis (figure 3.6; crystal data given in appendices). The torsion angle between the nitrogen atoms on the 2,2'-bipyridine unit was found to be 180.0°, as expected from the model. The bipyridinium units are not planar, indeed the torsion angle between the two pyridine rings is 32.0° - an unusual geometry - nearly 44% of related (dicationic) bipyridinium units in the Cambridge Crystallographic Database are planar.¹⁶

The implications of this conformation for cyclisation of this precursor at the two free nitrogen atoms cannot be overstated - the reacting centres are nearly 21Å apart - thus formation of oligomeric species is much more likely when attempting a ring closure reaction than is cyclisation.¹⁷ Using an aromatic electron donating molecule as a template for the synthesis of ring closed cyclophanes has met with some success - the template overcomes the unfavourable conformation of the precursor presumably by stabilising an intermediate tri-cationic species by way of EDA, electrostatic and hydrogen-bonding interactions. This strategy does not, however, produce high yields of products (as will be discussed later in section 3.3).

Given the limitation on the yields of product achievable by use of precursor **P1**, alternative strategies were designed and attempted which, it was hoped, would provide more efficient routes to target molecules. The first of these strategies involved 'pre-coordinating' precursor **P1** with a metal centre, thus 'fixing' the conformation of the bipyridine unit so that cyclisation became more favourable. As the target molecule often contained a metal centre such as ruthenium or osmium tris-bipyridyl as part of its molecular architecture, the pre-coordination motif was an appealing route. The second strategy employed to overcome the unfavourable conformation of precursor **P1** involved changing the substitution pattern from a 4,4'- to a 5,5'- disubstituted pattern so that the conformation of the central 2,2'-

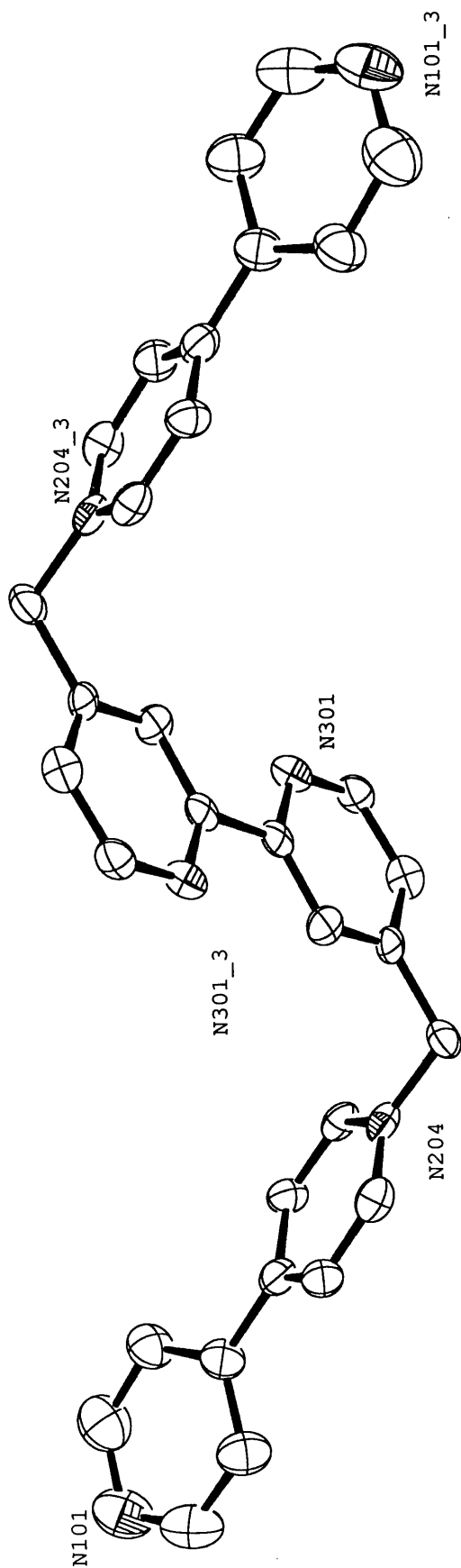


Figure 3.6: Crystal structure of precursor P1²⁺ (PF₆⁻ counterions omitted).

bipyridine unit became irrelevant to the cyclisation step. Employing this strategy has, of course, one major drawback in that the geometry and shape of the products (i.e. the dimensions of the cavity) are altered¹⁸ - hence the host-guest chemistry of the products formed by such a route is different from that of the target molecules.

The first of the routes described above was employed to synthesise both $\text{Os}(\text{bipy})_2(\mathbf{P1})(\text{PF}_6)_4$ and $\text{Ru}(\text{bipy})_2(\mathbf{P1})(\text{PF}_6)_4$. The effect of adding these metal centres to the precursor ligand may be determined by inspection of the reduction potentials of the ligands pyridinium substituent. In the 'free' precursor this reduction potential is found at -0.88V (all potentials quoted *vs* SCE) and in the ruthenium (II) complex the equivalent potential is found at -0.90V - thus very little perturbation has occurred to the reduction potential (and by extension, to the macro properties of the ligand other than its conformation) by metal ion coordination. The osmium complex follows this trend, with the ligand pyridinium reduction wave occurring at -0.85V . The ^1H NMR spectra of the ruthenium (figure 3.7) and osmium complexes of **P1** are, of course, slightly more complex than that of the 'free' precursor because two non-substituted bipyridine moieties have been added to the system. Coordination of the metal centres also causes certain signals to change their chemical shift. For instance, the 2,2'-bipyridine signals are substantially moved, whereas the resonance for the methylene spacer unit moves only slightly (by around 20Hz or 0.06ppm). Other changes to the ^1H NMR spectra include broadening of the signal corresponding to the protons α to the non-quaternised nitrogen from a doublet to a broad singlet in both the osmium and ruthenium complexes. Assignments of the ^1H NMR signals for **P1** in its ruthenium and osmium complexes are detailed in table 3.2.1.

The analytical data collected for the metal complexes of **P1** confirms the formation of the complexes but gives no clues as to the conformation of the new compounds. The UV-VIS absorption spectra of the complexes are not atypical for ruthenium and osmium tris bipyridyl complexes. The ruthenium complex shows the expected MLCT absorption band at around 455nm although the band is broader than that for simple $\text{Ru}(\text{bipy})_3^{2+}$. This broadening may be explained by changes in the excited MLCT states caused by the pyridinium substituents (see chapter 5). The osmium complex also has the expected MLCT absorption at 425 and 495nm - in

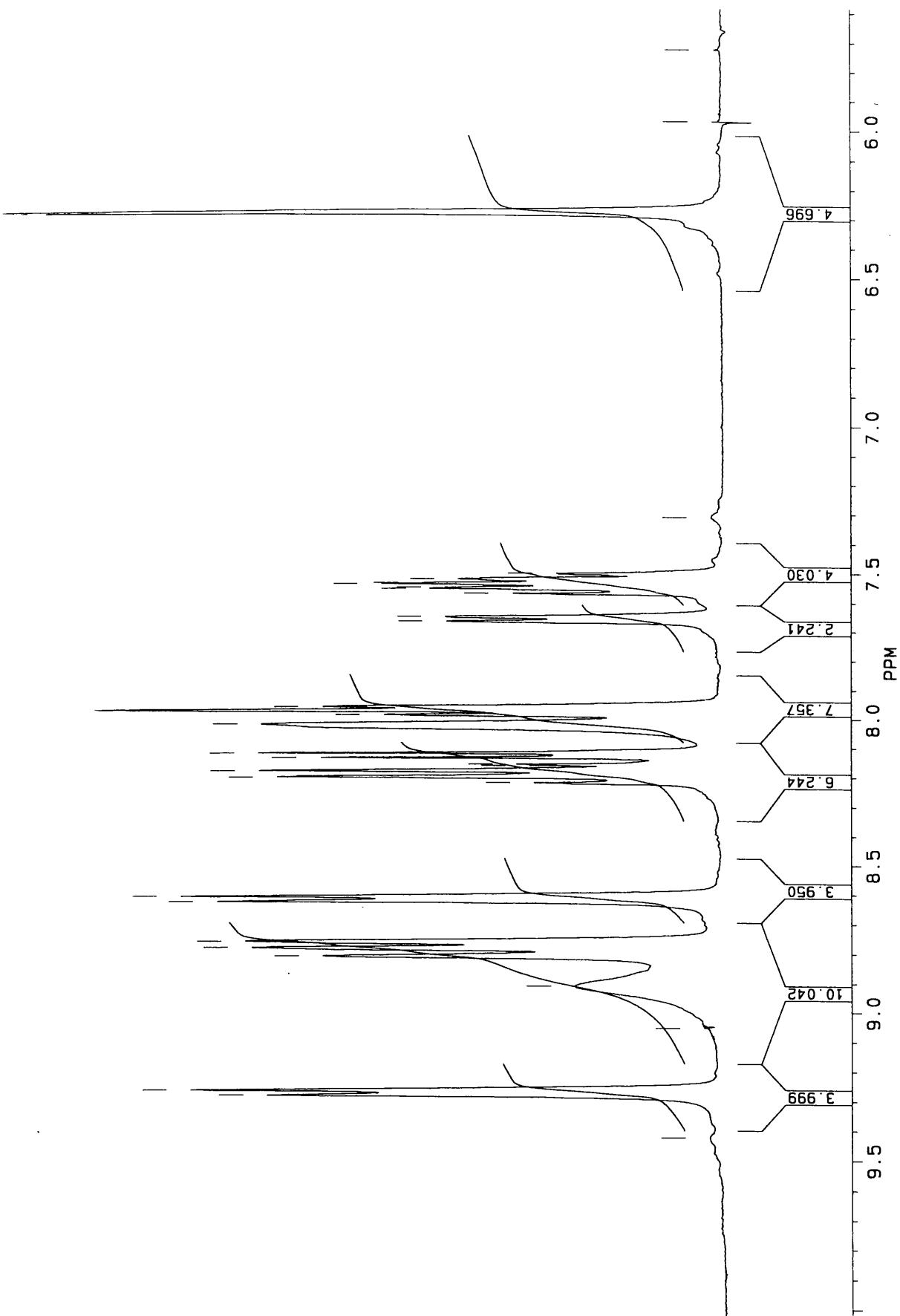


Figure 3.7: ^1H NMR spectrum of $[\text{Ru}(\text{bipy})_2(\text{P1})][\text{PF}_6]_4$ in d_6 -acetone at 360MHz and 298K.

contrast to the ruthenium complex, however, the asymmetric nature of the band is maintained despite derivatisation of the bipyridine ligand. Whilst no fluorescence could be observed for the osmium compound under steady state conditions, the ruthenium complex of **P1** is fluorescent albeit with a much reduced intensity and with a significantly red - shifted fluorescence maximum (again indicating the difference in the excited states between $\text{Ru}(\text{bipy})_3^{2+}$ and $\text{Ru}(\text{bipy})_2(\text{P1})^{4+}$).

Thus the spectroscopic and analytical data indicated that the ligand had entered into a tris chelate complex with the osmium and ruthenium metal centres. Molecular modelling of these complexes, using a molecular mechanics force-field indicated that the coordinated precursor **P1** should be in an ideal conformation for cyclisation at the free nitrogen atoms because the unfavourable 'transoid' conformation had been reversed by metal complexation. This model was confirmed by the determination of the solid state structure of $\text{Ru}(\text{bipy})_2(\text{P1})(\text{BF}_4)_4$ by X-ray diffraction analysis (figure 3.8, crystal data is given in appendices). The torsion angle between the nitrogen atoms on the 2,2'-bipyridyl portion of **P1** has changed from 180.0° to 2.2° thus the chelating unit is almost planar. The non-derivatised bipyridine molecules are also close to being planar (torsion angles of 0.4° and 2.5° with respect to the nitrogen atoms) as expected. The coordination geometry about the ruthenium atom is not perfectly octahedral (although all ruthenium - nitrogen bond lengths are in the range 2.045 to 2.069Å) - this may possibly be due to steric repulsion of the bulky **P1** ligand by the bipyridine ligands. The bipyridinium units are once again not planar, with the torsion angles about the central carbon - carbon bonds being 11.8° and 26.7° - these twists are assumed to be generated by the three dimensional packing of the compound in the solid state. The conformation is clearly in a favourable conformation for cyclisation, indeed the distance between the 'free' nitrogen atoms has fallen from around 21Å to 6.55Å - approximately the same size as, for example, a phenyl spacer unit.

The second strategy for incorporating 2,2'-bipyridine into cyclophane systems whilst overcoming the unfavourable conformation of precursor **P1** was to change the substitution pattern of the chelating unit from a 4,4'- to a 5,5'- pattern (figure 3.9). This strategy resulted in the synthesis of the precursor **P2** and the complementary non-chelating precursor **P3**.

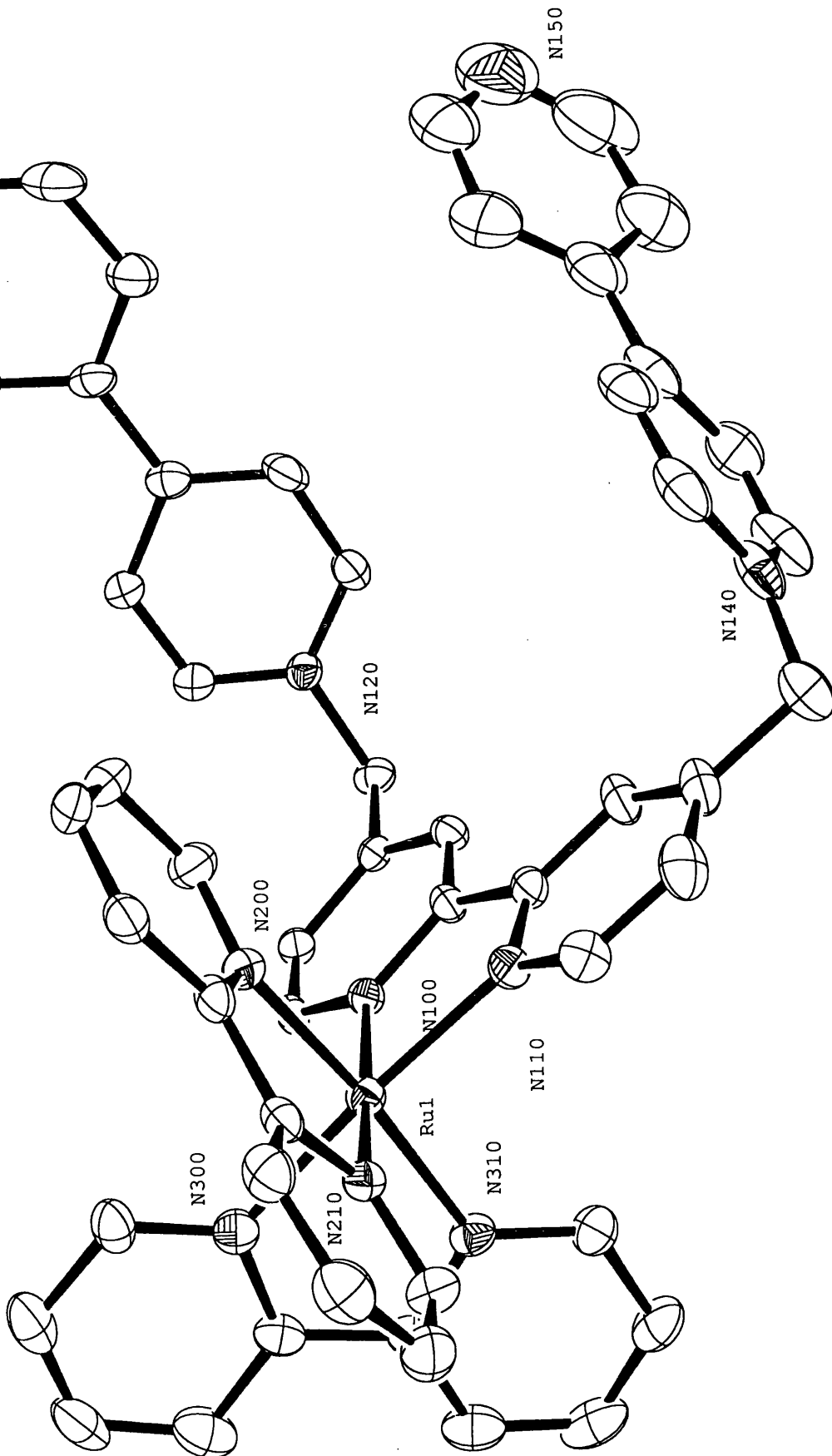


Figure 3.8: Crystal structure of Ru(bipy)₂(P1)⁴⁺ (BF₄ counterions omitted).

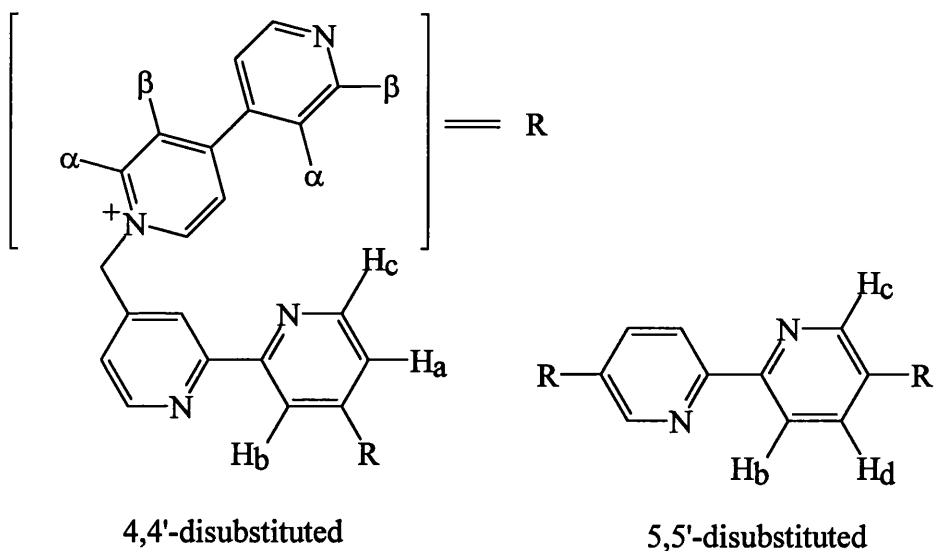


Figure 3.9: 2,2'-Bipyridine substitution patterns.

Compounds **P2** and **P3** have been synthesised previously,¹⁸⁻²⁰ but not for the purpose of incorporating chelating units into cyclophane structures. The ¹H NMR spectrum for compound **P2** is rather similar to that of **P1**, except that the change in substitution pattern is evident from the changes in the chemical shifts of the protons on the chelating unit (see table 3.2.1).

	P1	Ru(bipy)₂(P1)	Os(bipy)₂(P1)	P2*
Free N α,β	8.87, 8.00	8.90, 8.19	9.05, 8.25	8.93, 8.38
Quatr. N α,β	9.51, 8.77	9.28, 8.62	9.30, 8.65	8.87, 7.83
CH₂ spacer	6.33	6.28	6.31	5.89
H_a	7.64	7.65	obscured	-
H_b	8.66	8.81	obscured	8.56
H_c	8.80	8.11	obscured	8.84

Table 3.2.1: Selected ¹H NMR data for precursor ligands and complexes.

All ¹H NMR data was collected in d₆-acetone at 360MHz at 298K except * **P2** in d₃-acetonitrile at 360MHz at 298K.

3.3 Cyclophane L1

The cyclophane compound **L1**, cyclo[bisparaquat-*p*-phenylene-2,2'-bipyridine] tetrakis(hexafluorophosphate) was prepared by employing a template synthesis using the aromatic electron donor 1,5-bis[(hydroxyethoxy)ethoxy]naphthalene (compound **T1**) as the template. The means by which the template functions is well documented in the literature, the reviews of Stoddart *et al* being of particular interest in this regard.²¹ The template molecule **T1** was chosen in preference to its phenoxy equivalent (1,4-bis[2-{2-(2-hydroxyethoxy)ethoxy}ethoxy]benzene **T2**) because the naphthoxy template is known to form much stronger EDA complexes with viologen derivatives than does the phenoxy compound (association constants of **T1** are more than twice as great as those for **T2**)¹¹ - a fact that is reflected in the measured binding constants for the two templates with compound **L1** (section 3.3.1). Purification of the cyclophane involved separation of the product from the starting materials and from oligomeric species which were produced as a consequence of the aforementioned unfavourable conformation of precursor **P1**. A chromatographic separation was developed which allowed facile separation of these fractions. The elution of the colourless cyclophane product was followed by use of iron as an indicator. This works as a purple-red tris chelate is formed when bipyridine containing species elute.

The ¹H NMR spectrum of **L1** (figure 3.10) shows a rather simple pattern with signals corresponding to the methylene spacer units at 6.15 (CH₂-phenyl) and 6.27 (CH₂-bipy), the three 2,2'-bipyridine signals at 7.93, 8.22 and 8.78, the phenyl spacer at 7.75 and the viologen signals at 9.60, 8.67 (α and β to the nitrogen bound to the bipy unit) and at 9.38 and 8.59 (α and β to the nitrogen bound to the phenyl spacer). All chemical shifts quoted are for **L1** in d₆-acetone at 360MHz at 298K.

The electrochemical properties of **L1** are very different from its precursor **P1** in that two reduction waves for the paraquat subunit are found at -0.40 and -0.83V (*vs* SCE) instead of just one. The cyclophane also shows interesting host - guest and coordination chemistry as is discussed in sections 3.3.1 and 3.3.2. The connectivity and geometry of the cyclophane may be analysed from the solid state structure as determined by X-ray analysis (figure 3.11, crystal data is given in appendices).

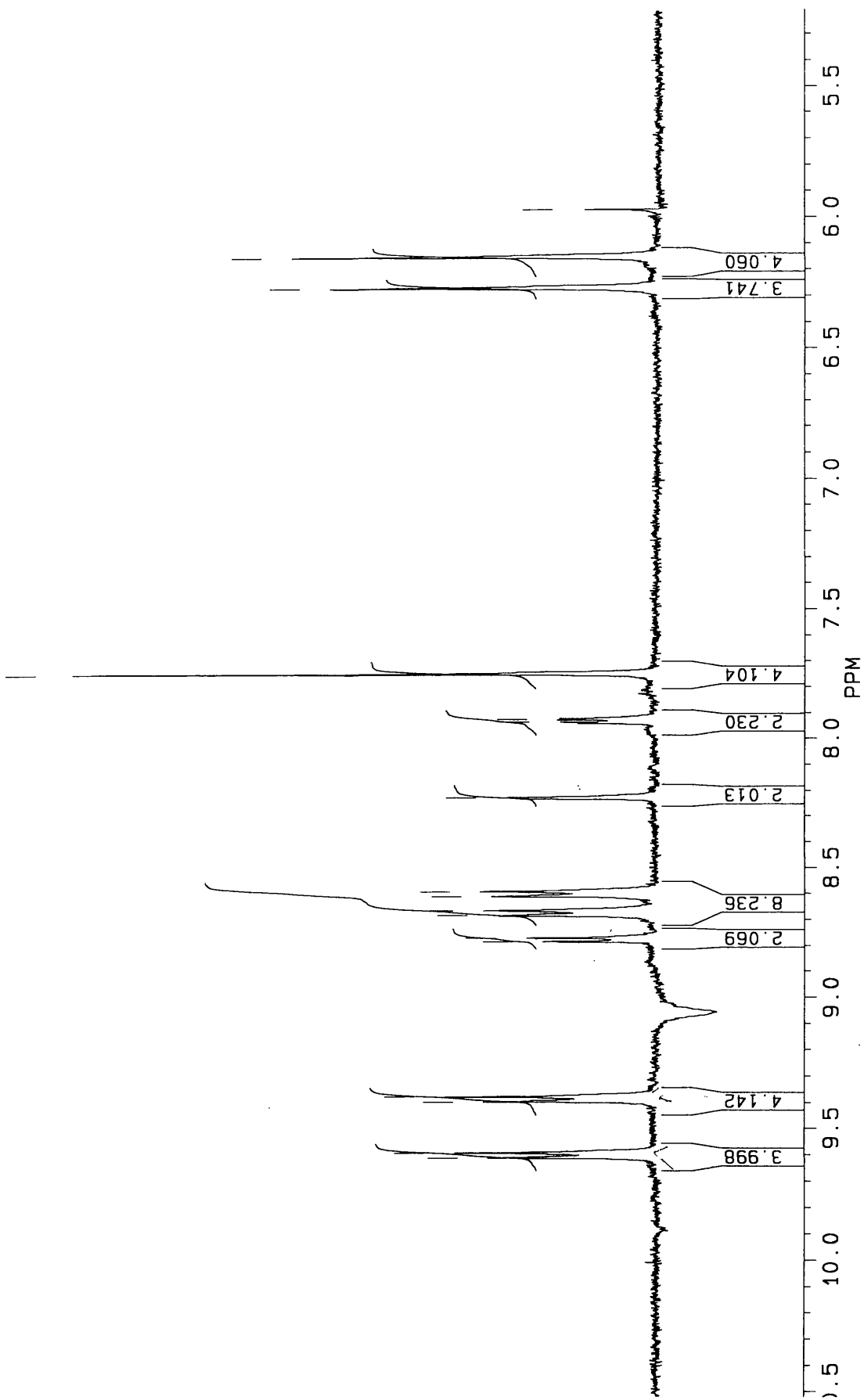


Figure 3.10: ¹H NMR spectrum of L1(PF₆)₄ in d₆-acetone at 360MHz and 298K.

The cyclophane has overall dimensions of approximately 12Å by about 6 - 7Å. The molecule is 'wedge' shaped in that the viologen units are not perfectly coplanar - they diverge from their narrowest point at the phenyl spacer (the methylene units being 5.77Å apart) to their widest at the 2,2'-bipyridine unit (the methylene units being 7.37Å apart at this point). The geometry is brought about in part by the 'cisoid' conformation of the bipyridine unit, the torsion angle between the nitrogen atoms being 17.7°. This geometry may not be the most favourable for forming EDA complexes with electron donating substrates, however evidence from solid state structures of this cyclophane with such donor molecules indicates that complex formation is still possible. Further, ¹H NMR evidence from metal cation binding experiments and from host-guest studies indicates that there is some conformational freedom in this cyclophane. In addition to their divergent configuration, the viologen units are significantly twisted about their central carbon - carbon bonds (torsion angles of 27.4° and 36.4°) - these twists may be the result of strain within the cyclic structure, which prevents the viologen units from adopting the expected planar geometry. The 2,2'-bipyridine unit is at an angle to the plane of the viologen units in the cyclophane giving the structure a bent 'dog - leg' appearance. The bond angle between the viologen nitrogen, the methylene spacer and the carbon on the 4- or 4'- position on the bipy unit is about 111°.

3.3.1 Host-Guest Chemistry of L1

Cyclophane structures bearing viologen subunits have a rich and well established host-guest chemistry with aromatic electron donors, whereby electron donor-acceptor (EDA) complexes are readily produced.^{10,11} The formation of EDA complexes may be easily followed by changes in the absorption spectrum of the receptor as a charge transfer interaction between the aromatic donor-acceptor pair produces a charge transfer band. Alternatively ¹H NMR spectroscopy may be employed, where addition of an aromatic electron donor to a solution of the guest cyclophane causes shifts in the resonances of the cyclophane. By employing the above techniques, the changes in the spectroscopic properties of the cyclophane upon formation of an EDA complex may be analysed so that the binding constant for the substrate with the cyclophane may be conveniently determined. In addition to determining the binding characteristics of cyclophane L1 it was desirable to

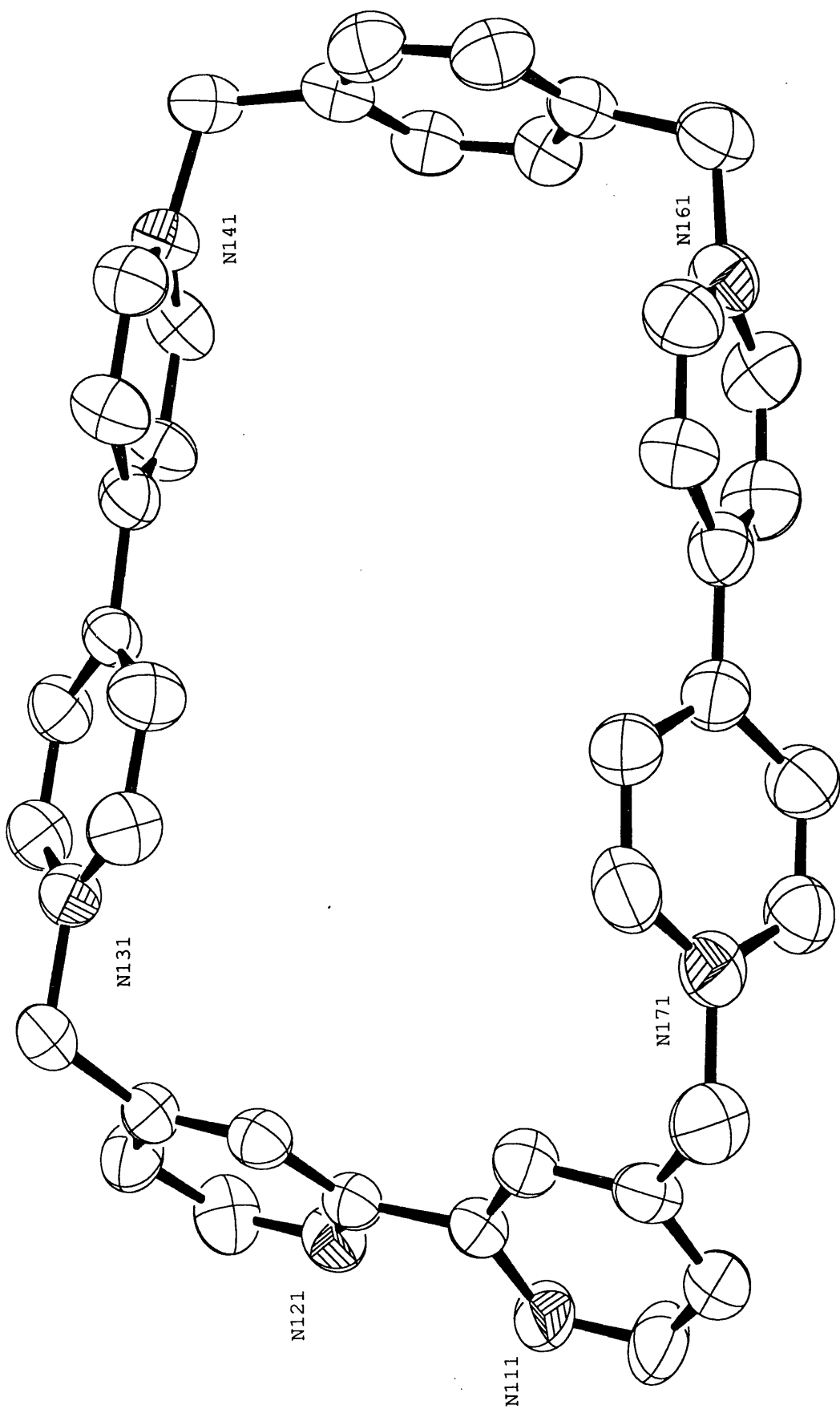


Figure 3.11: Crystal structure of cyclophane L1⁴⁺ (PF₆ counterions omitted).

compare the binding properties of this cyclophane both with its closely related analogue **L2** and with the simple non-chelating cyclophane depicted in figure 3.2. The binding properties of the simple cyclophane are well known^{10,11} in the literature. The aromatic electron donating substrates (figure 3.12) which were used in the binding studies were: 1,4-dihydroxybenzene (DHB), 1,4-dimethoxybenzene (DMB), N,N,N',N'-tetramethyl-1,4-phenylene diamine (TMPD), 1,5-bis[(hydroxyethoxy)ethoxy]naphthalene (**T1**) and 1,4-bis[2-{2-(2-hydroxyethoxy)ethoxy}ethoxy]benzene (**T2**).

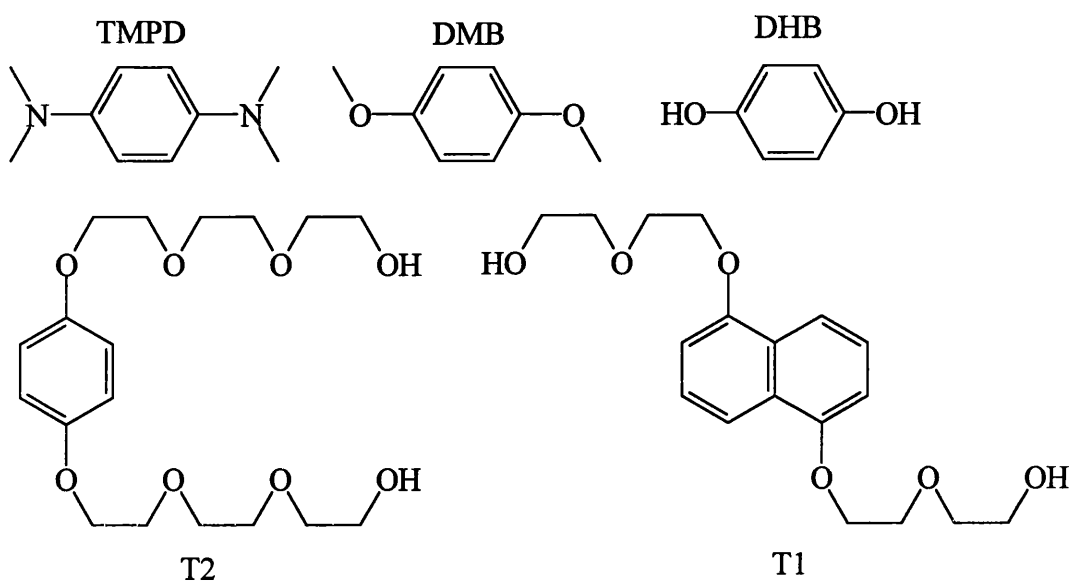


Figure 3.12: Aromatic electron donating substrates.

Upon addition of aliquots of an aromatic electron donor to a solution of cyclophane **L1**, a charge transfer band appears and grows in intensity as the concentration of donor increases. The absorption spectra from a typical experiment (in this case cyclophane **L1** with donor molecule **T2**) are shown in figure 3.13. By use of the equation:

$$b/\Delta A = 1/S_t K_{SL} \Delta \epsilon [L] + 1/S_t \Delta \epsilon_{SL}$$

where b = pathlength (1cm), ΔA = change in absorbance, K_{SL} = binding constant, $\Delta \epsilon_{SL}$ = molar extinction coefficient of the complex, $[L]$ = concentration of the donor substrate and S_t = concentration of the acceptor cyclophane, and by plotting $S_t/\Delta A$ vs $1/[L]$, a straight line plot is obtained which has a gradient equal to $1/K_{SL} \Delta \epsilon$ and a y-intercept equal to $1/\Delta \epsilon$ - thus the binding constant may be calculated. The Benesi - Hildebrand plot for the binding of **T2** with **L1** is given in figure 3.14 by way of an example of this type of analysis.

Benesi - Hildebrand was the most common technique employed to determine binding constants in the studies reported here. Techniques involving ^1H NMR were also employed (albeit less frequently) to confirm the binding constants derived by other means. The technique has been discussed previously (see section 2.4.2) but the analysis is rather similar to that discussed above in that a linearised form of the binding isotherm is used to plot a straight line graph of the reciprocal of the changes in chemical shift of the indicative experimental signal vs the reciprocal of the ligand concentration - the binding constant is obtained from the gradient. A typical plot obtained by these means for the binding of DMB with L1 is shown in figure 3.15.

The values for the binding constant and molar extinction coefficient, the method of measurement and the corresponding value of the binding constant for the simple cyclophane (c.f. figure 3.2) are given in table 3.3.1.

Donor Substrate	Cyclophane L1	Cyclophane L1	Cyclophane L1	Non-chelating Cyclophane
	K (M^{-1})	ϵ ($\text{M}^{-1}\text{cm}^{-1}$)	Technique	K (M^{-1})
DHB	< 1	-	Abs.	18
DMB	1.2, 2.2	454	Abs., NMR [#]	18
TMPD	6.7	1667*	Abs.	42
T1	> 3100	1086	Abs.	> 5000
T2	90.0	370	Abs.	2241

Table 3.3.1: Binding data for cyclophane L1.

All data was collected in dry degassed acetone except [#]NMR data which was collected in *d*₆-acetone. The value for ϵ for TMPD* is twice the expected value¹⁰ - this may be due to aerial oxidation of the donor molecule, thus the value of the binding constant may be inaccurate. Due to the exceptionally weak binding of DHB with L1 no value for ϵ could be obtained.

The trend of the binding constants displayed in the table above are well established^{10,11} in the literature. The simple benzene - based systems (DHB, DMB and TMPD) are bound by the acceptor cyclophane by virtue of their electron donating properties, i.e. they form EDA complexes with the electron accepting viologen units of the cyclophane. The benzene-based donor T2 has a larger binding constant than the more simple systems because the polyether 'arms' covalently

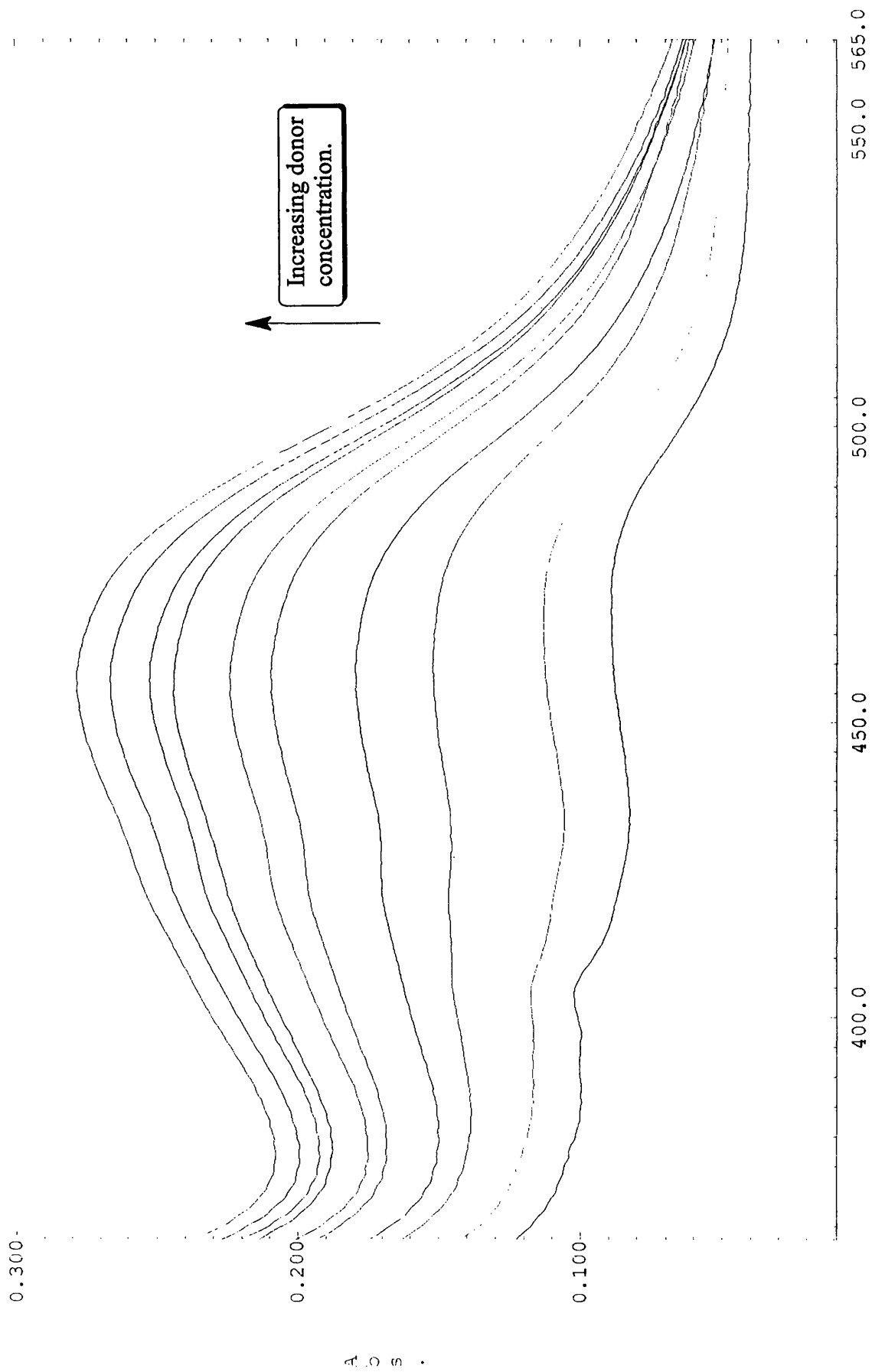


Figure 3.13: Absorption spectra showing progressive binding of T2 to L1⁴⁺ in acetonitrile.

Benesi-Hildebrand Analysis of Binding of T2 to L1

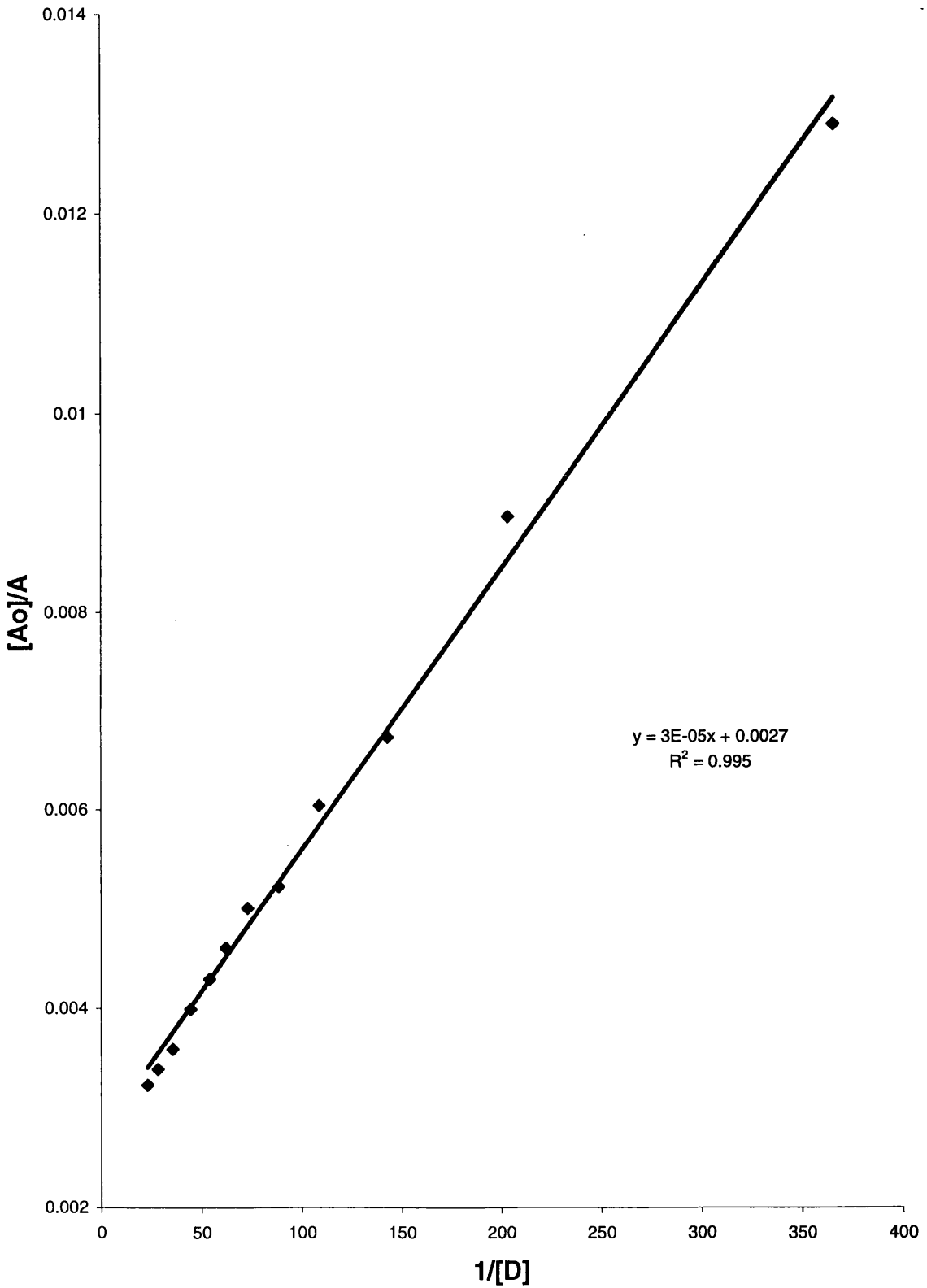


Figure 3.14: Benesi-Hildebrand analysis of binding of T2 to L1⁴⁺.

Analysis Of Binding Of DMB with Cyclophane L1 from NMR Data.

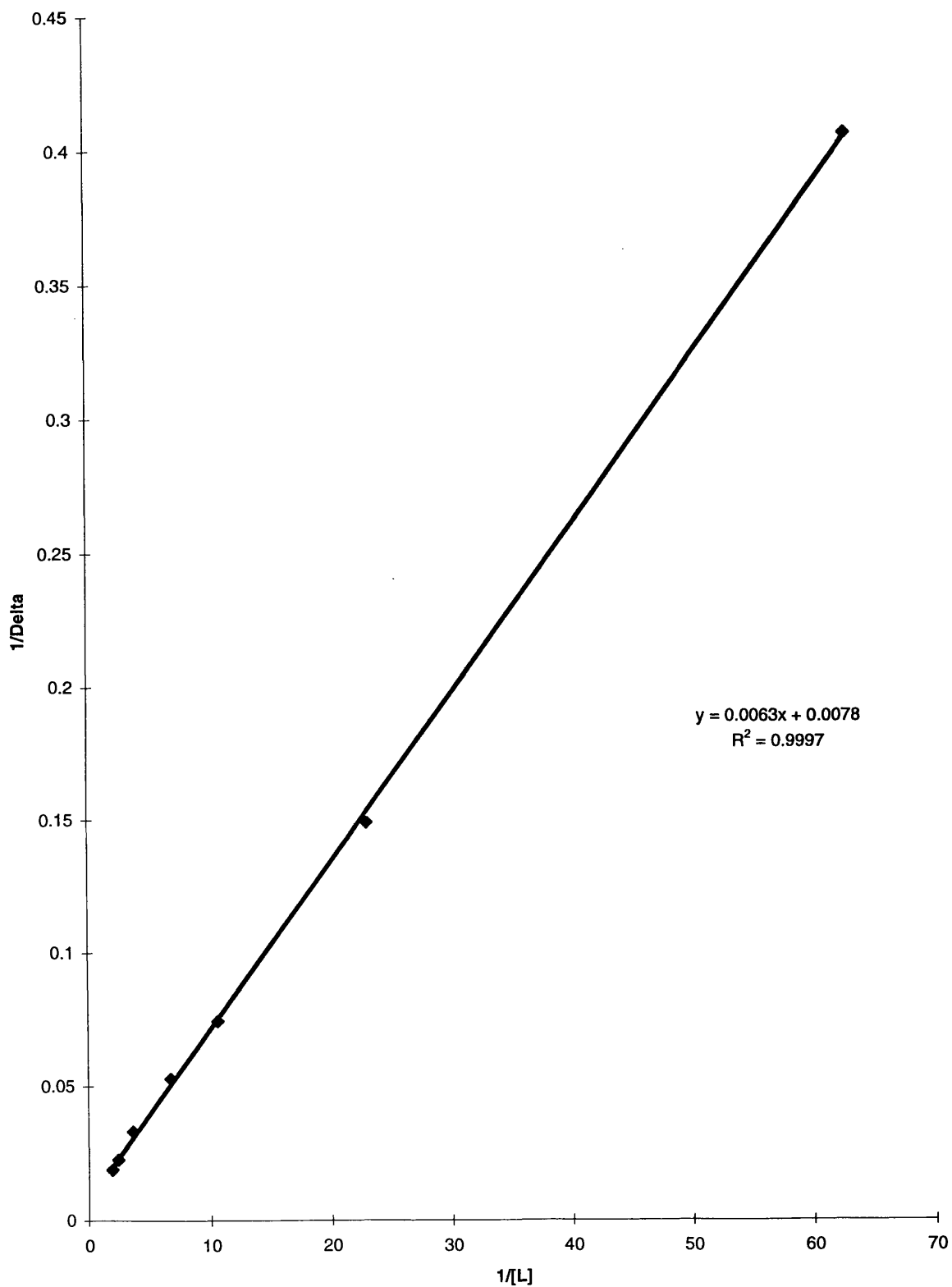


Figure 3.15: Analysis of binding of DMB to L1⁴⁺ as followed by ¹H NMR spectroscopy.

attached to the electron donating unit stabilise the EDA complex by virtue of their hydrogen-bonding and electrostatic interactions with the viologen units. The compound **T1** has the largest binding constant because it possesses a more easily oxidised donor centre than **T2**, thus it forms stronger EDA complexes.

Indeed, cyclophane **L1** forms a very strong complex with the template molecule **T1** - an result that is expected from related literature studies¹¹ and the observed improved yield of **L1** on employing **T1** rather than **T2** as template molecule in its synthesis. The geometry of the binding interaction is evident from the solid state crystal structure of the complex between **L1** and **T1** as presented in figures 3.16 and 3.17 (crystal data is given in appendices).

There are many notable features of this structure, relating both to the conformation of the cyclophane and the geometry of the EDA interaction. The cyclophane adopts a conformation which is different to that in the uncomplexed case, with the 2,2'-bipyridine unit being 'transoid' with respect to the nitrogen atoms with a torsion angle of 141.8°. The viologen units are once again twisted about their central carbon-carbon bonds (torsion angles of 20.3° and 19.2°) again possibly due either to strain within the cyclophane or due to packing requirements. The cyclophane maintains its wedge shape, with the distance between the methylene units at the phenyl spacer being 5.79Å whereas at the bipyridine unit the equivalent distance is 8.44Å. The bent 'dog-leg' shape of the cyclophane is lost in this structure, presumably because of the 'transoid' conformation of the chelating unit. There are two molecules of donor molecule **T1** for every one cyclophane unit, with one molecule being bound inside the cyclophane cavity and the other being bound 'alongside' the cyclophane. The result of this arrangement is that a π -stack of alternating acceptor-donor-acceptor-donor units is produced along the crystallographic *c* axis. The closest contact distances for the donor-acceptor pairs are approximately 3.6 to 3.7Å. The long axes of the naphthalene units are offset by +55° and by -65° respectively for the inside and alongside units from the long axes of the viologen acceptor units as is often the case in such systems.¹⁶ The inside and alongside naphthalene units have different orientations, possibly due to the need to keep the long polyether 'arms' on each molecule a far apart as possible whilst maintaining the offset geometry of their interaction with the viologen acceptors. The polyether 'arms' of the donor molecules engage in weak hydrogen bonding

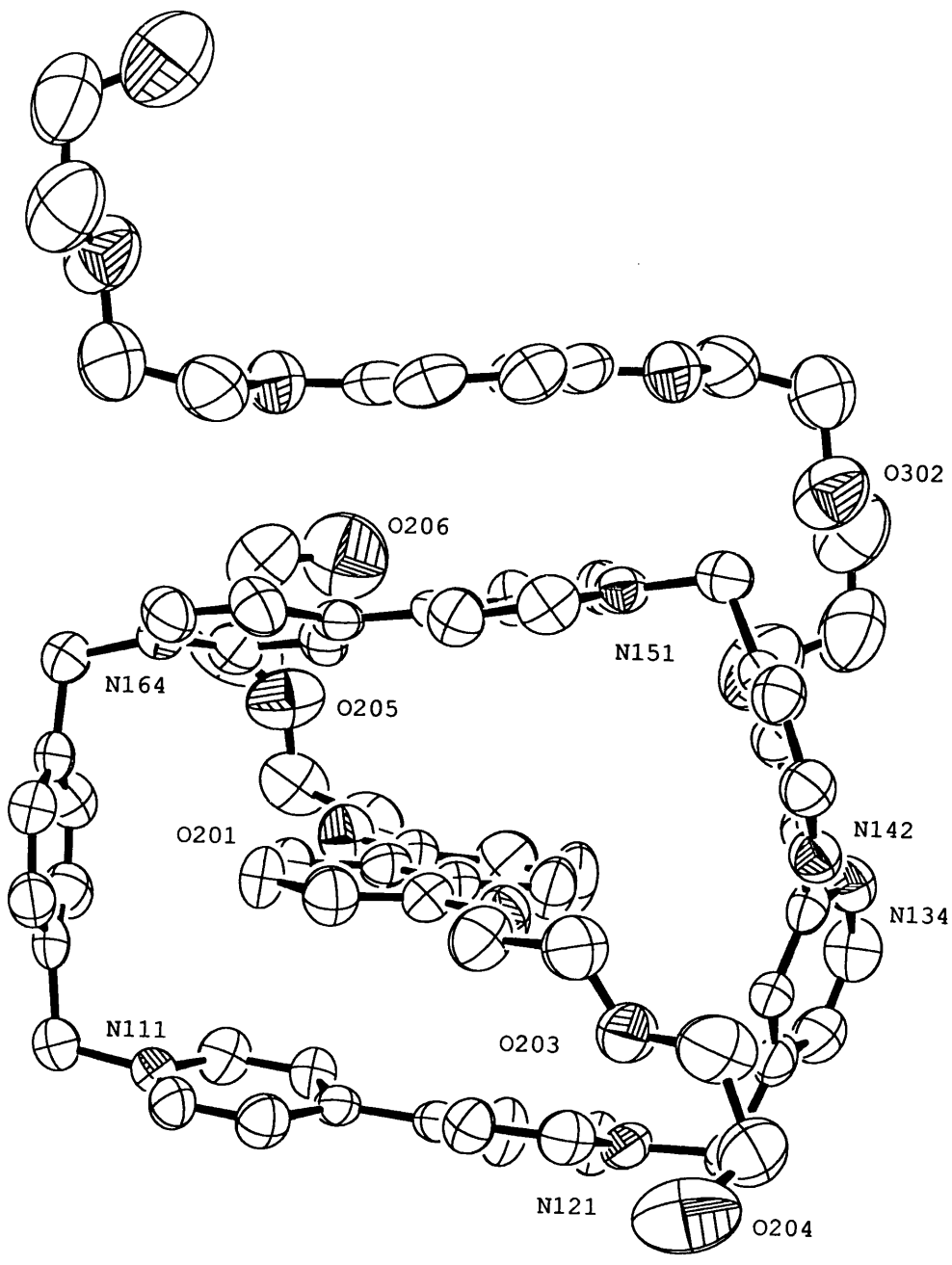


Figure 3.16: Crystal structure of $L1^{4+} \cdot [T1]_2$ (PF_6 counterions omitted).

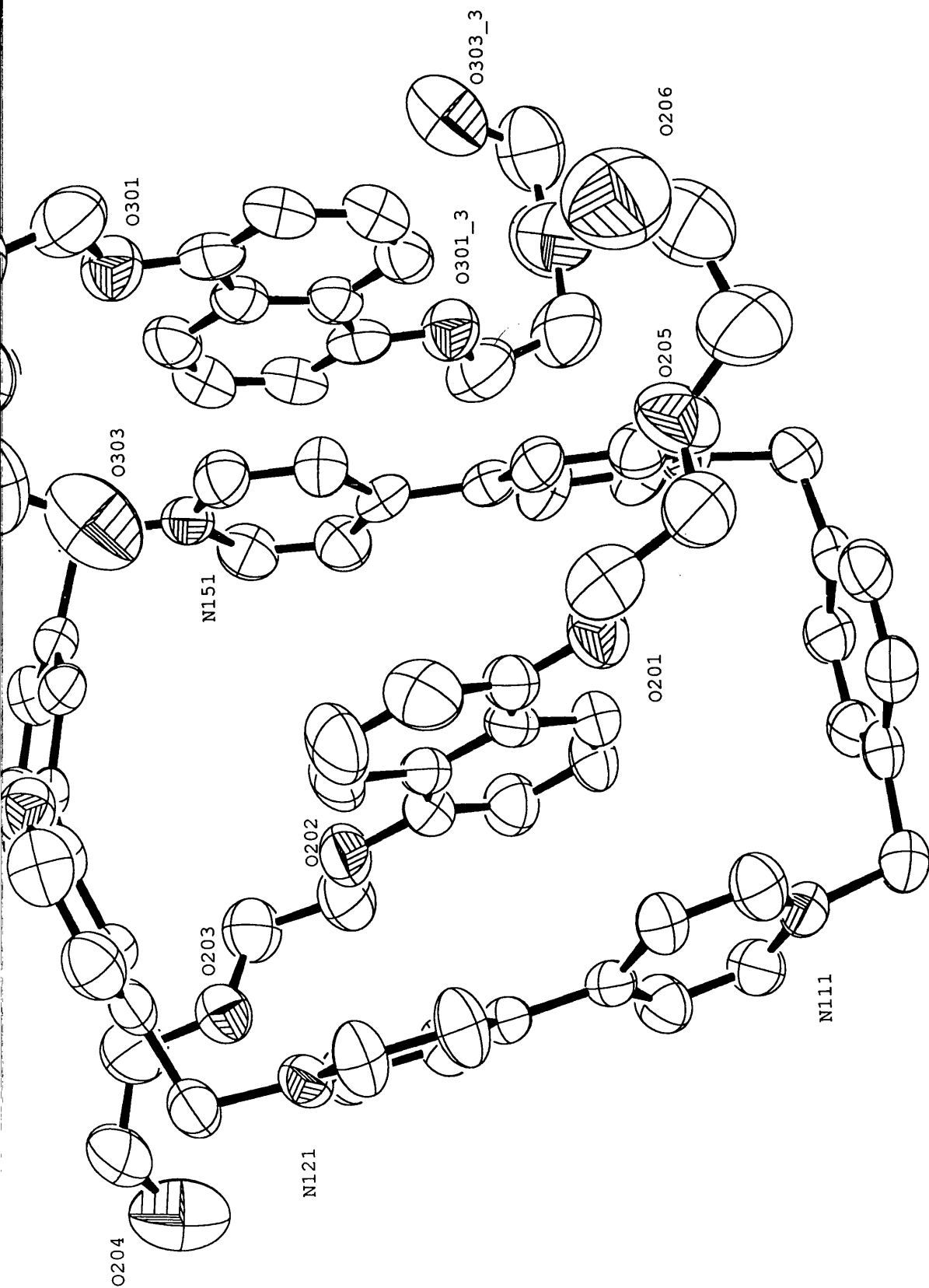


Figure 3.17: Crystal structure of $L1^{4+} \cdot [Tl]_2$ (PF₆ counterions omitted).

interactions with the 'acidic' protons which are on the positions α and β to the positively charged quaternary nitrogen atoms on the viologen subunits, the average C-H-O distances being between 3.2Å and 3.5Å.

3.3.2 Coordination Chemistry of L1

As was discussed previously, 2,2'-bipyridine has a rich and varied coordination chemistry. The coordination chemistry of cyclophane **L1** was approached in two distinct ways so as to achieve two different aims. The first of these involved adding simple metal salts to the cyclophane with the aim of constructing polymolecular arrays in which the metal centre acted as a central pinion around which dimeric (in the case of cations which form tetrahedral complexes) or trimeric (where cations form octahedral complexes) species are formed. The second approach was to append photoactive metal centres such as ruthenium and osmium tris bipyridine onto the acceptor cyclophane so that light induced electron transfer reactions may be investigated. The latter metal centres were added to the molecular architecture either before the cyclisation step (employing the pre-coordination motif) or after cyclisation once the free ligand had been synthesised.

The first of the approaches outlined above was used to produce aggregates of ligand **L1** with Cu (I), Zn (II) and Fe (II) from their simple $\text{Cu}(\text{CH}_3\text{CN})_4(\text{BF}_4)$, $\text{Zn}(\text{CF}_3\text{SO}_3)_2$ and $\text{FeSO}_4 \cdot 7\text{H}_2\text{O}$ salts respectively. The formation of cyclophane - metal complexes was followed by ^1H NMR spectroscopy because the resonances corresponding to the chelating unit move substantially upon complexation. In addition to the expected bipyridine shifts however, a number of other signals most notably those for the phenyl spacer and the those corresponding to the protons α and β to the nitrogen on the pyridinium ring closest to the 2,2'-bipyridine unit are considerably shifted on complexation. Figure 3.18 shows three ^1H NMR spectra corresponding to: (a) the 'free' cyclophane **L1**, (b) **L1** with an aliquot of $\text{FeSO}_4 \cdot 7\text{H}_2\text{O}$ added and (c) $\text{Fe}(\text{L1})_3(\text{PF}_6)_{14}$. From this figure it may be seen that upon complexation of **L1** there are significant changes to its NMR spectrum: the methylene signal at 6.27ppm (next to the bipyridine unit) moves substantially to 6.18ppm, the phenyl signal at 7.75ppm moves to 7.88ppm, all three bipyridine signals are moved significantly (one to under the phenyl resonance), both β signals

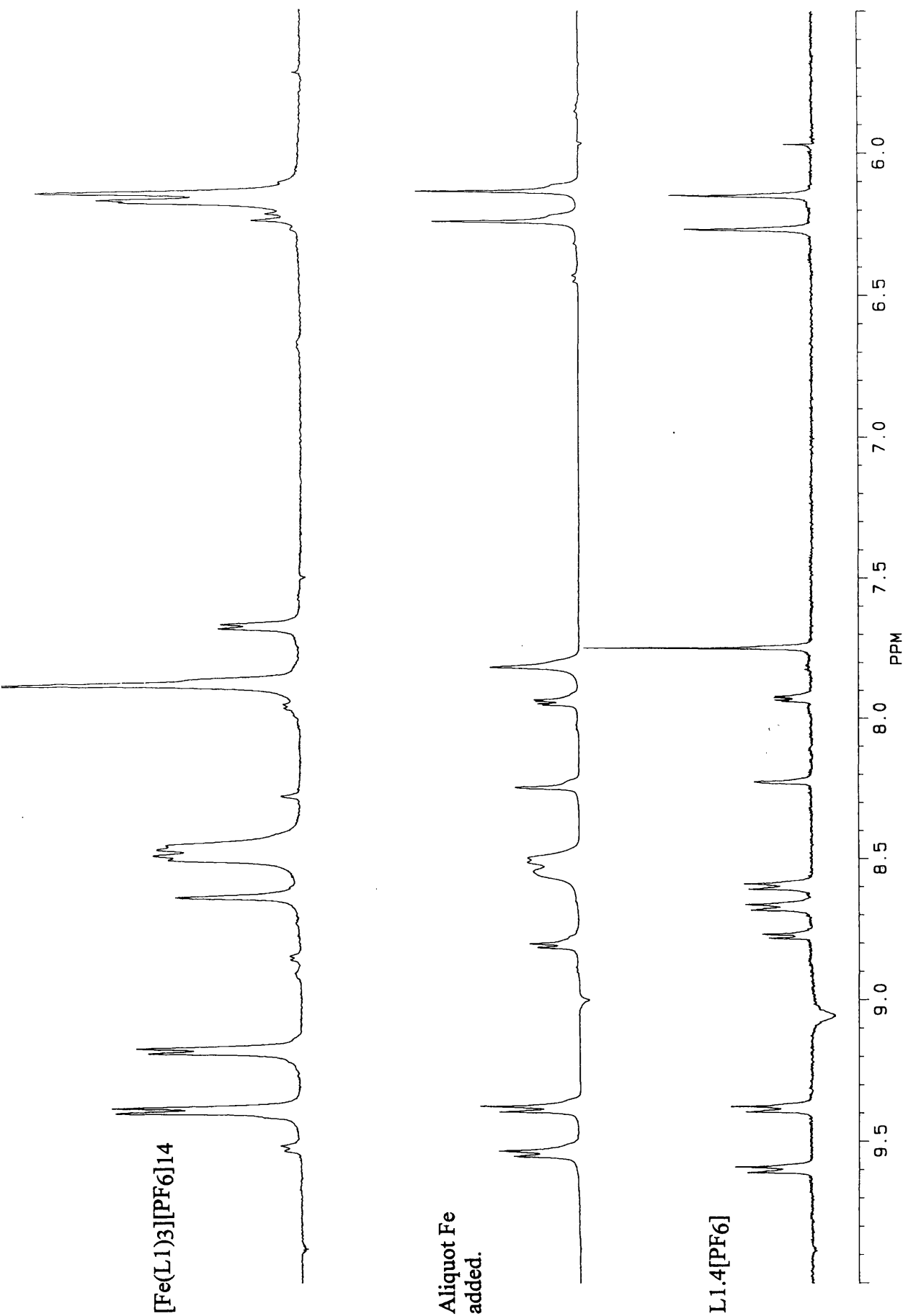


Figure 3.18: ^1H NMR spectra of $\text{L}1(\text{PF}_6)_4$ and its iron complex in d_6 -acetone at 360MHz and 298K.

broaden and move together to produce a broad multiplet at 8.47-8.49ppm and the both sets of α signals move upfield by approximately 72Hz (0.2ppm). Similar changes are found in the NMR spectra of the zinc (II) and copper (I) complexes (see table 3.3.2 for a summary of selected ^1H NMR data for these complexes). The implication of the movement of the majority of the cyclophane resonances upon complexation is that changes occur in the conformation of the entire cyclophane when it binds a metal centre. The nature of these conformational changes are not clear and are not able to be deduced from spectroscopic techniques. However, given the conformational fluidity present in cyclophane **L1** (as observed in the crystal structures of **L1** and its complex with the donor molecule **T1**) it is possible to speculate that in the solution phase the structure of **L1** has the chelating unit in the 'transoid' conformation - however, upon complexation with a metal cation the conformation of the bipyridine unit must 'flip' with the remainder of the cyclophane structure adjusting to accommodate this change.

	CH(α)	CH(β)	Phenyl	CH ₂	H _a	H _b	H _c
L1	9.38 9.60	8.60 8.67	7.75	6.15 6.27	7.93	8.22	8.77
Cu(L1)₂	9.40 9.44	8.56	7.89	6.21 6.25	8.71	8.17	8.78
Fe(L1)₃	9.18 9.39	8.48	7.88	6.15 6.18	7.67	8.63	7.88
Zn(L1)₂	9.44 9.57	8.57	7.87	6.19 6.27	8.39	9.00	9.12

Table 3.3.2: Selected ^1H NMR data for **L1 and its coordination complexes.**

All NMR data was recorded in d_6 -acetone (n.o. = not observed).

The geometry of the iron-cyclophane complex is obvious from its absorption spectrum, in that it is characteristic for an iron tris bipyridyl complex. This formulation was confirmed by analytical data. The geometry of the copper (I) complex would be expected to be tetrahedral about the metal centre, thus a dimeric (with respect to **L1**) aggregate should be formed. The analytical evidence for this geometry is not overwhelming but mass spectrometry appears to support the assertion that this complex is dimeric. Zinc (II) is generally regarded as forming

rather labile complexes, indeed it may form either 4, 5 or 6 coordinate complexes. However, evidence obtained from mass spectrometry again indicates that a dimeric complex is formed.

Having synthesised polymolecular arrays of cyclophane **L1**, it is convenient to investigate how cation chelation affects the host-guest chemistry and redox properties of the cyclophane. As an example, the cyclic voltammogram of $\text{Fe}(\text{L1})_3(\text{PF}_6)_{14}$ (vs Ag/AgNO_3) is presented in figure 3.19. The reduction potentials of the viologen for this tris chelate are found at -0.37V and -0.81V (as opposed to -0.40V and -0.83V for the 'free' cyclophane) - thus incorporation of the cyclophane into the trimeric complex does not appear to significantly perturb its electrochemical properties.

In contrast to the redox properties, however, the host-guest complexes of the zinc (II) and iron (II) complexes of **L1** exhibit substantially different properties to those of the free cyclophane (the host-guest chemistry of the copper (I) complex was not investigated due to apparent oxidation of the metal centre leading to uncertain complex stoichiometry). The iron complex $\text{Fe}(\text{L1})_3(\text{PF}_6)_{14}$ possesses a tris chelate geometry around the central ion which gives the complex a 'propeller' shape, with each blade of the propeller being a cyclophane unit - a molecular mechanics model of the complex is presented in figure 3.20.

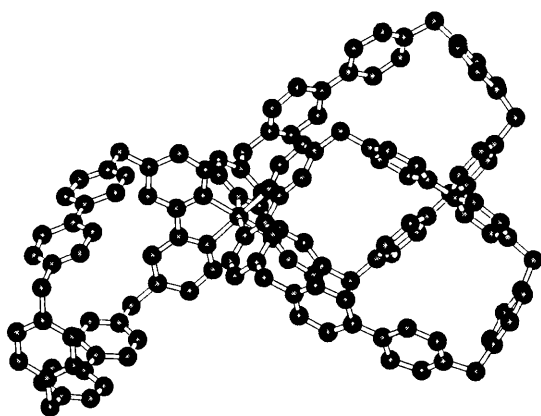


Figure 3.20: Molecular mechanics model of $\text{Fe}(\text{L1})_3(\text{PF}_6)_{14}$.

The template molecule **T2** was added in aliquots to a solution of $\text{Fe}(\text{L1})_3(\text{PF}_6)_{14}$ dissolved in d_6 -acetone, with the aim of following the progressive binding of **T2** into each of the cyclophane cavities by ^1H NMR spectroscopy. As **T2** binds to free cyclophane **L1** with a binding constant of 90M^{-1} it was expected that

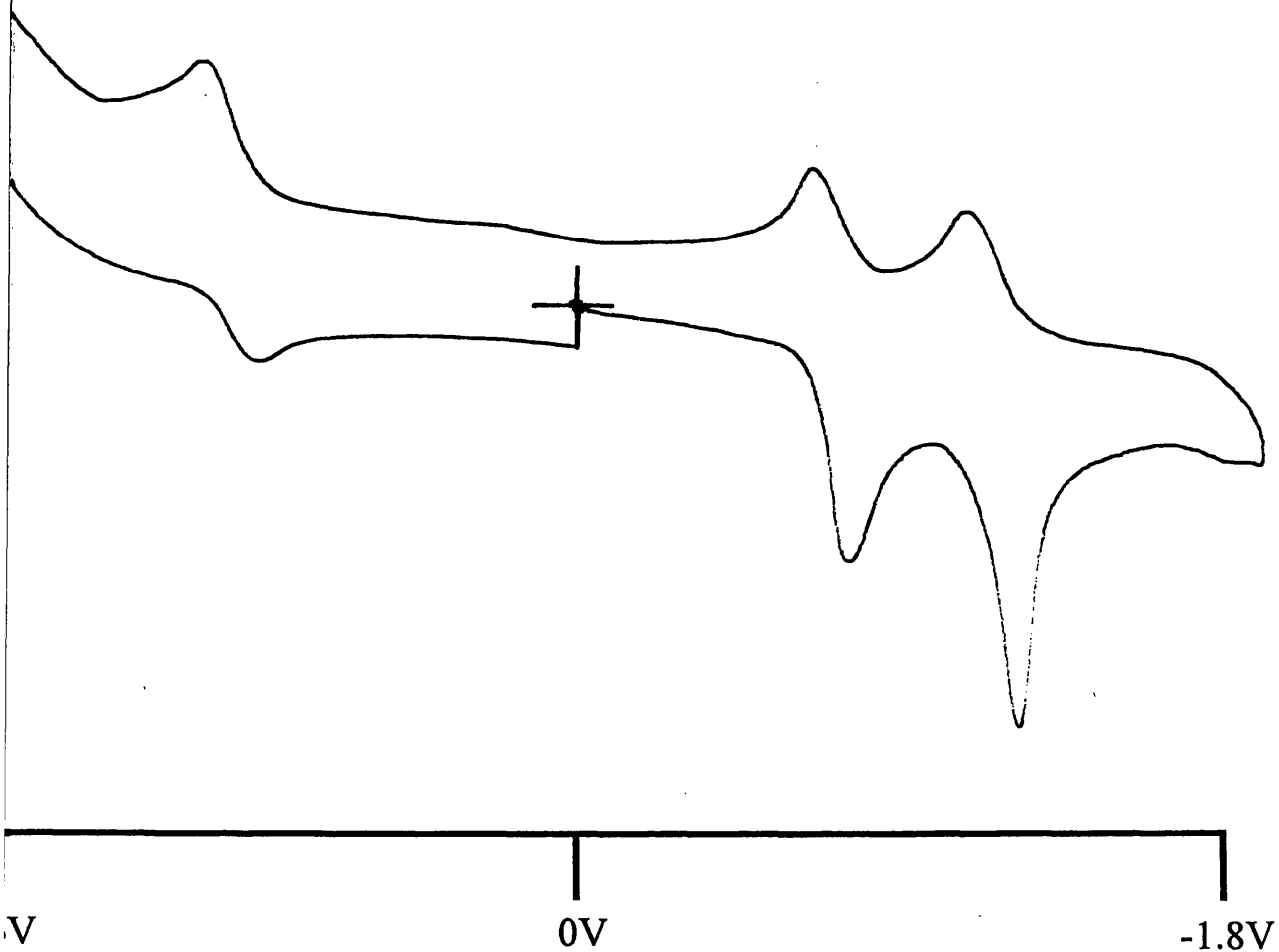


Figure 3.19: Cyclic voltammogram of $\text{Fe(L1)}_3(\text{PF}_6)_{14}$ in N_2 degassed acetonitrile with 0.2M tetrabutylammonium tetrafluoroborate background electrolyte. Scan rate was 50mVs^{-1} , reference electrode was Ag/AgNO_3 .

the complexed cyclophanes would exhibit similar behaviour, thus binding a total of three donor molecules. The somewhat unexpected result of these studies was no binding of **T2** occurred with $\text{Fe}(\text{L1})_3(\text{PF}_6)_{14}$ - no shifts in the ^1H NMR spectra could be observed. A possible explanation for this behaviour may be that each of the blades of the propeller prevents binding of substrates into the cavity of any of the others by a simple steric crowding or blocking phenomenon. From figure 3.20 it is possible to envisage how such an effect could occur.

The zinc-cyclophane complex $\text{Zn}(\text{L1})_2(\text{PF}_6)_8(\text{CF}_3\text{SO}_3)_2$ also exhibits interesting substrate binding properties. The simple aromatic electron donor DMB is found to bind to the dimeric complex with a binding constant of 0.85M^{-1} - a value which is rather similar to that found for the free cyclophane ($1.2 - 2.2\text{M}^{-1}$). The data fits a Benesi - Hildebrand analysis adequately - a straight line plot is obtained as expected (with $R^2 = 0.99$) thus the cyclophane ligands must be acting independently to form 1:1 complexes with the donor molecule. In contrast to the simple binding of DMB, however, when the template molecule **T2** is added to $\text{Zn}(\text{L1})_2(\text{PF}_6)_8(\text{CF}_3\text{SO}_3)_2$ more complex binding behaviour is observed. Initially, a charge transfer (CT) band corresponding to formation of the **L1.T2** EDA complex grows in strongly until a certain concentration is reached. After this point the CT band increases in intensity in smaller increments. Plotting the rate of increase in absorbance vs substrate concentration and fitting the data to 1:1 or 1:2 binding isotherms is inconclusive - neither stoichiometry represents a perfect model for this system. Upon carrying out a Benesi - Hildebrand analysis of the data, a non-linear plot is obtained (figure 3.21), which has a distinct point of inflection at a specific donor concentration. It is possible to plot the sets of points before and after this point and thus obtain two perfectly linear plots. By employing this technique, two binding constants may be derived - the first being in the range $60 - 90\text{M}^{-1}$ and the second being in the range $6 - 12.0\text{M}^{-1}$. The former binding constant is very close to that expected for the binding of **L1** with **T2** (90M^{-1}) whilst the second is much lower than expected for this system. It is apparent that Benesi - Hildebrand analysis is not adequate for this system, and that the values for the binding constants derived in the manner described above must be treated with some circumspection. However, one possible interpretation of the behaviour observed in this system may be that initially one **T2** molecule binds to one of the cyclophane binding sites in

Benesi Hildebrand Analysis of Binding of T2 to Zn (L1)2.

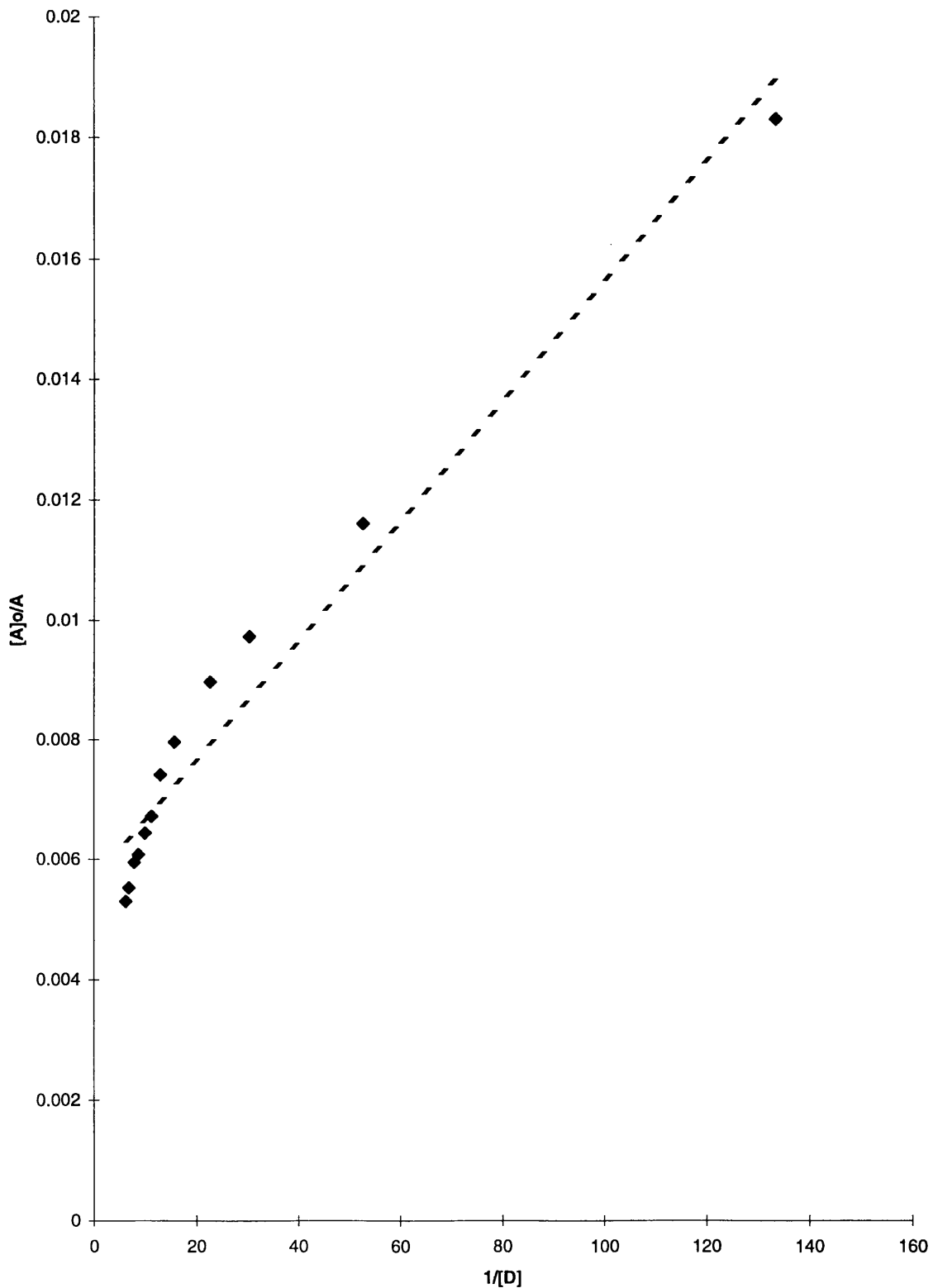


Figure 3.21: Benesi-Hildebrand analysis of binding of T2 to Zn(L1)₂¹⁰⁺.

$Zn(L1)_2(PF_6)_8(CF_3SO_3)_2$, but subsequently binding of a second molecule of **T2** is hindered by an allosteric effect. The allosteric effect may be explained by considering the lengthy polyether 'arms' of the substrate molecule - it is possible that these arms may partially block the second binding site by interacting with the other electron deficient cyclophane in addition to the first *via* hydrogen-bonding or electrostatic attractions. This effect is, at present, still under investigation.

The creation of photoactive molecular assemblies by appending ruthenium or osmium tris bipyridyl moieties onto cyclophane **L1** has been successfully carried out by either of two routes. The 'pre-coordination' route was developed as a means of circumventing the need to synthesise and purify free cyclophane **L1** as, for the reasons discussed in section 3.2, this synthetic route had previously proved troublesome. Subsequently, it became possible to produce **L1** in reasonable quantities so that simple complexation of the ligand with $Ru(bipy)_2Cl_2$ became a viable route to the desired product. The complexes were characterised by 1H NMR spectroscopy and by mass spectrometry. The NMR spectra of the metal complexes are convoluted, as the non-derivatised bipyridine units add an additional four signals to the aromatic region of the 1H NMR spectrum. The NMR spectra of the osmium and ruthenium bipyridyl complexes are essentially very similar. As the ruthenium complex was of greater interest due to its perceived photoinduced electron transfer capabilities, a two dimensional COSY 1H NMR experiment was performed on this compound (figure 3.22) in order to accurately assign its NMR spectrum.

The 1H - 1H COSY NMR experiment was carried out at room temperature and 400MHz. The data from the experiment allowed the assignment of the signals as presented in figure 3.23. The assignment of the signals confirms that the complex has the expected formulation, although the geometry of the system is not unambiguously defined by this type of NMR experiment. The 1H NMR spectrum shows significant perturbation of the signals corresponding to the cyclophane ligand upon complexation as in the polymolecular cyclophane aggregates described previously. This may again be interpreted as being caused by changes in the conformation of the cyclophane caused by cation chelation.

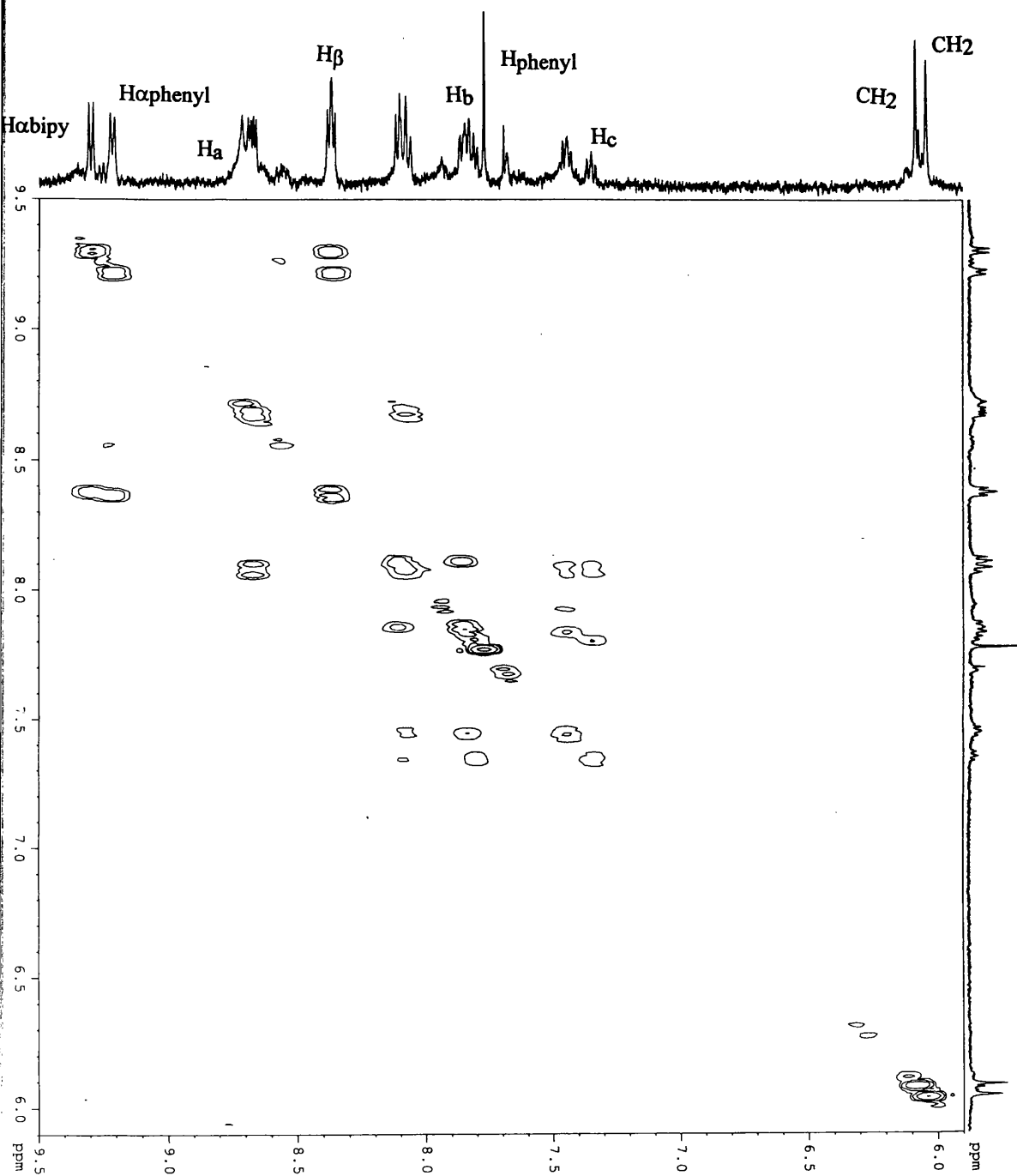


Figure 3.22: ^1H - ^1H COSY spectrum of $[\text{Ru}(\text{bipy})_2(\text{L1})][\text{PF}_6]_6$ in d_6 -acetone at 400MHz and 298K.

Signals grouped together as 'bipy' signals.

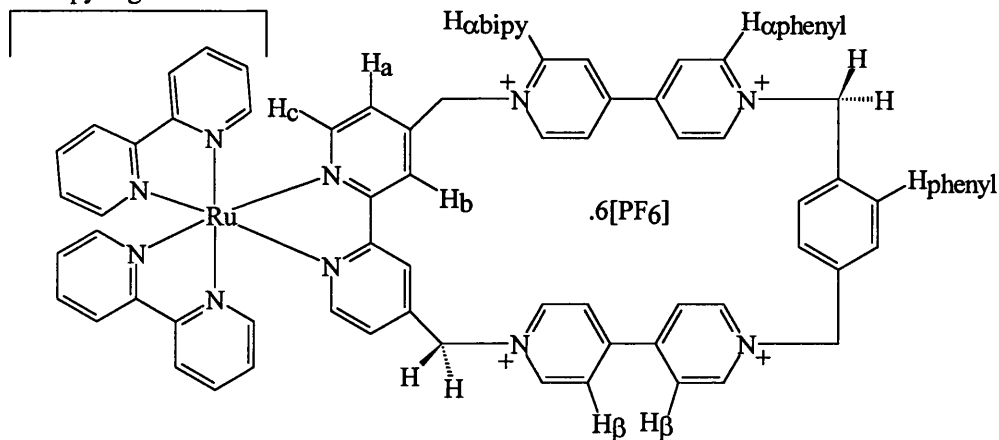


Figure 3.23: Ru(bipy)₂(L1)(PF₆)₆ ¹H NMR signal assignments from COSY experiment.

The spectroscopic and photophysical properties of the complex Ru(bipy)₂(L1)(PF₆)₆ are described in chapter 5. The redox properties of this compound and its osmium analogue are however summarised in table 3.3.3.

	$E_{1/2}$ (V)	ΔE (V)	$E_{1/2}$ (V)	ΔE (V)
L1	-0.40	0.21	-0.83	0.22
Ru(bipy)₂(L1)	-0.40	0.14	-0.86	0.14
Os(bipy)₂(L1)	-0.41	0.12	-0.75	0.26

Table 3.3.3: Selected electrochemical data for L1 and its Ru and Os complexes.

The table indicates that complexation of the ligand L1 by ruthenium and osmium tris bipyridyl centres leads to only small changes in the electrochemical properties of the ligand - the largest difference being found in the second reduction wave of the osmium-bipyridyl-cyclophane complex.

3.4 Cyclophane L2

The cyclophane L2, cyclo[bisparaquat-bis(2,2'-bipyridine)] tetrakis (hexafluorophosphate) was synthesised by a template route using donor molecule T1 as template in a procedure directly analogous to that used to prepare ligand L1.

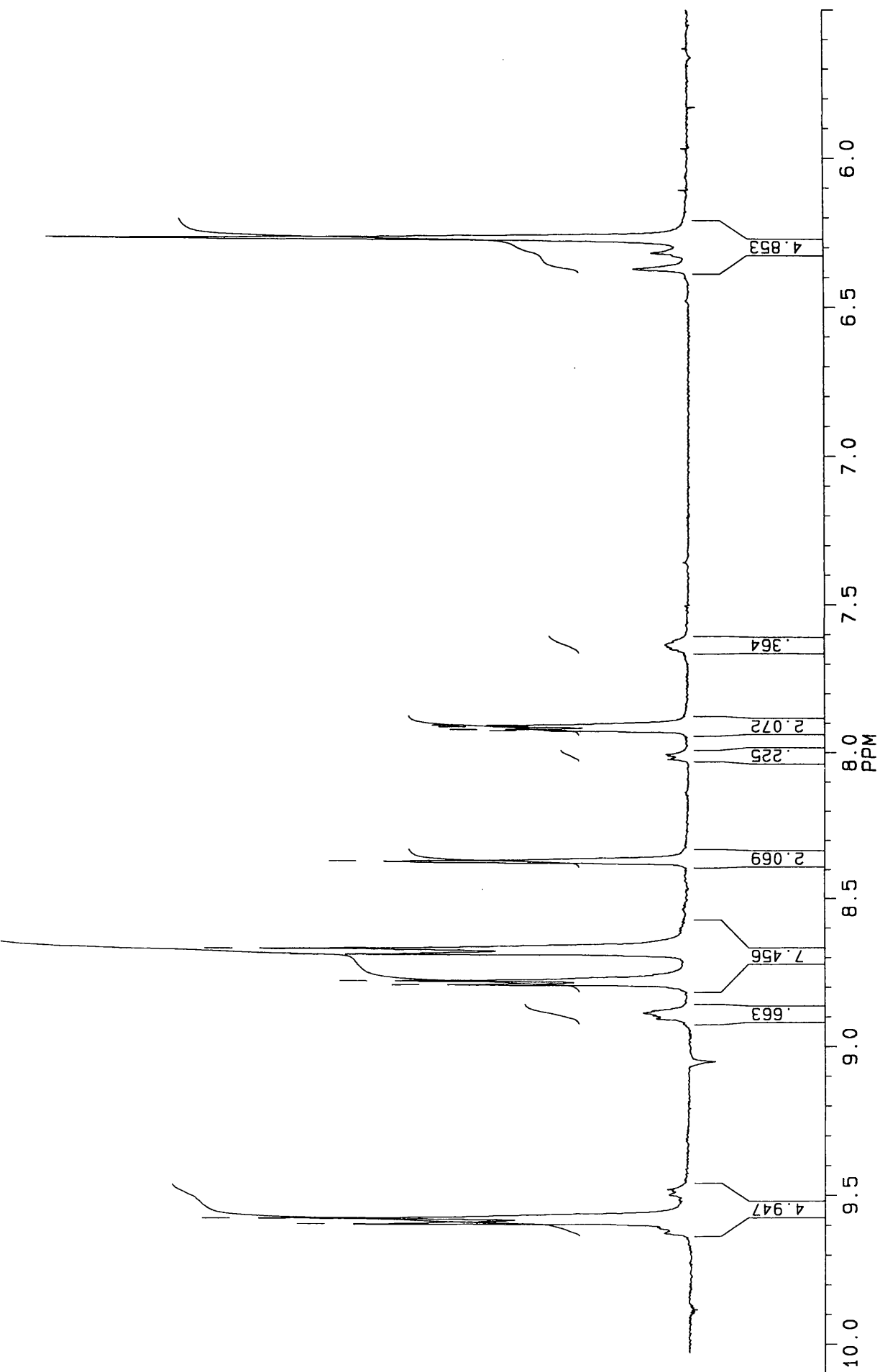


Figure 3.24: ^1H NMR spectrum of $\text{L2}(\text{PF}_6)_4$ in d_6 -acetone at 360MHz and 298K.

Compound **T1** was chosen as the template for this reaction because it is known to form strong EDA complexes with viologen derivatives thus it greatly increases the efficiency and yield of the synthetic procedure (as discussed in section 3.3). The pure cyclophane may be obtained by employing a similar chromatographic procedure to that used to purify cyclophane **L1**.

The ^1H NMR spectrum of compound **L2** (figure 3.24) is very simple indeed due to the highly symmetric nature of the cyclophane. The methylene spacer units are found at a chemical shift of 6.27ppm, the 2,2'-bipyridine signals at 7.92, 8.37 and 8.77ppm and the protons α and β to the pyridinium nitrogens come into resonance at 9.57 and 8.67ppm respectively. All chemical shifts quoted are for a d_6 -acetone solution of the cyclophane at 360MHz and 298K.

The electrochemical properties of the cyclophane are similar to those described previously for cyclophane **L1**, with the viologen units undergoing reduction at potentials of -0.34V and -0.74V (*vs* SCE). The host-guest properties and coordination chemistry of compound **L2** are, however, quite different to those described for **L1** because the phenyl spacer unit has been replaced with a second chelating unit, thus altering both the size of the internal cavity and the nature of the cyclophane as a ligand. These features will be discussed in sections 3.4.1 and 3.4.2.

The connectivity and geometry of the cyclophane may be observed from the solid state structure as determined by X-ray analysis (figure 3.25, crystal data is given in appendices).

The cyclophane has overall dimensions of *ca* 14.5Å long by 7.3Å wide. The molecule has a plane of symmetry about the central carbon - carbon bonds of the 2,2'-bipyridine units and hence the long axes of the viologen subunits are coplanar. The viologen units are twisted as in the analogous structures of cyclophane **L1**, with the torsion angle about the central carbon - carbon bond being 30.5°. The 2,2'-bipyridine chelating units may be described as being in a 'cisoid' conformation, with the torsion angle between the nitrogen atoms being 33.6°. The overall shape of the cyclophane (figure 3.25) is a 'chair' (c.f. cyclohexane conformations) whereby the 'seat' part corresponds to the plane in which the viologen units are orientated and the 'back' and 'legs' of the chair corresponding to the two bipyridine units (the angle between these and the 'seat' being 112.1° at the methylene spacer unit). A consequence of incorporating two 2,2'-bipyridine units into the cyclophane in place

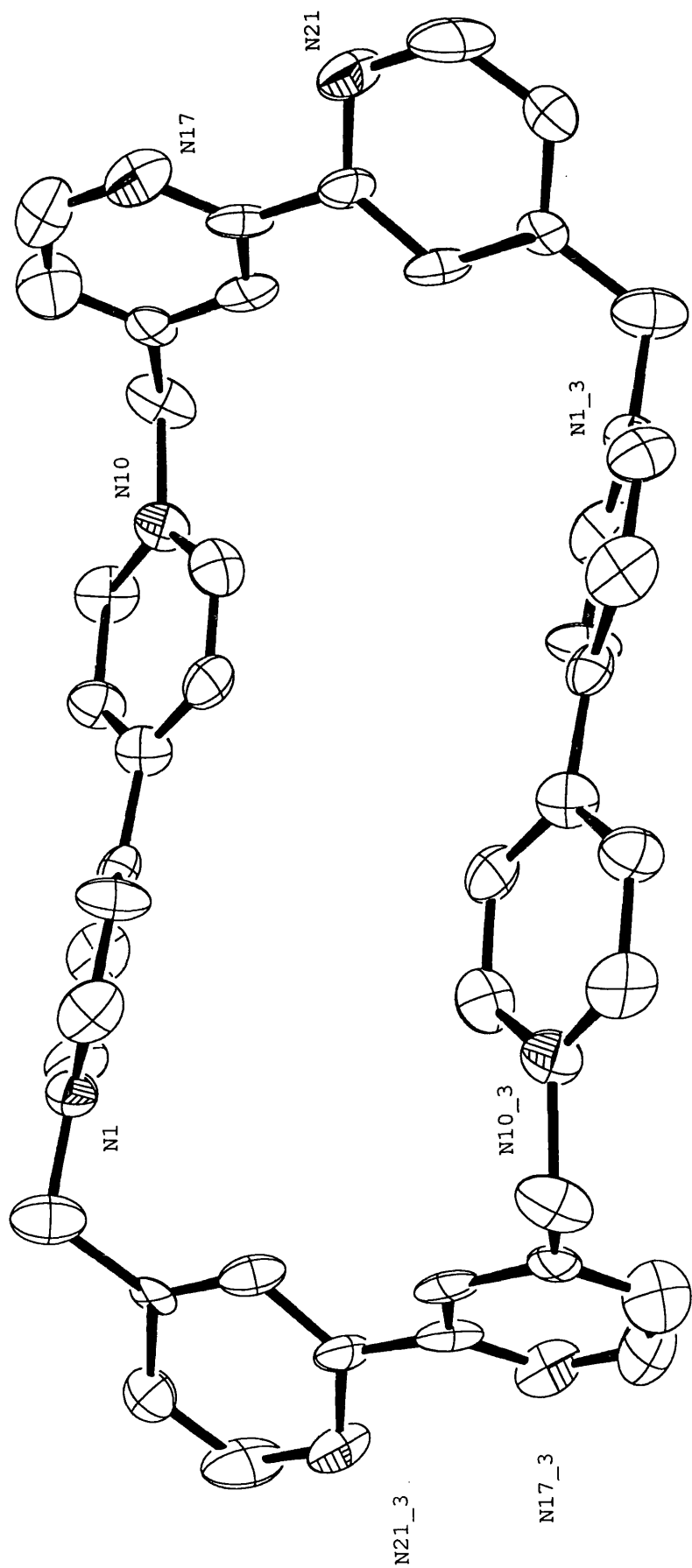


Figure 3.25: Crystal structure of cyclophane L2⁴⁺ (PF₆ counterions omitted).

of phenyl spacers (c.f. the non-chelating cyclophane depicted in figure 3.2) is that the dimensions of the cavity are increased. The strength (in terms of association constants) of EDA interactions is distance dependant: a distance of 3.3Å being an ideal distance for formation of a π - π stack,¹⁶ thus by increasing the distance between the viologen acceptors (to approximately 7.3Å) a profound effect on the binding properties of the cyclophane may be expected.

3.4.1 Host-Guest Chemistry of L2

Absorption spectroscopy (UV-VIS) combined with Benesi - Hildebrand analysis was used to follow the binding of the aromatic electron donating compounds DHB, DMB, TMPD and T2 (depicted in figure 3.12) with cyclophane L2. The binding of compound T1 with cyclophane L2 was followed using the alternative technique of fluorescence quenching. This technique, discussed in section 2.4.3, was employed because the compound T1 has a very strong absorption in the UV part of the spectrum which may lead to inaccurate determination of binding constants as the UV absorbance may contribute to the intensity of the charge transfer band. By adding aliquots of the cyclophane to a solution of the fluorophore, the fluorescence of the substrate may be quenched progressively. The fluorescence quenching may be used to calculate the binding constant of the interaction by employing the equation:

$$F_0/F = 1 + K[L]$$

where F_0 = the initial fluorescence intensity at zero quencher concentration, F = the fluorescence intensity at a given acceptor concentration, K = the binding constant and $[L]$ = the acceptor concentration.

Plotting F_0/F vs $[L]$ produces a straight line graph, with the gradient being equal to the binding constant.

The binding characteristics of cyclophane L2 are summarised in table 3.4.1, along with the values for the corresponding binding constants for cyclophane L1 and the non-chelating cyclophane depicted in figure 3.2.

Donor Substrate	Cyclophane L2	Cyclophane L2	Cyclophane L2	Cyclophane L1	Literature Standard
	K (M ⁻¹)	ϵ (M ⁻¹ cm ⁻¹)	Technique	K (M ⁻¹)	K (M ⁻¹)
DHB	0.9	303	Abs.	<1	18
DMB	1.4	179	Abs.	1.2,2.2	18
TMPD	2.5	10,000*	Abs.	6.7	42
T1	1593	-	Fluor.	> 3100	> 5000
T2	2	667	Abs.	90	2241

Table 3.4.1: Binding data for cyclophane L2.

All data was collected in dry degassed acetonitrile. The value for ϵ for TMPD* is an order of magnitude greater than the expected value¹⁰ - this may be due to aerial oxidation of the donor molecule, thus the value of the binding constant may be inaccurate.

The binding constants of DHB and DMB with both cyclophanes, L1 and L2, are very low - it is thus difficult to discern any trend in the relative binding properties of the two cyclophanes from these data other than to note that the incorporation of 2,2'-bipyridine units (thus increasing the dimensions of the cyclophane cavity) greatly lowers the binding affinity of these substrates for the cyclophanes as compared to the non-chelating acceptor. This feature is repeated for all the aromatic donor substrates, however the binding of TMPD, T1 and T2 displays an additional trend in that acceptor L1 binds these substrates more strongly than does L2 but considerably less strongly than the simple non-chelating cyclophane. This trend may be explained by considering the dimensions of the three cyclophane structures. The simple cyclophane (dimensions 6.8Å x 10.3Å)⁵ has the ideal geometry for binding aromatic electron donor molecules, both because of the spacing of its two viologen units and their coplanar arrangement. Compound L1 deviates from this geometry where one phenyl unit has been replaced with a larger bipyridine unit, thus the viologen units no longer have an ideal orientation or spacing for binding donor substrates. Whilst the introduction of a second bipyridine unit in L2 restores the coplanarity of the viologen units, the distance between them increases thus the binding of donor substrates is further weakened.

By changing the substitution pattern on the chelating unit, and by introducing biphenyl rather than phenyl spacer units, it would thus be expected that binding of simple aromatic electron donors would be extremely weak.¹¹ The large acceptor cavities produced by incorporation of such units would, however, allow the binding of larger substrates such as metal 'sandwich' complexes based on ferrocene or cobaltocenium and their derivatives.¹²

3.4.2 Coordination Chemistry of L2

Due to the fact that cyclophane **L2** has two 2,2'-bipyridine chelating sites, it has very different properties as a ligand to those of the analogous compound **L1**. The cyclophane was envisaged as a 'linker' unit in that it may be possible to connect metal centres together using this ligand. Indications that the ligand may perform such a function were immediately obvious upon its isolation, where the elution of fractions from the chromatographic purification process were monitored by testing with iron sulphate. The red solid produced by the testing procedure indicated that iron (II) tris bipyridyl complexes were being produced, however the solid could not be further analysed due to its insoluble nature. This lack of solubility may be explained by consideration of the intricate three dimensional polymer that must result from incorporation of this ligand into octahedral complexes where three **L2** ligands surround each iron centre.

To further investigate the coordination chemistry of the ligand, NMR experiments were carried out where copper (I) ($\text{Cu}(\text{CH}_3\text{CN})_4(\text{BF}_4)$) and zinc (II) ($\text{Zn}(\text{CF}_3\text{SO}_3)_2$) solutions were added to solutions of the ligand. Upon addition of small (2 μL) aliquots of a 1mM copper (I) solution to the ligand, an initial broadening of all ^1H NMR signals was observed. This was interpreted as evidence that complexation of the ligand was beginning to occur. After further addition of copper (I) solution, a precipitate was observed in the NMR tube and a featureless ^1H NMR spectrum was obtained. The precipitate could not be re-dissolved, thus formation of a polymeric assembly would seem to have occurred in a process directly analogous to that observed in the case of the iron complex. A similar experiment was carried out using a zinc (II) solution - it was expected that an identical result to that found with the copper (I) salt would be obtained. Initially the experiment took an identical course, with a precipitate being produced - however

upon addition of further aliquots of the zinc (II) solution to the sample, the precipitate was observed to re-dissolve, accompanied by the return of ^1H NMR signals corresponding to the complexed cyclophane (see table 3.4.2).

	CH(α)	CH(β)	CH₂	H_a	H_b	H_c
L2	9.57	8.67	6.29	7.96	8.40	8.82
[Zn]₂(L2)	9.61	8.66	6.40	8.36	8.96	9.14

Table 3.4.2: Selected ^1H NMR data for L2 and its zinc complex.

All ^1H NMR data was collected in d_6 -acetone at 360MHz.

This effect may be explained by the lability of zinc - bipyridine complexes. Initially a polymeric structure is formed in a similar manner to that proposed for the copper (I) reaction, but upon increasing the concentration of Zn (II) ions the polymeric structure dissociates into oligomeric species, until dissolution can once again occur. At a 2:1 ratio of Zn(II) to ligand L2, largely monomeric species (with respect to the cyclophane) must predominate in solution and addition of further aliquots of zinc (II) solution has no effect.

3.5 Cyclophanes L3 and L4

Cyclophanes **L3** and **L4** were prepared from precursors **P3** and **P2** (see section 3.2), respectively. Despite the expectation that the cavities of these cyclophanes would be too large to effectively bind simple aromatic electron donors,^{18,20} the template molecule **T1** was employed in the hope that even weak binding to the cyclophane precursors would increase the efficiency of the synthetic strategy. The low yields obtained from this approach (1.1% for **L3** and 8.2% for **L4**) would tend to indicate that no template effect occurred during the course of the cyclophane syntheses. Related cyclophanes, based on non-chelating biphenyl spacers (produced by the group of Stoddart, see figure 3.26) have been synthesised in yields of only 2% where no template was used²⁰ - thus the poor yields obtained of **L3** and **L4** are consistent with a purely statistical synthesis.

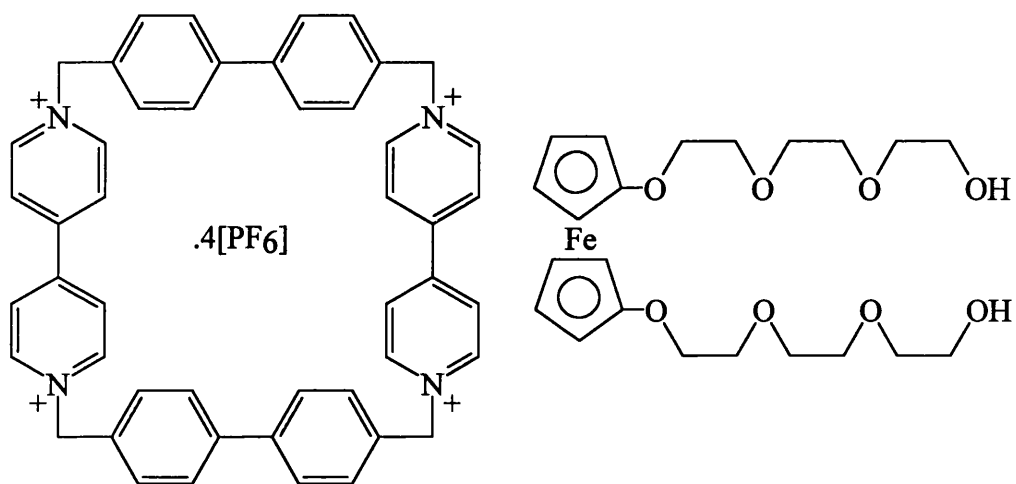


Figure 3.26: A biphenyl-based electron acceptor cyclophane and its template.

Stoddart and co-workers recognised that the cavities of these larger cyclophanes were of the correct size to bind ferrocene and its derivatives²⁰ (ferrocene was previously known to enter into EDA complexes with electron accepting molecules)²². Thus ferrocene derivatives (in particular polyether derivatised ferrocene compounds, see figure 3.26) could act as efficient templates for the synthesis of such cyclophanes. By employing this strategy, yields of the biphenyl - based cyclophane were increased to 32%.

This strategy was not employed in the synthesis of cyclophanes **L3** and **L4** because test reactions, where simple ferrocene derivatives (e.g. methyl alcohol, carboxylate, methyl ester) were stirred at room temperature with 2,2'-bipyridine, resulted (under certain conditions) in the abstraction of the iron atom from the ferrocene complex thus forming $\text{Fe}(\text{bipy})_3^{2+}$. Given that the syntheses of cyclophanes **L3** and **L4** involve lengthy periods of stirring (ca. 7days) the use of ferrocene-based templates did not appeal as a synthetic strategy.

Purification of the cyclophanes **L3** and **L4** was effected by the chromatographic system developed for cyclophanes **L1** and **L2**. The ^1H NMR spectra of **L3** and **L4** are unremarkable in that the signals corresponding to the viologen components of the cyclophane are very similar to those described previously for **L1** and **L2**. The changed substitution pattern of the larger cyclophanes leads to changes in the ordering of the signals corresponding to the bipyridine chelating unit (figure 3.27), in addition cyclophane **L3** has a multiplet at 7.69-7.76ppm corresponding to the biphenyl spacer instead of a singlet at 7.75ppm as is the case in the analogous phenyl containing cyclophane **L1**.

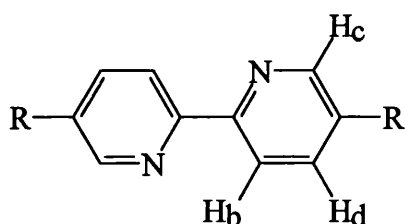


Figure 3.27: Substitution pattern of 2,2'-bipyridine unit in cyclophanes L3 and L4.

Assignments of the ^1H NMR signals for compounds **L3** and **L4** are presented in table 3.5.1.

	CH(α)	CH(β)	CH ₂	H _b	H _c	H _d
L3	9.53 9.59	8.75 8.78	6.20 6.33	8.41	9.01	8.27
L4	9.59	8.75	6.33	8.42	9.02	8.28

Table 3.5.1: Selected ^1H NMR data for L3 and L4.

All ^1H NMR data was collected in d_6 -acetone at 360 MHz.

The electrochemical properties of cyclophanes **L3** and **L4** are rather similar to those of the cyclophanes discussed previously. The viologen units of cyclophane **L3** undergo two-electron reduction at -0.39V and -0.84V and those incorporated into cyclophane **L4** undergo reduction at -0.38V and -0.80V (*vs* SCE). By way of a comparison, under the same conditions the viologen units of **L1** are reduced at potentials of -0.40V and -0.83V, thus it may be seen that the effect of changing the substitution pattern of the chelating unit on the electrochemical behaviour of the electron accepting units is very small indeed.

3.5.1 Host-Guest and Coordination Chemistry of **L3** and **L4**.

Due to the very small quantities of **L3** and **L4** that could be produced by the synthetic strategy outlined above, only a limited investigation of the binding properties of these ligands was possible. As discussed in section 3.4.1, the binding of simple aromatic electron donors was unlikely to occur in the cyclophanes **L3** and **L4**. Stoddart and co-workers have reported^{18,20} that ferrocene is readily bound by analogous non-chelating cyclophanes (with a binding constant of 80M^{-1}). However, upon adding ferrocene to compound **L3**, no colour change was observed (a green colour corresponding to formation of an EDA complex had been reported by Stoddart) - this indicated that no binding interaction had occurred. Upon stirring a solution of **L3** and ferrocene in dry degassed acetonitrile for several hours a colour change was observed - however upon investigation of this effect by absorption spectroscopy it was deduced that the blue/green colour could be attributed to the production of reduced viologen units rather than formation of a charge transfer band as had been expected.

Given that ferrocene derivatives (e.g. the molecule depicted in figure 3.26) have significantly higher binding constants than simple ferrocene^{18,20} (e.g. 1600M^{-1} *vs* 80M^{-1}) a novel ferrocene-based compound (figure 3.28), 1,1'-ferrocene di(carboxy-4-methylene-4'-methyl-2,2'-bipyridine) was developed.

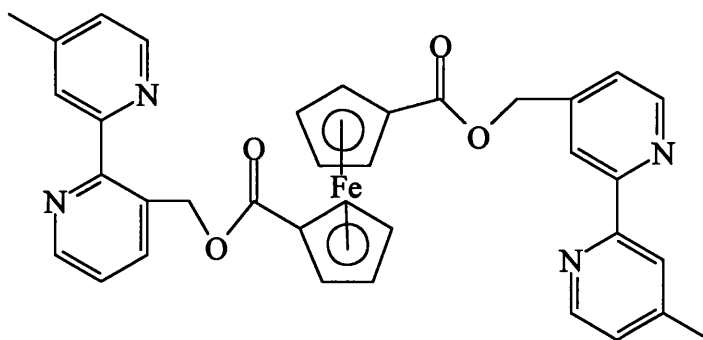


Figure 3.28: Novel ferrocene based guest molecule.

This compound has, in addition to a ferrocene donor subunit, two cation chelating 2,2'-bipyridine units - these units were included in the molecular architecture so that they could augment the binding of the ferrocene unit by forming complexes with tetrahedral metal centres in combination with the chelating units of cyclophane **L4**. The ferrocene compound, whilst it could be isolated after a great deal of purification, was extremely unstable in solution. The bipyridine units may well perform a 'back-biting' operation resulting in the abstraction of the iron atom from the ferrocene unit leading to the production of $\text{Fe}(\text{bipy}')_3^{2+}$ species. It was thus impossible to study the host-guest chemistry of this molecule with compounds **L3** and **L4**.

The coordination chemistry of cyclophane **L3** with copper (I) was, however, investigated in an NMR experiment. Upon addition of an aliquot of copper (I) solution ($\text{Cu}(\text{CH}_3\text{CN})_4(\text{BF}_4)$ in dry degassed d_6 -acetone) to a solution of **L3** in d_6 -acetone a broadening of the ^1H NMR signals corresponding to the cyclophane is observed. This may be interpreted as evidence that complexation of the ligand by the copper (I) centres is occurring. When the concentration of copper (I) ions has reached a level where the ratio of ligand to $[\text{Cu}^{\text{I}}]$ is 2:1, the ^1H NMR spectra has a quite different appearance to that of the free ligand (see table 3.5.2).

	CH(α)	CH(β)	CH ₂	H _b	H _c	H _d
L3	9.53	8.75	6.20	8.41	9.01	8.27
	9.59	8.78	6.33			
Cu(L3)₂	9.56	8.78	6.21	7.98	7.86	7.55

Table 3.5.2: Selected ¹H NMR data for L3 and its copper complex.

All ¹H NMR data was collected in d₆-acetone at 360 MHz.

Whilst the signals corresponding to the 2,2'-bipyridine chelating unit undergo significant shifts upon complexation, the viologen and biphenyl signals do not display notable changes in their chemical shifts - although these signals are broadened and thus no longer resolved into sharp singlets or doublets. Despite the fact that the signals corresponding to the methylene spacer units coalesce into one broad signal upon complexation, the lack of significant change to the chemical environment of the viologen and biphenyl units indicates that the conformation of the cyclophane is not altering to accommodate the binding of the metal centre. This feature of ligand **L3** is a consequence of the substitution pattern of the chelating unit, whereby the conformation of the cyclophane is insensitive to the orientation of the nitrogen atoms in the chelating unit, and it represents a stark contrast to the coordination chemistry of ligands **L1** and **L2**.

3.6 References

- [1] Diederich, F. in *Supramolecular Chemistry*, NATO ASI Series, (Eds. Balzani, V.; De Cola, L.), Kluwer Academic Publisher, Dordrecht, 1992.
- [2] Vögtle, F. *Cyclophanes*, Wiley, Chichester, 1993.
- [3] Lehn, J.M. *Supramolecular Chemistry*, VCH, Weinheim, 1995.
- [4] Ashton, P.R.; Chemin, A.; Claessens, C.G.; Menzer, S.; Stoddart, J.F.; White, A.J.P.; Williams, D.J. *Eur. J. Org. Chem.*, 1998, **6**, 983.
- [5] Anelli, P.L.; Ashton, P.R.; Ballardini, R.; Balzani, V.; Delgado, M.; Gandolfi, M.T.; Goodnow, T.T.; Kaifer, A.E.; Philp, D.; Pietraszkiewicz, M.; Prodi, L.; Reddington, M.V.; Slawin, A.M.Z.; Spencer, N.; Stoddart, J.F.; Vicent, C.; Williams, D.J. *J. Am. Chem. Soc.*, 1992, **114**, 193.
- [6] Asakawa, M.; Ashton, P.R.; Brown, C.L.; Fyfe, M.C.T.; Menzer, S.; Pasini, D.; Scheuer, C.; Spencer, N.; Stoddart, J.F.; White, A.J.P.; Williams, D.J. *Chem. Eur. J.*, 1997, **3**, 1136.
- [7] Anelli, P.L.; Asakawa, M.; Ashton, P.R.; Brown, G.R.; Hayes, W.; Kocian, O.; Pastor, S.R.; Stoddart, J.F.; Tolley, M.S.; White, A.J.P.; Williams, D.J. *J. Chem. Soc. Chem. Commun.*, 1995, 2541.
- [8] Ashton, P.R.; Boyd, S.E.; Menzer, S.; Pasini, D.; Raymo, F.M.; Spencer, N.; Stoddart, J.F.; White, A.J.P.; Williams, D.J.; Wyatt, P.G. *Chem. Eur. J.*, 1998, **4**, 299.
- [9] Asakawa, M.; Ashton, P.R.; Boyd, S.E.; Brown, C.L.; Menzer, S.; Pasini, D.; Stoddart, J.F.; Tolley, M.S.; White, A.J.P.; Williams, D.J.; Wyatt, P.G. *Chem. Eur. J.*, 1997, **3**, 463.
- [10] Benniston, A.C.; Harriman, A.; Philp, D.; Stoddart, J.F. *J. Am. Chem. Soc.*, 1993, **115**, 5298.
- [11] Asakawa, M.; Dehaen, W.; L'abbe, G.; Menzer, S.; Nouwen, J.; Raymo, F.M.; Stoddart, J.F.; Williams, D.J. *J. Org. Chem.*, 1996, **61**, 9591.
- [12] Raymo, F.M.; Stoddart, J.F. *Chem. Ber.*, 1996, **129**, 981.
- [13] Rebek, J.; Trend, J.F.; Wattley, R.V.; Chakravorti, S. *J. Am. Chem. Soc.*, 1979, **101**, 4333.
- [14] Vögtle, F. *Supramolecular Chemistry*, Wiley, Chichester, 1991.

- [15] For recent examples see: (a) Hasenknopf, B.; Lehn, J.M.; Kneisel, B.O.; Baum, G.; Fenshe, D. *Angew. Chem. Int. Ed. Engl.*, 1996, **35**, 1838. (b) Marguisrigault, A.; DupontGervais, A.; van Dorsselaer, A.; Lehn, J.M. *Chem. Eur. J.*, 1996, **2**, 1395. (c) Hasenknopf, B.; Lehn, J.M.; Boumediene, N.; DupontGervais, A.; van Dorsselaer, A.; Kneisel, B.O.; Fenshe, D. *J. Am. Chem. Soc.*, 1997, **119**, 10956.
- [16] Benniston A.C.; Yufit, D.S.; Mackie, P.R. *Acta Cryst.*, 1997, **C53**, 1899.
- [17] Benniston A.C.; Mackie, P.R.; Harriman, A. *Tetrahedron Lett.*, 1997, **38**, 3577.
- [18] Asakawa, M.; Ashton, P.R.; Menzer, S.; Raymo, F.M.; Stoddart, J.F.; White, A.J.P.; Williams, D.J. *Chem. Eur. J.*, 1996, **2**, 877.
- [19] (a) Beer, P.D.; Wheeler, J.W.; Grieve, A.; Moore, C.P.; Wear, T. *J. Chem. Soc. Chem. Commun.*, 1992, 1225. (b) Beer, P.D.; Fletcher, N.C.; Grieve, A.; Wheeler, J.W.; Moore, C.P.; Wear, T. *J. Chem. Soc. Perkin Trans. II*, 1996, 1545.
- [20] Ashton, P.R.; Menzer, S.; Raymo, F.M.; Shimizu, G.K.H.; Stoddart, J.F.; Williams, D.J. *J. Chem. Soc. Chem. Commun.*, 1996, 487.
- [21] See for example: (a) Stoddart, J.F. in *Frontiers in Supramolecular Organic Chemistry and Photochemistry*, (Eds. Schneider, H.J.; Dürr, H), VCH, Weinheim, 1991. (b) Fyfe, M.C.T.; Stoddart, J.F. *Acc. Chem. Res.*, 1997, **30**, 393. (c) Gillard, R.E.; Raymo, F.M.; Stoddart, J.F. *Chem. Eur. J.*, 1997, **3**, 1933.
- [22] Togni, A.; Hobi, M.; Rihs, G.; Rist, G.; Albinati, A.; Zanello, P.; Zech, D.; Keller, H. *Organometallics*, 1994, **13**, 1224.

Chapter Four

Catenanes

4.1 Introduction

[2]Catenanes represent a fascinating class of compounds in which the two cyclic components are inseparable not because they are covalently bound but because of their molecular topology.¹ Thus, the two rings of a catenane may be said to be held together by mechanical bonds, or in the language of Wasserman, topological bonds.² The chemistry of such compounds is well established and modern synthetic strategies such as those devised by Stoddart³ and Sauvage⁴ and co-workers have led to the ability to build-in functional subunits at any stage of the synthetic procedure. The recent advances made in catenane chemistry have eliminated the need for the tedious preparation of pre-catenanes (as is the case in directed syntheses) by employing template syntheses.²

The means by which [2]catenanes may be synthesised and the properties which may be expected from mechanically linked systems has been discussed at length in section 1.6. There are a number of strategies by which catenanes may be produced, for example: statistical threading, directed synthesis, from Möbius strips or by use of template syntheses based on transition metals, π - π (EDA) interactions or hydrogen bonding interactions.

The [2]catenane structures discussed in this chapter were constructed by the modular chemical approach developed by Stoddart⁵ and co-workers, in which molecular size fragments are incorporated into a polymolecular array in a highly controlled and totally precise manner. In this type of strategy the molecular components are assembled in a template directed synthesis. Upon completion of the self-assembly process, the weak non-covalent interactions which controlled the assembly are implanted and imbedded into the molecular assemblies they helped to create.⁶ Self-assembly is employed both because it is an extremely powerful tool for the creation of extremely large, highly ordered functional supramolecular systems and because it provides a means by which chemists can mimic, in a modest manner, the self-assembling, self-organising and self-replicating systems that abound in nature.⁷ In addition, catenanes are ideal target structures for construction by self-assembly processes because natural self-assembly processes are easier to recreate in relatively simple synthetic systems if they contain an element of mechanical entanglement.⁶

The means by which [2]catenanes may be produced by the self-assembly is presented in cartoon form in figure 4.1. There are two equivalent pathways to the target catenane, both of which involve a ‘clipping’ process, where a linear fragment is threaded through a cyclic molecule and subsequently ring closed to produce the catenane. This procedure differs from a purely statistical approach because the linear and cyclic units recognise each other - the recognition process controls the ring closing reaction.⁸

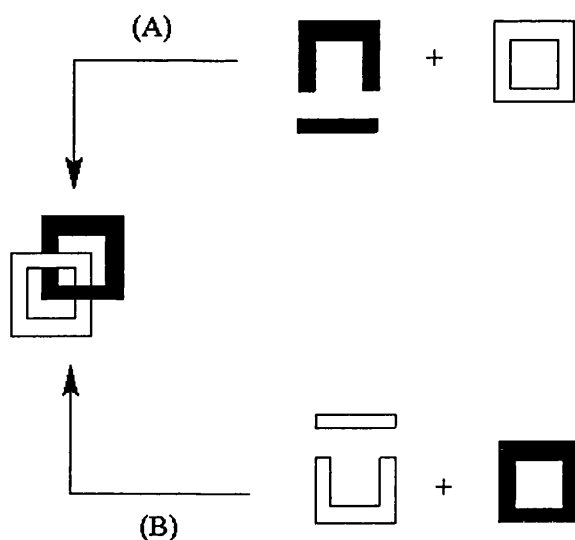


Figure 4.1: The means by which a [2]catenane may self-assemble.

The complexation of π -electron deficient endoreceptors (e.g. the paraquat dication) inside crown ethers containing π -electron rich aromatic rings has allowed the self-assembly of a large number of interlocked and intertwined structures,⁷ as discussed in section 1.6.5. The first [2]catenane structure constructed using EDA interactions as the driving force for the reaction is presented in figure 4.2.⁹ The catenanes discussed in this chapter may be regarded as derivatives of this simple system, where either phenyl spacer units on the acceptor cyclophane are replaced with chelating units or the phenoxy donor units are replaced with their naphthoxy analogues.

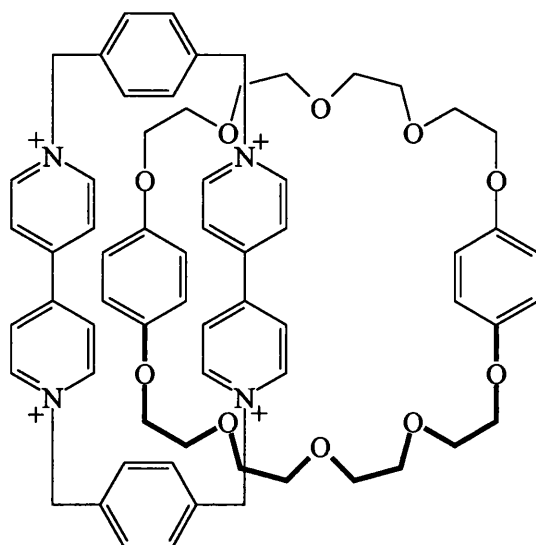


Figure 4.2: The first EDA-based [2]Catenane.

This method of catenane construction was pioneered by Stoddart and co-workers and as there are many reviews^{3,6,8} of self-assembly of [2]catenanes by use of π - π interactions, this topic will not be discussed further at this juncture.

The [2]catenanes reported in this chapter all contain the cation chelating 2,2'-bipyridine unit as part of their molecular architecture. The bipyridine unit was employed as an exoreceptor¹⁰ whereby metal moieties were bound to the outside of the interlinked structures. This provides a sharp contrast to the work of Sauvage where catenates are assembled around a metal centre which occupies a central position in the supramolecular structure⁴ (figure 4.3).

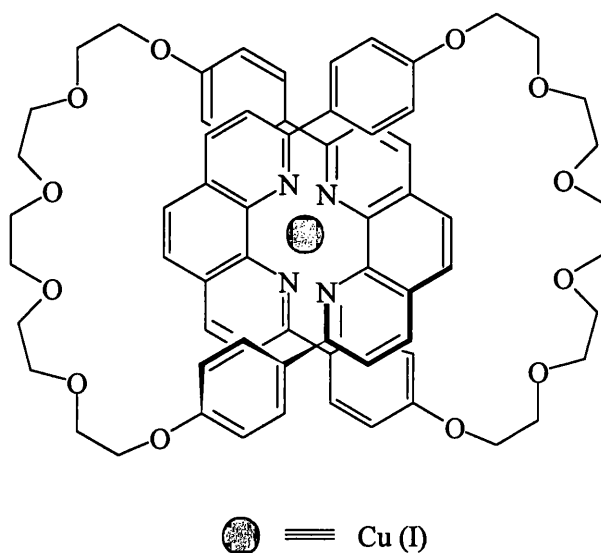


Figure 4.3: An example of a transition metal templated catenane structure.

The coordination chemistry of 2,2'-bipyridine is well established² and has been discussed previously in section 3.1. The use of such units allows the arrangement of catenated structures into polymolecular arrays such as metallo-polymers, thus providing a means for producing polycatenane structures - a much sought after arrangement as such species are expected to have interesting mechanical and electronic properties.¹¹ Additionally, complexation of such ligands by a metal centres may well have profound effects on the properties of the catenane ligands due to the charge of the metal centres, the geometry of its coordination sphere and its electronic properties - i.e. whether it is an electron donor or acceptor in the ground or excited states.

The precursors from which the [2]catenanes described in this chapter were constructed are identical to those discussed in section 3.2. The 'free' catenane ligands are more easily purified by column chromatography than are their analogous cyclophanes. This results from their colour (red or purple) because it is easier to determine when they elute. In addition, they are less strongly adsorbed onto stationary phases than the non-interlocked species, thus, a wider variety of techniques may be employed to purify them. Given the ease with which the catenanes could be purified, the most common synthetic strategy employed involved cyclising the acceptor cyclophane precursor **P1** in the presence of an aromatic crown ether compound. In addition, it was found that complexes such as $[\text{Os}(\text{bipy})_2(\text{L5})](\text{PF}_6)_6$ could be prepared by the 'pre-coordination' route¹² from the precursor complex $[\text{Os}(\text{bipy})_2(\text{P1})](\text{PF}_6)_4$, albeit in low yield. The structural formulae of the precursor units are presented in figure 4.4 as an *aide memoire*.

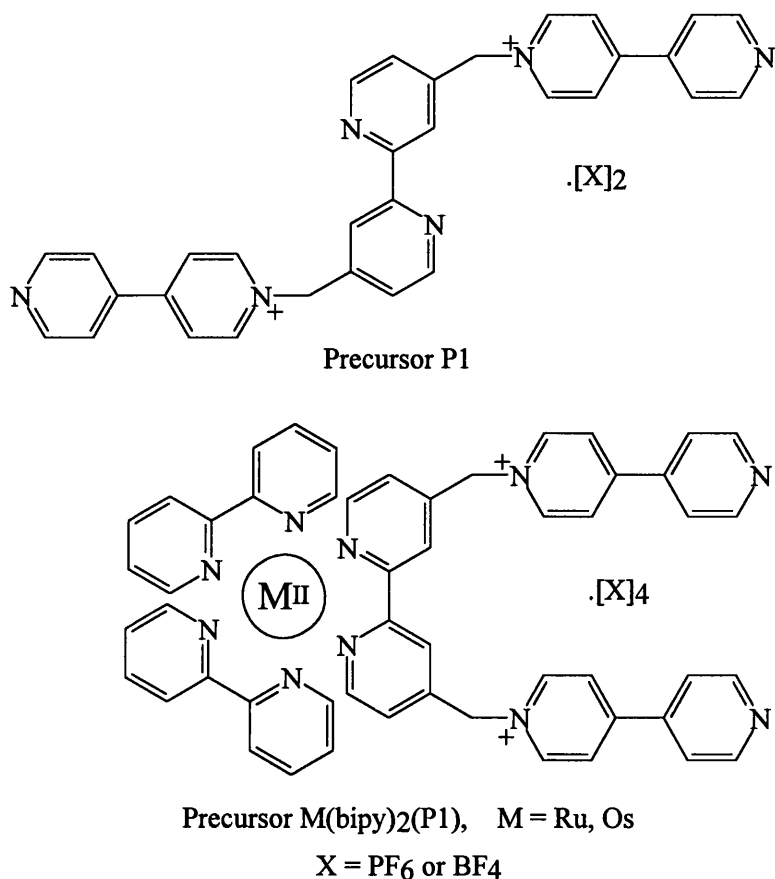


Figure 4.4: Catenane precursors.

4.2 [2]Catenane L5

The [2]catenane **L5**, [2]-[34C10]-[cyclo(bisparaquat-*p*-phenylene-2,2'-bipyridine)]catenane tetrakis(hexafluorophosphate) was prepared by a template methodology, where precursor **P1** was added to a solution of the aromatic crown ether **34C10** followed by α,α' -dibromo-*p*-xylene. The crown ether, in addition to being one of the cyclic components of the catenane, acts as a template for the reaction by stabilising tricationic pre-catenane intermediates by way of EDA, electrostatic and hydrogen bonding interactions.^{5,7} The reaction produced significant quantities of impurities, which were ascribed as being oligomeric compounds¹² (given the disposition of the precursor towards cyclisation), partially formed pre-catenane pseudo-rotaxane^{3b} intermediates and starting materials. The catenane is, however, easily separated from these impurities by means of column chromatography due to the fact that the catenane is the only species to maintain a colouration as it passes down a column. This colouration is caused by a charge

transfer transition which arises as a result of the EDA interaction between the electron accepting viologen and the electron donating phenoxy units on the two ring components of the catenane.¹³

The one dimensional ¹H NMR spectrum of **L5** in d₃-acetonitrile at 300K and 360MHz is presented in figure 4.5. It may be seen from the figure that the spectrum of the [2]catenane is rather simple despite the complex nature of the system. The signals at high-field (at 3.38, 3.59, 3.86 and 3.89ppm) correspond to the polyether chain portion of the **34C10** component of the catenane. The aromatic components of this macrocycle are broadened into the baseline because of the rapid movement of the crown component in the catenane structure.⁷ Analogous catenane structures in the literature, such as that presented in figure 4.2, are known to undergo a variety of processes involving the crown ether component including 'rocking' and 'rattling' motions of the aromatic subunit whilst it is bound within the acceptor cyclophane in addition to revolutions and rapid positional exchanges that occur for the macrocycle as a whole.⁷ By cooling the sample and obtaining its ¹H NMR spectrum it is possible to locate the missing phenoxy signals.¹² The signals at 5.79 and 5.84ppm correspond to the methylene spacer units of the acceptor cyclophane. The signals which correspond to the 2,2'-bipyridine unit may be found at 7.88 (partially obscured by the phenyl spacer resonance), 8.02 and 8.92ppm. The viologen signals are found between 7.68 and 7.75ppm (protons which are β to the nitrogen atoms) and between 8.83 and 8.96ppm (protons which are in the corresponding α positions). The chemical shifts of the resonances listed above show a very significant solvent dependency, the ordering of the signals being changed radically as a result. Thus, the equivalent ¹H NMR spectrum in d₆-acetone (see section 2.3.3 (e)) is significantly different to the spectrum in acetonitrile, however, the range of temperatures that are obtainable in acetonitrile lead to the use of this solvent in preference to acetone.

The electrochemical properties of the [2]catenanes described in this chapter are quite different to those of their analogous cyclophanes because the first reduction wave of the electron accepting viologen units is split into two distinct potentials.⁵ This effect may be explained by considering the environment immediately surrounding the two electrochemically active subunits. One viologen unit is completely encapsulated by the phenoxy substituents of the crown ether (the 'inside'

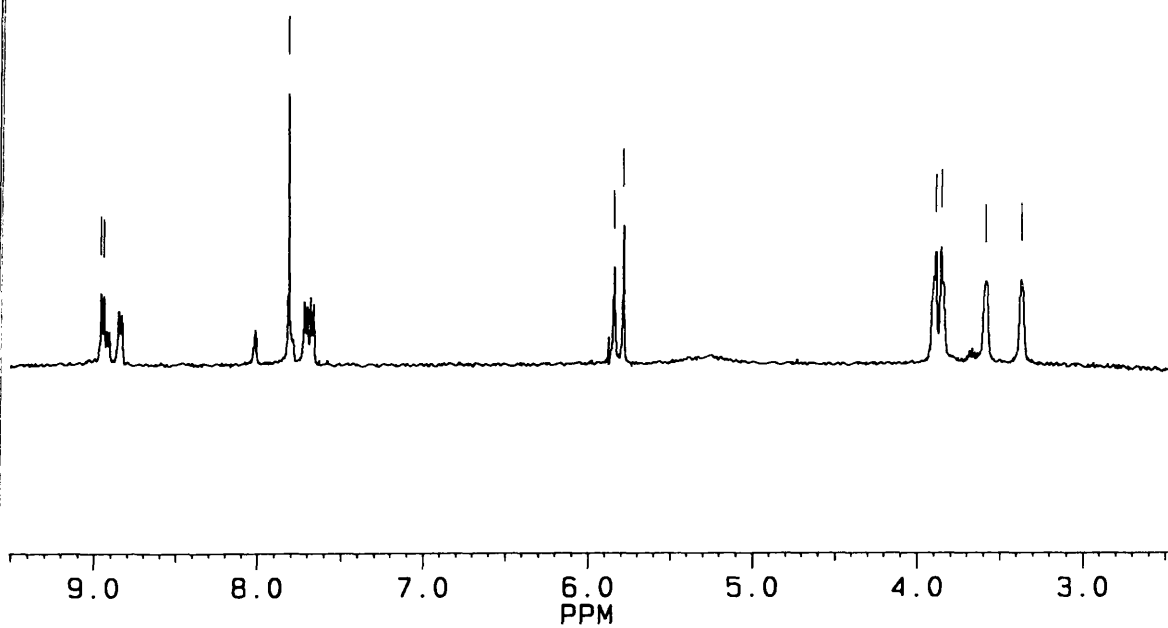


Figure 4.5: ^1H NMR spectrum of $\text{L5}(\text{PF}_6)_4$ in d_3 -acetonitrile at 360MHz and 298K.

viologen) whereas the other is in proximity to only one such donor unit (figure 4.6). The 'inside' viologen is thus stabilised by encapsulation by two donor units *via* EDA interactions and is thus less easily reduced than the 'alongside' acceptor unit.

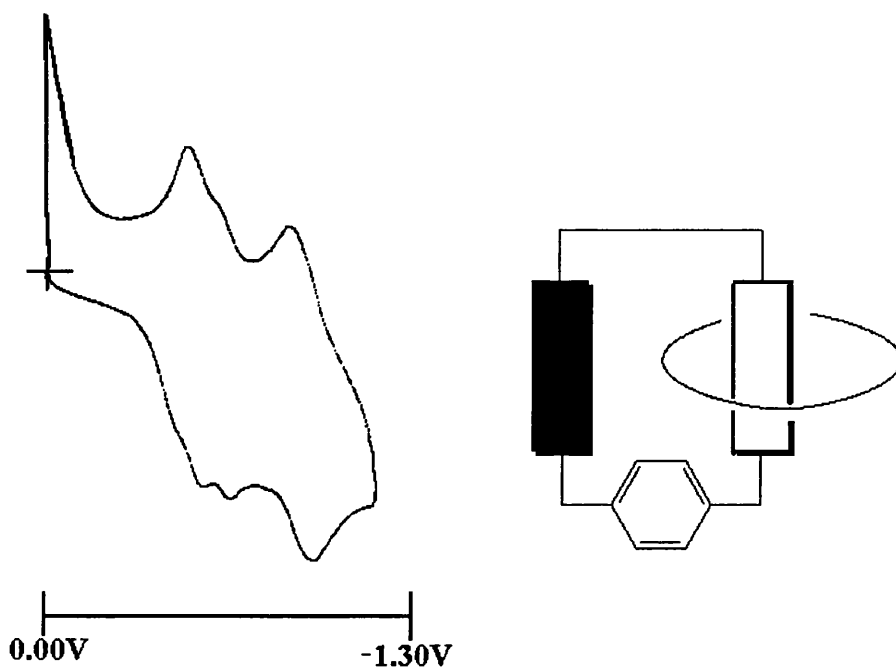


Figure 4.6: The electrochemical properties of L5.

The first reduction potentials for the inside and alongside viologen units are found at -0.54 and -0.41V (*vs* SCE) respectively. The second viologen reduction potential (-0.91V) for L5 is less strongly affected by this redox asymmetry because the mono-reduced viologen units no longer form very strong EDA complexes with the phenoxy donor units thus the acceptor units become electrochemically equivalent.

The electrochemical properties of the compound are more easily understood when the solid state structure of L5, as determined by X-ray analysis, is considered (figure 4.7, crystal data is given in appendices). The most immediately striking aspect of this structure is the nature of the two interlocked rings. The electron donating crown ether component forms part of an acceptor - donor - acceptor - donor π -stack as expected, however it is apparent that the aromatic subunits of the crown encapsulate one viologen acceptor unit whilst the other may be described as being merely 'alongside' this complex. Indeed, the average distances between the phenoxy unit bound within the acceptor cavity and the two acceptor units are

different. The 'encapsulated' viologen unit forms a 'tighter' EDA complex with the crown (the donor-acceptor distance being approximately 3.7Å) than does the 'alongside' viologen (the contact distance in this case being approximately 4.0Å). The means by which this arrangement arises is evident from consideration of the geometry of the acceptor cyclophane. In this component, the cation chelating 2,2'-bipyridine unit is again 'transoid' with respect to the nitrogen atoms, the torsion angle being 141.0°. Whilst this conformation leads to loss of the 'dog-leg' bend in the shape of the acceptor cyclophane, it accentuates the 'wedge' shape of the cyclophane where the long axes of the electron accepting units diverge from the phenyl spacer unit (where the methylene linking units are separated by 5.75Å) to the bipyridine unit (where the distance between the methylene linkers is 8.34Å). Thus, the divergent nature of the planes of the viologen units acts in combination with the increased distance between them to produce encapsulation of one viologen in preference to the other in the solid state. Analogies to the solution phase electrochemical properties of **L5** may be drawn where the electron acceptors were shown to be in different electrochemical environments whilst being chemically equivalent. A further interesting aspect of the solid state structure of **L5** which may support the above argument are the torsion angles of the 'inside' and 'alongside' viologen units. The encapsulated acceptor unit has a twist about its central carbon-carbon bond of 20.8° whereas the same twist for the corresponding non-encapsulated viologen is 38.0°. Hence the 'inside' viologen has greater planarity and is in position to form stronger EDA complexes by better orbital overlap with the electron donating moiety.

4.2.1 Coordination Chemistry of **L5**

As was the case with cyclophane **L1**, [2]catenane **L5** was expected to have a rich and varied coordination chemistry. Unlike its cyclophane analogue, however, **L5** cannot display interesting host-guest chemistry because the central cavity of the acceptor cyclophane is occupied by the crown ether component of the catenane. Thus, the construction of large polymolecular clusters with the aim of investigating potential changes in the host-guest properties of the system would have been fruitless activity. Whilst a dimeric (with respect to the catenane) structure was

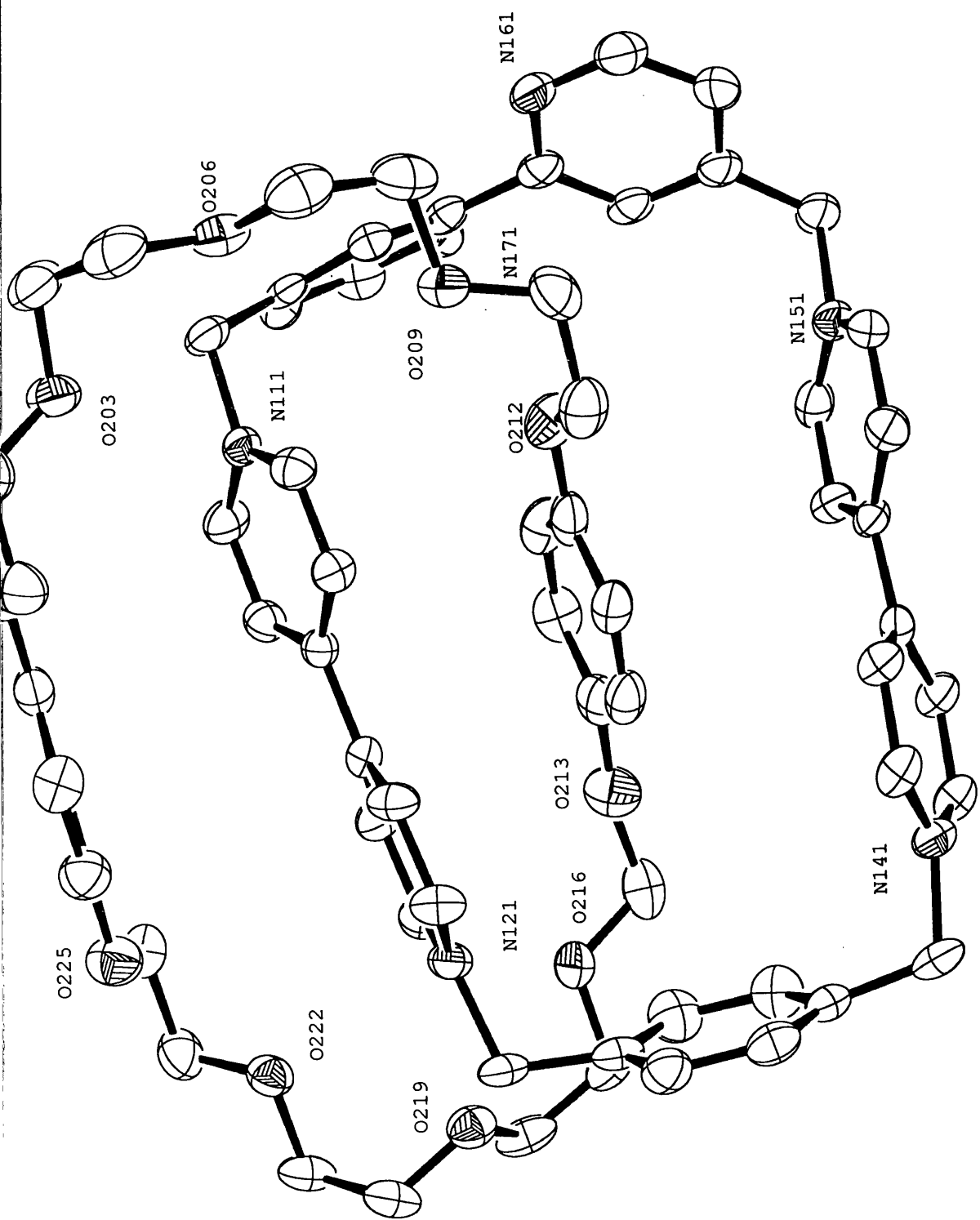


Figure 4.7: Crystal structure of cyclophane L5⁴⁺ (PF₆ counterions omitted).

constructed using a copper (I) centre and analysed by FAB mass spectrometry, the construction of polycatenane aggregates with **L5** was not systematically attempted. Rather, the main aim in studying the coordination chemistry of the [2]catenane was to append photoactive osmium and ruthenium bipyridyl moieties to **L5** and to then study the photoinduced electron transfer properties of the metal - ligand complex.¹⁴ The spectroscopic properties of the complex $\text{Ru}(\text{bipy})_2(\text{L5})(\text{PF}_6)_6$ will be discussed in chapter 5. The osmium complex was constructed with the aim of providing a comparison with the ruthenium analogue, but given that the compound $\text{Os}(\text{bipy})_2(\text{L1})(\text{PF}_6)_6$ did not show any interesting photophysical properties, it was not expected to be of any great interest as regards the creation of a model for the photosynthetic reaction centre.

In order to confirm that polymolecular aggregates of **L5** could be produced, a solution of copper (I) ($\text{Cu}(\text{CH}_3\text{CN})_4(\text{BF}_4)$ in acetonitrile) was added to a solution of the catenane in acetonitrile. A number of peaks were detected by fast atom bombardment (FAB) mass spectrometry which corresponded to degradation products of the complex $\text{Cu}(\text{L5})_2(\text{PF}_6)_8(\text{BF}_4)$. The dimeric compound, which has a molecular weight of 2578 a.m.u., displays typical behaviour for hexafluorophosphate containing compounds in that the mass spectra of such compounds frequently feature a series of peaks at various m/z values corresponding to the loss of 'n' PF_6 units. The peaks found in the mass spectrum of $\text{Cu}(\text{L5})_2(\text{PF}_6)_8(\text{BF}_4)$ represent the $[\text{M}-2(\text{PF}_6)]^+$, $[\text{M}-3(\text{PF}_6)]^+$ and $[\text{M}-(\text{PF}_6)(\text{BF}_4)]^+$ ions. Thus, evidence was obtained that it was possible to construct large polymolecular arrays without resorting to the use of covalent bonds - the four component rings of the $\text{Cu}(\text{L5})_2(\text{PF}_6)_8(\text{BF}_4)$ complex were held together by a combination of 'mechanical' bonds and by metal - ligand coordination.

The complex $\text{Os}(\text{bipy})_2(\text{L5})(\text{PF}_6)_6$ was synthesised by the pre-coordination method.¹² The yield of catenane product obtained by this method was disappointing (2.2%) particularly given the success of the strategy in preparing $\text{Os}(\text{bipy})_2(\text{L1})(\text{PF}_6)_6$ and $\text{Ru}(\text{bipy})_2(\text{L5})(\text{PF}_6)_6$ (yields of 60-70%). The dramatic differences in the yields of the two osmium complexes may be explained by both the reaction conditions and the different chromatographic strategies employed. The osmium-cyclophane complex was synthesised using a high dilution, high temperature strategy and accordingly no template molecule was used. Despite this,

the vigorous conditions and the low concentration of reactants combined with an efficient and rapid purification process using both alumina to remove impurities and size exclusion chromatography to separate the product from the starting materials lead to a high yield of Os(bipy)₂(L1)(PF₆)₆. In contrast, the osmium-catenane analogue could not be synthesised by this route because high temperatures disfavoured formation of the [2]catenane. This occurs because the EDA complex between the aromatic crown ether **34C10** and the acceptor cyclophane precursor dissociates in vigorous conditions. Given this restriction a room temperature strategy was employed in combination with a standard dilution (i.e. not high dilution) reaction. The result of this strategy was that a great many impurities were found to be present in the crude residue and a prolonged purification process using silica was necessary. Thus, it was difficult to isolate significant quantities of Os(bipy)₂(L5)(PF₆)₆ employing this strategy. It was, however, possible to obtain both FAB mass spectra and ¹H NMR data for this compound. Selected ¹H NMR data for this compound is presented in table 4.2.1.

Compound	CH(α)	CH(β)	Phenyl	CH ₂	Polyether
L5	9.28 9.33	8.10 - 8.14	8.00	6.08 6.15	3.46, 3.61, 3.89 -3.93
Os(bipy) ₂ L5	9.41	8.13 - 8.28	8.03	6.13 6.28	3.32, 3.46, 3.62, 3.82
Ru(bipy) ₂ L5	9.35	8.02 - 8.22	7.98	6.10 6.23	3.46, 3.62, 3.71, 3.82, 3.93-4.10

Table 4.2.1: Selected ¹H NMR data for [2]catenane L5 and its complexes.

All ¹H NMR data was obtained at 360MHz, at 298K in d₆-acetone.

From this table it may be seen that in contrast to the trend identified for cyclophane L1 and its metal complexes, catenane L5 and its metal complexes do not display large chemical shifts upon complexation. There were some small changes to the ¹H NMR spectrum of L5 upon complexation, including: the signals corresponding to the protons α and β to the nitrogen atom on the viologen unit collapse to multiplets rather than distinct doublets, and the methylene spacer signals move downfield by an average of 40Hz (0.11ppm). However, the key parameter for determining whether conformational change has occurred to the acceptor cyclophane

remains the resonance corresponding to the phenyl spacer. This signal has a chemical shift of 8.00ppm in the 'free' catenane and in its osmium and ruthenium compounds the equivalent signal appears at 8.03 and 7.98 ppm respectively. Given experimental errors inherent in NMR spectroscopy (slight changes in conditions, magnet properties, etc) there would seem to be very little change in the chemical shift of this resonance. Thus it may be postulated that the conformation of the acceptor cyclophane is not significantly changed upon complexation. Such behaviour would be in-keeping with decreased conformational fluidity of the acceptor cyclophane, possibly due to the binding of the crown ether component in its central cavity. However, such an interpretation is difficult to support when the solid state structure of **L5** is considered, where the acceptor cyclophane clearly still has the ability to deform into a conformation which allows a 'transoid' bipyridine conformation. The apparent discontinuity between these pieces of evidence may possibly be ascribed to a preferential packing geometry of the catenane in the solid state - the lowest energy solution phase structure may well be quite different to that of the solid state.

The ruthenium complex of **L5** was not synthesised by the pre-coordination route given the difficulties that were encountered with its osmium analogue. Rather, this compound was produced by synthesising **L5** and subsequently appending a ruthenium-bipyridyl centre to the catenane. This simplified route proved to be a facile route to the desired complex, which was easily purified by size exclusion chromatography. The ^1H NMR data for this compound is rather similar to that of its osmium analogue in that the signals corresponding to the protons α and β to the nitrogen atoms on the viologen units have also collapsed into multiplets, the methylene resonances are shifted by approximately the same extent ($\sim 40\text{Hz}$ or 0.11ppm) and the phenylene spacer unit has remained largely unmoved. Selected ^1H NMR data is presented in table 4.2.1. This compound was subjected to extensive photophysical investigation¹⁴ as will be discussed in chapter 5.

4.3 [2]Catenane L6

[2]Catenane L6, [2]-[1/5DN38C10]-[Cyclo(bisparaquat-*p*-phenylene-2,2'-bipyridine)]catenane tetrakis(hexafluorophosphate) was prepared in a manner directly analogous to that used to prepare compound L5. The crown ether 1/5DN38C10 is known to form stronger EDA complexes with aromatic electron acceptors due to the fact that it is more easily oxidised than its phenoxy equivalent.¹⁵ This feature may be clearly observed on a quantitative basis by considering the binding constants for the analogous cyclophane L1 with the aromatic electron donor molecules T1 and T2. The binding constant for the molecule containing the naphthoxy residue is $>3100\text{M}^{-1}$ as compared to 90M^{-1} for the phenoxy containing thread. It was hoped that this increased binding strength would increase the yield of catenane L6 as compared to the analogous L5 and indeed this effect was observed - the yield of catenated product improved from ca. 5% to over 30% on changing the crown ether from 34C10 to 1/5DN38C10.

It was further expected that the stronger EDA complexes formed by the naphthoxy - crown would accentuate the redox asymmetry that was created between the two viologen units in the acceptor cyclophane of compound L5. Hence [2]catenane L6 would provide an enhanced model for the photosynthetic reaction centre upon complexation with a photoactive metal centre such as ruthenium-tris-bipyridyl.¹⁴ Indeed, this effect is clearly evident in the electrochemical properties of L6. The cyclic voltammogram for compound L6 in acetonitrile presented in figure 4.8 is strikingly different from that of compound L5 in that both the first (at -0.43V and -0.53V vs SCE) and second reduction waves (at -0.83V and -0.97V vs SCE) of the viologen subunits are split into two one electron reductions. As was discussed previously, the first reduction potentials of the 'inside' and 'alongside' viologen subunits for [2]catenanes such as those described here are usually different due to the encapsulation of one of the acceptor units by the aromatic crown ether. In catenane L5 this resulted in the one electron reduction firstly of the 'alongside' acceptor unit and then the encapsulated 'inside' acceptor, followed at a more reducing potential by a two electron reduction of the almost equivalent mono-reduced acceptor units.⁵ In catenane L6 however, both the first and second reduction

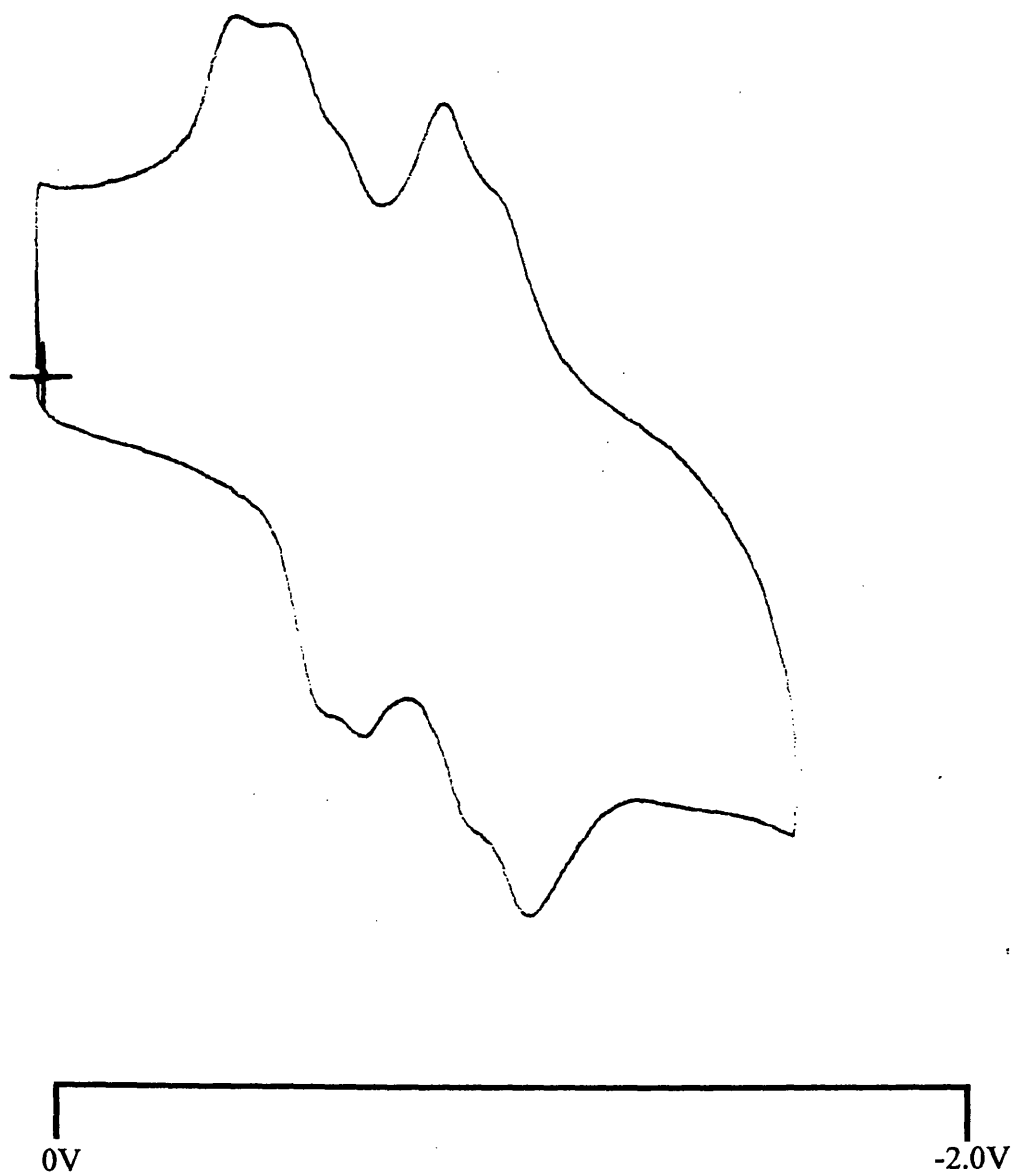


Figure 4.8: Cyclic voltammogram of L6.(PF₆)₄ in N₂ degassed acetonitrile with 0.2M tetrabutylammonium tetrafluoroborate background electrolyte. Scan rate was 50mVs⁻¹, reference electrode was Ag/AgNO₃.

waves of the viologen acceptor units are split because in contrast to its phenoxy equivalent, the naphthoxy residue is a sufficiently strong electron donor to form a significant EDA complex with a mono-reduced viologen unit.¹⁵ Thus, the encapsulated and 'alongside' acceptor units maintain their redox asymmetry even after both have been through a one electron reduction process.

Compound **L5** is intensely red in solution, with an absorption maximum at 450nm. In contrast catenane **L6** is an intense purple substance. The colours arise from the charge transfer (CT) process that occurs upon formation of an EDA complex¹³ and the change in wavelength of the CT band in **L6** (to 500nm, $\epsilon = 765\text{M}^{-1}\text{cm}^{-1}$) indicates that the energy of the charge transfer state is lower (by ca. $20,000\text{cm}^{-1}$) than in **L5**. This effect results from the ease of oxidation of the naphthoxy residues of the crown **1/5DN38C10** as compared to its phenoxy equivalent in **34C10**.

The ¹H NMR spectrum of **L6** at ambient temperature is rather more complex than that of **L5**. This is caused to a large extent by the more complicated pattern that is produced by the naphthoxy residue as compared to the more simple phenoxy equivalent (figure 4.9).¹⁵

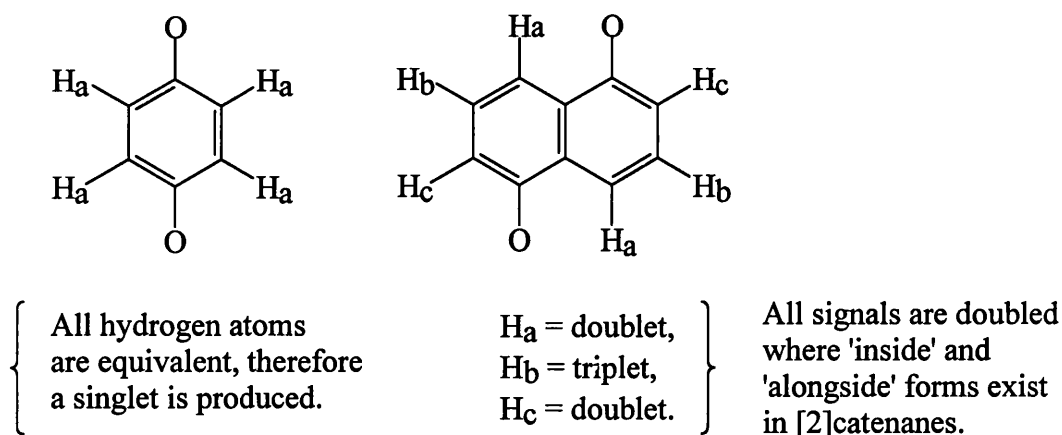


Figure 4.9: Expected multiplicities of ¹H NMR signals from 1,4-phenoxy and 1,5-naphthoxy residues.

All the expected signals for the acceptor cyclophane segment of the [2]catenane are present at room temperature. The signals corresponding to the protons on the viologen subunits are sharp doublets at 9.41 and 9.26ppm (protons α to the nitrogen atom) and at 7.91 and 7.82ppm (protons β to the nitrogen atom); the phenylene spacer resonance is a sharp singlet at 8.28ppm and the 2,2'-bipyridine

chelating unit has well resolved signals at 9.04, 8.43 and 8.04ppm. Interestingly, however, the methylene linking units are not sharp singlets as is the case with the analogous catenane **L5** or cyclophane **L1** - a broad signal is observed at 6.13ppm which integrates as 8 protons i.e. all four methylene units. The crown ether ^1H NMR signals are more difficult to assign because whilst the polyether portion of the macrocycle is obvious (in the range 3.00 - 4.30ppm) the signals corresponding to the naphthoxy residues are either broadened into the baseline or are at considerably higher field than expected.

In an attempt to locate all the signals expected for the naphthoxy residues, a series of variable temperature one dimensional ^1H NMR experiments were carried out with the aim of finding a temperature at which the signals coalesced and could be assigned either by inspection or by employing two dimensional techniques. Due to the complexity of the NMR spectra at low temperatures, the latter technique was found to be necessary. Two dimensional COSY experiments were undertaken first at 298K (400MHz, d_6 -acetone, figure 4.10) and then at 213K (360MHz, d_6 -acetone, figure 4.11). The ambient temperature COSY experiment plotted in figure 4.10 shows a rather simple pattern of correlation cross peaks because at 298K an averaged spectrum is produced by the rapid movements of the rings of the catenane. The spectrum confirms the assignment of the signals corresponding to the acceptor cyclophane as described above. As these signals were well characterised, the main points of interest in this spectrum were the doublet at 6.49ppm coupled to the triplet at 5.81ppm and the signals in the 'polyether region' of the spectrum in the range 3.0 to 4.5ppm. It is possible to state, by comparison to analogous catenanes in the literature,¹⁵ that the doublet and triplet pair belong to the 'inside' naphthoxy residue and that the 'missing' doublet must be moved to high field by the shielding effects of C-H $\cdots\pi$ and EDA interactions on these protons. This signal could not be identified at 298K as no correlation peak was produced with the doublet-triplet pair. The signals corresponding to the 'alongside' protons must be broadened into the baseline by rapid movement of the highly flexible polyether chain around the outside of the acceptor cyclophane cavity. The signals which are believed to correspond to the polyether portion of the crown ether component produce few correlation cross peaks.

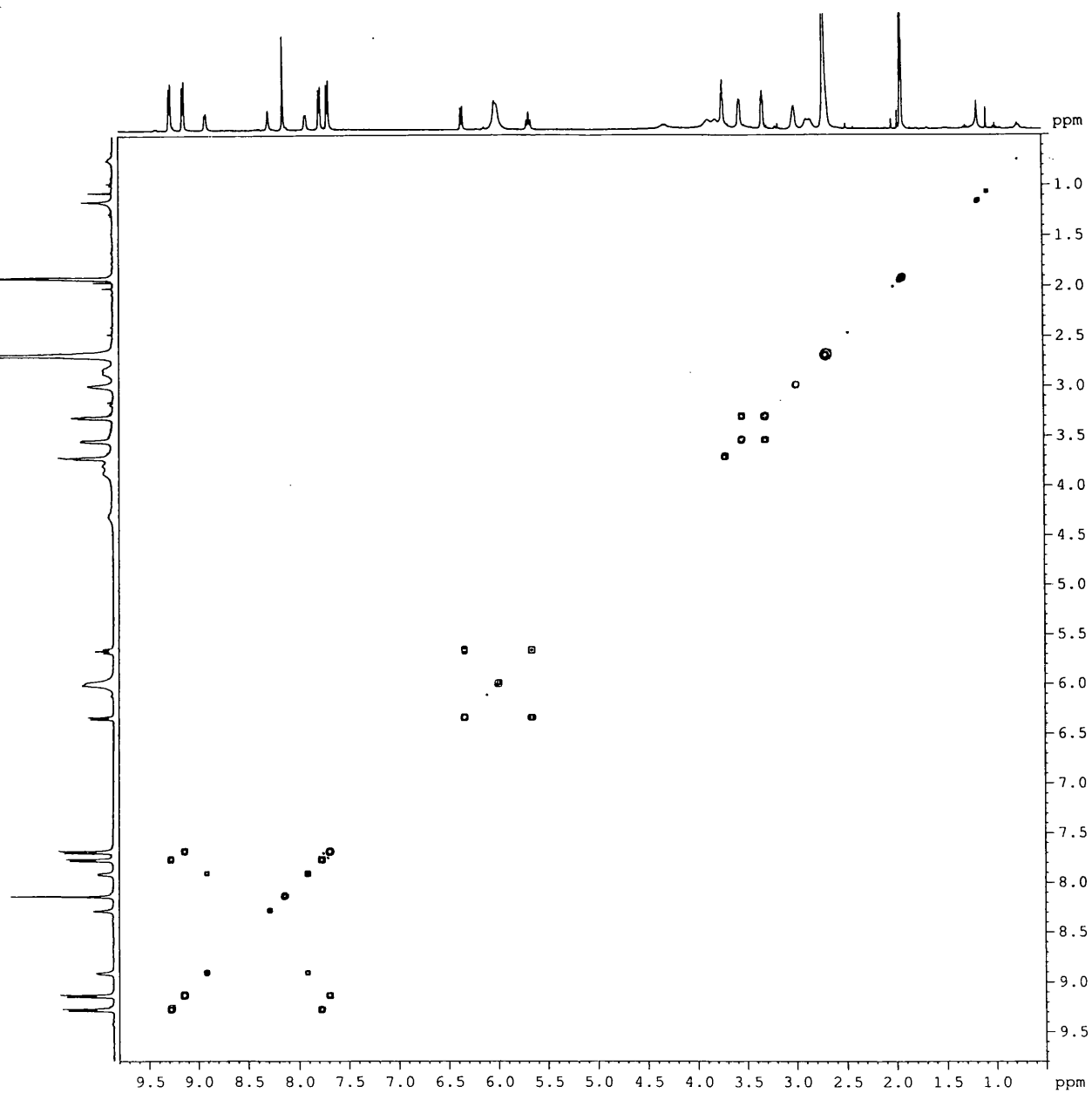


Figure 4.10: ¹H-¹H COSY spectrum of L6.(PF₆)₄ in d₆-acetone at 400MHz and 298K.

E100C IN ACETONE AT 213K.

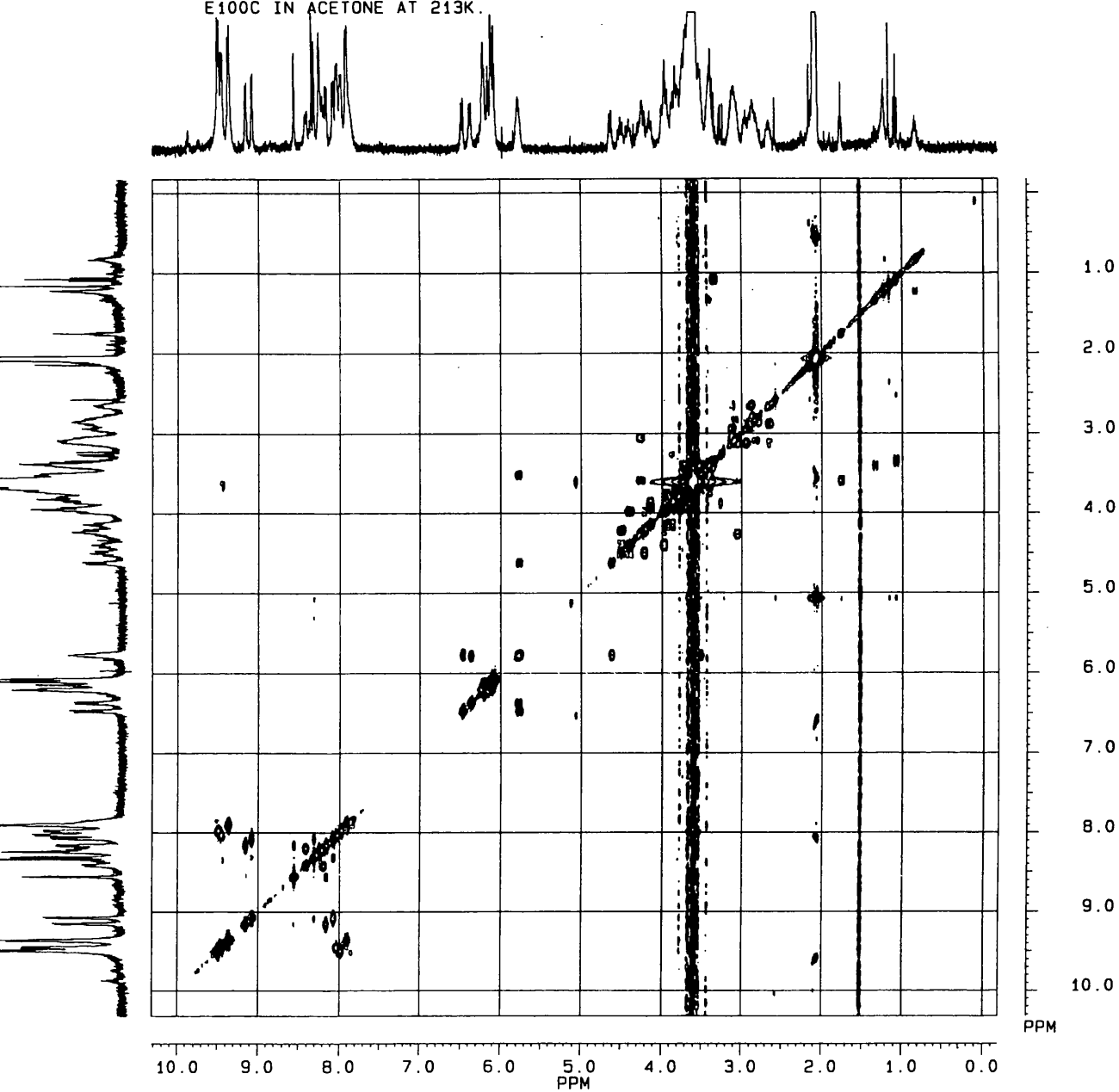


Figure 4.10: ^1H - ^1H COSY spectrum of $\text{L6} \cdot (\text{PF}_6)_4$ in d_6 -acetone at 360MHz and 213K.

The ^1H - ^1H COSY NMR spectrum of compound **L6** presented in figure 4.11 was obtained at 213K and at 360MHz in d_6 -acetone. At this temperature, the spectrum is very much more complicated than the equivalent spectrum at ambient temperature because the conformations that were rapidly interconverting at higher temperatures are now ‘frozen out’ - i.e. the rapid revolutions and movements of the component rings become inhibited. Whilst it is possible to correlate the ‘new’ peaks and tentatively assign them to different isomers (although the exact nature of these isomers remains uncertain) this was not the aim of the experiment. The goal was to attempt to locate and identify the ‘missing’ resonances of the naphthoxy residues of the crown ether component. To this end the experiment proved successful in that a number of naphthoxy signals were identified as detailed in table 4.3.1.

Signal	H_a	$\text{H}_{a'}$	H_b	$\text{H}_{b'}$	H_c	$\text{H}_{c'}$
Chemical Shift	3.55	4.61	5.71-5.82	5.71-5.82	6.41	6.50

Table 4.3.1: Chemical shifts of ‘inside’ naphthoxy residue of L6.

From the chemical shifts of these signals it seems likely that they represent protons on a naphthoxy unit which is bound within the acceptor cyclophane - however the signals for the pairs of protons H_a , H_b and H_c are no longer equivalent as explained in figure 4.9. The ‘freezing out’ of the rotations of the bound naphthoxy unit has created an asymmetry in this unit whereby C-H--- π interactions between the phenyl spacer of the acceptor cyclophane and H_a and the chelating 2,2'-bipyridine unit and $\text{H}_{a'}$ hold the naphthoxy residue rigidly in place, creating a doubling or broadening of the resonances as compared to the room temperature spectrum (figure 4.12).

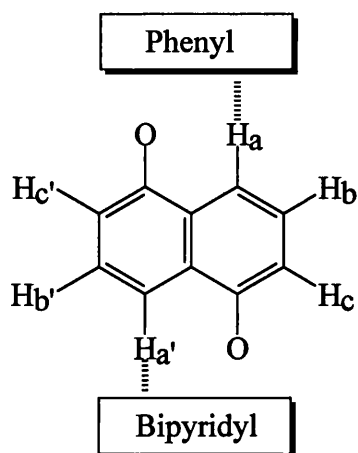


Figure 4.12: Low temperature induced asymmetry in the ‘inside’ naphthoxy residue of compound L6.

The location of the signals corresponding to the ‘alongside’ naphthoxy residue remains unclear given the interpretation of the low temperature COSY spectrum above. The complex nature of the ^1H NMR spectrum at this temperature in the 7.5 to 8.5ppm region of the spectrum may mask the signals corresponding to these protons, however this seem unlikely. A more plausible explanation is that the crown ether portion of the **1/5DN38C10** crown is still sufficiently flexible so that in combination with the open ‘wedge shaped’ nature of the acceptor cyclophane the crown ether can rapidly exchange its position and thus remain broadened into the baseline of the NMR spectrum even at 213K. Such a result indicates phenomenal conformational freedom within catenane **L6**.

The coordination chemistry of catenane **L6**, especially the complex of the ligand with photoactive metal centres such as ruthenium tris bipyridyl has yet to be fully investigated but it is anticipated that the stronger EDA complexes formed between the crown compound **1/5DN8C10** and viologen acceptor units should enhance the redox asymmetry inherent in such compounds. Thus, upon electron transfer from a secondary donor to the catenane, it is hoped that unidirectional electron transfer may occur¹⁴ (see chapter 5 for a discussion of this effect with compound $\text{Ru}(\text{bipy})_2(\text{L5})(\text{PF}_6)_6$) to the uncomplexed viologen unit in preference to the encapsulated acceptor unit. Such a system may provide a model for the photosynthetic reaction centre.

4.4 [2]Catenane L7

[2]Catenane L7, [2]-[34C10]-[cyclo(bisparaquat-bis-2,2'-bipyridine)] catenane tetrakis(hexafluorophosphate) was prepared by a route analogous to that employed to synthesise catenanes L5 and L6, where precursor P1 was stirred for 10 days with the aromatic crown ether 34C10 and 4,4'-bisbromomethylene-2,2'-bipyridine in an acetonitrile solution. Purification of the red product was effected by use of standard chromatographic techniques and by a number of recrystallisations. The yield of catenane produced by this synthetic strategy was disappointingly low (1.1%). Evidence from FAB mass spectrometry indicates that the formation of oligomeric material represents a significant proportion of the products produced by this reaction, with the oligomer depicted in figure 4.13 being particularly prevalent. Interestingly, the FAB mass spectrum also indicates that significant quantities of cyclophane L2 are produced as by-products in this synthesis (the m/z peaks are too intense to be mere degradation products of L7). This result is interesting because cyclisation must have occurred without the aid of a template as such a reaction would have resulted in production of the desired catenane.

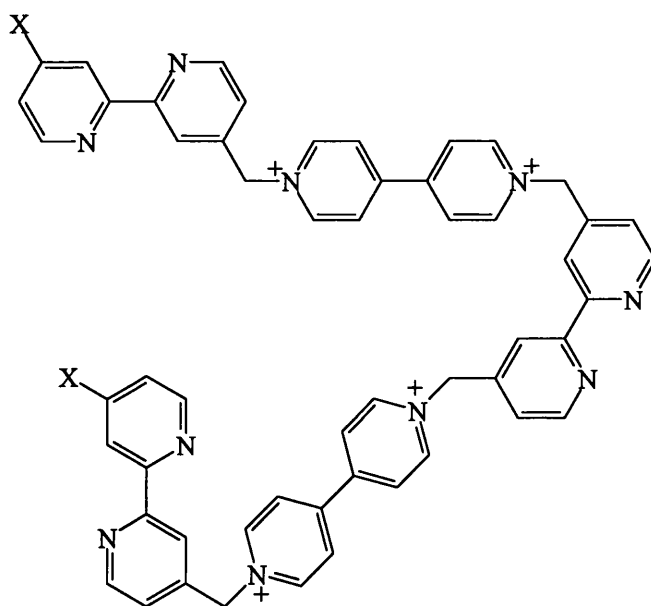


Figure 4.13: The major oligomeric impurity in the synthesis of L7.

An ^1H NMR experiment was carried out to follow the course of the reaction, with the aim of determining where the problem lay in the synthesis of L7. The reaction was carried out using the standard procedure but on a reduced scale, with

NMR spectra being recorded at regular intervals (every 1-3 hours initially, twice daily thereafter). Over the course of the reaction it was possible to observe the consumption of the precursor **P1** and the growth of a number of peaks representing a number of products, most likely including oligomers, the desired catenane and the cyclophane **L2**. This made interpretation of the spectra obtained towards the end of the reaction rather difficult.

The absorption spectrum of the crude reaction mixture demonstrated the existence of an (or several) EDA complex(s) by the presence of a charge transfer (CT) band (maximum at 460nm). Upon heating the solution however, the intensity of the charge transfer band decreased. This may be interpreted as evidence that a significant proportion of the intensity of the charge transfer band arises from pseudo-rotaxane species which may be thermally de-threaded thus destroying the EDA complex and the CT interaction. The remaining intensity corresponds to the concentration of interlocked catenane species which cannot be de-threaded (although the frequency of rotation of the ring components can be increased).

The explanation for the production of significant quantities of non-ring-closed and pseudo-rotaxane species is most obviously related to the fact that the cyclisation reaction involves the linking of two 2,2'-bipyridine derivatives, both of which are in unfavourable conformations to produce the desired product.¹² The same effect is in operation where the analogous cyclophane **L2** is produced, however the cyclophane is produced by employing the efficient naphthoxy containing template **T1** whereas catenane **L7** is assembled around the much poorer electron donating macrocycle **34C10**, which is clearly less effective at producing the desired product.

Despite the very poor yield of the synthetic strategy, the electrochemical properties of the catenane were briefly investigated and ¹H NMR and FAB mass spectra of **L7** were also obtained. The cyclic voltammogram (CV) of **L7** was obtained from a very weak analyte solution because of the difficulty in obtaining sufficient quantities of pure material. Two broad reduction waves were observed against a very strong background current due to the nature of the analyte solution. The reductions occurred at potentials of -0.43V and -0.73V (vs SCE) and correspond to two electron reductions of the viologen acceptor subunits. Whilst it was expected that the first reduction wave would be split into two one electron reductions corresponding to the 'inside' and 'alongside' viologen units as was the

case with compound **L5**, the fact that only one broad wave was recorded is unsurprising given the conditions of the experiment. The first reduction potential occurs at the expected value as compared to catenane **L5**, however, the second reduction potential is approximately 0.18V more positive than in **L5**, although this result must be regarded with some circumspection given the conditions employed.

The high m/z region of the FAB mass spectrum of **L7** is presented in figure 4.14. The peaks displayed on the spectrum are characteristic for the hexafluorophosphate salt of the tetracationic catenane - each peak represents loss of 'n' PF_6 units ($n = 1-3$).

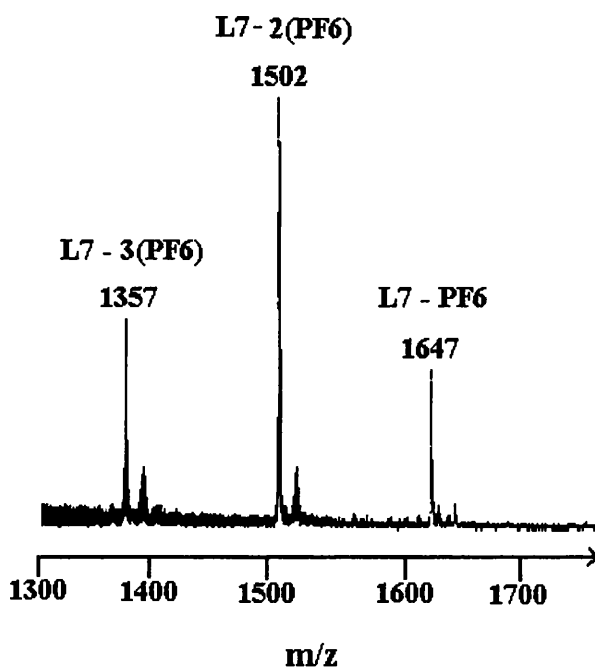


Figure 4.14: Partial FAB mass spectrum of L7 (NBA matrix).

The ^1H NMR spectrum of **L7** is rather simple as compared to **L5** and **L6** because the acceptor cyclophane is highly symmetric (the encapsulated and non-encapsulated viologen units being equivalent on the NMR timescale) and the crown ether **34C10** does not give rise to complicated NMR signals as its naphthoxy analogue does. The signals corresponding to compound **L7** are assigned in table 4.3.1.

Signal	Chemical Shift
CH(α)	9.40
CH(β)	8.30
Bipyridyl	7.91, 8.37, 8.88
CH ₂	6.25
Phenoxy*	6.39
Polyether	3.37, 3.52, 3.85, 3.91

Table 4.3.1: Assignment of the ¹H NMR spectrum of L7.

All ¹H NMR data was obtained at 360MHz and at 298K in d₆-acetone. The phenoxy signal* is believed to be the 'inside' phenoxy residue - the 'alongside' signal may be broadened into the baseline.

From the table it may be seen that in contrast to the analogous catenane L5, a sharp singlet most likely corresponding to the 'inside' phenoxy residue of the crown ether is observed at 6.39ppm. The fact that this signal is resolved for this system but not for L5 may imply that there are differences between the dynamic processes in the two systems. It is possible that circumrotation of the crown ether may be hindered by the incorporation of a second 2,2'-bipyridine units in place of a phenyl spacer, thus the 'inside' and 'alongside' phenoxy units may become distinguishable at room temperature. Due to the small quantities of product that were isolable it was difficult to carry out a rigorous investigation of this effect.

The coordination chemistry of catenane L7 was not investigated, again due to the lack of material available.

4.5 References

- [1] Benniston A.C. *Chem. Soc. Rev.*, 1996, 427.
- [2] Vögtle, F. *Supramolecular Chemistry*, Wiley, Chichester, 1991.
- [3] See for example: (a) Fyfe, M.C.T.; Stoddart, J.F. *Acc. Chem. Res.*, 1997, 30, 393. (b) Gillard, R.E.; Raymo, F.M.; Stoddart, J.F. *Chem. Eur. J.*, 1997, 3, 1933.
- [4] See for example: (a) Dietrich-Buchecker, C.O.; Sauvage, J.P. *Chem. Rev.*, 1987, 87, 795. (b) Sauvage, J.P. *Acc. Chem. Res.*, 1990, 23, 319. (c) Dietrich-Buchecker, C.O.; Sauvage, J.P. *New J. Chem.*, 1992, 16, 277.
- [5] Anelli, P.L.; Ashton, P.R.; Ballardini, R.; Balzani, V.; Delgado, M.; Gandolfi, M.T.; Goodnow, T.T.; Kaifer, A.E.; Philp, D.; Pietraszkiewicz, M.; Prodi, L.; Reddington, M.V.; Slawin, A.M.Z.; Spencer, N.; Stoddart, J.F.; Vicent, C.; Williams, D.J. *J. Am. Chem. Soc.*, 1992, 114, 193.
- [6] Stoddart, J.F. in *Frontiers in Supramolecular Organic Chemistry and Photochemistry*, (Eds. Schneider, H.J.; Dürr, H), VCH, Weinheim, 1991.
- [7] Amabilino, D.B.; Ashton, P.R.; Brown, C.L.; Córdova, E.; Godinez, L.A.; Goodnow, T.T.; Kaifer, A.E.; Newton, S.P.; Pietraszkiewicz, M.; Philp, D.; Raymo, F.M.; Reder, A.S.; Rutland, M.T.; Slawin, A.M.Z.; Spencer, N.; Stoddart, J.F.; Williams, D.J. *J. Am. Chem. Soc.*, 1995, 117, 1271.
- [8] Ashton, P.R.; Bissell, R.A.; Philp, D.; Spencer, D.; Spencer, N.; Stoddart, J.F. in *Supramolecular Chemistry*, NATO ASI Series, (Eds. Balzani, V.; De Cola, L.), Kluwer Academic Publisher, Dordrecht, 1992.
- [9] Ashton, P.R.; Goodnow, T.T.; Kaifer, A.E.; Reddington, M.V.; Slawin, A.M.Z.; Spencer, N.; Stoddart, J.F.; Vicent, C.; Williams, D.J. *Angew. Chem. Int. Ed. Engl.*, 1989, 28, 1396.
- [10] Lehn, J.M. *Supramolecular Chemistry*, VCH, Weinheim, 1995.
- [11] (a) Amabilino, D.B.; Ashton, P.R.; Balzani, V.; Boyd, S.E.; Credi, A.; Lee, J.Y.; Menzer, S.; Stoddart, J.F.; Venturi, M.; Williams, D.J. *J. Am. Chem. Soc.*, 1998, 120, 4295. (b) Ashton, P.R.; Boyd, S.E.; Claessens, C.G.; Gillard, R.E.; Menzer, S.; Stoddart, J.F.; Tolley, M.S.; White, A.J.P.; Williams, D.J. *Chem. Eur. J.*, 1997, 3, 788. (c) Ashton, P.R.; Brown, C.L.; Chrystal, E.J.T.; Parry,

- K.P.; Pietraszkiewicz, M.; Spencer, N.; Stoddart, J.F. *Angew. Chem. Int. Ed. Engl.*, 1991, **30**, 1042.
- [12] Benniston A.C.; Mackie, P.R.; Harriman, A. *Tetrahedron Lett.*, 1997, **38**, 3577.
- [13] Benniston, A.C.; Harriman, A.; Philp, D.; Stoddart, J.F. *J. Am. Chem. Soc.*, 1993, **115**, 5298.
- [14] Benniston, A.C.; Mackie, P.R.; Harriman, A. *Angew. Chem. Int. Ed. Engl.*, 1998, **37**, 354.
- [15] (a) Ashton, P.R.; Brown, C.L.; Chrystal, E.J.T.; Goodnow, T.T.; Kaifer, A.E.; Parry, K.P.; Philp, D.; Slawin, A.M.Z.; Spencer, N.; Stoddart, J.F.; Williams, D.J. *J. Chem. Soc. Chem. Commun.*, 1991, 634. (b) Ashton, P.R.; Ballardini, R.; Balzani, V.; Blower, M.; Ciano, M.; Gandolfi, M.T.; McLean, C.; Philp, D.; Prodi, L.; Spencer, N.; Stoddart, J.F.; Tolley, M.S. *New J. Chem.*, 1993, **17**, 689. (c) Asakawa, M.; Ashton, P.R.; Boyd, S.E.; Brown, C.L.; Gillard, R.E.; Kocian, O.; Raymo, F.M.; Stoddart, J.F.; Tolley, M.S.; White, A.J.P.; Williams, D.J. *J. Org. Chem.*, 1997, **62**, 24.

Chapter Five

Photophysical Studies

5.1 Introduction

The photophysical properties of three closely related compounds, all based on the ruthenium tris-bipyridyl unit, have been investigated by transient absorption and fluorescence spectroscopy. The compounds (figure 5.1) may be regarded as a progression from the simplest compound, $\text{Ru}(\text{bipy})_2(\text{P1})^{4+}$ - a complex involving the acyclic precursor **P1**, to the more complex cyclised analogue $\text{Ru}(\text{bipy})_2(\text{L1})^{6+}$, and ending with the most complicated system, $\text{Ru}(\text{bipy})_2(\text{L5})^{6+}$ - a complex featuring a [2]catenane as a ligand. The first compound in this series, $\text{Ru}(\text{bipy})_2(\text{P1})^{4+}$ was investigated using nanosecond (10^{-9} s) time resolved laser flash photolysis equipment. The aim of this study was to determine whether the compound behaved in a similar way to the more complicated systems in the series (undergoing photoinduced electron transfer)¹ or whether it behaved simply as a $\text{Ru}(\text{bipy})_3^{2+}$ derivative.² The compounds $\text{Ru}(\text{bipy})_2(\text{L1})^{6+}$ and $\text{Ru}(\text{bipy})_2(\text{L5})^{6+}$ were subjected to examination by picosecond (10^{-12} s) time resolved transient absorption spectroscopy. The aim of these experiments was to determine whether electron transfer occurred between the excited state of the ruthenium tris-bipyridyl centres and the electron accepting units to which they are bound.³ It was hoped that the most sophisticated compound in the series, $\text{Ru}(\text{bipy})_2(\text{L5})^{6+}$ might act as a model for the photosynthetic reaction centre.⁴

The properties expected from molecular and supramolecular systems were discussed in section 1.7. It was stated that one of the key functions that the systems discussed in this thesis were to achieve was photoinduced electron transfer. This property has also been discussed previously, particularly as regards its theoretical background (Marcus theory)⁵ and the factors which influence feasibility and rates of electron transfer. Such factors include solvent effects (e.g. reorganisation),⁶ electrolyte effects⁷ and through bonds or through space interactions.⁸ The theories behind and factors influencing photoinduced electron transfer will not, therefore, be discussed further in this chapter, except with specific reference to the properties of the systems of interest.

The photophysical and electrochemical properties of $\text{Ru}(\text{bipy})_3^{2+}$ were also briefly discussed in chapter 1. The excited state properties of $\text{Ru}(\text{bipy})_3^{2+}$ are well known and a great number of publications on various aspects of these may be found in the literature.⁹ For example, the profound effect that solvents have on the

properties of ruthenium tris-bipyridyl have been studied in great detail and reviewed extensively.¹⁰ As most of the results described in this chapter were obtained in acetonitrile (with the obvious exception of the determination of the effect of solvent polarity on the rates of forward and back electron transfer for $\text{Ru}(\text{bipy})_2(\text{L1})^{6+}$) this will not be discussed at length in this chapter.

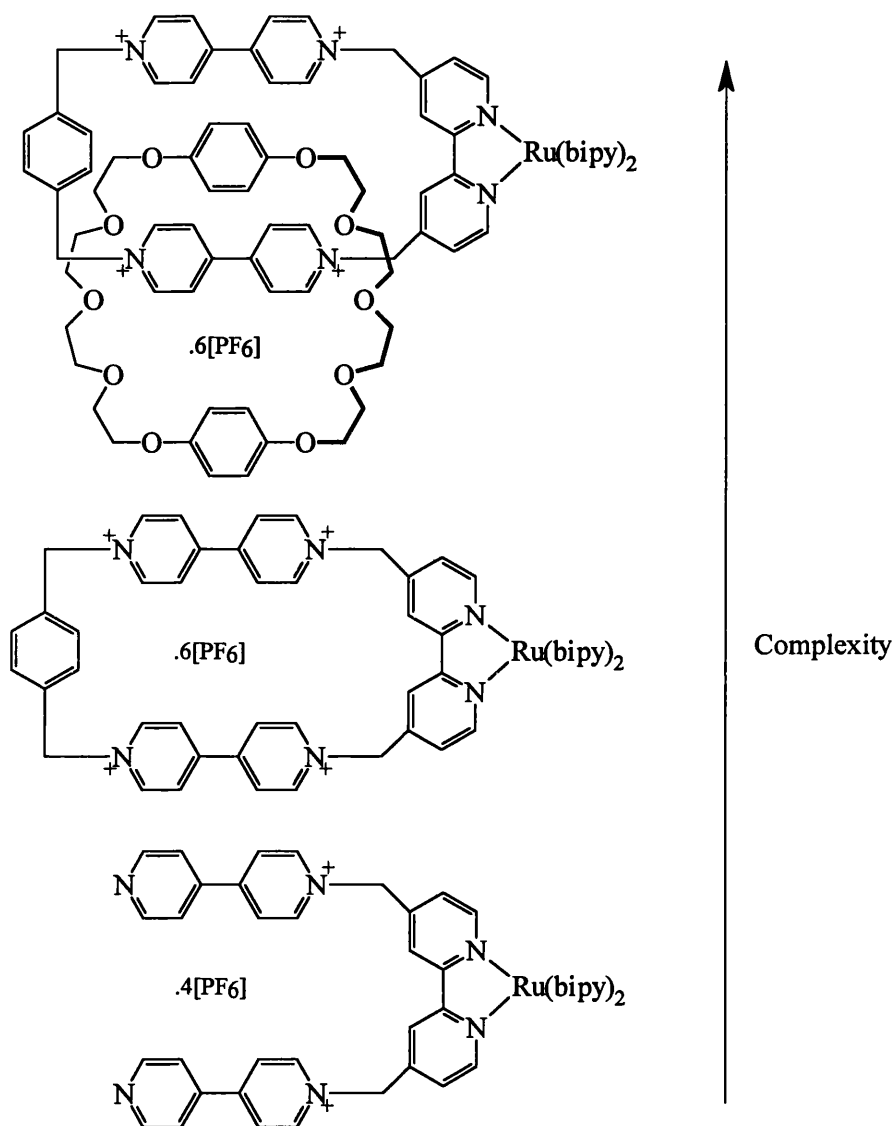


Figure 5.1: Compounds studied by time-resolved optical spectroscopy.

Ruthenium tris-bipyridyl complexes can perform photoinduced electron transfer reactions because of the relative ordering of the energies of the occupied and unoccupied orbitals in the complex. The d, π^* excited state of $\text{Ru}(\text{bipy})_3^{2+}$ can, for example, readily donate a π -electron to methyl viologen in a thermodynamically

favourable reaction.¹ The charge-transfer excited state is brought about by photoexcitation whereby a metal-centred electron (t_{2g}) is promoted to a ligand based π^* orbital. The MLCT state consists of a manifold^{2,11} of closely spaced thermally equilibrated states. The promoted electron, which is localised on the bipyridyl ligands, is available for donation to suitable electron acceptors.

The excited state of ruthenium tris-bipyridyl can be quenched by a variety of electron acceptors (and donors) and by energy transfer processes.¹ The quenching of $\text{Ru}(\text{bipy})_3^{2+}$ by $\text{Cr}(\text{CN})_6^{3-}$ provides an example of energy transfer. Energy transfer occurs in this case because electron transfer is not thermodynamically allowed. It should be noted however, that there are comparatively few examples of energy transfer¹² involving $\text{Ru}(\text{bipy})_3^{2+}$.

The quenching of the excited state of ruthenium tris-bipyridyl by methyl viologen, where the metal complex acts as an electron donor, involves a thermodynamically allowed electron transfer process which produces a strongly blue coloured intermediate $\text{MV}^{\cdot+}$. Energy transfer between these two reactants is not a significant competitive quenching mechanism¹ because both the singlet and triplet excited state of the methyl viologen dication lie at higher energies than that of the excited state of $\text{Ru}(\text{bipy})_3^{2+}$.

A fundamental problem with the application of ruthenium tris-bipyridyl/methyl viologen systems as supramolecular devices, e.g. for converting light into charge separated species, is that rapid charge recombination occurs between the radical ion pair produced by the photoinduced electron transfer process. A number of means of preventing this back electron transfer have been described. The most effective strategy is to separate the products of the electron transfer process¹ either by use of a barrier e.g. in micelles or lipid bilayers in vesicles (compartmentalise the products) or by separating the products to a great distance by use of highly polar solvents. In either case, subsequent oxidation of a sacrificial electron donor (e.g. secondary amines) by the $[\text{Ru}^{3+}]$ complex regenerates the photosensitiser and allows recycling of the system so that quantities of reduced viologen may be built up. This has been employed (with appropriate catalysts) in water splitting systems.

Substitution of bipyridyl ligands has a significant effect on the energy levels within the chelating molecule - this is manifested in the properties of the complex.² As a consequence of varying the energy of the MLCT state, for example, the

absorption bands arising from the d,π^* charge transfer transitions and the associated emission bands may have very different energies, transition intensities and quantum efficiencies. There are a large number of examples of complexes involving ruthenium and derivatised bipyridyl complexes. A brief summary of some recent examples which pertain to the systems under investigation in this chapter are outlined in the following text.

The complex $\text{Ru}(\text{bipy})_2(\mathbf{P1})$ possesses two nitrogen atoms on the extremes of the bipyridinium 'arms' of the $\mathbf{P1}$ ligand, which are capable of capturing and reacting with protons and other electrophiles. If donation of electrons from the nitrogen atoms to such electrophilic entities resulted in changes in the electron accepting ability of the bipyridinium units (of which the nitrogen atoms are a part) then the fluorescence of the ruthenium tris-bipyridyl centre may well be quenched. The complex would then have the potential to act as a sensor for protons (pH sensor), metal cations and suitable organic Brønsted acids such as carboxylic acids. Analogies in the literature are abundant, the systems based on $\text{Ru}(\text{bipy})_2(5,5'$ -diaminomethyl-2,2'-bipyridyl) derivatives being particularly relevant¹³ (figure 5.2).

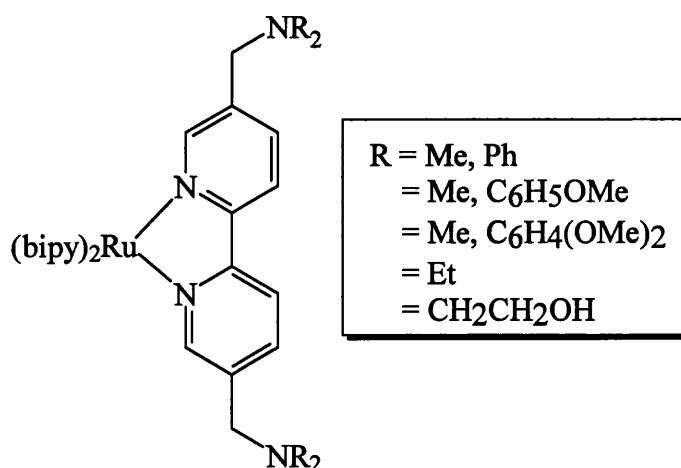


Figure 5.2: $\text{Ru}(\text{bipy})_2(5,5'$ -diaminomethyl-2,2'-bipyridyl)²⁺.

The aminomethyl derivatised bipyridyl complexes depicted above act as a proton sensors by either of two mechanisms. The first three compounds presented in figure 5.2 show no fluorescence at high pHs as the amine units act as electron donors to the excited state of the $\text{Ru}(\text{bipy})_3^{2+}$ unit *via* a photoinduced electron transfer process. Lowering the pH results in protonation of the amine units, thus destroying their electron donating ability and so the compound fluoresces. In

contrast, the last two compounds act in a manner which is expected to be more directly analogous to $\text{Ru}(\text{bipy})_2(\text{P1})^{4+}$ in that upon protonation at low pH values the ammonium subunits act as electron acceptors and thus the fluorescence of the $\text{Ru}(\text{bipy})_3^{2+}$ moiety is quenched.

Derivatives of ruthenium tris-bipyridyl in which an electron accepting methyl viologen unit is covalently bound to the photoactive metal centre have been investigated by a number of groups. A simple case, where methyl viologen is joined to a bipyridyl ligand by a propyl linking chain was presented by Mallouk, Bard and co-workers.¹⁴ It was found that electron transfer from the excited state of the photosensitiser to the electron acceptor occurred as expected, but that some luminescence was still evident. They demonstrated that this luminescence was produced by degradation products of the complex where the viologen unit had been displaced by reaction with oxygen. Kelly and Rodgers¹⁵ presented a closely related set of compounds (figure 5.3) where the viologen acceptor unit was bound to a variety of ruthenium bipyridyl complexes *via* amide linkages.

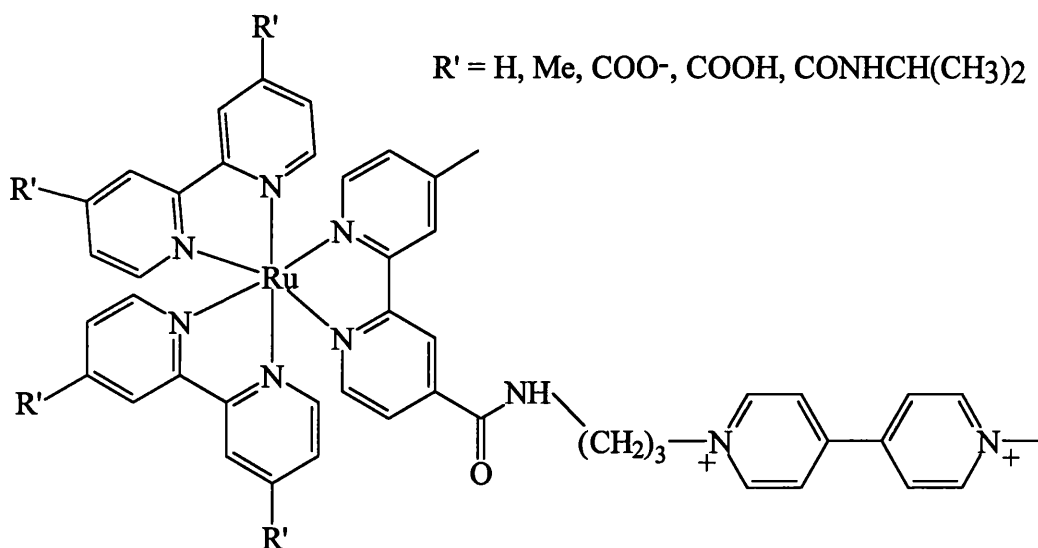


Figure 5.3: Mixed ligand ruthenium tris-bipyridyl complexes.

By varying the R' groups on the two of the bipyridyl ligands and by changing the spacer length between the $\text{Ru}(\text{bipy}')_3$ unit and the electron accepting viologen unit, it was found that rates of photoinduced electron transfer could be tuned. The variations were attributed to the variable π^* orbital energies on the $(\text{R}')_2$ -

2,2'-bipyridyl ligands and to the changes in thermodynamic driving force caused by changing the donor - acceptor separation.

A related structure in which viologen acceptor units bearing pyrrole subunits were joined to a $\text{Ru}(\text{bipy})_3^{2+}$ centre by ester linkages has been employed by Deronzier and Essakalli¹⁶ to assemble a pyrrole polymer on an electrode surface. The result of such an electropolymerisation was to produce a thin film which could act as a photoelectrode when irradiated by visible light. Matsuo and co-workers¹⁷ have constructed a modified gold electrode in which a sulfur containing $\text{Ru}(\text{bipy})_3^{2+}$ derivative was adsorbed onto the surface simultaneously with a sulfur containing viologen derivative. Photoexcitation of the monolayer generated an appreciable current caused by an intermolecular electron transfer process from the photosensitiser to the electron acceptor. The addition of triethanolamine as a sacrificial electron donor for the oxidised $[\text{Ru}^{3+}]$ species 'completes the circuit' and allows facile electron flow (figure 5.4).

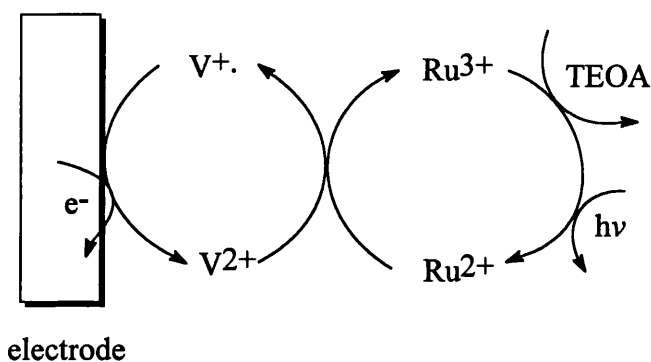


Figure 5.4: Mechanism of electron flow on a supramolecular donor-acceptor modified electrode surface.

The photosensitiser - relay - acceptor triad complexes synthesised by Dürr and Willner *et al*¹⁸ have been described previously in section 1.7.3. These systems employ sterically hindered viologen units as electron relays which are covalently bound secondary viologen units which act as electron acceptors. Related [2]catenane¹⁹ and supramolecular dialkoxybenzene-tethered systems²⁰ have been synthesised and employed by the same group to prove that photoinduced electron transfer may occur between ruthenium tris-bipyridyl photosensitisers and electron accepting units to which they are not covalently bound. Such assemblies are held together by EDA (electron donor acceptor) interactions between electron rich phenoxy donors and electron deficient viologen units, as has been discussed

previously. This methodology is particularly relevant in section 5.4, where the properties of $\text{Ru}(\text{bipy})_2(\text{L5})(\text{PF}_6)_6$ are discussed.

Thus, the intriguing photophysical properties of $\text{Ru}(\text{bipy})_3^{2+}$ have been thoroughly investigated and exploited by a great many workers. These studies have provided inspiration for the design, synthesis and investigation of the properties of the systems described below.

5.2 Properties of $\text{Ru}(\text{bipy})_2(\text{P1})(\text{PF}_6)_4$

The absorption spectrum of $\text{Ru}(\text{bipy})_2(\text{P1})^{4+}$ shows the expected bands corresponding to both MLCT and metal/ligand based transitions. The MLCT band is however, somewhat broader for the mixed ligand complex than for simple $\text{Ru}(\text{bipy})_3^{2+}$ as shown in figure 5.5. The broadening of the MLCT band may be attributed to the presence of two types of ligand²¹ in the complex which produce two MLCT transitions at slightly different energies.

The triplet MLCT state of the compound is formed within the 15ns laser pulse, and is observed to decay with a rate constant $k_{\text{obs}} = 3.81 \times 10^6 \text{ s}^{-1}$ at 298K in nitrogen outgassed dry acetonitrile solution. This gives a lifetime for the excited state of 262ns ($\tau = 1/k_{\text{obs}}$) as compared to a value of 1100ns measured for $\text{Ru}(\text{bipy})_3^{2+}$ under the same conditions. By comparing the rates of decay of the excited states of the two compounds it is possible to determine what effect the bipyridinium substituents have on the properties of the derivatised 2,2'-bipyridine ligand. This may be achieved by calculating a Hammett²² σ constant using the formula:

$$p\sigma = \log k_x - \log k_h$$

where p = a parameter which depends on the type of reaction under investigation, but which is often ~ 1 , k_x = the rate constant for decay of the excited state for a reactant bearing a substituent 'x' and k_h = the rate constant for decay of the excited state for a non-derivatised reactant. If the value for σ is negative then 'x' may be said to be an electron-releasing group and conversely if the constant is positive then the substituent is deemed electron-withdrawing. The value for the constant in this case is +0.76 thus the bipyridinium substituents in **P1** may be considered to be

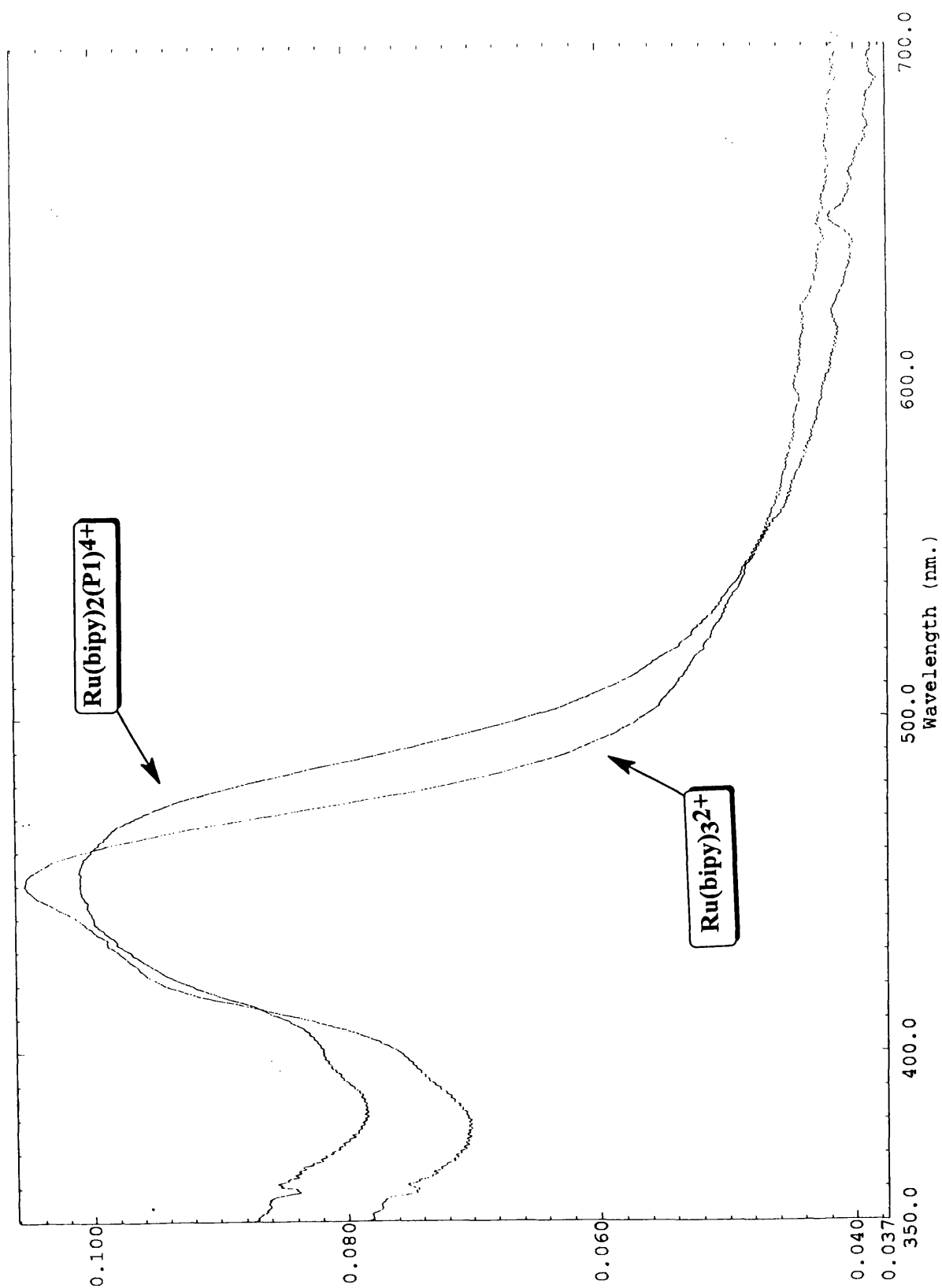


Figure 5.5: Absorption spectra of Ru(bipy)_3^{2+} and $\text{Ru(bipy)}_2(\text{P1})_4^+$ in dry acetonitrile.

electron withdrawing. This property leads to a lowering of the energy of the MLCT states (as the π^* orbital of **P1** will be of lower energy than those of non-derivatised 2,2'-bipyridine). Thus the broadening of the MLCT band in the absorption spectrum (especially to longer wavelengths) is explained. A further consequence of the lower energy of the MLCT states is that the fluorescence maximum for the compound should be red-shifted to longer wavelengths as compared to $\text{Ru}(\text{bipy})_3^{2+}$. This shift is indeed observed, with the maximum moving from 610nm for the simple compound to 630nm for $\text{Ru}(\text{bipy})_2(\text{P1})^{4+}$.

The methyl viologen dication, when in its mono-reduced $\text{MV}^{\cdot+}$ form absorbs³ light at between 610 and 625nm, giving a characteristic blue colouration. Transient absorption measurements in this wavelength range indicated no such absorption occurs after excitation of $\text{Ru}(\text{bipy})_2(\text{P1})^{4+}$. There are two possible explanations for this behaviour: either the bipyridinium cationic substituent cannot act as an efficient electron accepting unit, or electron transfer and subsequent charge recombination is so rapid that it cannot be observed on the nanosecond timescale. Electrochemical data for the compounds $\text{Ru}(\text{bipy})_2(\text{P1})^{4+}$ and $\text{Ru}(\text{bipy})_2(\text{L1})^{6+}$ indicate that the mono-cationic bipyridinium units are more difficult to reduce than their dicationic equivalents (-0.90V and -0.40V respectively vs SCE). Thus it may be surmised that electron transfer is less likely to occur from the photosensitiser to the bipyridinium unit in $\text{Ru}(\text{bipy})_2(\text{P1})^{4+}$. The fact that the compound fluoresces under steady state conditions at 298K (albeit with a much reduced quantum yield) whereas the fluorescence of $\text{Ru}(\text{bipy})_2(\text{L1})^{6+}$ is completely quenched, supports the conclusion that electron transfer to the bipyridinium units in $\text{Ru}(\text{bipy})_2(\text{P1})^{4+}$ is not significant.

The quantum yield (ϕ) of the fluorescence of $\text{Ru}(\text{bipy})_3^{2+}$ in acetonitrile at 298K is 0.062.² The equivalent quantum yield for $\text{Ru}(\text{bipy})_2(\text{P1})^{4+}$ may be calculated from the relationship between laser energy and fluorescence intensity for the two compounds. Within a certain range, fluorescence intensity shows a linear dependency on laser energy. The gradients of the straight-line plots for the compounds may be employed to calculate the unknown quantum yield by the means outlined below:

$$\phi = \text{no. photons emitted/no. photons absorbed} \propto L_o/I_o(1-10^A) \propto m$$

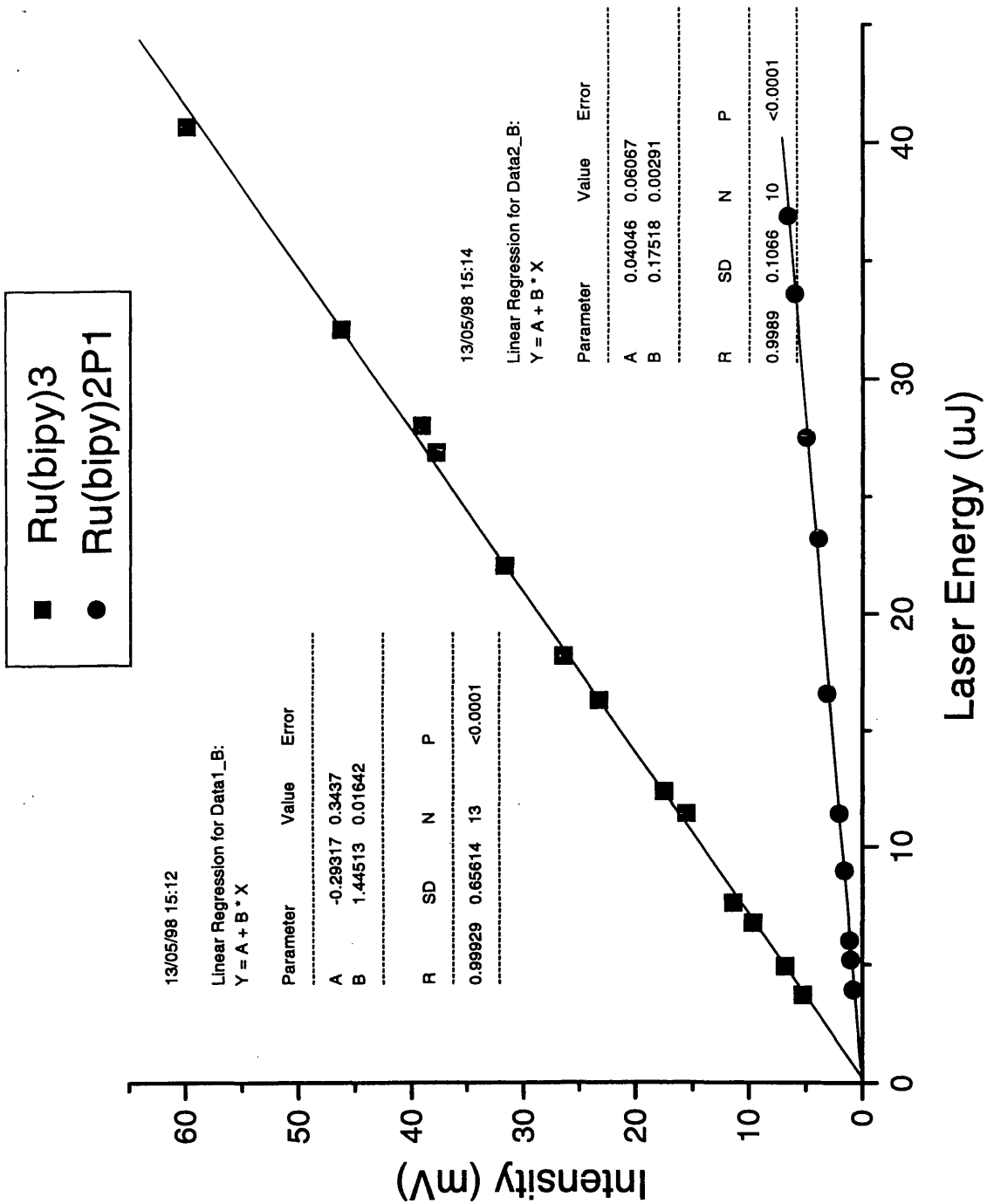


Figure 5.6: Laser energy - luminescence intensity plots for Ru(bipy)₃²⁺ and Ru(bipy)₂(P1)⁴⁺ in dry acetonitrile.

where L_o = laser energy, $I_o(1-10^A)$ = intensity of transmitted light and m = the gradient of the laser energy-intensity plot. The expression above leads to the simple series of ratios:

$$\phi_{RuP1}/\phi_{Std.} = L_o^{RuP1}/L_o^{Std.} = m_{RuP1}/m_{Std.}$$

hence the quantum yield for the fluorescence of $Ru(bipy)_2(P1)^{4+}$ may be easily calculated. The laser energy-intensity plots for the standard compound and for the unknown are presented in figure 5.6 - by comparison of the respective gradients the quantum yield for $Ru(bipy)_2(P1)^{4+}$ was calculated to be equal to 0.0075. This value does not, however, represent an accurate value for the quantum yield because the fluorescence maxima of the compound and the standard are not coincident. The intensity measurements were made at 610nm, thus the values recorded for $Ru(bipy)_2(P1)^{4+}$ do not represent maximum value of the fluorescence intensity. However, by comparing the intensities at 610nm and 630nm (where the maximum occurs) and scaling the value for the quantum yield appropriately, the true value of the quantum yield was obtained and found to be 0.0092. Thus, $Ru(bipy)_2(P1)^{4+}$ fluoresces with an intensity approximately one seventh that of $Ru(bipy)_3^{2+}$.

The behaviour of the observed rate constant for the decay of the excited state of $Ru(bipy)_3^{2+}$ under variable temperatures is not simple. The Arrhenius plot ($\ln k_{obs}$ against the reciprocal of the temperature) for $Ru(bipy)_3^{2+}$ is curved^{2,11} rather than linear as might have been expected. This result is explained by a three state model of the excited state of the compound (figure 5.7) where the observed rate of decay of the emitting state is a combination of temperature independent radiative and non-radiative rate constants (k_r and k_{nr}) and a second non-radiative rate constant (k_o'), which shows a temperature dependence:

$$k_{obs} = k_r + k_{nr} + k_o' \exp(-E_a/k_b T)$$

where k_b is the Boltzmann constant and E_a is the activation energy for the non-radiative process. The energy barrier for the activated process has been calculated² to be $42.57 \text{ kJ mol}^{-1}$ (3560 cm^{-1}).

In contrast to the behaviour observed for $Ru(bipy)_3^{2+}$, the derivatised compound shows a linear relationship between $\ln k_{obs}$ and the reciprocal of temperature (figure 5.8).

Arrhenius Plot for Decay of Fluorescence of Ru(bipy)2(P1).

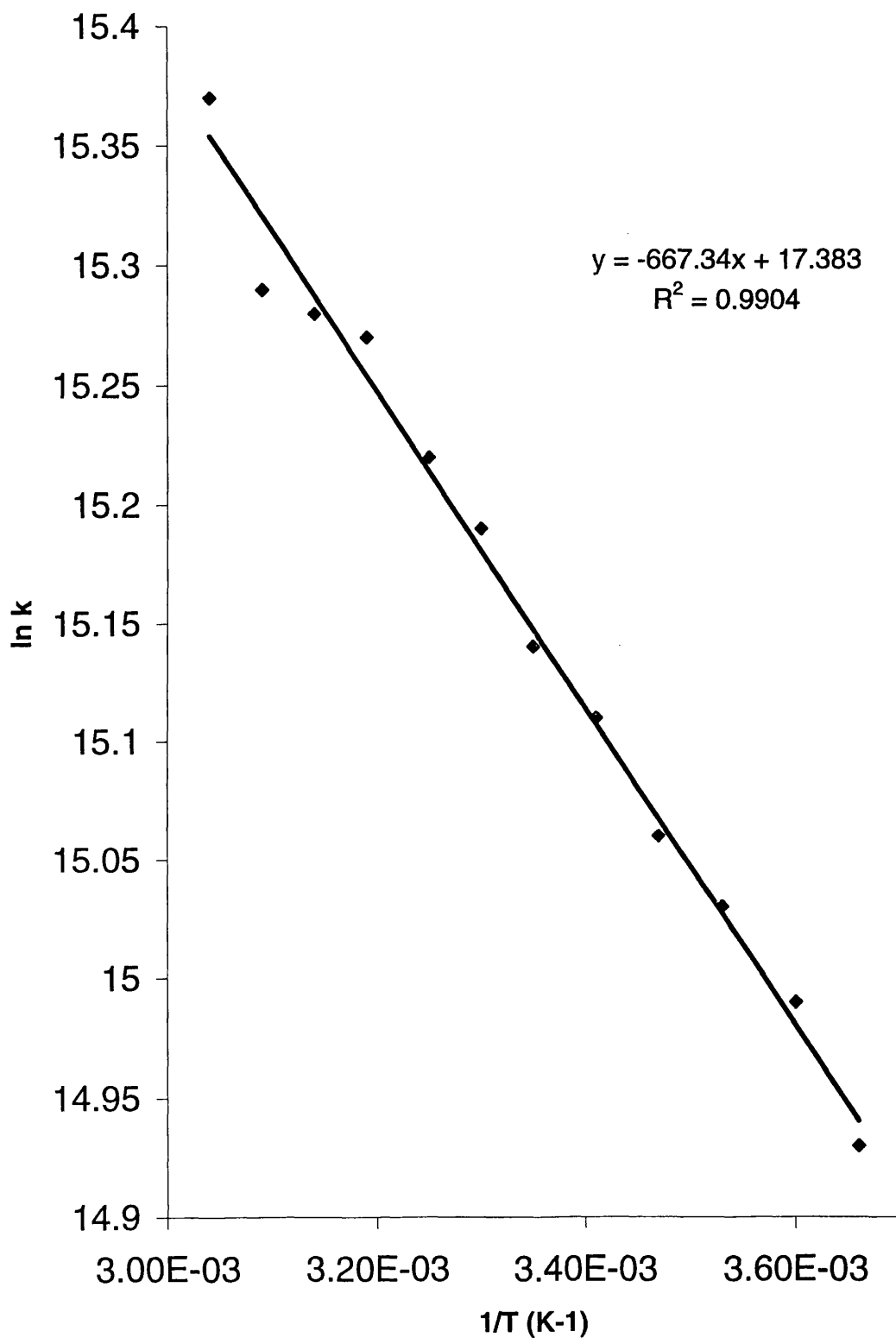


Figure 5.8: Arrhenius plot for decay of fluorescence of Ru(bipy)2(P1)⁴⁺ in dry acetonitrile.

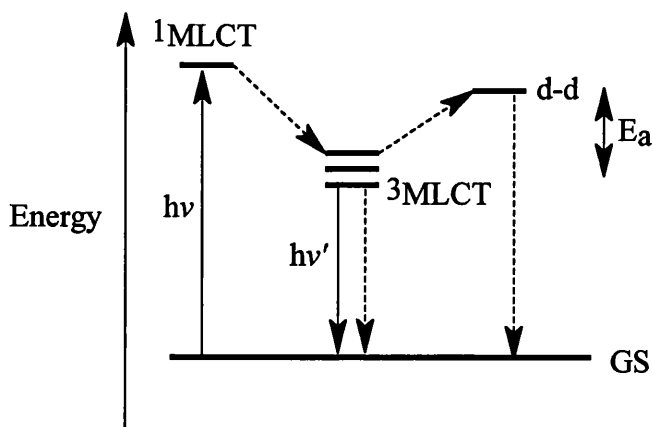


Figure 5.7: Energy level diagram showing the three state model of the excited state of $\text{Ru}(\text{bipy})_3^{2+}$.

The value for the activation energy obtained from the Arrhenius plot is 5.55kJmol^{-1} , with the pre-exponential factor being equal to 3.54×10^7 . Clearly the compound is not behaving in a similar manner to that observed for simple $\text{Ru}(\text{bipy})_3^{2+}$. If, as stated previously, the effect of derivatising a 2,2'-bipyridine unit with two electron withdrawing bipyridinium units is to lower the energy of the π^* orbitals of the ligand, then the energy of the $^3\text{MLCT}$ state would also be expected to be of lower energy than in $\text{Ru}(\text{bipy})_3^{2+}$. Further, the excited electron would be expected to be preferentially localised on the lower lying orbitals of the **P1** moiety. Such a model explains the absorption and steady state fluorescence spectra but not the observed linear Arrhenius plot obtained for the rate of decay of the excited state of the compound. If the triplet MLCT state was lower in energy for $\text{Ru}(\text{bipy})_2(\text{P1})^{4+}$ than for $\text{Ru}(\text{bipy})_3^{2+}$ and if the energy of the metal based d-d state is unperturbed by the mixed ligand set then it would be expected that the activation energy for the temperature dependent non-radiative rate constant would be increased in the derivatised compound. This conjecture is not borne out by the data, where an activation barrier of a mere 5.5kJmol^{-1} was calculated.

It is clear from consideration of the time-resolved data that the excited state of $\text{Ru}(\text{bipy})_2(\text{P1})^{4+}$ does not behave in manner which fits with a conventional three state model. The excited state of the complex decays more rapidly than does simple $\text{Ru}(\text{bipy})_3^{2+}$ ($k_{\text{obs}} = 3.81 \times 10^6$ and 9.1×10^5 respectively) hence it is apparent that efficient non-radiative relaxation routes are available. It may be speculated that the

'arms' of the **P1** unit act as a 'rotor' which, through vibronic interactions with the solvent, provides a facile quenching pathway which may explain the observed data.

Both compounds, $\text{Ru}(\text{bipy})_2(\text{P1})^{4+}$ and $\text{Ru}(\text{bipy})_3^{2+}$ react with molecular oxygen. The observed rate constant for decay of an excited state under nitrogen is the sum of the radiative and non-radiative rate constants:

$$k_{\text{obs}} = k_r + k_{\text{nr}}$$

In oxygenated solution, however, an additional quenching process occurs, so that the observed rate constant may be described as:

$$k_{\text{obs}} = k_r + k_{\text{nr}} + k_q[\text{Q}]$$

where Q is molecular oxygen in this case. By comparing the observed rate constants in oxygenated and oxygen-free solutions it is possible to calculate the bimolecular rate constant for reaction of a complex with oxygen (assuming $[\text{O}_2] = 9.1 \text{ mmol}$ in acetonitrile). The values obtained for the bimolecular rate constants for reaction of $\text{Ru}(\text{bipy})_2(\text{P1})^{4+}$ and $\text{Ru}(\text{bipy})_3^{2+}$ with oxygen are thus $9.83 \times 10^8 \text{ M}^{-1}\text{s}^{-1}$ and $2.76 \times 10^9 \text{ M}^{-1}\text{s}^{-1}$ respectively. It is apparent from these constants that the simple non-derivatised complex reacts more rapidly with oxygen than does the substituted complex. This result is not unexpected, as $\text{Ru}(\text{bipy})_2(\text{P1})^{4+}$ is less electron rich than the non-derivatised complex - thus it will react less rapidly with electrophilic triplet oxygen.

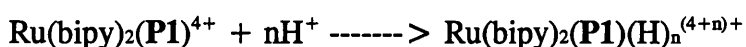
Whilst $\text{Ru}(\text{bipy})_2(\text{P1})^{4+}$ was constructed in order to expedite the synthesis²³ of $\text{Ru}(\text{bipy})_2(\text{L1})^{6+}$ and its catenane equivalent $\text{Ru}(\text{bipy})_2(\text{L5})^{6+}$, investigation of the photophysical properties of the compound has revealed an interesting deviation from the classical excited state behaviour of $\text{Ru}(\text{bipy})_3^{2+}$. In addition to these properties, it was found that upon addition of trifluoroacetic acid (TFAA) to a solution of $\text{Ru}(\text{bipy})_2(\text{P1})^{4+}$ the fluorescence of the complex may be completely quenched. This property allows the possibility that the complex may act as a pH sensor, such as that described in section 5.1 above, where fluorescence intensity is diminished at lower pH values. Initial experiments were carried out using steady state conditions in aerated conditions. Addition of TFAA to the complex under these conditions led to the expected quenching which was found to obey Stern-Volmer conditions¹:

$$I_0/I = 1 + k_{\text{DTR}}[\text{Q}]$$

where I_0 = fluorescence intensity at zero quencher concentration, I = fluorescence intensity at all other quencher concentrations, k_{D} = Stern-Volmer constant, $\tau_{\text{R}} =$

lifetime of the emitting state and $[Q]$ = quencher (acid) concentration. Whilst the value obtained for k_D is not reliable because of the conditions in which the measurements were made, the initial experiments indicated that dynamic quenching was the dominant process in the pH range investigated.

Time-resolved experiments, using dry, nitrogen outgassed acetonitrile solutions of TFAA and $\text{Ru}(\text{bipy})_2(\text{P1})^{4+}$ were conducted in order to accurately determine the values for the bimolecular rate constant of quenching, the equilibrium constant for the reaction:



and to attempt to determine whether one or two protons were required to quench the fluorescence of the 'di-topic' ruthenium tris-bipyridyl based receptor.

Five solutions were studied, each with the same concentration of $\text{Ru}(\text{bipy})_2(\text{P1})^{4+}$ but with different concentrations of TFAA: the concentrations of these solutions are detailed in table 5.2.1.

Solution	Abs. (532nm)	$[\text{H}^+]$ (M)	k_{obs} (s^{-1})	k_q ($\text{M}^{-1}\text{s}^{-1}$)
1	0.078	0	3.81×10^6	0
2	0.075	0.001	6.05×10^6	2.24×10^9
3	0.077	0.002	8.38×10^6	2.28×10^9
4	0.076	0.004	1.37×10^7	2.47×10^9
5	0.076	0.005	1.45×10^7	2.14×10^9

Table 5.2.1: Selected photophysical data for the interaction between TFAA and $\text{Ru}(\text{bipy})_2(\text{P1})^{4+}$.

The rate constants measured for each of these solutions were found to increase with the concentration of acid (and so quencher concentration). By comparing the observed rate constants for the acidified solutions to that of the neutral solution a value for the bimolecular rate constant of the quenching reaction may be obtained. From table 5.2.1 the average value for k_q is found to be $2.28 \times 10^9 \text{ M}^{-1}\text{s}^{-1}$.

When the fluorescence intensity is measured against varying laser energy, a linear plot is obtained (such as those in figure 5.6). By performing such

measurements for each of the five solutions and determining the gradient of each line (figure 5.9) it is possible to calculate the equilibrium concentration of $\text{Ru}(\text{bipy})_2(\text{P1})^{4+}$ (A) as it is the only fluorophore in solution. Given that the initial concentrations of the receptor in the solutions are known, it is then possible to calculate the concentration of the $\text{Ru}(\text{bipy})_2(\text{P1})(\text{H})_n^{(4+n)+}$ complex (B). As $[\text{H}^+]$ is significantly larger than $[\text{Ru}(\text{bipy})_2(\text{P1})^{4+}]$, the equilibrium and initial concentrations of free acid are approximately the same. The concentrations of the species in solution for the five solutions are detailed in table 5.2.2.

Solution	Gradient	Ratio	$[\text{H}^+]_{\text{eq}}$ (M)	$[\text{A}]_{\text{eq}}$ (M)	$[\text{B}]_{\text{eq}}$ (M)
1	0.20147	N/A	0	8.28×10^{-5}	0
2	0.18294	0.908	0.001	7.51×10^{-5}	7.7×10^{-6}
3	0.13461	0.668	0.002	5.53×10^{-5}	2.75×10^{-5}
4	0.11359	0.564	0.004	4.97×10^{-5}	3.61×10^{-5}
5	0.10199	0.506	0.005	4.19×10^{-5}	4.09×10^{-5}

Table 5.2.2: Summary of concentrations of the species present in solutions 1 - 5.

The data presented in table 5.2.2 may be manipulated so that the equilibrium constant for the process:



may be calculated. The means by which this may be achieved is outlined below:

$$K = \frac{[\text{B}]_{\text{eq}}}{[\text{A}]_{\text{eq}}[\text{H}^+]^n}$$

$$\text{so } [\text{H}^+]^n = \frac{[\text{B}]_{\text{eq}}}{[\text{A}]_{\text{eq}}}K$$

$$\text{thus } n \log [\text{H}^+] = \log \left(\frac{[\text{B}]_{\text{eq}}}{[\text{A}]_{\text{eq}}} \right) + \log K$$

hence, by plotting $\log [\text{H}^+]$ vs $\log \left(\frac{[\text{B}]_{\text{eq}}}{[\text{A}]_{\text{eq}}} \right)$ a straight line is obtained (figure 5.10) which has a gradient equal to 'n' the number of moles of acid per mole of $\text{Ru}(\text{bipy})_2(\text{P1})^{4+}$ and a y-intercept equal to $\log K$. By employing this procedure the equilibrium constant was determined to be 1308M^{-1} and the value of 'n' was found to be 1.33.

Thus, it has been demonstrated that $\text{Ru}(\text{bipy})_2(\text{P1})^{4+}$ binds protons with a binding constant which is large enough to make the compound useful as a pH sensor

Plot of Laser Energy vs. Intensity at 650nm for Solutions 1 to 5

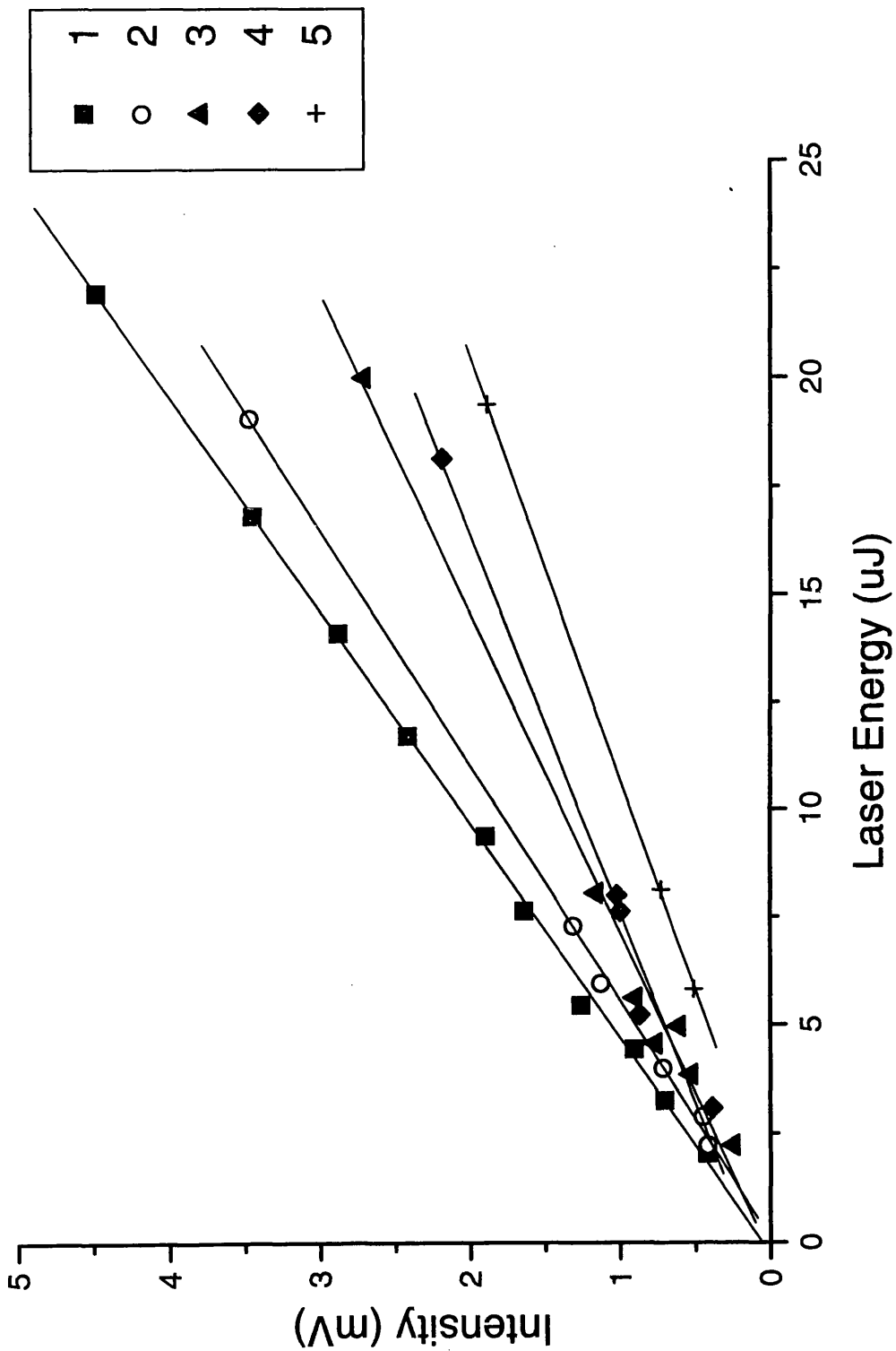


Figure 5.9: Laser energy - luminescence intensity plots for solutions 1 to 5 in dry acetonitrile.

Plot of Log [H+] vs. Log ([B]/[A])

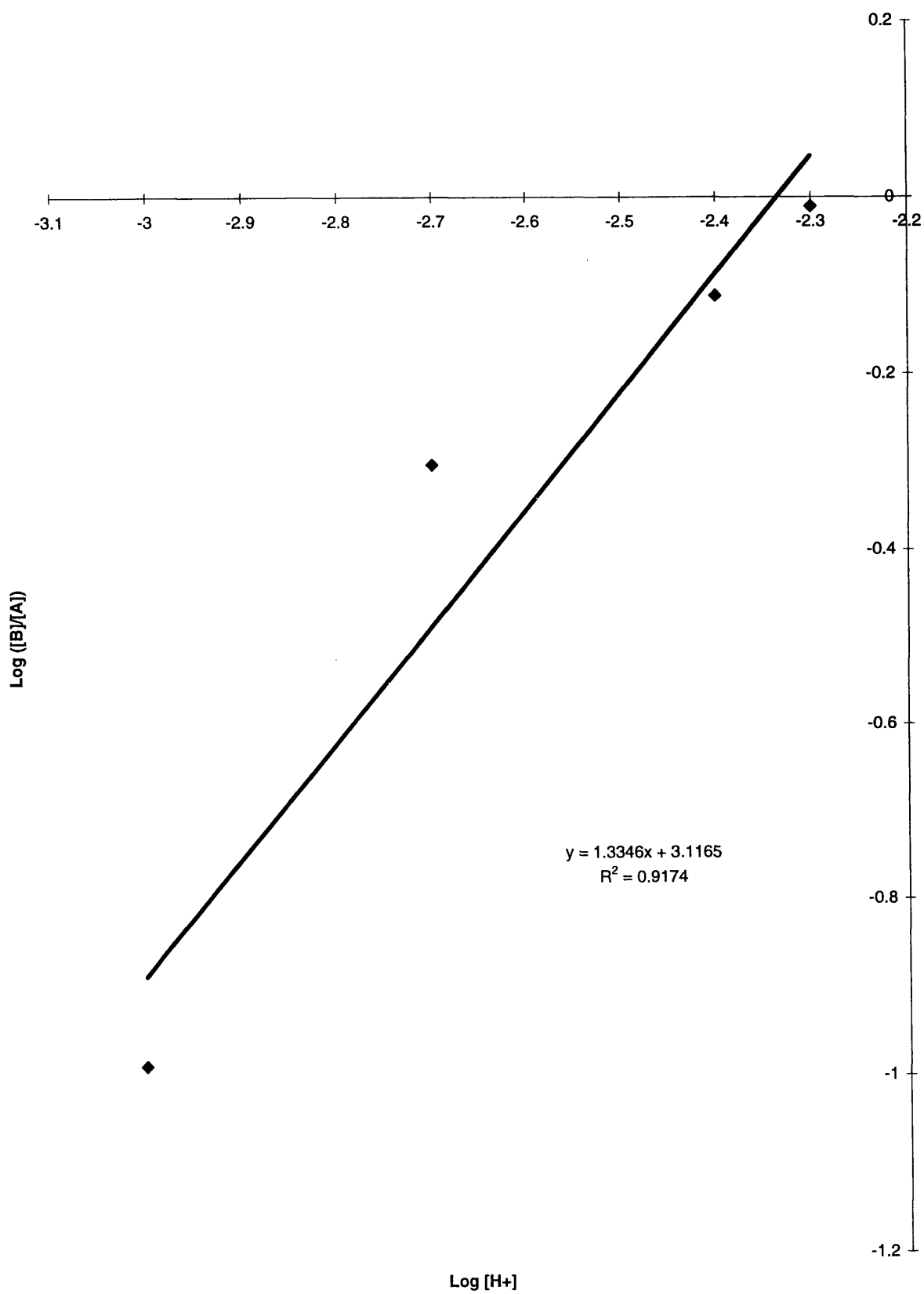


Figure 5.10: Plot of $\log [H^+]$ vs $\log [B]_{eq}/[A]_{eq}$.

but not so large to result in irreversible binding. The fact that an average of 1.33 protons is bound to each quenched receptor is unfortunate (a 1:1 ratio was hoped for) as this would undoubtedly distort pH measurements given that it has been reported that only one electron accepting unit is required to efficiently quench the fluorescence of Ru(bipy)₃²⁺ derivatives.

5.3 Properties⁴ of Ru(bipy)₂(L1)(PF₆)₆

The means by which Ru(bipy)₂(L1)⁶⁺ may be synthesised²³ were outlined in chapter 3. The compound was produced either by addition of a ruthenium bis-bipyridyl moiety to the 'free' cyclophane, or by employing a 'pre-coordination' route where the desired compound was obtained by cyclising Ru(bipy)₂(P1)⁴⁺ with α,α' -dibromo-*p*-xylene. The compound was characterised by mass spectrometry and by one and two dimensional NMR spectroscopy. The electrochemical properties of the compound were also discussed previously, with the viologen reduction waves occurring at potentials of -0.40 and -0.86V and the Ru^{II}/ Ru^{III} couple being measured at a potential of 1.23V (*vs* SCE).

The absorption spectrum of Ru(bipy)₂(L1)(PF₆)₆ in dry, degassed acetonitrile is similar to that of Ru(bipy)₂(P1)⁴⁺, with bands corresponding to MLCT, metal and ligand centred transitions²¹ being observed. Selected data for the main bands in the absorption spectrum together with their assignments are listed in table 5.3.1.

Wavelength (nm)	Absorption	Molar Extinction Coefficient (M ⁻¹ cm ⁻¹)	Assignment
253	1.937	69,200	MLCT
286	2.530	90,350	LC
432	0.458	16,350	MLCT
467	0.468	16,700	MLCT

Table 5.3.1: Selected absorption data for Ru(bipy)₂(L1)(PF₆)₆.

At room temperature and under steady-state conditions, Ru(bipy)₂(L1)(PF₆)₆ is not fluorescent⁴ due to efficient quenching of the emitting state by the electron accepting viologen units which are covalently bonded to the photoactive metal

centre. However, at 77K (in a butyronitrile glass) a weak luminescence characteristic of a Ru(bipy)₃²⁺ derivative was observed upon excitation at 565nm.

Transient absorption spectra for the compound were recorded at 293K. These studies indicated that the triplet MLCT state of the complex, which is formed within the laser pulse, has a lifetime of 12±2ps, as compared to standard Ru(bipy)₃²⁺ which has a lifetime of approximately 1μs. After decay of the triplet excited state, the transient absorption spectra suggest the presence of both [Ru^{III}] and mono-reduced viologen species, indicating that an electron transfer process may have occurred. The decay of these redox intermediates occurred by first-order kinetics, with a lifetime of 35±3ps. The overall process involving electron transfer and subsequent charge recombination is very rapid due to the proximity of the reacting species.

The fluorescence observed for the compound at 77K allowed the determination of the energy of the triplet emitting state at approximately 1.90eV. From the measured rate constant for the forward reaction, the thermodynamic driving force for the light-induced reduction of the viologen units in acetonitrile was estimated as $\Delta G^\circ = -34.7\text{kJmol}^{-1}$ (-0.36eV). This indicates that the charge separation process is likely to fall within the 'normal' Marcus region (see section 1.7.2). The back reaction (charge recombination) is thermodynamically more favourable, with an estimated free energy of $\Delta G^\circ = -154.4\text{kJmol}^{-1}$ (-1.60eV). Thus, the back reaction is expected to fall within the 'inverted' Marcus region. Measurement of the rates of forward and back electron transfer between 243 and 338K confirmed the above expectations, with the activation energies for the two processes (as determined from Arrhenius plots) being 6.7kJmol⁻¹ (0.070±0.002eV) for charge separation and 0.96kJmol⁻¹ (0.010±0.001eV) for charge recombination respectively.

The total reorganisation energy, λ , for the forward reaction was calculated to be about 82.0kJmol⁻¹ (0.85eV) based on the equation below:

$$E_a = (\lambda + \Delta G^\circ)^2 / 4\lambda$$

It was found that the rate constant for the forward electron transfer, in contrast to that of the charge recombination, is dependant upon the polarity of the surrounding solvent, as expressed in terms of the static dielectric constant ϵ_s (figure 5.11).

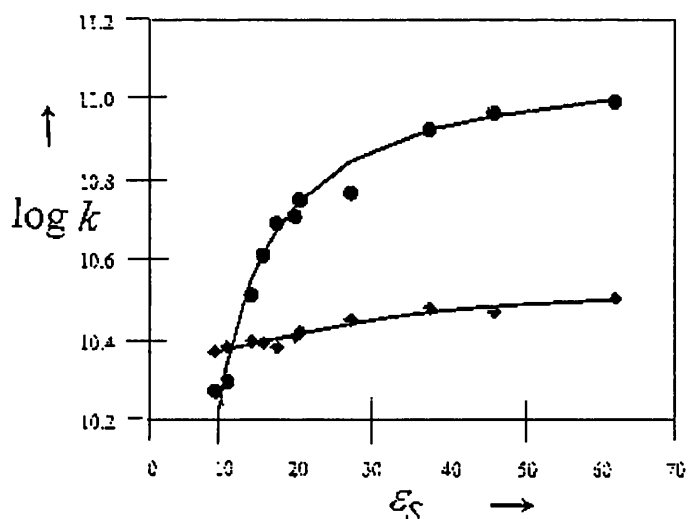


Figure 5.11: Effect of dielectric constant on the rate constants for forward electron transfer (●) and subsequent charge recombination (◆).

The solvents employed (and their static dielectric constants) were: propylene carbonate (62), dimethyl sulphoxide (46), acetonitrile (37.5), propionitrile (27.2), isobutyronitrile (20.4), butyronitrile (20.3), valeronitrile (19.7), hexanenitrile (17.3), 4-methylvaleronitrile (15.5), octanenitrile (13.9), 1,2-dichloroethane (10.6) and dichloromethane (8.9).

In highly polar solvents such as propylene carbonate and dimethyl sulphoxide, k_{cs} has an optimum value of about 10^{11} s^{-1} . This value decreases progressively as the polarity of the solvent is reduced. The reduced rate of electron transfer may be attributed to a smaller driving force in less polar solvents due to weaker solvation of the reactants and products. This effect may be understood in simple terms by considering the stabilisation of the radical ion pair (RIP) produced by the electron transfer process. A more polar solvent is better able to stabilise the charge transferred state by dissipating charge over a larger volume through dipole interactions over both the inner and outer solvent spheres.

The results obtained from the photophysical studies performed on $\text{Ru}(\text{bipy})_2(\text{L1})(\text{PF}_6)_6$ clearly indicate that charge separation is dependant upon driving force i.e. that electron transfer is under activation control ($-\Delta G^\circ = 0.4\lambda$). The effect of solvent polarity on the rate of electron transfer is thus an important consideration.

5.4 Properties⁴ of Ru(bipy)₂(L5)(PF₆)₆

The X-ray structure determinations of the reaction centre (RC) proteins of the purple photosynthetic bacteria *Rhodospseudomonas viridis* and *Rhodobacter sphaeroides* have allowed visualisation of the detailed placement²⁴ of the chromophores within these proteins. The chromophores are arranged within these proteins along a C₂ symmetry element. Two of the bacteriochlorophyll (BChl) molecules are closely associated spatially and electronically to form the dimeric primary donor known as the special pair (SP). Two more monomeric BChl molecules are placed in edge-to-edge positions relative to the SP. Each of these molecules are, in turn, adjacent to monomeric bacteriopheophytin (BPh) molecules which in turn are each next to a quinone moiety.

Photonic excitation of the SP causes an electron to migrate along the chain of electron acceptors until it rests finally on the quinone residue. The donor-acceptor separations and relative orientations within the RC play an important role in controlling the individual electron transfer steps.²⁵ An intriguing aspect of this electron transfer is the redox asymmetry between the two sets of co-factors, which is manifested in the unidirectional nature of the electron transfer process (as discussed in section 1.7.1).

Compound Ru(bipy)₂(L5)(PF₆)₆ was designed as a model compound for such natural systems, in that it contains two chemically identical electron acceptors which are bound to a photo-activated electron donating ruthenium centre. The electron acceptors have different reduction potentials because of encapsulation of one unit by an electron donating aromatic crown ether. The encapsulated viologen unit enters into an electron donor-acceptor (EDA) interaction with the crown, thus lowering its ability to accept electron density. This encapsulation further affects the electron accepting ability of the viologen unit by excluding access to it by polar solvent molecules.

The synthesis and characterisation by NMR spectroscopy and electrospray mass spectrometry of the compound were discussed in chapters 2 and 4. The electrochemical properties of the compound were investigated in dry, degassed acetonitrile. The metal centre undergoes a quasi-reversible one-electron oxidation with a half-wave potential $E^{\circ} = 1.29 \pm 0.02\text{V}$ (vs SCE). At higher potentials,

oxidation peaks can be resolved for the external and internal phenoxy units of the crown ether at $E^\circ = 1.44 \pm 0.02\text{V}$ and $E^\circ = 1.73 \pm 0.04\text{V}$ respectively. The viologen units undergo one electron reductions at $E^\circ = -0.32 \pm 0.01\text{V}$ and $E^\circ = -0.45 \pm 0.01\text{V}$ (reflecting their redox asymmetry) and a further two electron reduction at $E^\circ = -0.85 \pm 0.03\text{V}$. Thus it may be observed that there is a significant (130mV) redox asymmetry between the two electron accepting units in $\text{Ru}(\text{bipy})_2(\text{L5})(\text{PF}_6)_6$.

The redox asymmetry present in this compound leads to the expectation that light-induced electron transfer should occur selectively from the metal centre to the external viologen due to the more favourable thermodynamic driving force.

Upon excitation of the compound at 565nm, the triplet MLCT excited state of the complex was formed immediately. The excited state decayed by first order kinetics (with a lifetime of $17 \pm 2\text{ps}$) by way of an electron transfer to the electron accepting unit(s). The charge separation reaction ($k_{\text{CS}} = 5.9 \times 10^{10} \text{ s}^{-1}$) was followed by subsequent charge recombination ($k_{\text{CR}} = 2.4 \times 10^{10} \text{ s}^{-1}$) to restore the ground state. The $[\text{Ru}^{\text{III}}]$ and mono-reduced viologen intermediates persist for approximately $42 \pm 4\text{ps}$ as shown by the decay profiles presented in figure 5.12.

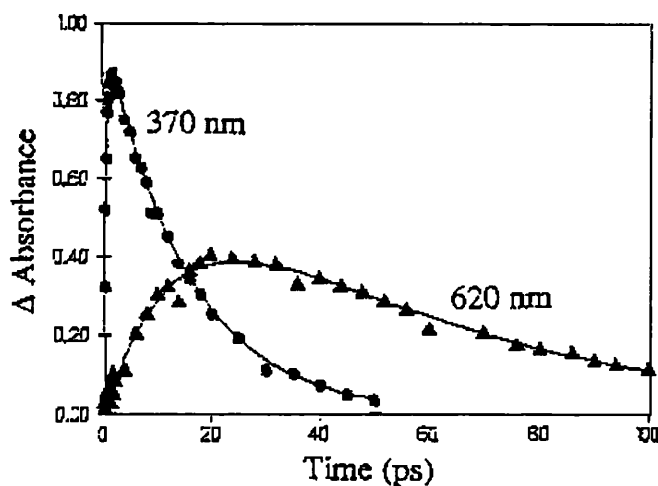


Figure 5.12: Decay profiles showing formation and decay of the excited state of the 370nm and of the mono-reduced viologen at 620nm.

The rate of the forward and back reactions were measured as a function of temperature and the activation energies of the two processes calculated from their respective Arrhenius plots. The activation energy for the charge separation process was found to be 5.98kJmol^{-1} ($0.062 \pm 0.002\text{eV}$), whereas charge recombination was found to be almost activationless. The forward electron transfer lies in the ‘normal’

Marcus region ($-\Delta G^\circ = 0.4\lambda$) in which the rate increases with driving force. In contrast, charge recombination occurs in the 'inverted' Marcus region ($\Delta G^\circ = 154.4\text{kJmol}^{-1}$ (1.6eV)), and with E_a equal to zero, the total reorganisation energy is estimated to be approximately 72.4kJmol^{-1} (0.75eV) (by application of the equation $E_a = (\lambda + \Delta G^\circ)^2/4\lambda$).

The rate of electron transfer to the external viologen ($\Delta G^\circ = -30.9\text{kJmol}^{-1}$ (-0.32eV)) should exceed that to the encapsulated electron acceptor ($\Delta G^\circ = -18.3\text{kJmol}^{-1}$ (-0.19eV)) by a factor of five provided that the reorganisation energy and the donor-acceptor coupling matrix element are identical for both viologen units. Thus 85% of the total electron transfer is estimated to occur between the excited donor unit and the external viologen residue. As such the model compound may be regarded as performing unidirectional electron transfer in a similar manner to that which occurs in the naturally occurring photosynthetic RC.

It is difficult, however, to distinguish between the two viologen units spectroscopically - thus it is not currently possible to prove that the proposed vectorial electron transfer has occurred. A possible solution to this problem may be to employ transient resonance Raman techniques, whereby it may be possible to distinguish between the viologen units and to determine the extents to which each has been reduced by the photoinduced electron transfer process.

5.5 References

- [1] Kavarnos, G.J. *Fundamentals of Photoinduced Electron Transfer*, VCH, New York, 1993.
- [2] (a) Krause, R.A. *Structure and Bonding*, 1987, **67**, 1. (b) Cook, M.J.; Lewis, A.P.; MaAuliffe, G.S.G.; Skarda, V.; Thomson, A.J.; Glasper, J.C.; Robbins, D.J. *J. Chem. Soc. Perkin Trans. II*, 1984, 1293. (c) Cook, M.J.; Lewis, A.P.; MaAuliffe, G.S.G.; Skarda, V.; Thomson, A.J.; Glasper, J.C.; Robbins, D.J. *J. Chem. Soc. Perkin Trans. II*, 1984, 1303. (d) Cook, M.J.; Lewis, A.P.; MaAuliffe, G.S.G.; Skarda, V.; Thomson, A.J.; Glasper, J.C.; Robbins, D.J. *J. Chem. Soc. Perkin Trans. II*, 1984, 1309.
- [3] A related example may be found at: Chen, P.; Danielson, E.; Meyer, T.J. *J. Phys. Chem.*, 1988, **92**, 3708.
- [4] Benniston, A.C.; Mackie, P.R.; Harriman, A. *Angew. Chem. Int. Ed. Engl.*, 1998, **37**, 354.
- [5] Marcus, R.A. *Ann. Rev. Phys. Chem.*, 1964, **15**, 155.
- [6] (a) Niwa, T.; Kikuchi, K.; Matsusita, N.; Hayashi, M.; Katagiri, T.; Takahishi, Y.; Miyashi, T. *J. Phys. Chem.*, 1993, **97**, 11960. (b) Blackbourn, R.L.; Hupp, J.T. *J. Phys. Chem.*, 1988, **92**, 2817.
- [7] Thompson, R.A.; Simon, J.D. *J. Am. Chem. Soc.*, 1993, **115**, 5657.
- [8] Gleiter, R. *Angew. Chem. Int. Ed. Engl.*, 1974, **13**, 696.
- [9] Balzani, V.; Barigelleti, F.; Belser, P.; Campagna, S.; Juras, A.; von Zelewsky, A. *Coord. Chem. Rev.*, 1988, **84**, 85.
- [10] Chen, P.; Meyer, T.J. *Chem. Rev.*, 1998, **98**, 1439.
- [11] Fernando, S.R.L.; Ogawa, M.Y. *J. Chem. Soc. Chem. Commun.*, 1996, 637.
- [12] for an example of an energy transfer process see: Creutz, C.; Chou, M.; Netzal, T.L.; Okumura, M.; Sutin, N. *J. Am. Chem. Soc.*, 1980, **102**, 1304.
- [13] Grigg, R.; Amilaprasadh Norbert, W.D.J. *J. Chem. Soc. Chem. Commun.*, 1992, 1300.
- [14] Clark, C.D.; Debad, J.D.; Yonemoto, E.H.; Mallouk, T.E.; Bard, A.J. *J. Am. Chem. Soc.*, 1997, **119**, 10525.
- [15] Kelly, L.A.; Rodgers, M.A.J. *J. Phys. Chem.*, 1995, **99**, 13132.

- [16] Deronzier, A.; Essakalli, M. *J. Chem. Soc. Chem. Commun.*, 1990, 242.
- [17] Yamada, S.; Kohrogi, H.; Matsuo, T. *Chem. Lett.*, 1995, 639.
- [18] (a) Seiler, M.; Dürr, H. *Synthesis*, 1994, 83. (b) Zahavy, E.; Seiler, M.; Marx-Tibbon, S.; Joselevich, E.; Willner, I.; Dürr, H.; O'Conner, D.; Harriman, A. *Angew. Chem. Int. Ed. Engl.*, 1995, **34**, 1005.
- [19] Hu, Y.Z.; van Loyen, D.; Schwarz, O.; Bossmann, S.; Dürr, H.; Huch, V.; Veith, M. *J. Am. Chem. Soc.*, 1998, **120**, 5822.
- [20] (a) Seiler, M.; Dürr, H.; Willner, I.; Joselevich, E.; Doron, A.; Stoddart, J.F. *J. Am. Chem. Soc.*, 1994, **116**, 3399. (b) Kropf, M.; Joselevich, E.; Dürr, H.; Willner, I. *J. Am. Chem. Soc.*, 1996, **118**, 655. (c) David, E.; Born, R.; Kaganer, E.; Joselevich, E.; Dürr, H.; Willner, I. *J. Am. Chem. Soc.*, 1997, **119**, 7778.
- [21] Ashton, P.R.; Balzani, V.; Credi, A.; Kocian, O.; Pasini, D.; Prodi, L.; Spencer, N.; Stoddart, J.F.; Tolley, M.S.; Venturi, M.; White, A.J.P.; Williams, D.J. *Chem. Eur. J.*, 1998, **4**, 590.
- [22] Perrin, D.D.; Dempsey, B.; Serjeant, E.P. *pKa Prediction for Organic Acids and Bases*, 1981, Chapman and Hall, London.
- [23] Benniston, A.C.; Mackie, P.R.; Harriman, A. *Tetrahedron Lett.*, 1997, **38**, 3577.
- [24] Johnson, D.G.; Svec, W.A.; Wasielewski, M.R. *Isr. J. Chem.*, 1988, **28**, 193.
- [25] Benniston, A.C. *Chem. Soc. Rev.*, 1996, 427.

Chapter 6

Future Directions

6.1 Introduction

The themes presented in this chapter relate to research which was undertaken with the aim of developing various aspects of the work described previously in chapters 3 to 5. Whilst significant advancement towards the goals outlined in the following text has been achieved, and a number of interesting results obtained, there remains some work to be done to fully realise the potential of the developments detailed below.

The first development to be described involves the replacement of the bipyridinium electron accepting unit in the [2]catenane and cyclophane systems discussed previously with the less well characterised 2,7-diazapyrenium (DAP^{2+}) unit (figure 6.1). This electron acceptor is larger than its methyl viologen equivalent and is known to form stronger complexes with the aromatic crown ether **34C10** - most likely due to its superior complementarity with the crown.¹ In addition, DAP^{2+} is fluorescent and the emitting singlet state of the acceptor overlaps and interacts with the charge transfer state of its complex with **34C10**, thus stabilising the radical ion pair which is generated by photoexcitation. Thus DAP^{2+} is expected to have very interesting properties when incorporated into cyclophanes, [2]catenanes and [2]rotaxanes.

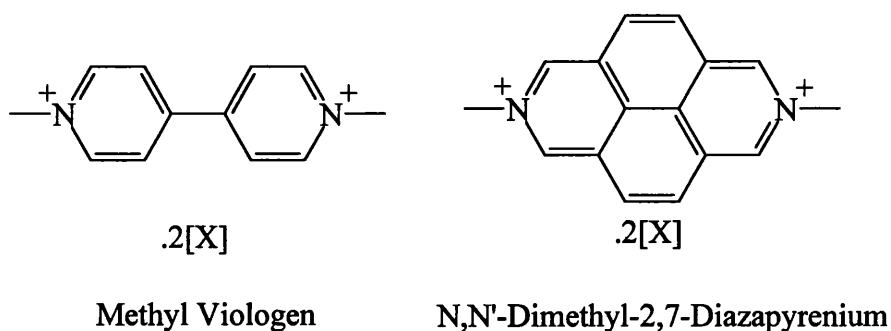


Figure 6.1: Methyl viologen and dimethyl 2,7-diazapyrenium.

The second development under investigation in this chapter involves supplanting the inefficient method for generation of cyclophanes and catenanes with a methodology which would be both simple and produce quantitative (or at least significantly improved) yields of cyclised products. The methodology employed to produce the ligands discussed previously in chapters 3 and 4 has involved supramolecular assembly by means of simple substitution reactions which are

directed by use of templates. In addition to being high yielding, an alternative strategy would be required to employ mild conditions so that template syntheses may still be employed. Cyclic systems containing amide functions constructed from acid chloride and amine compounds were described in section 1.6.6. Such systems generally assemble in excellent yields in reactions which employ very mild conditions - thus both requirements for the production of systems which are of interest in this project are met. It was decided, however, to attempt a related Schiff base type cyclisation reaction because this type of reaction also employs mild conditions and produces high yields.² The challenge which had to be met, however, was to incorporate electron accepting viologen and cation chelating 2,2'-bipyridine units into such a synthetic approach. The means by which this may be achieved is outlined in section 6.3.

6.2 Electron Donor-Acceptor Complexes

The self-assembly methodologies employed in the construction of the supramolecular systems discussed in this thesis rely upon complementarity interactions between π -electron rich aromatic units and π -electron deficient bipyridinium components. Non-covalent bonding interactions, such as electron donor acceptor (EDA) interactions, hydrogen bonding between polyether oxygen atoms and the 'acidic' protons on bipyridinium units and electrostatic interactions are largely responsible for the self-assembly of these systems.³

In order to obtain fundamental structural information regarding the nature of the interactions between such π -electron donors and acceptors, however, it is convenient to analyse simple 1:1 complexes between the two species, such as those presented in sections 6.2.1 and 6.2.2.

The nature of such complexes has been extensively investigated, particularly with regard to methyl viologen and its complexes. EDA complexes possess two important properties, namely facile electron transfer and reversibility.⁴ Reversibility requires that the free energy change involved in the interaction is low and that the activation energy is small or zero. Facile electron transfer is achieved where an acceptor-donor interaction involves either donors with low ionisation potentials,

acceptors with high electron affinities, or both. Charge-transfer becomes feasible once the molecules involved in the interaction have approached sufficiently closely to overcome their mutual repulsions, i.e. within van der Waals distances ($< 3\text{\AA}$). Such an approach is most easily allowed in interactions involving planar lamellar configurations,⁴ such as exists between paraquat dications and aromatic electron donors. Methyl viologen may undergo charge transfer (CT) interactions with a wide variety of chemical species⁵ including anions (halides, sulfides, tetraphenyl borate, benzilate, hexacyanoferrate and carboxylates), amines, phenols, hydroquinones and thiols. Such complexation often gives rise to a colouration which has been measured spectroscopically and attributed to charge transfer transitions.⁴ The absorption bands are broad and structureless and in most cases displaced to longer wavelength than the absorption bands of the constituent components of the complex. A study of the colourations reveals that absorption bands nearest the red end of the spectrum result from interactions of paraquat with molecules possessing low ionisation potentials i.e. good electron donors such as hydroquinone and its derivatives.

It has been shown that complexes between paraquat and neutral electron donors obey the approach derived by Mulliken for studying the energetics of weakly interacting EDA systems.⁴ The valence bond equation can be simplified to encompass a wide range of complex interactions in the following expression:

$$h\nu = I_D - E_A - C$$

where $h\nu$ is the energy involved in complex formation, I_D is the donor ionisation potential, E_A is the electron affinity of the acceptor and C is a term summing contributions from non-bonding interactions, polarisation and solvation.

In general EDA complexes have small free energies of formation so that the position of the equilibrium below should show reversibility with temperature, leading to an intensification of the CT band on cooling, assuming a negative enthalpy term for the forward reaction.



There are a multitude of examples of EDA complexes involving methyl viologen, both in solution and in the solid state. Both metal complexes^{6,7} such as $[\text{Cu}^{\text{I}}(\text{CN})_3]^{2-}$, $[\text{Zn}(\text{S}_2\text{C}_2\text{O}_2)_2]$ and $[\text{Fe}(\text{CN})_6]^{4-}$ and wholly organic aromatic donors⁸ such as indole, benzidine, *p*-cresol, *p*-methoxyphenol, pyrogallol, aniline, *p*-

toluidine, *N,N'*-dimethylaniline, *N,N'*-dimethyl-*p*-toluidine, hydroquinone, dimethoxybenzene, TMPD, etc. have been reported^{4,8} to form EDA complexes with methyl viologen.

The complex discussed in section 6.2.1 involves methyl viologen and the template molecule **T1**.⁹ This complex was investigated due to its important nature in the synthesis of cyclophanes **L1** and **L2** and also because of the extraordinary strength of its binding with these receptors. The second complex (section 6.2.2) also involves the template **T1** and the novel electron accepting unit *N,N'*-dimethyl-2,7-diazapyrenium. This electron acceptor was investigated because the diazapyrenium unit is known to demonstrate enhanced binding and spectroscopic properties as compared with methyl viologen.

6.2.1 [*N,N'*-Dimethyl-4,4'-bipyridinium][1,5-bis{(hydroxyethoxy)ethoxy}naphthalene][PF₆]₂

Upon mixing of equimolar acetonitrile solutions of *N,N'*-Dimethyl-4,4'-bipyridinium bis(hexafluorophosphate) (methyl viologen) and 1,5-bis{(hydroxyethoxy)ethoxy}naphthalene (figure 6.2) a dark red solution was produced almost instantaneously as a result of the formation of a charge transfer complex between the two molecular components.⁹

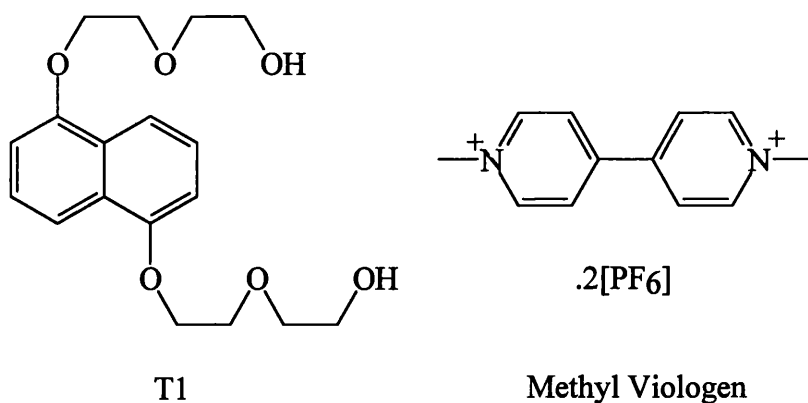


Figure 6.2: The components of EDA complex 6.2.1.

The stoichiometry of the complex was expected to be 1:1 - this was confirmed by FAB mass spectrometry and by an X-ray structural study which was performed on a crystalline sample obtained by slow vapour diffusion from the red solution. The FAB mass spectrum displayed a large peak at $m/z = 667$ which

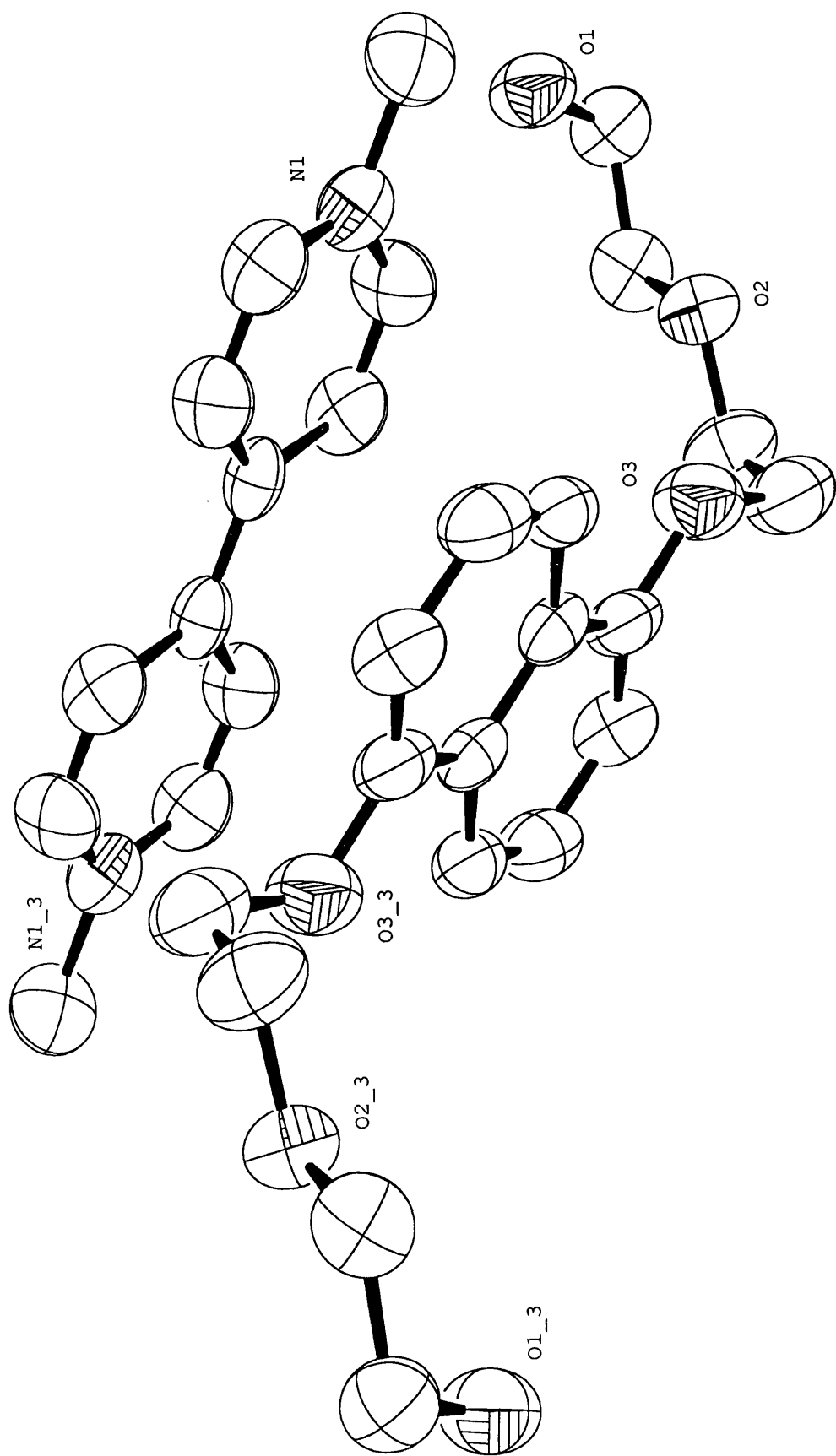


Figure 6.3: Crystal structure of [N,N'-dimethyl-4,4'-bipyridinium][1,5-bis{(hydroxyethoxy)ethoxy}naphthalene]²⁺ (PF₆ counterions omitted).

represented ($M\text{-PF}_6$) where $M = 814\text{Da}$ for the 1:1 complex. In addition, the FAB mass spectrum showed that small quantities of 1:2 (methyl viologen to **T1**) complex were present in the red solution. In the solid state however, the ratio of the electron acceptor to its complementary donor was strictly 1:1, as was determined by the X-ray structural study. The structure of the complex is presented in figure 6.3 (crystal data is presented in the appendices). The bipyridinium dication is found to be essentially planar, indeed nearly 44% of related dications in the Cambridge Structural Database are also planar or are nearly so.⁹ In the crystal, the naphthalene-containing molecules are stacked with the bipyridinium dications with an interplanar spacing of 3.33\AA . The plane normals of the donor molecule **T1** and the methyl viologen acceptor are inclined at 3.6° and 5.0° respectively to the crystallographic *b* axis. The 1:1 complexes form an infinite stack along the *b* axis. Each component of the complex occupies a special position, with centres of symmetry located in the middle points of the central carbon-carbon bonds of the each unit. The angle between the long axis of the template **T1** and that of the methyl viologen unit is approximately 63° - a value which is consistent with the angles found in the 2:1 complex between **L1** and **T1** of 55° and 65° . Each π -stack is joined to its near neighbours by short hydrogen bonds [$\text{O-H}\cdots\text{O}$, $\text{O}\cdots\text{O}$ distance = 2.812\AA] involving the polyether arms of the **T1** molecules.

Thus the complex between methyl viologen and the template molecule **T1** has been well characterised. To compare the properties of methyl viologen with those of dimethyl-2,7-diazapyrenium it is necessary to study the 1:1 complex of this electron acceptor with the electron donating compound **T1**.

6.2.2 [N,N'-Dimethyl-2,7-diazapyrenium][1,5-Bis{(hydroxyethoxy)ethoxy}naphthalene][PF₆]₂

N,N'-Dimethyl-2,7-diazapyrenium (DAP^{2+}) has been shown to display increased binding strength with the aromatic electron donating crown **34C10** as compared with methyl viologen (3900M^{-1} vs 50M^{-1}).¹ This effect may be attributed to both electronic and geometrical contributions, where the increased size of the DAP dication leads to increased π -overlap between the electron donor acceptor pair

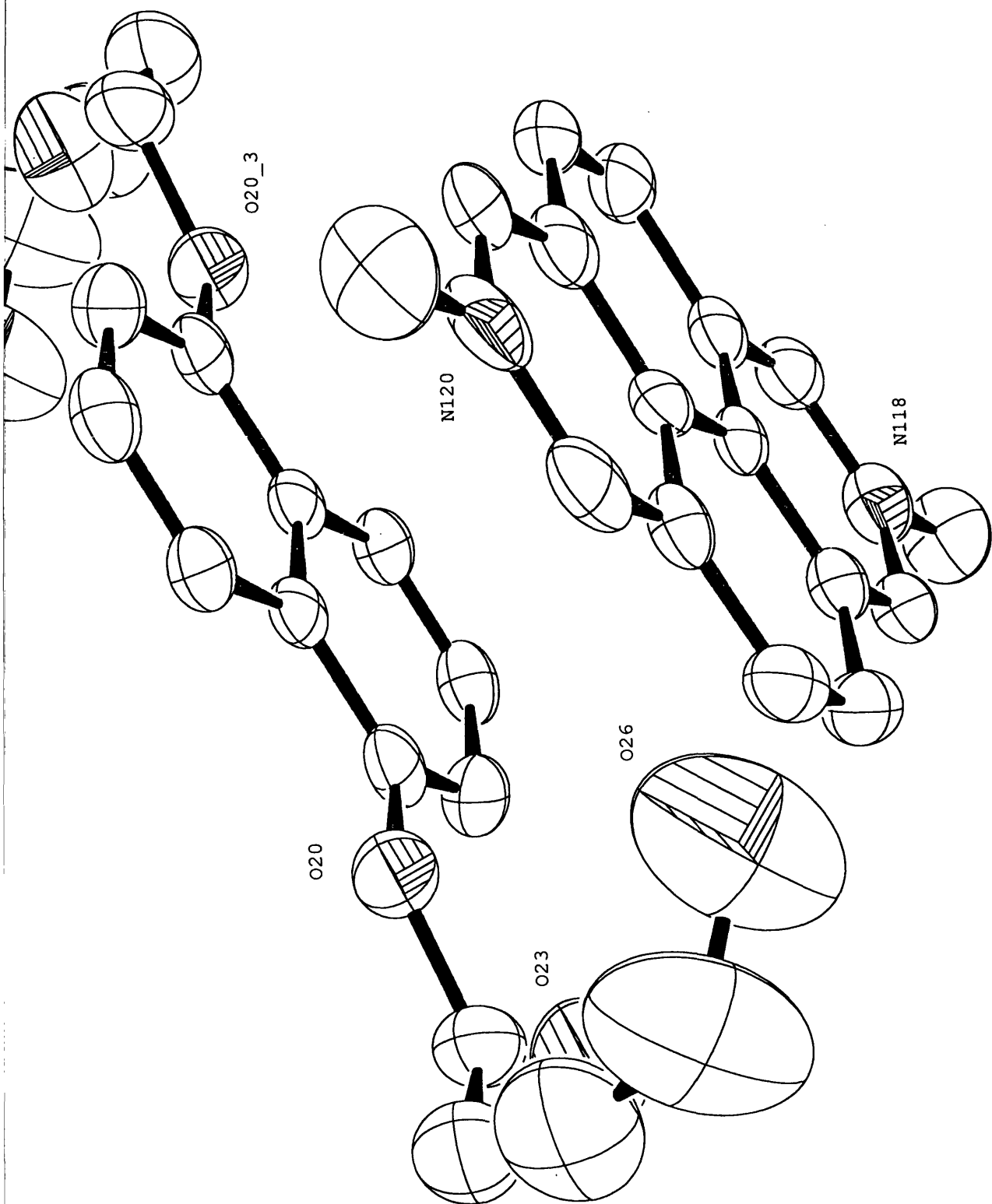


Figure 6.4: Crystal structure of [N,N'-dimethyl-2,7-biazapyrenium][1,5-bis{(hydroxyethoxy)ethoxy}naphthalene]²⁺ (PF₆ counterions omitted).

and ensures planarity of the acceptor. In addition, the size of the DAP dication may well provide a superior 'fit' to the crown ether as compared to methyl viologen, where electrostatic and hydrogen bonded interactions between the polyether segments of the crown and 'acidic' protons on the DAP dication play an important role in stabilising the EDA complex.

The DAP dication is fluorescent and the singlet emitting state may mix with the charge transfer state of the $[\text{DAP}^{2+}][\text{34C10}]$ complex thus stabilising the charge separated state and enabling ejection of the mono-reduced DAP from the oxidised crown.¹ Thus incorporation of the DAP dication into cation chelating cyclophanes and [2]catenanes may lead to interesting photophysical properties, e.g. long lived charge separated states, which would have potential as light harvesting devices.

The $[\text{N,N}'\text{-Dimethyl-2,7-diazapyrenium}] [1,5\text{-Bis}\{(\text{hydroxyethoxy})\text{ethoxy}\}\text{naphthalene}][\text{PF}_6]_2$ complex was produced in an analogous manner to its methyl viologen equivalent. The solution produced by mixing equimolar acetonitrile solutions of the acceptor and the donor was red-brown in colour, showing that production of a charge transfer complex had occurred. Interestingly, analysis of the red-brown material by FAB mass spectrometry failed to identify the presence of the 1:1 complex (or any other stoichiometry) however an X-ray structural analysis confirmed the identity of the coloured material. A crystalline sample suitable for such analysis was grown by slow vapour diffusion of di-isopropyl ether into an acetonitrile solution of the complex.

From figure 6.4 (crystal data is presented in the appendices) it may be seen that the naphthalene-containing molecules are stacked with the dimethyl-2,7-diazapyrenium dications, with an average interplanar spacing of 3.50Å. The plane normals of the donor molecule T1 and the DAP^{2+} acceptor are inclined with respect to the crystallographic a axis. The 1:1 complexes form an infinite stack along the a axis, however the stack is not as simple as that between methyl viologen and compound T1. Alternate DAP dications are displaced with respect to one another along the direction of the b axis by approximately 1.5Å and, in addition, the naphthalene containing molecules adopt two orientations regularly throughout the donor-acceptor stack. This stacking may be explained by packing forces whereby the polyether arms force the naphthalene units to adopt alternate conformations in order to minimise steric repulsions between them. The naphthalene molecules do not

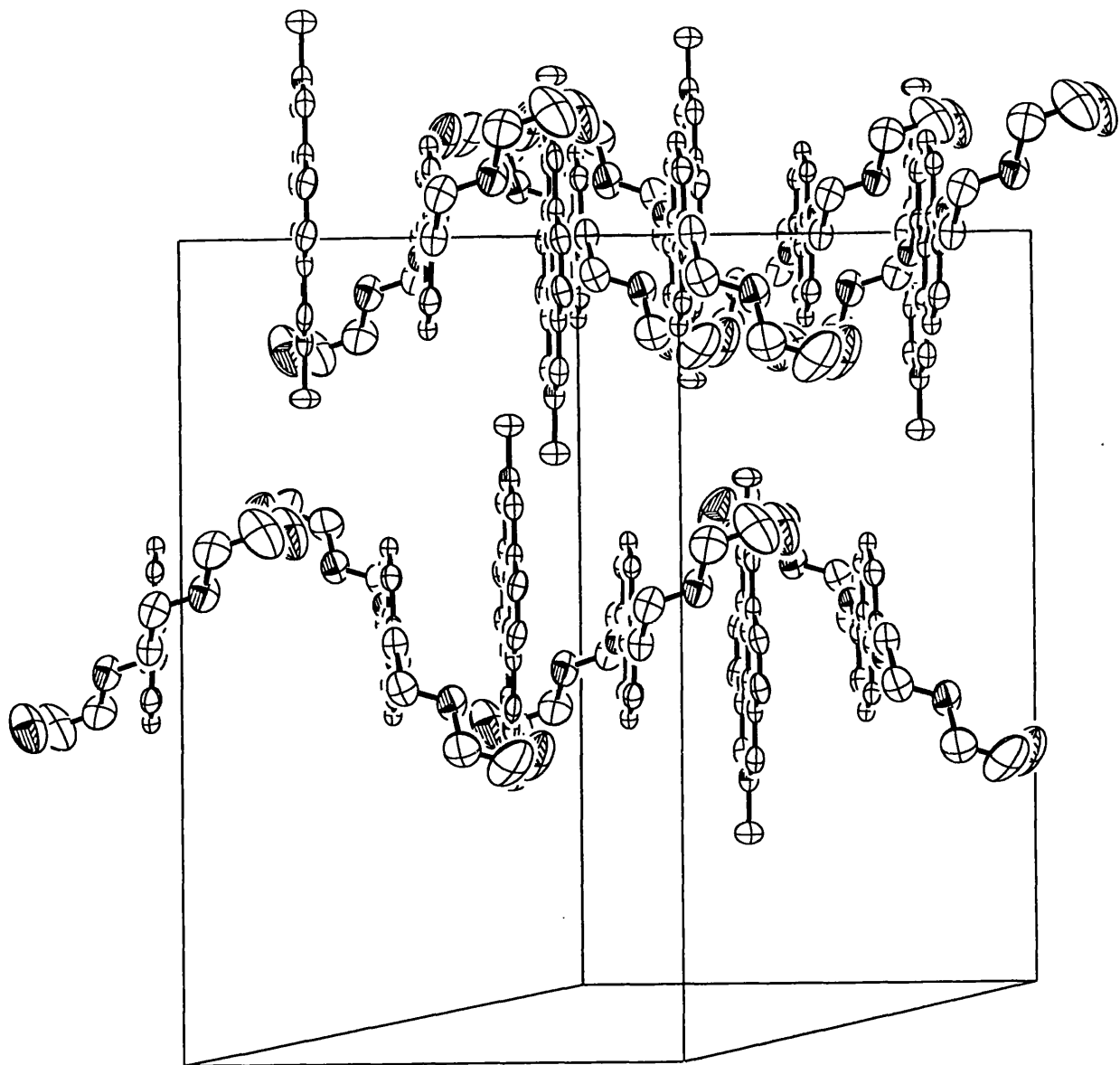


Figure 6.6: Packing diagram for [N,N'-dimethyl-2,7-biazapyrenium][1,5-bis{(hydroxyethoxy)ethoxy}naphthalene]²⁺ (PF₆ counterions omitted).

stack with the DAP dications in a perfectly symmetrical manner - they are displaced to one side of the long axis of the acceptor unit, presumably by stereoelectronic factors (figure 6.5).

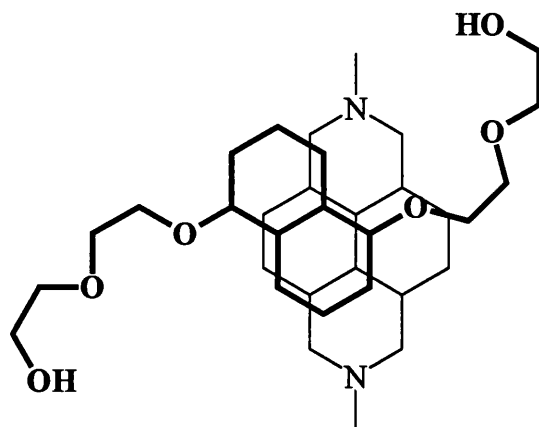


Figure 6.5: Geometry of the interaction between DAP^{2+} and T1.

This geometry coupled with the steric requirements of compound T1, would appear to lead to the displacement of the DAP dications in the stack. The angle between the long axis of the template T1 and that of the DAP^{2+} unit is approximately 31° . Interestingly, the geometry of the T1 molecules generates a pseudo-helical type structure (with respect to the polyether arms of the template molecule, see figure 6.6) along the axes of the π -stacks. The stacks are not connected by hydrogen bonds as was the case in the structure of the methyl viologen - T1 complex.

There is a complication with the structure described above in that some residual electron density remains in the electron density map of the DAP dication (figure 6.7). The electron density cannot be attributed to either of the component molecules or to extraneous water or solvent molecules due to its proximity to the carbon centres in the DAP dication. At the time of writing the residual electron density was under further investigation.

Thus, it is apparent that the DAP dication forms a similar EDA complex with the electron donating molecule T1 to that reported for methyl viologen, although the geometry of the interaction is less straightforward. It should therefore be relatively simple to incorporate the DAP dication into cyclic systems such as those described previously in chapters 3 and 4.

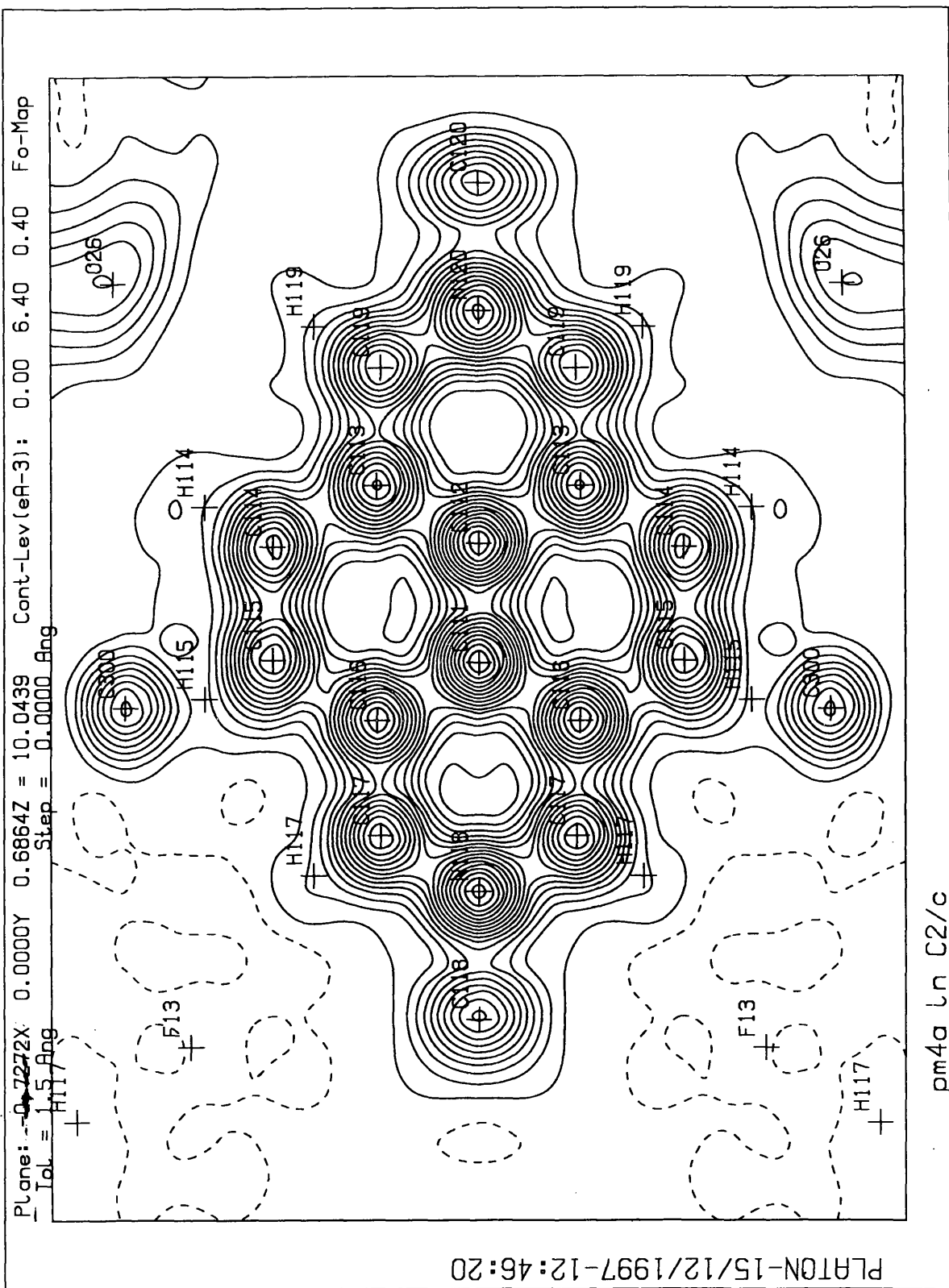


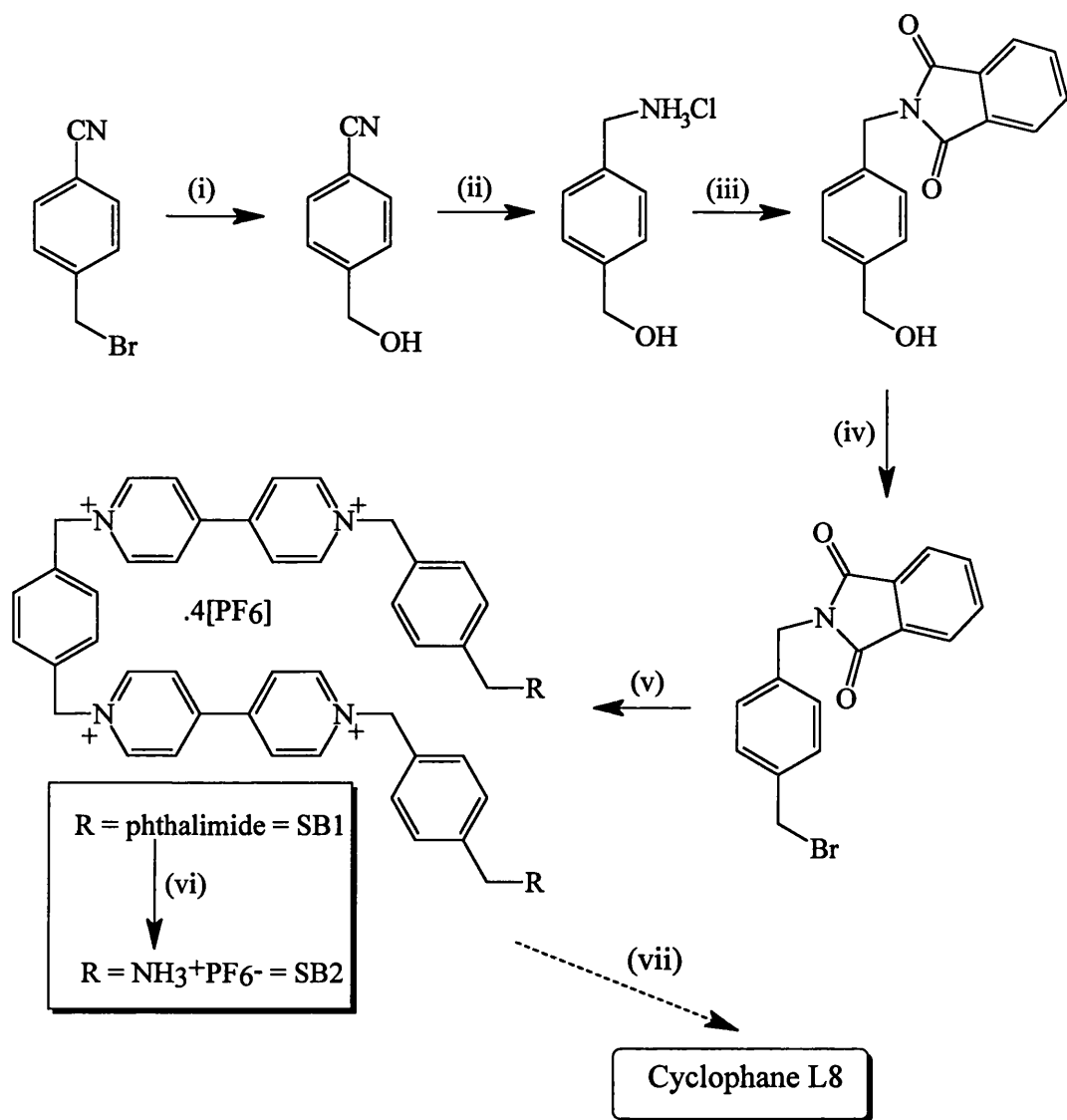
Figure 6.7: Electron density map of the DAP dication.

6.3 Schiff Base Chemistry

When primary amines add to aldehydes and ketones imines are produced.¹⁰ Where there is an aryl group either bonded to the nitrogen or to the carbonyl carbon stable imines are produced which are usually called Schiff bases. Such compounds are straightforward to produce and reactions usually proceed in high yields. A large number of Schiff base macrocyclic structures have thus been produced - the facile cyclisation reactions providing good yields of the desired products.² There are two strategies that may be employed when attempting Schiff base cyclisations, based on metal-templated or metal-free condensations. The former is the most common and simplest approach. The construction, complexation and properties of a wide range of Schiff base macrocycles have been extensively reviewed² and so will not be discussed in detail at this juncture. The wide range of sophisticated macrocyclic and macropolycyclic Schiff base structures in the literature have been largely employed for metal ion encapsulation. It has proved possible to introduce great specificity for various ions and to design ligands which are capable of coordination of two or more metal centres at pre-ordered distances in well defined arrays.² Such properties arise from the extreme versatility of the synthetic strategy.

By employing template syntheses and subsequently de-metallating the product, facile routes to a range of otherwise unobtainable functional macrocycles have been identified and the products used in liquid membrane transport, as precursors in the preparation of ceramic materials, as models of metalloenzymes and metalloproteins and as carriers in industrial separation procedures.

The aim of the synthetic strategy outlined in scheme 6.3.1 was to produce cyclophanes and catenanes which incorporated both cation chelating 1,10-phenanthroline and electron accepting viologen units whilst gaining the benefits of a facile Schiff base type cyclisation.



Scheme 6.3.1: Attempted Schiff base synthesis of cyclophane L8.

Reagents and conditions: (i) $\text{BaCO}_3/\text{H}_2\text{O}$ 85%; (ii) $\text{LiAlH}_4/\text{Et}_2\text{O}$, 2N $\text{HCl}_{(\text{aq})}$ 118%; (iii) phthalic anhydride, $\text{Na}(\text{CH}_3\text{COO})/\text{CH}_3\text{COOH}$ 12%; (iv) $\text{Si}(\text{Me})_3\text{Br}/\text{CHCl}_3$ 88.7%; (v) 1,1'-[1,4-phenylenebis(methylene)][bis-4,4'-bipyridinium] bis(hexafluorophosphate)/MeCN, $\text{NH}_4\text{PF}_6_{(\text{aq})}$ 63%; (vi) conc. $\text{HCl}/\text{CH}_3\text{COOH}$, $\text{NH}_4\text{PF}_6_{(\text{aq})}$ 45%; (vii) 1,10-phenanthroline-4,7-dialdehyde, pyridine, T1/DMSO/MeCN (1:6) or 1,10-phenanthroline-4,7-dialdehyde, pyridine/MeCN.

Steps (i) and (ii) in the above scheme were achieved by literature procedures,¹¹ the reagents employed being (i) BaCO_3 and (ii) LiAlH_4 . Step (iii) is a well known protection reaction and was carried out using standard procedures with phthalic anhydride as the protecting reagent. Step (iv) was also adapted from a literature preparation and involved the use of trimethylsilylbromide.¹² All four products were produced in reasonable yield and were characterised by NMR spectroscopy and mass spectrometry. Step (v) involved a standard $\text{S}_{\text{N}}2$ substitution

reaction where the precursor compound¹³ 1,1'-[1,4-phenylenebis(methylene)][bis-4,4'-bipyridinium].2[PF₆] was added slowly to a solution of the *p*-phthalimidomethylbenzyl bromide. The reaction proceeded in reasonable yield (63 %) and the product, **SB1**, was characterised by ¹H and ¹³C NMR spectroscopy in addition to FAB mass spectrometry. The mass spectrum contained peaks corresponding to the loss of n(PF₆⁻) counterions from the molecular ion, with m/z values of 1351 (n=1), 1206 (n=2) and 1061 (n=3). The interpretation of the ¹H NMR spectrum is presented in table 6.3.1.

Signal	Chemical Shift
CH ₂ -phthalimide	4.75
CH ₂ -viologen	5.87, 5.93
phenyl-phthalimide	7.47
phenyl-viologen	7.65
phthalimide	7.84
viologen CH(β)	8.61
viologen CH(α)	9.35

Table 6.3.1: Interpretation of the ¹H NMR spectrum of SB1.

¹H NMR data was obtained at 360MHz at 298K in d₆-acetone

The conversion of the protected amine to its unprotected ammonium salt (step (vi)) **SB2**, was accomplished by an established acid catalysed deprotection reaction. The more usual method involving hydrazine as the cleaving reagent could not be employed because of the sensitivity of the viologen derivatives in **SB1** to nucleophiles - they may easily be displaced by electron rich species in substitution reactions to produce 4,4'-bipyridine as the leaving group. Compound **SB2** was characterised by ¹H and ¹³C NMR spectroscopy and by FAB mass spectrometry. As with compound **SB1**, the mass spectrum shows the expected peaks corresponding to the loss of n(PF₆⁻) counterions at m/z values of 1383 (n=1), 1238 (n=2), 1093 (n=3) and 948 (n=4). The ¹H NMR spectrum of compound **SB2** is presented in figure 6.8. As may be seen from the figure, the signal corresponding to the methylene protons next to the amine functionality are partially obscured by a water peak at 4.26ppm. The methylene units which are located next to the viologen units

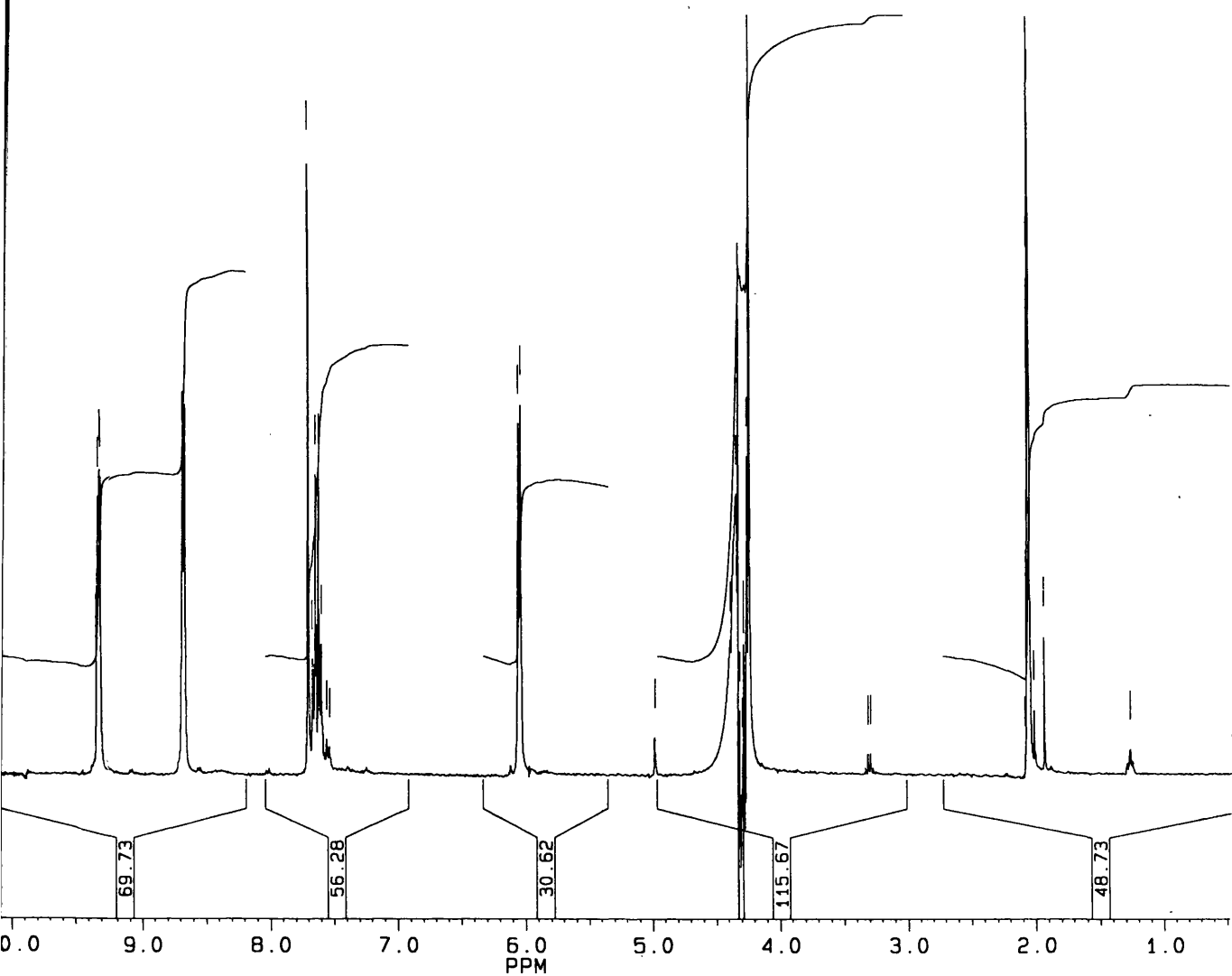


Figure 6.8: ^1H NMR spectrum of $\text{SB2}(\text{PF}_6)_4$ in d_6 -acetone at 360MHz and 298K.

come into resonance at 6.04 and 6.06ppm. The multiplet at 7.53-7.67ppm corresponds to the two phenyl units which link the viologen and amine functions and the singlet at 7.70ppm corresponds the phenyl spacer situated between the electron accepting units. The signals corresponding to the protons on the viologen units are found at 8.67 (protons β to the nitrogen atom) and at 9.31ppm (protons α to the nitrogen atom). Compound **SB2** was produced from **SB1** in reasonable yield (45.1%), however it appeared to be too unstable to withstand long term storage (even at 4°C) as the compound was found to decompose to give a brown solid and a noxious vapour after several days.

The final step (vii) was attempted on a number of occasions, using either compound **T1** as a template to produce free cyclophane **L8** or the crown ether **34C10** to synthesise the analogous [2]catenane **L9**. In addition, a high temperature (i.e. non-templated) cyclisation was attempted in the hope that such a strategy would produce the desired product. The aim of the reaction was to cyclise **SB2** by formation of imine functions with 1,10-phenanthroline-4,7-dicarbaldehyde¹⁴ (figure 6.9) in a standard Schiff base type reaction.

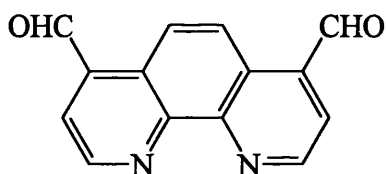


Figure 6.9: Formula of 1,10-phenanthroline-4,7-dicarbaldehyde.

It was hoped that the nitrogen atoms in the phenanthroline unit would act as catalysts for the reaction by deprotonating a quantity of the ammonium function of compound **SB2** - the protonated heterocycles subsequently activating the aldehyde carbonyl groups thus promoting the reaction.

Unfortunately, no evidence for successful reaction could be obtained using either FAB mass spectrometry or NMR spectroscopy.

In an attempt to discern why the cyclisation reaction had failed, the solubility of 1,10-phenanthroline-4,7-dicarbaldehyde was investigated. Although this unit is rather insoluble, it was found to dissolve in sufficient quantities in solvents such as DMF or DMSO to participate in simple coordination chemistry such as the formation of tris-chelates with iron centres. Given that the solubility of the di-aldehyde was not the source of the problem and that the amine was clearly soluble in

a variety of solvents, the reaction conditions were eliminated as the source of the problem. Production of water leading to a rapid equilibration of the products back to the reactants was also considered, but as the reactions were carried out using dry conditions (dry solvents etc.) and the addition of drying agents had no effect to the yield, this was also eliminated. Upon attempting a simple Schiff base reaction between benzaldehyde and **SB2** however, the source of the problem was tentatively identified. Instead of producing the predicted imine product, a white solid was produced by the reaction which appeared to be an aldol self-condensation product of benzaldehyde alone. Clearly, the amine functions in **SB2** are not reactive despite the introduction of mild bases (e.g. pyridine) to deprotonate them. Strong bases cannot be used as these would degrade the viologen part of the precursor molecule. It may prove possible in future reactions to produce cyclophane **L8** by using a large quantity of a hindered base such as DBU (1,8-diazabicyclo[5.4.0]undecene-7) to effect deprotonation of the ammonium units in **SB2**, thus enabling reaction to occur.

6.4 References

- [1] Benniston, A.C.; Harriman, A.; Yufit, D.S. *Angew. Chem. Int. Ed. Engl.*, 1997, **36**, 2356.
- [2] Guerriero, P.; Tamburini, S.; Vigato, P.A.; *Coord. Chem. Rev.*, 1995, **139**, 17.
- [3] Asakawa, M.; Ashton, P.R.; Boyd, S.E.; Brown, C.L.; Gillard, R.E.; Kocian, O.; Raymo, F.M.; Stoddart, J.F.; Tolley, M.S.; White, A.J.P.; Williams, D.J. *J. Org. Chem.*, 1997, **62**, 26.
- [4] White, B.G. *Trans. Faraday Soc.*, 1969, **65**, 2000.
- [5] Prasad, D.R.; Hoffman, M.Z. *J. Phys. Chem.*, 1984, **88**, 5660.
- [6] Fernando, Q.; Inoue, M.; Inoue, M.B.; Machi, L. *Inorg. Chim. Acta.*, 1992, **192**, 123.
- [7] Hofbauer, M.; Möbius, M.; Knoch, F.; Benedix, R. *Inorg. Chim. Acta.*, 1996, **247**, 147.
- [8] Bhardwaj, A.P.; Murthy, A.S.N. *Spectrochim. Acta*, 1982, **38A**, 207.
- [9] Benniston A.C.; Yufit, D.S.; Mackie, P.R. *Acta Cryst.*, 1997, **C53**, 1899.
- [10] March, J. *Advanced Organic Chemistry: Reactions, Mechanisms and Structure*, Wiley-Interscience, New York, 1992.
- [11] Bardsley, W.G.; Ashford, J.S.; Hill, C.M. *Biochem. J.*, 1971, **122**, 557.
- [12] Jung, M.F.; Hatfield, G.L. *Tetrahedron Lett.*, 1978, **6**, 4483.
- [13] Anelli, P.L.; Ashton, P.R.; Ballardini, R.; Balzani, V.; Delgado, M.; Gandolfi, M.T.; Goodnow, T.T.; Kaifer, A.E.; Philp, D.; Pietraszkiewicz, M.; Prodi, L.; Reddington, M.V.; Slawin, A.M.Z.; Spencer, N.; Stoddart, J.F.; Vicent, C.; Williams, D.J. *J. Am. Chem. Soc.*, 1992, **114**, 193.
- [14] Bishop, M.M.; Lewis, J.; O' Donoghue, T.D.; Raithby, P.R. *J. Chem. Soc. Chem. Commun.*, 1978, 476.

Chapter Seven

General Conclusions

The [2]catenanes and cyclophanes discussed in this work were successfully synthesised from simple precursor compounds, namely **P1**, **P2** and **P3**. Whilst precursors **P2** and **P3** had been synthesised previously, neither had been employed in the synthesis of catenanes and cyclophanes which incorporated both cation chelating 2,2'-bipyridine units in addition to electron accepting bipyridinium units. A model of the novel compound **P1** demonstrated that it should adopt a structure which was unfavourable towards cyclisation, caused by the lowest energy conformation of the central chelating unit. This was confirmed by a structure obtained from an X-ray diffraction study of a crystalline sample of the compound. In order to obtain a precursor which had a more favourable conformation towards cyclisation, a 'pre-coordination' strategy was adopted. This strategy involved appending a ruthenium or osmium bipyridyl moiety onto **P1** thus 'forcing' the compound into a conformation which favoured cyclisation at the 4,4'- positions. The crystal structure of $\text{Ru}(\text{bipy})_2(\text{P1})^{4+}$ confirmed that the precursor had indeed adopted the desired conformation on complexation. This compound was found to have interesting photophysical properties, whereby the complex did not behave as a typical $\text{Ru}(\text{bipy})_3^{2+}$ derivative because of changes to its excited state caused by the introduction of the **P1** ligand. Furthermore, it was observed that the compound reacted with protons to produce the non-fluorescent $\text{Ru}(\text{bipy})_2(\text{P1})(\text{H})_n^{(4+n)+}$ complex.

Free cyclophanes **L1**, **L2**, **L3** and **L4** were synthesised from their appropriate precursors by employing template syntheses based on EDA interactions between the electron accepting cyclophanes and complementary donor threads. It was found that the yield of such syntheses decreased with increasing distance between the electron accepting units, i.e. as cavity size increased and with the number of 2,2'-bipyridyl units included. Hence compound **L1** was produced in reasonable quantities, **L2** in smaller yields and **L3** and **L4** in yields of less than 10%.

Ruthenium and osmium tris bipyridyl complexes of cyclophane **L1** were produced by either appending metal centres to the free cyclophane (which had been synthesised by the template strategy) or by employing the pre-coordination strategy.

The second strategy resulted in higher yields of products, but involved the tedious preparation of $M(\text{bipy})_2(\text{P1})^{4+}$ precursors.

The structure of cyclophane **L1** was determined by X-ray diffraction techniques and confirmed that the cyclophane had a novel size and shape as compared to those in the literature - a feature caused by incorporation of a bipyridyl unit in the structure. The electrochemistry, host-guest and coordination chemistry of the compound were investigated. The binding constants were determined for the compound with a range of aromatic electron donors and the expected trend observed. A crystal structure of an inclusion complex between **L1** and the donor molecule **T1** was obtained, which shed light on the geometry and the factors which influence the stability of such EDA interactions. The complexation of **L1** with 'naked' Cu^I , Zn^{II} and Fe^{II} ions resulted in the production of dimeric and trimeric cyclophane aggregates. The host-guest properties of the cyclophane was observed to change in such environments. The addition of ruthenium and osmium bipyridyl centres to **L1** resulted in production of the expected monomeric complexes. Investigation of the electrochemical and photophysical properties of $\text{Ru}(\text{bipy})_2(\text{L1})^{6+}$ revealed that excitation of the compound led to a photoinduced electron transfer process. Upon irradiation it was shown that an excited state of ruthenium tris-bipyridyl was formed and that this donated an electron to the electron accepting units to which it was bound. The thermodynamic feasibility of electron transfer was found to be solvent dependant.

The crystal structure of cyclophane **L2** was determined, and showed that the incorporation of two bipyridyl units had indeed increased the cavity size within the compound. This data explained the decreased binding constants observed for the formation of inclusion complexes between **L2** and a range of electron donors as compared to those obtained for **L1**. Cyclophane **L2** has two cation chelating sites rather than one and so it was found to have different coordination chemistry to that observed for **L1**. Indeed, upon addition of 'naked' metal cations to the cyclophane, materials which were ascribed as being metallo-polymers were produced.

The [2]catenanes **L5**, **L6** and **L7** were synthesised by template syntheses whereby an aromatic crown ether acts as both a template for the construction of electron accepting cyclophane rings and as a constituent part of the interlocked

structure. It was found that using naphthalene-based donor crowns (**1/5DN38C10**) produced higher yields of product than their equivalent benzene-based systems (**34C10**). This effect was manifest in the significantly higher yield of **L6** as compared to that of **L5**. In contrast, [2]catenane **L7** was produced in very low yield. The poor yield was attributed to the relatively poor templating effect of **34C10** combined with the difficulties inherent in constructing systems which contain two 2,2'-bipyridyl chelating units.

The electrochemical properties of the catenane structures were investigated and a redox asymmetry between the two chemically identical electron acceptors was observed in each system. This effect was attributed to encapsulation of one acceptor unit by the donor crown ethers whilst the second acceptor remained 'outside' the complex. The encapsulated acceptor unit is less easily reduced than the outside acceptor because of enhanced electron donation from the crown ether. This effect was more pronounced for catenane **L6** than for **L5** or **L7** because of the increased electron donating ability of the naphthalene crown as compared to that of the benzo-crown.

[2]Catenane **L5** was shown to have interesting coordination chemistry in much the same way as its cyclophane precursor. Addition of Cu^{I} to the catenane resulted in formation of a dimeric aggregate. Addition of ruthenium and osmium bipyridyl centres to the catenane resulted in the expected complexes. The complex of $\text{Ru}(\text{bipy})_2(\text{L5})^{6+}$ was synthesised by this route and its electrochemical and photophysical properties probed. It was demonstrated that upon excitation of the ruthenium tris-bipyridyl centre the excited state of the complex is produced. Subsequent photoinduced electron transfer from the excited donor to the electron accepting units was shown to occur followed by rapid charge recombination. The redox asymmetry present within the molecule lead to the assertion that the electron transfer occurred in a vectorial fashion, i.e. that the electron transfer process involved the outside acceptor unit in preference to the encapsulated acceptor. As such, $\text{Ru}(\text{bipy})_2(\text{L5})^{6+}$ was proposed to function as a model of the photosynthetic reaction centre such as those in purple photosynthetic bacteria *Rhodospseudomonas viridis* and *Rhodobacter sphaeroides*, thus fulfilling the primary aim of the research discussed in this thesis.

Appendices

(i) Crystal data for P1.2[PF₆]

A single crystal of suitable size was attached to a fine glass fibre using frozen hydrocarbon oil and mounted on a goniometer head in a general position. Data were collected using the synchrotron radiation source at Daresbury (see section 2.1.4) using monochromatic X-ray radiation ($\lambda=0.6875\text{\AA}$). The structure was solved by direct methods (section 2.1.4). Aliphatic and aromatic hydrogen atoms were included at calculated positions, with C-H = 0.96 \AA , and were refined with a riding model with U_{iso} set to 1.2 times that of the attached C-atom. Refinement was by full-matrix least-squares on F^2 using all unique data. Neutral atom scattering factors, coefficients of anomalous dispersion and absorption coefficients were obtained from international tables. Thermal ellipsoid plots were obtained using the program ORTEP-3 for windows. All calculations were carried out using the WinGX package of programs.

cell formula	C ₆₄ H ₅₂ N ₁₂ F ₂₄ P ₄
M _r	1569.06
space group	P2(1)/n
crystal system	monoclinic
a (Å)	6.3652(9)
b (Å)	35.2563(112)
c (Å)	7.6591(17)
α (deg)	90.000(0)
β (deg)	108.033(17)
γ (deg)	90.000(0)
V (Å ³)	1634.37
Z	2
D _{calc} (gcm ⁻³)	1.594
F(000)	796
μ (mm ⁻¹)	2.4
Temperature (°C)	-113
crystal size (mm)	0.02 x 0.02 x 0.05
no. data collected	3444
no. unique data	2056
R _{int}	0.0830
no. parameters	235
final R1	0.0586
final R _w ²	0.1288
largest remaining feature in electron density map (e/Å ³)	0.36, -0.28
mean shift/esd	0.004
goodness of fit S	0.954

(ii) Crystal data for Ru(bipy)₂(P1).4[BF₄]

A single crystal of suitable size was attached to a fine glass fibre using frozen hydrocarbon oil and mounted on a goniometer head in a general position. Data were collected using the synchrotron radiation source at Daresbury (see section 2.1.4) using monochromatic X-ray radiation ($\lambda=0.6849\text{\AA}$). The structure was solved by direct methods (section 2.1.4). Aliphatic and aromatic hydrogen atoms were included at calculated positions, with C-H = 0.96 \AA , and were refined with a riding model with U_{iso} set to 1.2 times that of the attached C-atom. Refinement was by full-matrix least-squares on F^2 using all unique data. Neutral atom scattering factors, coefficients of anomalous dispersion and absorption coefficients were obtained from international tables. Thermal ellipsoid plots were obtained using the program ORTEP-3 for windows. All calculations were carried out using the WinGX package of programs.

cell formula	C ₁₀₄ H ₇₆ N ₂₀ F ₃₂ B ₈ Ru ₂
M _r	2502.47
space group	P-1
crystal system	triclinic
a (\AA)	13.1025(1)
b (\AA)	13.5227(1)
c (\AA)	16.4607(1)
α (deg)	94.579(1)
β (deg)	102.822(1)
γ (deg)	105.621(1)
V (\AA^3)	2708.33
Z	2
D _{calc} (gcm ⁻³)	1.534
$F(000)$	1255.8
μ (mm ⁻¹)	3.9
Temperature (°C)	-123
crystal size (mm)	0.12 x 0.06 x 0.02
no. data collected	16321
no. unique data	11274
R _{int}	0.0264
no. parameters	835
final R1	0.0473
final R _w ²	0.1193
largest remaining feature in electron density map (e/ \AA^3)	1.16, -1.07
mean shift/esd	0.007
goodness of fit S	0.930

(iii) Crystal data for L1.4[PF₆]

A single crystal of suitable size was attached to a glass fibre using acrylic resin and mounted on a goniometer head in a general position. Data were collected using a Stoe Stadi-4 diffractometer at the University of Edinburgh (see section 2.1.4) using monochromatic X-ray radiation ($\lambda=1.54178\text{\AA}$). The structure was solved by direct methods (section 2.1.4). Aliphatic and aromatic hydrogen atoms were included at calculated positions, with C-H = 0.96 \AA , and were refined with a riding model with U_{iso} set to 1.2 times that of the attached C-atom. Refinement was by full-matrix least-squares on F^2 using all unique data. Neutral atom scattering factors, coefficients of anomalous dispersion and absorption coefficients were obtained from international tables. Thermal ellipsoid plots were obtained using the program ORTEP-3 for windows. All calculations were carried out using the WinGX package of programs.

cell formula	C ₃₃₆ H ₂₉₆ N ₅₆ F ₁₉₂ P ₃₂
M_r	1569.06
space group	C2/c
crystal system	monoclinic
a (\AA)	29.9146(23)
b (\AA)	13.9686(13)
c (\AA)	24.8144(18)
α (deg)	90.000(0)
β (deg)	90.204(5)
γ (deg)	90.000(0)
V (\AA^3)	10369.01
Z	8
D_{calc} (gcm^{-3})	1.56
$F(000)$	4911.3
$\mu(\text{Cu-K}\alpha)$ (mm^{-1})	2.51
Temperature ($^{\circ}\text{C}$)	-53
crystal size (mm)	0.54 x 0.35 x 0.23
no. data collected	10062
no. unique data	9147
R_{int}	0.0295
no. parameters	685
final R1	0.0814
final R_w^2	0.2642
largest remaining feature in electron density map ($\text{e}/\text{\AA}^3$)	0.75, -0.39
mean shift/esd	0.000
goodness of fit S	1.046

(iv) Crystal data for L1.2(T1).4[PF₆]

A single crystal of suitable size was attached to a glass fibre using acrylic resin and mounted on a goniometer head in a general position. Data were collected using an Enraf-Nonius CAD4 diffractometer at the University of Glasgow (see section 2.1.4) using monochromatic X-ray radiation ($\lambda=0.71073\text{\AA}$). The structure was solved by direct methods (section 2.1.4). Aliphatic and aromatic hydrogen atoms were included at calculated positions, with C-H = 0.96 \AA , and were refined with a riding model with U_{iso} set to 1.2 times that of the attached C-atom. Refinement was by full-matrix least-squares on F^2 using all unique data. At the time of writing anion disorder had not been adequately modelled, hence unacceptable mean esd and goof values were obtained. Neutral atom scattering factors, coefficients of anomalous dispersion and absorption coefficients were obtained from international tables. Thermal ellipsoid plots were obtained using the program ORTEP-3 for windows. All calculations were carried out using the WinGX package of programs.

cell formula	C ₂₆₈ H ₂₈₀ N ₂₄ F ₉₆ P ₁₆ O ₃₆
M_r	1683.2
space group	P 21/n
crystal system	monoclinic
a (\AA)	10.3840(5)
b (\AA)	14.5560(5)
c (\AA)	48.6610(5)
α (deg)	90.000(5)
β (deg)	91.377(5)
γ (deg)	90.000(5)
V (\AA^3)	7352.96
Z	4
D_{calc} (gcm^{-3})	1.52
$F(000)$	3447.6
$\mu(\text{Mo-K}\alpha)$ (mm^{-1})	2.23
Temperature ($^{\circ}\text{C}$)	23
crystal size (mm)	0.20 x 0.20 x 0.20
no. data collected	19953
no. unique data	14827
R_{int}	0.0197
no. parameters	991
final R1	0.0918
final R_w^2	0.2696
largest remaining feature in electron density map ($\text{e}/\text{\AA}^3$)	0.876, -0.49
mean shift/esd	0.000
goodness of fit S	1.063

(v) Crystal data for L2.4[PF₆]

A single crystal of suitable size was attached to a fine glass fibre using frozen hydrocarbon oil and mounted on a goniometer head in a general position. Data were collected initially at the University of Durham and subsequently using the synchrotron radiation source at Daresbury (see section 2.1.4) using monochromatic X-ray radiation ($\lambda=0.6875\text{\AA}$). The structure was solved and refined by Dr. D.S. Yufit. Thermal ellipsoid plots were obtained using the program ORTEP-3 for windows.

cell formula	C ₈₈ H ₇₂ N ₁₆ F ₄₈ P ₈
M _r	1256.69
space group	P21/c
crystal system	monoclinic
a (Å)	8.6876(2)
b (Å)	15.3989(1)
c (Å)	18.7258(2)
α (deg)	90.007(0)
β (deg)	101.006(1)
γ (deg)	90.073(0)
V (Å ³)	2459.05
Z	2
D _{calc} (gcm ⁻³)	1.697
F(000)	1264
μ (Cu-K α) (mm ⁻¹)	2.90
Temperature (°C)	-123
crystal size (mm)	0.15 x 0.15 x 0.15
no. data collected	11896
no. unique data	5119
R _{int}	0.0393
no. parameters	346
final R1	0.0797
final R _w ²	0.2074
largest remaining feature	
in electron density map (e/Å ³)	1.27, -0.88
mean shift/esd	0.000
goodness of fit S	1.119

(vi) Crystal data for L5.4[PF₆]

A single crystal of suitable size was attached to a fine glass fibre using frozen hydrocarbon oil and mounted on a goniometer head in a general position. Data were collected using the synchrotron radiation source at Daresbury (see section 2.1.4) using monochromatic X-ray radiation ($\lambda=0.6849\text{\AA}$). The structure was solved by direct methods (section 2.1.4), and was refined by Dr L.J. Farrugia. Thermal ellipsoid plots were obtained using the program ORTEP-3 for windows. All calculations were carried out using the WinGX package of programs.

cell formula	C ₅₉₂ H ₇₀₄ N ₄₈ F ₁₉₂ P ₃₂ O ₁₀₄
M _r	1849.4
space group	Pbca
crystal system	orthorhombic
a (Å)	14.7510(27)
b (Å)	29.0775(55)
c (Å)	38.5238(68)
α (deg)	90.000(0)
β (deg)	90.000(0)
γ (deg)	90.000(0)
V (Å ³)	16523.71
Z	8
D _{calc} (gcm ⁻³)	1.49
<i>F</i> (000)	7631.1
μ (mm ⁻¹)	2.02
Temperature (°C)	-113
crystal size (mm)	0.16 x 0.07 x 0.02
no. data collected	61989
no. unique data	16783
R _{int}	0.1141
no. parameters	1100
final R1	0.0892
final R _w ²	0.2352
largest remaining feature in electron density map (e/Å ³)	0.76, -0.66
mean shift/esd	0.000
goodness of fit S	1.005

(vii) Crystal data for [N,N'-Dimethyl-4,4'-bipyridinium][1,5-bis
{(hydroxyethoxy)ethoxy}naphthalene].2[PF₆]

A single crystal of suitable size was attached to a glass fibre using acrylic resin and mounted on a goniometer head in a general position. Data were collected using an Enraf-Nonius CAD4 diffractometer at the University of Glasgow (see section 2.1.4) using monochromatic X-ray radiation ($\lambda=0.71069\text{\AA}$). The structure was solved and refined by Dr. D.S. Yufit. Thermal ellipsoid plots were obtained using the program ORTEP-3 for windows.

cell formula	C ₆₀ H ₇₆ N ₄ F ₁₂ P ₄ O ₁₂
M _r	698.0
space group	P21/n
crystal system	monoclinic
a (Å)	15.005(5)
b (Å)	6.829(5)
c (Å)	17.749(5)
α (deg)	90.000(5)
β (deg)	102.250(5)
γ (deg)	90.000(5)
V (Å ³)	1777.3
Z	4
D _{calc} (gcm ⁻³)	1.305
F(000)	728
μ (Mo-K α) (mm ⁻¹)	1.95
Temperature (°C)	20
crystal size (mm)	0.50 x 0.45 x 0.01
no. data collected	4009
no. unique data	2941
R _{int}	0.0463
no. parameters	229
final R1	0.0761
final R _w ²	0.2061
largest remaining feature in electron density map (e/Å ³)	0.57, -0.54
mean shift/esd	0.000
goodness of fit S	1.032

(viii) Crystal data for [N,N'-Dimethyl-2,7-diazapyrenium][1,5-bis
{(hydroxyethoxy)ethoxy}naphthalene].2[PF₆]

A single crystal of suitable size was attached to a glass fibre using acrylic resin and mounted on a goniometer head in a general position. Data were collected using an Enraf-Nonius CAD4 diffractometer at the University of Glasgow (see section 2.1.4) using monochromatic X-ray radiation ($\lambda=0.71073\text{\AA}$). The structure was solved by direct methods (section 2.1.4). Aliphatic and aromatic hydrogen atoms were included at calculated positions, with C-H = 0.96 \AA , and were refined with a riding model with U_{iso} set to 1.2 times that of the attached C-atom. Refinement was by full-matrix least-squares on F^2 using all unique data. As discussed previously, the difference map contains some spurious electron density peaks. These are as yet unexplained. Neutral atom scattering factors, coefficients of anomalous dispersion and absorption coefficients were obtained from international tables. Thermal ellipsoid plots were obtained using the program ORTEP-3 for windows. All calculations were carried out using the WinGX package of programs.

cell formula	C ₁₃₆ H ₁₆₈ N ₈ F ₄₈ P ₈ O ₃₂
M _r	908.25
space group	C 2/c
crystal system	monoclinic
a (\AA)	16.329(1)
b (\AA)	21.818(1)
c (\AA)	13.591(1)
α (deg)	90.000(0)
β (deg)	126.819(9)
γ (deg)	90.000(0)
V (\AA^3)	3876.42
Z	4
D _{calc} (gcm ⁻³)	1.556
F(000)	1792.0
μ (Mo-K α) (mm ⁻¹)	2.3
Temperature ($^{\circ}\text{C}$)	18
crystal size (mm)	0.38 x 0.23 x 0.18
no. data collected	5637
no. unique data	2450
R _{int}	0.0402
no. parameters	265
final R1	0.0725
final R _w ²	0.2201
largest remaining feature in electron density map (e/ \AA^3)	0.49, -0.25
mean shift/esd	0.003
goodness of fit S	0.890